

Alma Mater Studiorum – Università di Bologna

DOTTORATO DI RICERCA IN

Ingegneria Chimica dell' Ambiente e della Sicurezza

Ciclo XXVIII

Settore Concorsuale di afferenza: 09/D2 SISTEMI, METODI E TECNOLOGIE
DELL'INGEGNERIA CHIMICA E DI PROCESSO

Settore Scientifico disciplinare: ING-IND/24 PRINCIPI DI INGEGNERIA CHIMICA

***PRESSURE DRIVEN MEMBRANE TECHNOLOGY FOR FOOD
AND BIOTECHNOLOGY INDUSTRY***

Presentata da: *Dott. Ing. Valentina Morelli*

Coordinatore Dottorato

Prof. Ing. Serena Bandini

Relatore

Prof. Ing. Serena Bandini

Esame finale anno 2016

Index

<i>Abstract</i>	<i>iii</i>
<i>1. Introduction to membrane processes for Food and Biotechnology Industry</i>	<i>1</i>
<i>2. Sugar Chemistry & Sugar NF</i>	<i>27</i>
<i>3. Separation of oligosaccharide mixtures in Nanofiltration: Experimental study</i>	<i>59</i>
<i>4. Separation of oligosaccharide mixtures in Nanofiltration: Modelling and critical assessment</i>	<i>89</i>
<i>5. Conclusions</i>	<i>139</i>
<i>APPENDIX A: Materials & Methods</i>	<i>149</i>
<i>APPENDIX B: Fluid dynamic analysis on 1812 spiral wound modules</i>	<i>159</i>
<i>APPENDIX C: Membrane processes in Biotechnology applications</i>	<i>183</i>
<i>APPENDIX D: Experimental data</i>	<i>211</i>

Abstract

The increase in energy costs and the demands for products with greater nutritional value and of processing procedures less toxic to the environment are attractive factors for transferring membrane processing to food industry and biotechnology applications.

Sugar production is one of the most energy-intensive applications in the food industry, therefore membrane separation processes find many applications, nevertheless some limitation exist for application of membrane processes in the sugar industry, since the solutions exhibit high viscosity and high osmotic pressure, as well as criticalities still exist in modelling and process simulation.

This study focused mainly on *Food* applications of membrane processes. A brief graphical abstract of the main topics discussed is given in Fig. A.1.

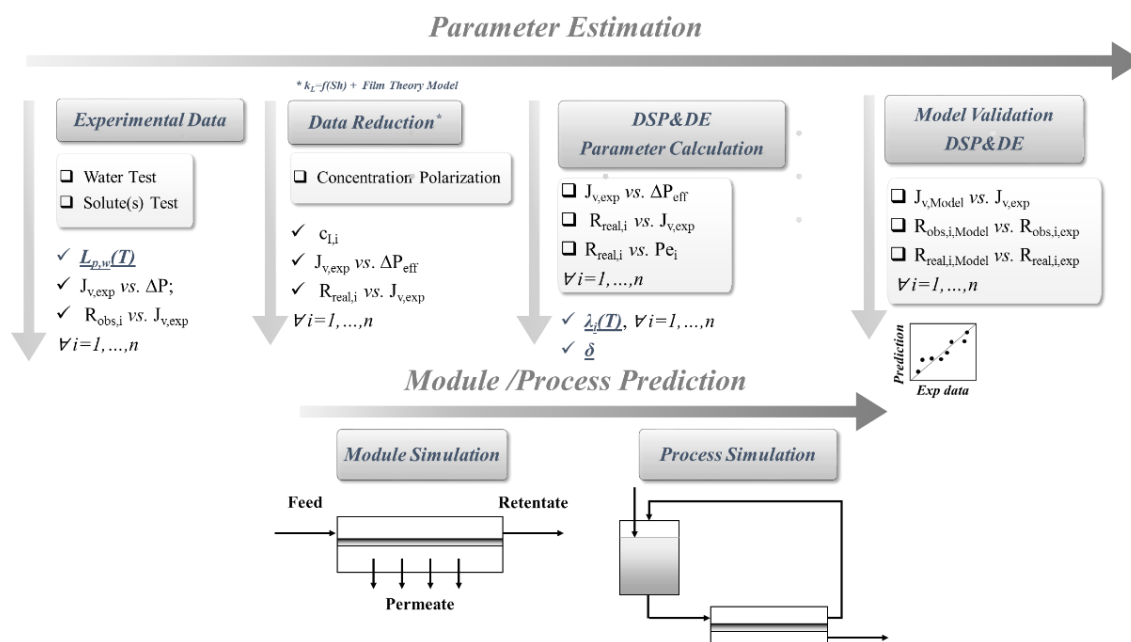


Figure A.1: Flow sheet of the modeling steps of the thesis, about pressure driven membrane processes for food applications.

After a general introduction on pressure driven membrane processes, sugar chemistry and sugar Nanofiltration, a critical summary of a wide experimental investigation is reported. In this work, separation performances of commercial polyamide *NF* membranes are investigated in a wide range of compositions in the feed side (from 5 to 300 g/dm³) at temperatures from 30 to 50°C; aqueous solutions containing monosaccharides (xylose,

glucose or fructose), disaccharides (maltose), and mixtures of them are studied, and the role of the electrolytes (NaCl, CaCl₂, NaHSO₃) on their rejection is investigated.

All the results obtained, performed with two module configurations (flat sheet and spiral wound membranes) have been organized in three main sections: (i) Hydraulic permeability, (ii) experimental investigation as it is, and (iii) Intrinsic membrane performances. Differently from literature, where typically aqueous solutions containing monosaccharides and oligosaccharides are used at low concentrations (from 9 to 80 g/dm³), at room temperature and only experimental data as it is are reported, a key point of this study is the critical evaluation based on intrinsic membrane performances.

The data processing discussed allows to introduce a revised Donnan Steric Pore & Dielectric Exclusion model (*DSP&DE*), in which:

- i) General equations of the model are introduced;
- ii) A critical assessment about model parameter calculation in literature is proposed and a new procedure for their calculation is suggested;
- iii) Model validation is performed at each experimental level (from flat sheet to SW, from single solutes to multicomponent mixtures).

Elaborations of experimental data with oligosaccharides put in evidence that the Stokes radius is not representative of the molecule shape because it does not account for: (a) molecule shape (such as deviations from sphericity); (b) change in hydration shell due to solution properties, and (c) solute-solute interactions.

The revised model provides useful elements to understand which kind of interactions (complex formation or dehydration) can affect sugars rejections in presence of strong electrolytes, however dehydration effects caused by temperature and electrolyte are the most evident.

The revised model is able to predict with good confidence both the temperature effect on membrane performances and rejections in multicomponent mixtures, ranging from laboratory to process/industrial scale, by comparison with literature data from 4040C1025 GE-DL module.

For completeness, the study provides in *Appendix*:

- Discussion about fluid dynamic analysis in 1812 Spiral Wound Modules and calculation of proper correlation for mass transfer coefficient (*Appendix B*);

- A preliminary study for membrane processes in biotechnology applications about :
(i) the recovery of *PHAs* (Polyhydroxyalcanoates) via Ultrafiltration; and (ii) the recovery and/or fractionation of *VFA* (*Volatile Fatty Acids*) by Nanofiltration
(*Appendix C*)

1. Introduction to membrane processes for Food and Biotechnology Industry

1.0 Preface.....	3
1.1 Pressure driven membrane processes.....	5
1.1.1 Membrane types.....	12
1.1.2 Polymers used in membrane manufacture.....	14
1.1.3 NF Membranes: State of art.....	16
1.1.4 Spiral-Wound module.....	17
1.2 Operating parameters.....	19
1.2.1 Concentration Polarization.....	20
1.2.2 The Film Theory.....	22
References.....	24

List of symbols

<i>Symbol</i>	<i>Units</i>	<i>Quantity</i>		
c	[g/dm ³]	concentration	<i>RO</i>	Reverse Osmosis
P	[bar]	pressure	<i>NF</i>	Nanofiltration
Δ		difference	<i>UF</i>	Ultrafiltration
Q	[dm ³ /h]	flow rate	<i>MF</i>	Microfiltration
J_v	[dm ³ /(hm ²)]	permeate flux		
J_S	[g/(hm ²)]	solute flux		
			<i>Subscript</i>	
R_{obs}	-	observed rejection	<i>i</i>	Solute/component
R_{real}	-	real rejection	<i>bulk</i>	bulk side
k_L	[m/s]	mass transfer coefficient	<i>I</i>	feed/membrane interface
D	[m ² /s]	diffusion coefficient	<i>F</i>	feed
δ	[m]	boundary layer thickness	<i>P</i>	permeate
A	[m ²]	membrane area	<i>R</i>	retentate

1.0 Preface

Membranes and membrane processes are not a recent invention, they are part of our daily life, exist as long as life exist, and they are also an essential structural component of living objects. We can distinguish between biological membranes, which are part of the living organism, and synthetic membranes that are man-made.

Many biological processes require membranes. The phospholipid bilayer is the basic structure of all biological membranes. Physically and chemically essential functions include metabolism and the process of the accumulation and usage of energy in the biological system. An essential function of the membrane is to keep a well-defined chemical composition inside of the membrane at a limited volume, which is different from the outside. Moreover biological membranes reproduce themselves continuously, controlling important physiological processes, carry out very complex and specific transport tasks. They accomplish them quickly, efficiently, and with minimal energy expenditure, frequently using active transport.

On the other side, synthetic membranes are not nearly as complicated in their structure or function as biological membranes. They exhibit only passive transport properties and are usually less selective and energy efficient. In general however, they have significantly higher chemical and mechanical stability, especially at elevated temperatures and pressures, while their selectivity is determined by their porous structure.

The preparation of synthetic membranes and their utilization on a large industrial scale, however, are a more recent development which has rapidly gained a substantial importance due to the large number of practical applications.

Today membrane processes have a wide industrial applications covering many existing and emerging uses in chemical, environmental, water treatment, pharmaceutical, medical, food, dairy and beverage industries. Membranes are used to produce water from the sea, to clean industrial effluents and recover valuable constituents, to concentrate, purify, or fractionate macromolecular mixtures in the food and drug industries, as well as to separate gases and vapors. They are also key components in energy conversion systems, and in artificial organs and drug delivery devices.

Membrane operations in the last years have shown their potentialities in the rationalization of production system. Their intrinsic characteristics of efficiency, operational simplicity and flexibility, relatively high selectivity and permeability for the transport of specific components, low energy requirements, good stability under a wide spectrum of operating conditions, environment compatibility, easy control and scale up have been confirmed in a

large variety of applications and operations, as molecular separation, fractionation, concentration, purification, etc., in a wide spectrum of operating parameters such as pH, temperature and pressure.

From a general point of view membrane processes are used to concentrate or fractionate a liquid to yield two liquids that differ in their composition. It stands out as alternatives to conventional processes for the chemical, pharmaceutical, biotechnological and food industries (Baker 2004). In many cases the low energy consumption, reduction in number of processing steps, greater separation efficiency and improved final product quality are the main attractions of these processes. Indeed, in many applications membrane processes compete directly with the more conventional techniques. However, compared to these conventional procedures membrane processes are often energy efficient, simple to operate and yield a higher quality product. The same is true for separation, concentration, and purification of drugs and food products or in pharmaceutical applications.

For instance, for surface water purification and waste-water treatment, micro- and ultrafiltration are competing with flocculation, sand bed filtration and biological treatment. In terms of versatility, centrifugation is perhaps the only method to match membrane technology (see Table 1.1), when concentration is required, however, an absolute requirement for centrifugal processes is the existence of a suitable density difference between the two phases that are to be separated, in addition to the two phases being immiscible.

The existing membrane applications include mainly: (i) dialysis for the purification of human blood (the artificial kidney); (ii) reverse osmosis for seawater desalination; (iii) ultrafiltration for the concentration of protein molecules (typically from cheese and milk); (iv) microfiltration for the sterilization of pharmaceutical and medical product (Winston Ho and Sirkar 1992).

The possibility of having the membrane systems as tools for a better design of chemical transformation is becoming realistic for interesting biological applications (i.e. *MBR, Membrane Bio Reactors*); synthetic membranes provide an ideal support to catalyst immobilization due to their available surface area per unit volume. Membrane based artificial organs such as the artificial kidney are a standard part of modern biochemical engineering and medicine.

The possibility of developing new nanostructured materials with specific configurations and morphology is offering powerful tools for the preparation of membranes with controlled selectivity and higher permeability (Strathmann, Giorno and Drioli 2011).

In this study (as suggested by the title of this work) we have focused on pressure driven membrane processes for food and biotechnology applications.

Membranes in their many configurations are used throughout the food processing industry for many years. They can be applied within the production process, i.e. for clarification and concentration, as well as used to treat the resulting wastewater prior to disposal or re-use. In biotechnology industry, membrane applications are increasingly being used in reaction, clarification and recovery schemes for the production of molecules, emulsions and particles. They are very well suited to biological processes, since they operate at relatively low temperatures and pressures and involve no phase changes or chemical additives, thereby minimizing the extent of denaturation, deactivation, and/or degradation of biological products (Zeman and Zydney 1996).

The increase in energy costs and the demands for products with greater nutritional value and of processing procedures less toxic to the environment are attractive factors for transferring membrane processing to food industry and biotechnology applications.

In addition to food and biotechnology applications, the growth of bio resource based chemicals, functional monomers as well as fuels leads to an increased demand for new separation processes. Current research focuses on the utilization of lignocellulosic materials as a bio-renewable feedstock, thus the role of membranes in view of the new biorefinery concept is crucial for downstream processes (Abels, Cartensen and Wessling 2013).

In this chapter a general introduction to membrane science and technology is given. It begins with the definition of technical terms and provides a description of membrane structures and processes that are used in mass separation. The discussion of engineering considerations such as mass transfer in membrane modules and concentration polarization and their consequences in practical applications in food and biotechnology industries will follow later.

1.1 Pressure driven membrane processes

Technically filtration is defined as the separation of two or more components from a fluid aqueous stream based primarily on size differences [(Van der Bruggen, Vandecasteele, et al. 2003), (Daufin, et al. 2001)]. The primary role of a membrane is to act as a selective barrier: it should permit passage of certain components and retain certain other components

of a mixture. By implication, either the permeating stream or the retained phase should be enriched in one or more components, selectively.

In pressure driven membrane processes (reverse osmosis, nanofiltration, ultrafiltration, and microfiltration, *RO*, *NF*, *UF* and *MF* respectively) a pressure (P_F as shown in Fig. 1.1) exerted on the solution at one side of the membrane is the driving force that separates it into a permeate and a retentate (P and R respectively). In other applications, concentration gradients or electrical potential gradients may also be used as additional driving forces (Baker 2004).

Membranes involved may be typically polymeric, organo-mineral, ceramic, or metallic, and filtration techniques differ in pore size, from dense (no pores) to porous membranes. Moreover, depending on the type of technique, salts, small organic molecules, macromolecules, or particles can be retained, just as the applied pressure will differ.

Pressure-driven membrane processes use thus the pressure difference (ΔP) between the feed and the permeate side as the driving force to transport the solvent (usually water) through the membrane. Particles and dissolved components are (partially) retained based on properties such as size, shape, and charge.

According to a further grading, pressure-driven membrane processes can be classified by several criteria:

- The characteristics of the membrane (pore size);
- Size and charge of the retained particles or molecules;
- Pressure exerted on the membrane.

This classification distinguishes intrinsically microfiltration, ultrafiltration, nanofiltration, and reverse osmosis.

The hydrostatic pressure gradient exerted (ΔP) is the driving force used to achieve the desired hydrodynamic flow (J_v) through the membrane (and through a deposited layer that may develop during the filtration process).

In its simplest form, as shown in Fig. 1.1, a generic membrane technology consists merely of pumping the feed solution under pressure over the surface of a membrane of the appropriate chemical nature and physical configuration.

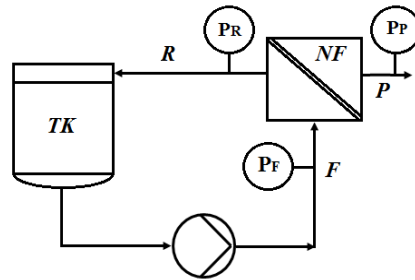


Figure 1.1: Operating principle of membrane technology, “cross-flow” configurational mode, where the feed (F) is pumped from the feed tank over the surface of the membrane, resulting in two stream, permeate (P) and retentate (R)

The pressure exerted on the solution at one side of the membrane represent the driving force to separate it into a Permeate (P) and a Retentate (R). Permeate is usually a diluted stream (or pure water), whereas the retentate is a concentrated solution.

The pressure gradient across the membrane would force solvent and in some case smaller species through the pores of the membrane, while the larger molecules/particles would be retained. Thus, one feed stream is split into two product stream. The retained stream (R) will thus be enriched in the retained macromolecules, and will also contain some of the soluble solutes. In fact, the permeable solutes may be at the very same or higher concentration than in the permeate stream, depending on how the membrane separates or rejects the solute. However, since the retentate now forms a much smaller volume than in the feed a purification of the retained species is reached.

As well as by the pressure, separation performance of a membrane is influenced by its chemical composition, temperature, feed flow rate and interactions between components in the feed flow and the membrane surface.

The four major pressure driven membrane processes are Microfiltration (MF), Ultrafiltration (UF), Nanofiltration (NF) and reverse osmosis (RO), and cover a wide range of particle/molecular sizes and applications. What distinguishes the more common pressure driven processes is the application of hydraulic pressure to speed up the transport process, as well as the nature of the membrane itself controls which components permeate and which are retained preferentially, as shown in Table 1.1.

In its ideal definition, RO retains all components other than the solvent (e.g. water) itself, while ultrafiltration retains only macromolecules or particles larger than about 10-200 Å (about 0.001-0.02 μm). Because UF deals with the separation of fairly large molecules,

such as proteins, starch or pigments, the osmotic pressures involved are fairly low; in contrast, pressure involved in *RO* would be fairly high (of order 35-100 bar) in order to overcome the high osmotic pressure of the small solutes, like salts. *NF* has lower osmotic pressure to work and thus will need lower operating pressure (10-30 bar). *UF* and *MF*, on the other hand, would thus need fairly low pressures for operation, and thus lower equipment and operating (mainly pumping) costs. Table 1.1 shows some typical example of components that fall under these four main processes.

When pressure-driven flow through a membrane is used to separate micron-sized particles from fluids, the process is called Microfiltration.

Table 1.1: Principal characteristics typical of solutes retained of commercial pressure driven membrane separation processes

<i>Separation Process</i>	<i>Application</i>	<i>Species retained</i>	<i>Cut off (kDa)</i>	<i>Driving force</i>	<i>Pressure (bar)</i>	<i>Centrifugation*</i>
<i>MF</i>	Clarification	Suspended and emulsified solid, Yeats	>200	Hydrostatic Pressure	0.5-3	High speed centrifuge 5000-10,000 G
<i>UF</i>	Clarification/ Concentration	Colloids, Proteins, Bacteria	1-200	Hydrostatic pressure vs. small osmotic pressure	2-10	Ultra-centrifuge 10,000-100,000 G
<i>NF</i>	Concentration/ Purification	Divalent salt (SO ₄ ²⁻ , PO ₄ ²⁻), Oligosaccharides Dextrans	0.1-1	Hydrostatic pressure vs. osmotic pressure	6-30	–
<i>RO</i>	Purification	Monovalents salts, Monosaccharides	< 0.1		10-80	–

*comparison of centrifugation and filtration processes

Microfiltration (MF) is a membrane process that involves the use of membranes with a pore size of 0.2–2 µm, and can selectively separate particles with molecular weights of >200 kDa.

MF is generally defined to be the filtering of a suspension containing colloidal or fine particles with linear dimensions within the range of 0.025 to 10 µm. This size range covers a wide variety of natural and industrial particles (i.e. viruses, bacteria, synthetic polymer spheres, yeast cells). These particles are generally large, consequently the osmotic pressure for *MF* is negligible, and the transmembrane pressure drop, which drives the filtration

process, is lower than 0.2 MPa. *MF* is primarily used to separate particles and bacteria from other smaller solutes.

In the food processing industry *MF* is commonly used for clarification instead of centrifugation and for sterilization in place of heat. It is primarily used to remove suspended solids (*SS*), fat and high molecular weight (*HMW*) proteins. In the dairy industry, for example, it can be used to clarify cheese whey, as well as de-fat and reduce the microbial load of milk.

In biotechnology applications, tangential flow microfiltration competes with centrifugation, depth filtration and expanded-bed chromatography for the initial harvest of therapeutic products from mammalian, yeast and bacterial cell cultures. In contrast to centrifugation, *MF* membranes generate a particle-free harvest solution that requires no additional clarification before subsequent purification (van Reis and Zydney 2001).

The most common application of microfiltration is sterile filtration (bacterial removal) prior to final formulation of many biotechnological products, and in the initial clarification of fermentation broths to remove suspended cells, other particulate debris, or antibiotics recovery (Charcosset 2006).

Ultrafiltration (UF) is primarily a size-exclusion-based pressure driven membrane separation process. Typical rejected species include sugars, biomolecules, polymers, and colloidal particles. Most *UF* membranes are described by their nominal molecular weight cut-off (*MWCO*)¹. The *MWCO* of any given membrane can vary with changing feed chemistries as well as with factors such as molecular orientation, molecular configuration, operating conditions, etc. As a consequence of the high molecular weight of species separated in a *UF* process, osmotic pressure differentials are smaller, simultaneously the liquid phase diffusivity is also lower, hence membrane fouling and concentration polarization problems are significant.

UF involves the use of membranes with a molecular weight cut off (*MWCO*) in the range of 1–300 kDa and a pore size of ~0.01µm. *UF* processes operate from 2 to 10 bar, although in some cases up to 25-30 bars have been used. Feed liquid phase mass transfer resistance and resistance due to gel layer formation on the membrane surface are extremely important effects in *UF* processing.

¹ *MWCO* is usually defined as the smallest molecular weight specie for which the membrane shows more than 90% rejection

UF membrane processes are generally used in the food, beverage, and dairy industries, for effluent treatment, and for biotechnology and medical applications [(Baker 2004), (Winston Ho and Sirkar 1992)]. *UF* is ideal for fractionation, concentration and purification. For example, *UF* can be used to fractionate milk for cheese production. A particularly large market for *UF* is in the specialty milk-based beverages. Another industry where *UF* has found popularity is the fruit juice industry, where permeate rather than retentate is the product of interest. Here, *UF* can be used to clarify a wide variety of fruit juices by removing impurities, such as yeast, bacteria and colloids, together with proteins, tannins and polysaccharides, which all helps to impart stability to the final product.

Not to mention that *UF* has numerous applications in the biotechnology field. In the last decade *UF* has become the method of choice for protein concentration and buffer exchange, largely replacing size-exclusion chromatography in these applications, purification of plasmid *DNA* as well as virus-like particles [(Kurnik, et al. 1995), (Kahn, et al. 2000), (Cruz, et al. 2000)].

*Reverse osmosis (RO)*² technology has grown extensively in recent years, since when thin-film composite (*TFC*) membranes has provided better flux performance and enhanced separations of organic under lower operating pressures than those obtained with cellulosic membranes. These materials are more pH, temperature, and chlorine resistant than the traditional cellulose acetate membranes. The ideal reverse osmosis membrane should be resistant to chemical and microbial attack, and the separation and mechanical characteristics should not change after long-term operation.

RO is characterized by a *MWCO* of about 100 Da, and the process involves pressures 5–10 times higher than those used in *UF*. It uses pressures between 4 and 10 MPa and concentrates particles with molar masses below 350 Da and this technique reject nearly all solutes and desalinate water (Baker 2004).

Applications of *RO* membranes include treatment of water and hazardous wastes, separation processes in the food, beverage, and pulp and paper industries, recovery of organic and inorganic materials from chemical processes, etc. One of the main advantage of using *RO* is the reduction in the costs associated with evaporation, or even the elimination of this step.

² *Osmosis* is a natural phenomenon in which water flows through a semipermeable (no solute flow) membrane from the side with lower solute concentration to the higher solute concentration side until equilibrium of solvent (water) chemical potential is restored. To reverse the flow of water, a pressure difference greater than the osmotic pressure difference is applied; as a result, separation of water from solutions become possible. This phenomenon is termed *Reverse Osmosis*.

These membranes, originally developed for desalination, have found a small niche in the biopharmaceutical industry; more often they are used for the concentration of antibiotics, peptides, or salts (Kalyanpur 2002).

Nanofiltration (NF) lies between the separation characteristics of *RO* and *UF* process which is widely used for several applications such as water softening and wastewater treatment. The pore size of the *NF* is in the range of 0.5–1 nm. This application concentrates, fractionates or purifies aqueous solutions of organic solutes with molecular weight between 100 and 1000 Da and mixture of monovalent/multivalent salts and uses pressures between 1 and 4 MPa [(Baker 2004), (Salehi, Razavi and Elahi 2011)]. Since, the *NF* membrane shows an amphoteric behavior, depending on pH, positive or negative charged ions will be attracted and repelled due to Donnan effect. *NF* carries quite distinctive properties such as pore radius and surface charge density which influences the separation of various solutes (Salehi, Razavi and Elahi 2011).

NF membranes also have a useful (peculiar) property in that they can separate dissociated forms of a compound from the undissociated form; e.g., organic acids such as lactic, citric, and acetic pass through easily at low pH but are rejected at higher pH when in their salt forms.

NF can also be applied for more challenging applications, involving fractionation rather than purification. The nature of the membrane controls which components will permeate and which will be retained, since they are selectively separated according to their molar masses or particle size. It is well known that *NF* membranes can be used for salt fractionation since the rejection of monovalent salts is lower than that of multivalent salts (Bandini and Bruni 2010). *NF* appears as an important alternative to conventional methods of food processing, and it is a technology is still evolving, finding more and more applications in food processing and appears as an important alternative to conventional methods. Recent research has highlighted the potential for *NF* use in wide ranging, including water softening, wastewater treatment, vegetable oil processing, beverage, dairy and sugar industry (Salehi, Razavi and Elahi 2011). *NF* has been established as greater separation efficiency technology: it successfully reduces the wastewater, in can be performed at low temperatures, it is characterized by reduction in number of processing steps and it presents a promising choice toward the achievement of cost effective process.

1.1.1 Membrane types

As seen in the previous section, membrane processes involve very different applications and hence it might be expected that a number of very different membranes are necessary. This is especially so because even for a single process one type of membrane is not sufficient to cover all possible applications.

Membranes can be classified by: (i) nature of the membrane (natural or synthetic), (ii) structure of the membrane (porous or nonporous), (iii) application (gas-gas, gas-liquid or liquid-liquid separation), and (iv) mechanism of membrane action (adsorptive, diffusive, ion exchange, osmotic, or nonselective (inert) membranes).

Synthetic membranes may be polymeric, organo-mineral, ceramic, and filtration techniques may differ in pore size, from dense (no pores) to porous membranes. Depending on the type of process (technique), salts, small organic molecules, macro-molecules, or particles can be retained, and so the applied pressure as well as the mechanical stability will differ [(Van der Bruggen, Vandecasteele, et al. 2003), (Cheryan 1998)].

Most membrane type are asymmetric, consisting of a thin separation layer (0.1 to 1 μm) supported by one or more thicker layers with larger pores. The supporting layers do not contribute to the resistance against the mass transfer; the permeability of the membrane is determined solely by the thin active layer. When the different layers consist of different polymer materials, the membrane are classified as thin film composite (*TFC*) membranes. Traditional material used in pressure-driven membrane processes are organic polymers.

Membranes are usually classified according to the size of the separated components, and thus in *MF* applications are specified in microns (i.e., μm). However, in *UF* membranes, it is customary to refer to the “molecular weight cut-off” (*MWCO*) instead of particle size. Thus, *UF* covers particles and molecules that range from about 1000 in molecular weight to about 500,000 Daltons. The most important membrane qualities are:

- high selectivity;
- high permeability;
- mechanical stability;
- temperature stability; and
- chemical resistance.

Firstly, membranes should combine high permeability and high selectivity, with sufficient mechanical stability. Selectivity is placed first on the list because low selectivity leads to a multi stage process, which is not economical compared with conventional process, whereas low permeability can be compensated by an increase in membrane surface area. The

separation efficiency is expressed by the rejection of a given compound, which ranges from 0 for complete permeation to 1 ($R=100\%$) for complete rejection. In industrial full-scale installations, the recovery, REC^3 , typically is around 80%.

MF membranes have the largest pores, ranging from 0.1 to 10 μm , and the highest permeability, so that a sufficient water flux is obtained at a low pressure. For microfiltration, the most often used materials are the hydrophobic polytetrafluoroethylene (PTFE), poly(vinylidene fluoride) (PVDF), polypropylene (PP), polyethylene (PE) and the hydrophilic materials cellulose esters, polycarbonate (PC), polysulfone/poly(ether sulfone) (PSf/PES), polyimide/poly(ether imide) (PI/PEI), aliphatic polyamide (PA), and polyetheretherketone (PEEK).

UF membranes have smaller pores (from 2 to 100 nm), and the permeability is considerably lower than in *MF*, so higher pressures are needed. Ultrafiltration membranes must be prepared by phase inversion. Materials used are polysulfone/poly(ether sulfone)/sulfonated polysulfone, poly(vinylidene fluoride), polyacrylonitrile and related block-copolymers, cellulosic such as cellulose acetate, polyimide/poly(ether imide), aliphatic polyamide, and polyetheretherketone. Polymer blends, e.g., with polyvinylpyrrolidone (PVP) are commonly used to increase the hydrophilicity of the membranes. Nanofiltration membranes are made of aromatic polyamide, polysulfone/poly(ether sulfone)/sulfonated polysulfone, cellulose acetate, or poly(piperazine amide).

In *NF* the pore size are smaller than in *UF*, typically around 1 nm, which corresponds to dissolved compounds with a molecular weight of about 300. Nanofiltration membranes are made of aromatic polyamide, polysulfone/poly(ether sulfone)/sulfonated polysulfone, cellulose acetate, or poly(piperazine amide). *NF* membranes also have a surface charge: polymeric *NF* membranes contain ionizable groups (carboxylic or sulfonic acid groups) which results in a surface charge in the presence of a feed solution.

Partitioning between the charged membrane and the bulk solution is characterized by the contribution of Donnan equilibrium, of Dielectric exclusion and hindrance; all of them allow also steric retention of ions with a size below the pore size of the membrane. Most *NF* membranes are composite materials supported by polymer substrate and manufactured in a spiral wound design as opposed to a flat sheet or tube geometry, the predominant model used today for industrial applications is the spiral configuration, whereas Polyamide (PA)

³ REC : defined as the ratio between permeate stream (Q_P) and feed stream (Q_F)

is typically used as the main component of the skin [(Baker 2004), (Hong, Miller e Bruening 2006)].

RO membranes are dense membranes without predefined pores. As a result, permeation is slower and rejection is not a result of sieving effect, but of a different diffusivity of the solutes with the membrane. The low permeability of *RO* membranes requires high pressures and, as a consequence, relatively high energy consumption. This effect is even more pronounced in the presence of osmotic pressure due to the high concentrations of dissolved components that counteract the effect of the exerted pressure. Reverse osmosis membranes can be made of cellulose triacetate, aromatic polyamide or interfacial polymerization of polyamide and poly(ether urea). Most membrane types are asymmetric, i.e. consisting of a thin separating layer (0.1 to 1 μm) supported by one or more thicker layers with larger pores. The supporting layers do not contribute to the resistance against mass transfer; the permeability of the membrane is determined solely by the thin active layer. These asymmetric membranes were a breakthrough for industrial application of membrane filtration because they combine high flux with sufficient mechanical strength. When the different layers consist of different polymer materials, the membranes are classified as thin film composite (*TFC*) membranes.

1.1.2 Polymers used in membrane manufacture

Among all the materials used to manufacture membranes (over 130 materials have been documented in literature), only few was approved for use in food and biotechnology applications. Moreover those material is limited by the high pressure values in pressure driven membrane processes. A brief summary of the membrane chemistry is presented in this section, towards understanding the behavior, performance, and limitations of particular materials.

Cellulose Acetate (CA) is a classic membrane material. The raw material is cellulose, which is a polymer of β -1,4 linked glucose units. One primary and two secondary hydroxyl groups and the β -glucosidic oxygen are in the equatorial position. Cellulose and its derivatives are generally linear, rod like, and rather flexible molecules, which are considered as fairly important characteristics for *RO* and *UF* applications. Cellulose acetate is prepared from cellulose by acetylation (i.e. reaction with acetic anhydride, acetic acid, and sulfuric acid). There are several advantages to the use of *CA* as membrane material:

- Hydrophilicity (which minimizes fouling);

- Wide range of pore size (covering from *RO* to *UF* applications)
- Low cost.

Among the disadvantages of *CA* membranes there are a fairly narrow temperature range, maximum recommended temperature is 35°C, as well as a rather narrow pH range (pH 5-6.5⁴). Another problem is the poor resistance to chlorine (less than 1 ppm is suggested under continuous operation), moreover *CA* is highly biodegradable, it is highly susceptible to microbial attack due to the nature of its cellulose backbone, not to mention that the lower the temperature the higher the risk of microbiological growth.

One important physical property that affects membrane quality is the degree of polymerization of the cellulose, the optimum appears to be 100-200 or 100-300, which would result in molecular weights of about 25,000-80,000.

Recently cellulose matrix have been studied as affinity support for biotechnology applications. Memtek Corporation⁵ has introduced hydrophilic affinity micro porous membranes composed of reactive aldehyde sites for covalent coupling to the groups of proteins and other ligands (Hermanson, Krishna Mallia and Smith 1992).

Polyamide (PA) membranes are characterized by having an amide bond in its structure (-CONH-). This class of materials overcomes some of the problems associated with *CA* membranes. Temperature, pH, biofouling as well as chlorine tolerance are higher. Typically *PA* form the contact skin layer in many composite membranes.

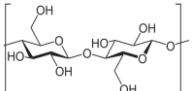
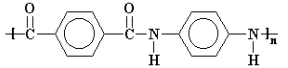
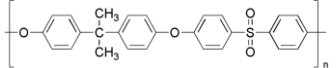
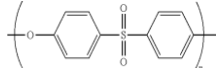
Polysulfone (PS) membranes are widely used in *MF* and *UF*. Polysulfone itself is characterized by having in its structure diphenylene sulfone repeating units. The -SO₂ group in the polymeric sulfone is quite stable. Repeating phenylene rings contribute to high degree of molecular immobility, producing high rigidity and strength. *Polysulfone (PS)* and *Polyethersulfone (PES)* are widely used, and are considered breakthroughs for *MF* and *UF* applications because of wide temperature limits (up to 75°C), wide pH tolerance as well as good chlorine tolerance.

To conclude, *Polyvinylidene fluoride (PVDF)* is a hydrophobic material, although some *PVDF* membrane has its surface modified to make it more hydrophilic (especially for biotechnology applications, where the fouling is severe). These class of material is very popular for *MF* and *UF* applications, because to its good chlorine tolerance. Table 1.2 summarizes the main characteristics of these membrane materials.

⁴ <http://www.gewater.com/>

⁵ <http://memteccorp.com/>

Table 1.2: Polymeric materials used for the manufacture of membranes

Membrane Polymer	Structure	T_{max} (°C)	pH range	Chlorine tolerance (ppm)
Cellulose Acetate (CA)		30-35	5.0-6.5	1
Polyamide (PA)		50-55	3.0-10.0	5,000
Polysulfone (PS)		75	1.0-13.0	200
Polyethersulfone (PES)		125		

1.1.3 NF Membranes: State of art

With properties between Ultrafiltration and Reverse Osmosis, *NF* membranes have been used extensively in many interesting applications especially in water and wastewater treatment. Other interesting applications include those in food, pharmaceutical and biotechnology applications.

NF membranes possess pore size typically of 1 nm which corresponds to molecular weight cut-off of 300-500 Da. *NF* membranes in contact with aqueous solution are also slightly charged due to the dissociation of surface functional groups or adsorption of charge solutes. For example, polymeric *NF* membranes contain ionizable groups such as carboxylic groups and sulfonic acid groups which result in charged surface in the presence of a feed solution; the dissociation of these surface groups is strongly influenced by the pH of the contacting solution and where the membrane surface chemistry is amphoteric in nature, the membrane may exhibit an isoelectric point at a specific pH.

Similar to *RO* membranes, *NF* membranes are able in the separation of inorganic salts and small organic molecules. Key distinguish characteristics are low rejection of monovalent ions, high rejection of divalent ions and higher fluxes compared to *RO* membranes. These properties have allowed *NF* to be used for water and wastewater treatment, pharmaceutical and biotechnology, and food engineering.

A wide literature is available about *NF* membrane properties [(Van der Bruggen, Manttari and Nystrom 2008) , (Hilal, et al. 2004)] as well as (Schaefer, Fane and Waite 2005) have written a comprehensive reference book on *NF*. Other recent reviews covered the chemical

modification of *NF* membranes (Van der Bruggen 2009), fouling [(Al-Almoudi 2010), (Tang, Chong and Fane 2011)], as well as effect of pH and salt (Luo and Wan 2013).

NF is an extremely complex process and depends on the micro hydrodynamic and interfacial phenomena occurring at the membrane surface and within the membrane nanopores. Rejection for *NF* membranes may be attributed to a combination of steric, Donnan, dielectric, and transport effects. The transport of neutral solutes is based on size exclusion and has been well established through numerous studies.

Most of *NF* membranes possess a porous active layer, and characterization of these nanopores in terms of pore size and distribution is a key element to understanding sieving aspect of these membranes. Thus membrane characterization is widely documented in literature because plays a crucial role, and as documented by (Mohammad, et al. 2015) can be performed by:

- Atomic Force Microscopy (*AFM*), which allows the direct measurement of pore size and distribution, surface roughness, topography;
- Neutral solutes rejection studies and model application, which allows the indirect measurement of pore size;
- Scanning electron microscope (*SEM*) for imaging of the membrane surface, membrane cross section and fouling.

A more detailed discussion about membrane characterization will be presented in *Chapter 4*.

1.1.4 Spiral-Wound module

Commercially, flat sheet membranes are installed in spiral wound modules and used in mainly water desalination and purification. In most cases the company which produces the membranes also produces the appropriate modules. This module type provides a rather large membrane area per unit volume, but requires in certain applications a substantial amount of pre-treatment.

Spiral wound is one of the most compact and inexpensive designs, and is characterized by a high packing density ($> 900 \text{ m}^2/\text{m}^3$) and a simple design. These membrane elements are designed around flat sheets: two flat sheets are placed together with their active sides facing away from each other and are wound around a permeate collecting tube with a special mesh being use as spacers (usually made of polypropylene). Both sheets are separated from each other and are glued together on three sides, the fourth open side is fixed around the

perforated center tube. Another mesh like spacer of the required thickness (the feed channel spacer) is placed on one side of this envelope and the whole assembly rolled around the center tube in a spiral configuration. A simplified sketch of the basic concept is depicted in Fig. 1.2:

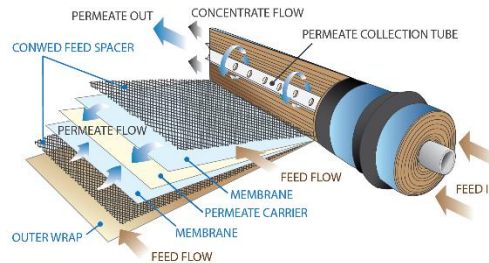


Figure 1.2: Detailed structure of a spiral wound module with axial feed flow

The feed is pumped lengthwise along the unit, while the permeate is forced through the membrane sheets into the permeate channel and spirals toward the perforated center collected tube. Usually, several elements are assembled in one pressure vessel.

In terms of fluid flow characteristics, spiral wound modules are basically flat sheet arranged on top of each other to form several narrow slits for fluid flow. The feed channel height is controlled by the thickness of the spacer in the feed channel. The advantage of a narrow channel height is that much more membrane area can be packed into a given pressure vessel.

The classic spiral wound module is characterized by cross flow and accurate modelling must, therefore, take into account the two-dimensional nature of velocity, pressure and concentration distribution for both feed and permeate channels.

These modules operate in turbulent flow. The velocity in the feed channel is calculated by dividing the volumetric flow rate by the cross sectional area. Typically the velocity in spiral wound unit ranges from 0.1 to 0.6 m/s, being higher for the larger mesh spacer. These are “superficial” velocities, corresponding to Reynolds number of 100-1300: nominally this is the laminar flow region (i.e. in tubular modules), but the additional turbulence contributed by the spacers, should also be taken into account. The spacer enhances turbulence, despite low Reynolds numbers.

Other configurations are plate-and-frame and tubular modules, used mainly in the chemical and food processing industry and in treating certain waste waters. Capillary type membrane modules dominate the hemodialysis market but are also applied in ultrafiltration and the production of ultra-pure water [(Strathmann, Giorno and Drioli 2011), (Cheryan 1998)].

1.2 Operating parameters

The terminology used for pressure-driven membrane processes (such as *NF*) was reviewed by (Gekas 1988). The driving force of the process is the pressure across the membrane.

The main physical operating parameters that affect membrane performances are: feed flow rate (Q_F), trans membrane pressure (ΔP), turbulence near the membrane surface (provided by stirring in a bench-top test cell, or by cross flow in an industrial module), temperature (T) and concentration of the solute(s) (c). Additional factors include pH, ionic strength (in particular for Electrolyte solutions), and other features that may affect the shape and conformation of the solutes.

The process is generally evaluated in terms of two parameters: observed solute rejection R_{obs} , and permeate flux J_v .

The definitions of these parameters are given below:

$$R_{obs} = 1 - \frac{c_P}{c_{bulk}} \quad (1.1)$$

$$J_v = \frac{Q_P}{A} \quad (1.2)$$

c_P , c_{bulk} in Eq. (1.1) are permeate and bulk concentration respectively, and Q_P , A in Eq. (1.2) represent permeate flow rate and membrane area, respectively. All these factors mentioned above affect rejection values. In pressure driven membrane processes it is important to account for the effect of concentration polarization.

Besides concentration polarization, others parameters that affect membrane performances are viscosity and density of the feed fluid. The viscosity can be controlled by two factors: solids concentration in the feed and temperature (Hwang and Kammermeyer 1998). An increase in feed concentration alters the viscosity, density and diffusivity of the feed solution, causing a decrease in permeate flow rate (Satyanarayana et al., 2000). An increase in temperature results in a decrease in fluid viscosity and increase in molecular mobility, that is, in diffusivity. For its part, an increase in tangential velocity increases the permeate flow rate by provoking greater turbulence, causing a dispersion in the solute molecules concentrated on the membrane surface, reducing the thickness of the gel layer [(Cheryan 1998), (Cheng and Lin 2004)].

There is a linear relationship between flow rate and the inverse of the solvent viscosity for *NF* and *UF* membranes, indicating that the main mass transport mechanism in these systems is convection (Tsui and Cheryan 2004).

1.2.1 Concentration Polarization

The term concentration polarization is used to describe the accumulation of membrane rejected solute at the membrane surface where the solute concentration is much higher than that of the bulk feed solution. This is shown schematically in Fig.1.3:

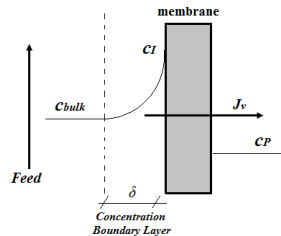


Figure 1.3: Concentration profiles during membrane processing of partially or completely rejected solutes

This phenomenon is an additional complication that arises when macromolecules (such as proteins, in *UF*) and other relatively large solutes (such as sugars, in *NF*) or particles are filtered. These compounds, being largely rejected by the membrane, tend to form a layer on the surface of the membrane. Depending on the type of solid, this layer could be fairly viscous (in case of sugars) or gelatinous (with proteins). Thus, a further resistance to the permeate flow is encountered, in addition to those of the membrane and boundary layer. As water passes through the membrane, the convective flow of solute to the membrane surface is much larger than the diffusion of the solute back to the bulk feed solution; as a result, the concentration of the solute at the membrane surface increases ($C_I > C_{bulk}$).

During Nanofiltration solutes in the feed are brought to the membrane surface by convective transport, and a portion of the solvent (water frequently) is removed from the fluid. This results in a higher local concentration of the rejected solute at the membrane surface as compared to the bulk, regardless of whether the solutes are partially or completely rejected by the membrane. This solute buildup is known as “concentration polarization” and is chiefly responsible for the marked deviation in flux compared to pure water flux.

Analogous to the velocity boundary layer, there will also be a concentration boundary layer that separates the region of higher concentration near the wall (i.e., near the membrane surface) from the lower, more uniform concentration in the bulk of the liquid (see Fig. 1.3). This concentration boundary layer is thinner than the corresponding velocity boundary layer since mass transfer by molecular diffusion is generally a much slower process than momentum transfer. In addition, the length over which the concentration boundary layer develops will be much longer.

Concentration polarization is more pronounced at higher pressure, lower velocities, and any other conditions which bring solute to the membrane surface very rapidly. When these operating conditions aggravate polarization effects, rejection will increase. The additional layer formed next to the membrane surface will cause the local concentration of the solute at the membrane surface, c_I (interfacial concentration) to be higher than in the bulk solution where samples are taken, thus, the true rejection, R_{real} , will differ from the apparent (observed) rejection, R_{obs} , where:

$$R_{real} = 1 - \frac{c_P}{c_I} \quad (1.3)$$

Where c_I refers to membrane surface concentration. Since $c_I > c_{bulk}$ because of the concentration polarization, R_{real} will be greater than R_{obs} . It is easy to measure c_P and c_{bulk} , on the other hand, R_{obs} values would only be valid under similar operating and polarization conditions, which in many cases is difficult to scale-up on industrial systems.

Concentration polarization is responsible of negative effects, such as:

- (i) Decrease in water flux due to an increase in osmotic pressure at the membrane surface;
- (ii) Increase in solute flux through the membrane;
- (iii) Precipitation of the solute if the surface concentration exceeds its solubility limit, plugging membrane pores and hence reducing water flux;
- (iv) Changes in separation properties of the membrane;
- (v) Fouling.

If the concentration of a rejected species is high enough, the secondary layer formed on the membrane surface may impede the passage of lower molecular solutes, in addition, higher concentrations lead to a decrease in the apparent *MWCO* (Cheryan 1998).

The extent of concentration polarization can be reduced by promoting good mixing of the bulk feed solution near the membrane surface. This can be done by modifying the membrane module to enhance the mixing, by including turbulence promoters in the feed channel, or by increasing the feed flow rate to increase the axial velocity and so promote turbulent flow, increasing Reynolds number.

Concentration polarization can have a major impact on membrane processes. The increased solute concentration on the membrane surface results in a significantly higher osmotic pressure, causing a decrease in the driving force of the process, and thus a decrease of the flux.

On the other hand the lower flux in polarization-limited system is due to the hydrodynamic resistance of the boundary layer. Initially, as a result of convective transport of solute to the membrane, solute buildup will cause a steep concentration gradient within the boundary layer. This causes a back transport of the solute into the bulk because of diffusion. Eventually, a steady state is reached where the two phenomena balance each other. Solute concentration in the gel layer reaches a maximum.

Changing the operating conditions, such as lowering pressure or feed concentration, or increasing the feed velocity, should revert the system back to the pressure controlled operating regime. Concentration polarization, differently from fouling, is an irreversible phenomenon.

1.2.2 The Film Theory

The flow of fluid in the bulk stream influences the back transfer of accumulated solute into the bulk, thus keeping this boundary layer thin. This concept forms the basis of the film theory.

The first model proposed to explain the effects of concentration polarization in *UF* was the gel-polarization model (Porter 1972). In the following years many works and reviews about concentration polarization have been reported [(Gekas and Hallstrom 1987), (Sablani, et al. 2001)].

Concentration polarization greatly complicates the modeling of membranes systems because experimental determination of the wall concentration is very difficult. For very high flow rates, enough mixing occurs, and the wall concentration can be assumed equal to the bulk concentration ($c_{bulk} \cong c_l$); however at lower flow rates this assumption could cause substantial error. One of the simplest and widely used theory for modeling flux in mass-transfer controlled systems is the *Film theory*. As solution is filtered, solute is brought to the membrane surface by convective transport at a rate J_s , defined as:

$$J_s = J_v c_{bulk} \quad (1.4)$$

Where J_v is the permeate flux and c_{bulk} is the bulk concentration of the rejected solute. The resulting concentration gradient causes the solute to be back-transported in to the bulk of the solution due to diffusional effects. Neglecting axial concentration gradients, the rate of back-transport of solute will be given by:

$$J_s = D \frac{dc}{dx} \quad (1.5)$$

Where D is the diffusion coefficient and the term $\frac{dc}{dx}$ is the concentration gradient over differential element in the boundary layer.

The *Film theory*, developed by (Brian 1966), simplifies a complex transport problem to a one-dimensional mass transfer problem by assuming axial solute convection near the membrane surface is negligible. At steady state, integrating the one dimensional convection-diffusion mass balance (the *Navier-Stokes* diffusion-convection equation) from the membrane surface out to a finite mass boundary (*film*) layer thickness, δ , assuming that the boundary layer is stagnant and its thickness does not change with channel length, yields the relationship between concentration polarization and permeate flux. The result is:

$$\frac{J_v}{k_L} = \ln \frac{c_I - c_P}{c_{bulk} - c_P} \quad (1.6)$$

Where k_L is the mass transfer coefficient, having the same units as the flux J_v , and is calculated as:

$$k_L = \frac{D}{\delta} \quad (1.7)$$

Where δ is the thickness of the boundary layer over which the concentration gradient exists. From Film theory, the intrinsic rejection can be calculated from the apparent (measured) rejection by the following relationship:

$$\ln \left[\frac{1 - R_{obs}}{R_{obs}} \right] = \ln \left[\frac{1 - R_{real}}{R_{real}} \right] + \frac{J_v}{k_L} \quad (1.8)$$

Where J_v is the flux and k_L is the mass transfer coefficient. Thus, whenever rejection data are reported, the mass transfer characteristics for the apparatus used should be known. This will allow the value k_L to be known, along with the volume flux J_v . Equation (1.3) could then be used to determine the true rejection, R_{real} .

In this model there is no pressure term; no effect of pressure was assumed, and thus this model will be valid only in the pressure-independent region. The flux will be controlled by the rate at which solute is transferred back from the membrane surface into the bulk fluid. Flux only can be improved by enhancing mass transport as much as possible, such as by reducing the thickness of the boundary layer.

References

- Winston Ho, W.S., and Kamalesh K. Sirkar. *Membrane Handbook*. 1992.
- Abels, C., F. Cartensen, and M. Wessling. "Membrane processes in biorefinery applications." *Journal of Membrane Science* 444 (2013): 285-317.
- Al-Almoudi, A.S. "Factors affecting natural organic matter (NOM) and scaling fouling in NF membranes: a review." *Desalination* 259 (2010): 1-10.
- Baker, R.W. *Membrane Technology and Applications*, Second Edition. John Wiley & Sons, 2004.
- Bandini, S., and D. Vezzani. "Donnan Equilibrium and Dielectric Exclusion for Characterization of Nanofiltration Membranes." *Desalination* 149 (2002): 477-483.
- Bandini, S., and D. Vezzani. "Nanofiltration modeling: The role of dielectric exclusion in membrane characterization." *Chemical Engineering Science* 58, no. 13 (2003): 3303-3326.
- Bandini, S., and L. Bruni. Transport phenomena in nanofiltration membranes. Vol. 2, in *Comprehensive membrane science and engineering*, by E. Drioli and L. Giorno, 67-89. Oxford: Elsevier, 2010.
- Brian, P. "Mass transport in reverse osmosis." In *Desalination by Reverse Osmosis*, by P. Brian. 1966.
- Charcosset, C. "Membrane processes in biotechnology: An overview." *Biotechnology Advances* 24 (2006): 482-492.
- Cheng, T., and C.T. Lin. "A study on cross flow ultrafiltration with various membrane orientations." *Separation Purification Technology* 39 (2004): 13-22.
- Cheryan, Munir. *Ultrafiltration and Microfiltration*. CRC Press, 1998.
- Cruz, PE, CC Peixoto, K. Devos, J.L. Moreira, E. Saman, and M.J.T. Carrondo. "Characterization and downstream processing of HIV-1 core and virus-like-particles produced in serum free medium." *Enzyme Microb. Technol.* 26 (2000): 61-70.
- Cuartas-Urbe, B., M.C. Vincent-Vela, S. Alvarez-Blanco, M.I. Alcaina-Miranda, and E. Soriano-Costa. "Nanofiltration of sweet whey and prediction of lactose retention as a function of permeate flux using the Kedem-Spiegler and Donnan Steric Partitioning models." *Separation and Purification Technology* 56 (2007): 38-46.
- Daufin, G., J.-P. Escudier, H. Carrère, S. Bérot, L. Fillaudeau, and M. Decloux. "Recent and emerging applications of membrane processes in the food and dairy industry." *Trans IChemE* 79 (June 2001): 89-102.
- Gekas, V. "Terminology for pressure-driven membrane operations." *Desalination*, 1988: 77.
- Gekas, V., and B. Hallstrom. "Mass transfer in the membrane concentration polarization layer under turbulent cross flow." *Journal of Membrane Science* 30 (1987): 153.

- Hermanson, Greg T., A. Krishna Mallia, and Paul K. Smith. *Immobilized Affinity Ligand Techniques*. 1st Ed. 1992.
- Hilal, N., H. Al-Zoubi, N.A. Darwish, A.W. Mohammad, and M. Abu ARabi. "A comprehensive review of nanofiltration membranes: treatment and pretreatment, modelling and atomic force microscopy." *Desalination* 170 (2004): 281-308.
- Hong, S., M.D. Miller, and M.L. Bruening. "Removal of dyes, sugars, and amino acids from NaCl solutions using multilayer polyelectrolyte nanofiltration membranes." *Industrial and Engineering Chemistry Research* 45 (2006): 6284-6288.
- Hwang, S.T., and K. Kammermeyer. "Membranes in separations." In *Ultrafiltration and Microfiltration Handbook*, by M. Cheryan, 526. Chicago: Technomic Publications, 1998.
- Kahn, D.W., M.D. Butler, Cohen, M. Gordon, J.W. Kahn, and M.E. Winkler. "Purification of plasmid DNA by tangential flow microfiltration." *Biotech. Bioeng.* 69 (2000): 101-106.
- Kalyanpur, M. "Downstream processing in the Biotechnology Industry." *Molecular Biotechnology* 22, no. 1 (2002): 87-98.
- Kumar, V.S., K.S. Hariharan, K.S. Mayya, and S. Han. "Volume average reduced order Donnan Steric Pore Model for nanofiltration membranes." *Desalination* 322 (2013): 21-28.
- Kurnik, R.T., et al. "Buffer exchange using size exclusion chromatography, countercurrent dialysis, and tangential flow microfiltration: models, development, and industrial application." *Biotech. Bioeng.* 45 (1995): 149-157.
- Luo, J., and Y. Wan. "Effects of pH and salt on nanofiltration- a critical review." *Journal of Membrane Science* 438 (2013): 18-28.
- "Membrane technology benefits the food processing industry." *Filtration & Separation* 41, no. 8 (2004): 32-33.
- Mohammad, A.W., Y.H. Teow, W.L. Ang, Y.T. Chung, D.L. Oatley-Radcliffe, and N. Hilal. "Nanofiltration membranes review: Recent advantages and future prospects." *Desalination* 356 (2015): 226-254.
- Porter, M.C. *Industrial Engineering Chem. Production Res. Develop.* 11, no. 3 (1972): 234.
- Sablani, S.S., M.F.A. Goosen, R. Al-Belushi, and M. Wilf. "Concentration polarization in ultrafiltration and reverse osmosis: a critical review." *Desalination* 141 (2001): 269-289.
- Salehi, F., S.M.A. Razavi, and M. Elahi. "Purifying anion exchange resin regeneration effluent using polyamide nanofiltration membrane." *Desalination* 278 (2011): 31-35.
- Schaefer, A.I., A.G. Fane, and T.D. Waite. *Nanofiltration-principles and Applications*. 1st. Kidlington, UK: Elsevier Advanced Technology, 2005.

- Strathmann, H., L. Giorno, and E. Drioli. *An Introduction to Membrane Science and Technology*. 2011.
- Tang, C.Y., T.H. Chong, and A.G. Fane. "Colloidal interactions and fouling of NF and RO membranes: a review." *Adv. Colloid Interface* 164 (2011): 126-143.
- Tsui, E.M., and M. Cheryan. "Characteristics of nanofiltration membranes in aqueous ethanol." *Journal of Membrane Science* 237 (2004): 61-69.
- Van der Bruggen, B. "Chemical modification of polyethersulfone nanofiltration membranes: a review." *J. Appl. Polym. Sci.* 114 (2009): 630-642.
- Van der Bruggen, B., C. Vandecasteele, T. Van Gestel, W. Doyen, and R. Leysen. "An overview of pressure-driven membrane processes in wastewater treatment and drinking water production." *Environmental Progress* 22 (April 2003): 46-56.
- Van der Bruggen, B., M. Manttari, and M. Nyström. "Drawback of applying nanofiltration and how to avoid them: a review." *Sep. Pur. Technol* 63 (2008): 251-263.
- van Reis, R., and A. Zydney. "Membrane separations in biotechnology." *Current Opinion in Biotechnology* 12 (2001): 208-211.
- Zeman, L.J., and A.L. Zydney. *Microfiltration and ultrafiltration. Principles and applications*. New York: Marcel Dekker, 1996.

2. Sugar Chemistry & Sugar NF

2.0 Introduction.....	27
2.1 Classification of Carbohydrates.....	29
2.1.1 Monosaccharides.....	30
2.1.2 Disaccharides.....	31
2.1.3 Polysaccharides.....	32
2.2 Sugar Chemistry in water solution.....	32
2.2.1 Hydration.....	34
2.2.2 “Salting out” effect.....	37
2.2.3 Sweetness and sweetener.....	38
2.2.4 Solubility.....	40
2.3 Sugar fractionation: state of the art.....	41
2.3.1 Conventional technique: the isomer separation case.....	41
2.3.2 Nanofiltration.....	44
References.....	53

2.0 Introduction

Carbohydrates are one of the most abundant classes of organic compounds that can be found on earth. This large natural resource has long interested chemist and biochemist because of its predominant role in biological and industrial applications. Among the well-known carbohydrates are various sugars, starches, and cellulose, all of which are important for the maintenance of life in both plants and animals, and which today play a pivotal role in food and biotechnology technology.

Carbohydrates are a major class of naturally occurring organic compounds, which come by their name because they usually have, or approximate, the general formula $C_n(H_2O)_m$ with $n \geq 3$, $m \geq 1$.

Although the structures of many carbohydrates appear to be quite complex, the chemistry of these substances usually involves only two functional groups- ketone or aldehyde carbonyls and alcohol hydroxyl groups. The carbonyl groups normally do not occur as such, but are combined with hydroxyl groups to form hemiacetal or acetal linkages.

An understanding of stereochemistry is particularly important to understanding the properties of carbohydrates: configurational and conformational isomerism play an important role for this class of organic compounds.

The structural characteristics of oligosaccharides, including the types of monosaccharides, substitutions and linkages building the structure, as well as the molecular weight, obviously influence their physico-chemical properties and in turn define the properties of the resulting solution as well as the membrane separation performance [(Geankoplis and Toliver 2003), (Pinelo, Jonsson and Meyer 2009)].

In commercial usage, the term “sugar” usually refers to sucrose, a disaccharide obtained from sugar cane and sugar beet. Today’s trend in commercial application is to use the term “sugar” without reference to its origin (Pancoast and Junk 1980). Glucose, sucrose, cellulose and starch are household names even if the common man may not know that glucose is a constituent of the other three. Within this group, one comes across a wide range of molecular sizes (from monomers to oligomers to polymers), and shapes. The predominant functional group is the hydroxyl ($-OH$), several of which occur in a carbohydrate. Another key functional group is the carbonyl group ($C=O$), which plays a pivotal role in the chemical behavior of carbohydrates.

Sucrose, the refined sugar of commerce, is represented by the following structural formula (Fig. 2.1):

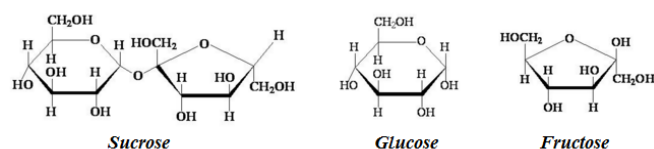


Figure 2.1: Sucrose, Glucose and Fructose structural formula. Sucrose is a disaccharide with one molecule of α -D-glucose condensed with one molecule of β -D-fructose.

Sucrose is a α -D-glucopyranosyl- β -D-fructofuranoside, technically. It is a disaccharide with one molecule of α -D-glucose in the pyranose (or 6-membered) ring and is condensed with one molecule of β -D-fructose in the furanose (or 5-member) ring form.

α -D-glucose is generally referred to as dextrose in its food applications, as well as β -D-fructose is also known as levulose, but more commonly as fructose. This structure is quite stable both in the dry form and in solution, but it is subject to hydrolysis in acid solution or when attacked by invertase enzyme. This hydrolysis reaction is also termed inversion, because of the net change in optical rotation (α)_D.

Upon hydrolysis a mixture of α -D-glucose (α -D-glucopyranose) and β -D-fructose (β -D-fructopyranose) is formed, technically named “Invert sugar syrup”.

There are three methods that are used to produce invert syrup: (i) the oldest procedure is the use of invertase, which is still used to some extent; secondly (ii) acid inversion, using hydrochloric acid, is widely used in both batch and in continuous systems; (iii) the third method is to use an ion-exchange resin.

Total invert sugar is, by definition, sucrose which is essentially completely hydrolyzed to an equimolecular ratio of dextrose and fructose. The limiting factor for the solubility of total invert is the solubility of dextrose. When one sugar is dissolved in an aqueous solution of another, the solubility of the latter is usually reduced due to the salting-out effect of the added sugar.

(Van der Linden 1919) firstly showed that the solubility of sucrose was less in an invert sugar solution than in pure water.

In this section sugar properties will be investigated in view of membrane processes application, however the first attempt is to introduce their classification.

2.1 Classification of Carbohydrates

Carbohydrates are primarily classified according to their molecular size and the number of monosaccharide units.

The simple sugars, or monosaccharides, are the building blocks of carbohydrate chemistry. They are polyhydroxy aldehydes or ketones with five, six, seven, or eight carbon atoms that are classified appropriately as pentoses (C5), hexoses (C6), heptoses (C7), or octoses (C8), respectively. They can be designated by more specific names, such as aldohexose or ketohexose, to denote the kind of carbonyl compound they represent (see Fig. 2.2). For example, an aldopentose is a five-carbon sugar with an aldehyde carbonyl; a ketohexose is a six-carbon sugar with a ketone carbonyl.

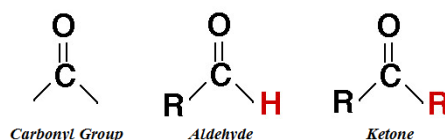


Figure 2.2: Representation of Carbonyl groups

It is important to keep in mind that the carbonyl groups of sugars usually are combined with one of the hydroxyl groups in the same molecule to form a cyclic hemiacetal or hemiketal. These structures once were written as follows, and considerable stretch of the

imagination is needed to recognize that they actually represent oxacycloalkane ring systems.

Oligosaccharides are made up of two or more monosaccharide units; for example, disaccharides, such as sucrose, lactose and maltose, are hydrolysable to yield two monosaccharide units. In the case of sucrose, the monomers obtained are glucose and fructose. Raffinose, which can be isolated from molasses, is a trisaccharide; this compound on hydrolysis yields one molecule each of glucose, galactose, another aldohexose, and fructose.

As already mentioned, cellulose and starch are polysaccharides, being polymeric compounds. Another example of a polysaccharide is glycogen, commonly known as animal starch. Others carbohydrates which do not conform to the general formula $C_n(H_2O)_m$ include deoxy sugars and amino sugars.

2.1.1 Monosaccharides

Monosaccharides are monomers. The most important member of this group is Dextrose (a C6), which is an aldohexose as it has six carbon atoms, five hydroxyl groups (one primary and the other four secondary) and an aldehyde function at one end, as in the Fischer representation. Dextrose is the hexose sugar *D-glucose* obtained by the complete hydrolysis of starch.

The optical activity exhibited by (+)-*Glucose* was first observed by Biot in the year 1817. Two years earlier he had recorded that sucrose was optically active. However, the stereochemistry of glucose and other monosaccharides remained obscure until Fischer began his pioneering studies. The molecular formula, formation of a penta acetate and reduction of Tollen's reagent established that glucose is a pentahydroxy aldehyde having six carbon atoms. The presence of the aldehyde group could be confirmed by oxidation with bromine water, the product being gluconic acid. Glucose cyanohydrin, on hydrolysis followed by reduction with hydriodic acid gave n-heptanoic acid showing that glucose is a straight-chain aldohexose. On catalytic hydrogenation over a nickel catalyst glucose yielded glucitol or sorbitol, which is 1,2,3,4,5,6-hexahydroxyhexane. However, structure that emerged from the above mentioned reactions could not account for all the known properties of glucose.

Fructose, which is an isomer of glucose (C6), has a keto carbonyl function and is known as a ketohexose. This hexose sugar is a natural constituent of many foods, and is a very hygroscopic sugar

When it crystallizes from solution it has the β -D-fructo-pyranose configuration. The crystals are anhydrous. (Shallenberger and Birch 1975) reported that the percentage distribution of the isomers of mutarotated D-fructose at 20°C is 68.4-76.0 for β -pyranose, 28.0-31.6 for β -furanose, and 4.0 for α -pyranose. Increasing temperature favors the formation of the pyranose configuration.

Fructose has the highest sweetness value of any of the commercial sugars; compared to sucrose, crystalline fructose is about 1.7-1.8 times sweeter than sucrose. When in solution, however, certain factors affect the sweetness intensity. These include concentration of sugar, temperature, and pH. Since the sweetness level is reduced with increasing temperature, fructose has a more effective application at normal or cool food temperatures. Monosaccharides having fewer carbon atoms are also known. For example, arabinose and ribose are aldopentoses, that is, they are C5 compounds with an aldehyde group and four hydroxyls.

Xylose, a pentose sugar, is an intermediate product in xylitol production. Xylitol is a sugar alcohol having sweetness equal to sucrose but it does not cause dental carries and, thus, it is used as a sweetener by e.g. the confectionary industry (P.M. Olinger 2001). Xylose can be hydrolyzed from xylan-rich materials like rice husk, corn stalk, wheat straw and flax straw. Potential sources for xylose are birch and other hardwoods that have a xylan-rich hemicellulose structure.

2.1.2 Disaccharides

Combinations of two or more of the simple sugars through glycoside linkages give substances known as polysaccharides. They also are called oligosaccharides if made from two to ten sugar units. The simplest oligosaccharides are disaccharides made of two molecules of simple sugars that can be the same or different.

The best known disaccharide is sucrose or cane sugar. As mentioned earlier, on hydrolysis it gives one molecule each of D(+)-Glucose and D(-)-Fructose. Since it does not reduce Tollen's reagent or react with phenylhydrazine, it is evident that it does not have a free carbonyl group. Nor does it exhibit mutarotation. Therefore, it is obvious that glucose and fructose are combined through their anomeric carbon atoms that are C-1 of glucose and C-

2 of fructose as shown in structure 26. This linkage is known as the glycoside bond. The configuration at the anomeric carbon atom of the glucose unit is α -, whereas that at the corresponding position in the fructose part is β .

In contrast to sucrose, *D(+)-Lactose*, which is the milk sugar, reduces Tollen's reagent, exhibits mutarotation and reacts with phenylhydrazine to form an osazone derivative. On acidic or enzymatic hydrolysis (brought about by the action of emulsin which specifically cleaves β -glycosidic linkages), one molecule each of *D(+)-Glucose* and *D(+)-Galactose* are obtained. The observation that lactosazone on hydrolysis gives galactose and glucosazone shows that in lactose, the glucose unit retains its anomeric hydroxyl group. Further experiments involving methylation followed by hydrolysis show that the anomeric carbon atom (C-1) of galactose is linked through an oxide bond to C-4 of glucose as shown in Maltose (28) and cellobiose are both diglucosides, each being made of two glucose units. Both are reducing sugars. In both the compounds, C-1 of one glucose unit is linked to C-4 of the other unit through an oxide bond. The only difference is the configuration of the glucosidic bond; in maltose it is α -, whereas in cellobiose it is β . Maltose forms the structural unit of starch, while cellobiose has a similar function in cellulose.

2.1.3 Polysaccharides

Among polysaccharides the best known are cellulose, starch and chitin. As mentioned earlier, the monomeric unit in both cellulose and starch is D-glucose but the glucosidic bond in cellulose is β and in starch it is α . Apart from this important difference, cellulose and starch differ from each other in several other respects. In cellulose, where the disaccharide unit is cellobiose, several molecules of the latter combine in a linear manner to form the polymer. Further, parallel strands of the polysaccharide thus formed link together by hydrogen bonding. The resulting ropelike structure makes cellulose a strong structural material. Starch, on the other hand, is not a homogeneous substance; it can be separated into the water-soluble amylose and water-insoluble

2.2 Sugar Chemistry in water solution

A mixture composed of water and small sugars is not as simple as it seems to be when molecular structure is investigated. Sugar molecules are neutral, but are sensitive to solvent polarity. As concentration increases, depending on sugar type, solute-solvent interactions

became more complex. Among small carbohydrates, the most studied one is sucrose for which literature is particularly rich in information.

The sucrose molecule can readily interact with water as well as other sucrose molecules through hydrogen bonding. Therefore, at least three types of molecular interactions take place in sucrose solutions:

- (i) Water-water;
- (ii) Sucrose-water (Solvation or Hydration);
- (iii) Sucrose-sucrose (Complex formation).

As well as aggregates between formed complexes are possible, all resulting in the formation of intermolecular hydrogen bonds.

The hydration of sugars is a crucial factor affecting properties such as water activity, solubility, and osmotic pressure. When dealing with uncharged solutes in aqueous environment, the so-called hydrodynamic model is the most common tool used to describe their rejection with a NF membrane. This model assumes the membrane, with uniform radius, having a proper pore geometry, defined as membrane pore radius, r_p , and the solute size is described, generally, by the Stokes radius.

In this study, different type of neutral solutes are investigated in order to better understand their behavior in solution; in nanofiltration applications rejection is the most useful tool for understanding their behavior.

Neutral solutes investigated and their molecular structure are summarized in Tab. 2.1, from mono-saccharides (xylose, glucose, fructose) to di-saccharides (maltose and lactose).

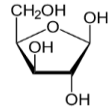
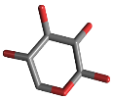
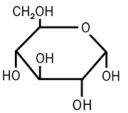
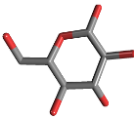
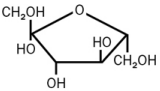
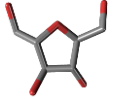
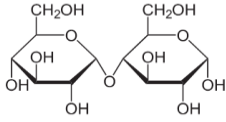
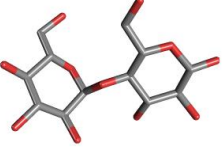
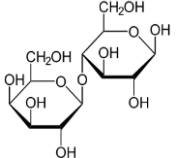
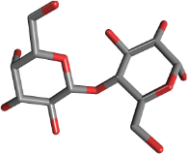
Since molecular weight is not able to describe the molecule steric hindrance, the 3-D structure put in evidence the spherical (or semi-spherical) nature regarding mono-saccharides whereas underlines the deviation from spherical nature of di-saccharides.

Both 2-D as well as 3-D figures represent very well the orientation of the free molecule alone, free to rotate in the space, and deviations from “sphericity”.

Besides orientation and steric hindrance, sugar chemistry in aqueous solution is quite complex. Small carbohydrates in aqueous solution are known to establish hydrogen bonds with water molecules: the number and strength of these bonds depend on solute conformation (orientation of –OH groups in the space) anomeric effect and on the proportion of ring isomers in the solution (Seuvre and Mathlouthi 2010); sugar hydration is influenced by the stereochemistry of the solute and the molecular conformation.

The aim in this section is to show the complex behavior of sugar in solution, starting from literature studies.

Table 2.1: Molecular weight (MW), 2-D and 3-D structure, Diffusivity, Stokes radius (r_{Stokes}) and pK_a constant of interesting oligosaccharides.

Solute	Molecular Weight (g/mol)	2-D Structure	3-D Structure	$D^\circ(25^\circ\text{C})$ (m^2/s)	r_{Stokes} (nm)	pK_a^1 (25°C) ^[d]
Xylose (XY)	150.13			$7.495 \cdot 10^{-10}$ [b] $7.5 \cdot 10^{-10}$ [c]	0.65 [c]	12.15
Dextrose (DX)	180.16	 <i>α-D-Glucopyranose</i>		$6.790 \cdot 10^{-10}$ [a] $6.728 \cdot 10^{-10}$ [b]	0.361 [a]	12.28
Fructose (FR)	180.16			$6.860 \cdot 10^{-10}$ [a]	0.357 [a]	12.03
Maltose (ML)	342.29			$4.80 \cdot 10^{-10}$ [a]	0.470 [a]	11.94
Lactose (LT)	342.29			$5.66 \cdot 10^{-10}$ [a]	0.433 [a]	11.98

^[a] (Ribeiro 2006); ^[b] (Sjoman, et al. 2007) (Shibusawa and Gakkaishi 1987); ^[c] (Taylor and Francis 2006) *D.R. Lide (Ed.) CRC Handbook of Chemistry and Physics, Taylor & Francis, Boca Raton, FL, 2006*

^[d] (Bhattacharyya and Roherer 2012)

2.2.1 Hydration

It is well known that carbohydrates present a very high affinity for water molecules, as well as water is known as a highly solvating (hydrating) agent. It is the nature of such

¹ pK_a is defined as the negative logarithm of the acidity constant in aqueous solution at 25°C

interactions that is responsible for most of the biological features, such as solubility, as well as sweet taste.

The number and strength of hydrogen bonds established between sugar and water molecules depends on sugar conformation (disposition of the hydroxyl groups in space), anomeric effect and on the proportion of ring isomers (pyranose or furanose) at equilibrium in solution. Moreover equatorial *OHs* are known to be more hydrated than axial ones because of a better fit with water structure (Seuvre and Mathlouthi 2010). In particular sugar hydration is influenced by the stereochemistry of the solute and the molecular conformation (Franks 1985).

Different studies showed that the hydration of a carbohydrate does not depend only on the number of *OH* groups and on the potential hydrogen binding sites, but also on their relative orientation. Moreover, the water structure is influenced by the ions arising from the dissolution of the electrolytes. Hydration plays an important role at low temperature and low concentration, especially when monosaccharides are processed (Sjoman, et al. 2007). As concentration increases, sugar-sugar interactions (i.e. *complexation*) become preponderant and n_h decreases. Among small carbohydrates, the most studied is sucrose for which the literature is particularly rich in information using all types of experimental techniques as well as molecular modelling in order to describe molecule hydration (Gharsallaoui, et al. 2008).

The hydration of sugars is a decisive factor for properties such as water activity, glass transition temperature, melting temperature, solubility (for instance fructose is more soluble than glucose in water) and osmotic pressure (Ben Gaida, Dussap and Gros 2006). It is well known that increase in temperature provokes an increase of water activity coefficient and a decrease in hydration number (as shown in Fig. 2.4)

Sugar hydration has been investigated for many years and several measured methods have been proposed to calculate overall sugar hydration and dependence on sugar concentration (NMR², NIR³, water activity or density measurements), as shown in Tab. 2.2. As a general rule, the hydration number (n_h) given in literature for saccharides greatly varies with the technique used to determine it. There is a considerable variation depending on the measurement method used, as suggested by (Ben Gaida, Dussap and Gros 2006).

² Nuclear Magnetic Resonance spectroscopy

³ Nuclear and Near-Infrared

Although maltose is comparable to sucrose, shows different hydration behavior; its hydration numbers are higher than that of sucrose, in the whole range of concentrations investigated. However the hydration layers of carbohydrates in aqueous solutions cannot be exactly described based upon present knowledge (Sjoman, et al. 2007).

Table 2.2: Hydration number (n_h), and technique adopted to calculate it for sugars from literature, temperature ranging between 20 and 25°C

<i>Solute</i>	n_h	<i>Methodology-technique</i>	<i>Ref.</i>
<i>Dextrose</i> (<i>DX</i>)	2.45-1.83	water activity, 20°C	(Cooke, Jónsdóttir and Westh 2002)
	3.56-1.35	density, 20°C	(Gharsallaoui, et al. 2008)
	3.26	viscosity measurements, 25°C	(Seuvre and Mathlouthi 2010)
	1.93±0.02	water activity data	(Ben Gaida, Dussap and Gros 2006)
<i>Fructose</i> (<i>FR</i>)	2.24-1.5	water activity, 20°C	(Cooke, Jónsdóttir and Westh 2002)
	3.83-1.89	density, 20°C	(Gharsallaoui, et al. 2008)
	2.93	viscosity measurements, 25°C	(Seuvre and Mathlouthi 2010)
	3.39±0.02	water activity data	(Ben Gaida, Dussap and Gros 2006)
<i>Maltose</i> (<i>ML</i>)	4.75-3.79	water activity 20°C	(Cooke, Jónsdóttir and Westh 2002)
	8.17-3.45	density, 20°C	(Gharsallaoui, et al. 2008)
	6.93	viscosity measurements, 25°C	(Seuvre and Mathlouthi 2010)
	4.48±0.02	water activity data	(Ben Gaida, Dussap and Gros 2006)
	14.2	acoustic data, 25°C	(Branca, Magazù, et al. 2001)
	11.7	viscosity data, 25°C	
<i>Sucrose</i> (<i>SC</i>)	1.8	NMR	Allen and Wood (1974)
	21	NIR	
	5.3	viscosity	(Mathlouti and Génétolle 1994)
	5	water activity data	(Akhumov 1981)
	13.8	ultrasound velocity and density data	(Galema and Høiland 1991)
	5-0.85	density, 20°C	(Gharsallaoui, et al. 2008)
	6.59	viscosity measurements, 25°C	(Seuvre and Mathlouthi 2010)
	13.1	acoustic data, 25°C	(Branca, Magazù, et al. 2001)
	11.2	viscosity data, 25°C	
3.13±0.02	water activity data	(Ben Gaida, Dussap and Gros 2006)	
<i>Xylose</i> (<i>XY</i>)	1.33±0.22	water activity data	(Ben Gaida, Dussap and Gros 2006)

There is a considerable variation depending on the measurement method used, as indicated in Tab. 2.2 and Fig.2.3 for some sugars, particularly at high molecular weight.

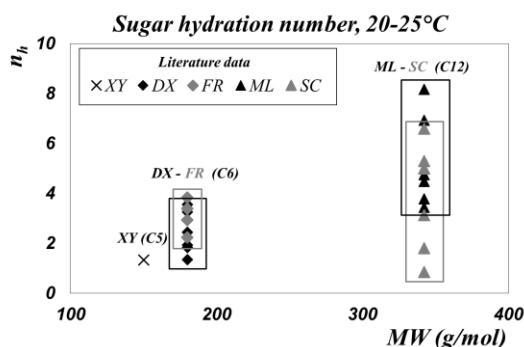


Figure 2.3: Literature data (from Tab.2.2) of sugar hydration number n_h as a function of molecular weight (MW). Temperature ranging from 20 to 25°C. Xylose (C5) 150.16 g/mol, Dextrose and Fructose (C6) 180.16 g/mol, Maltose and Sucrose (C12) 342.29 g/mol.

As illustrated in Tab 2.2 is not yet possible to set the hydration number values *a priori* for sugars to represent the hydration of these compounds in aqueous solution. From numerous literature data we can observe general trend of hydration number, n_h , as well as apparent molar volume, V_ϕ , as a function of temperature, concentration and salt in solution.

As can be seen in Fig. 2.4 *a-b*, n_h decreases with increasing temperature and solute concentration. A similar relationship between hydration number and temperature was also found by (Branca, Magazù, et al. 2001) for sucrose and maltose.

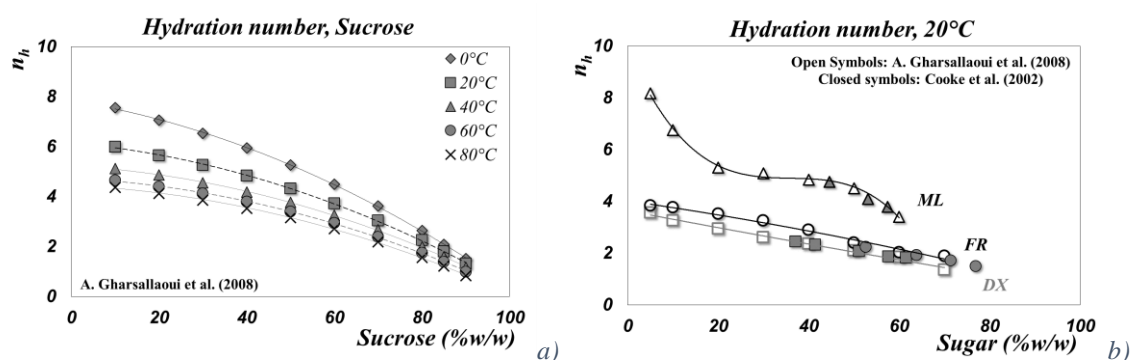


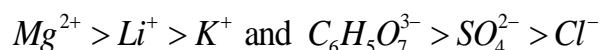
Figure 2.4:(a) Hydration number of sucrose solution at temperatures between 0 and 80°C and concentration between 10 and 90 %w/w (Gharsallaoui, et al. 2008); (b) Variation of hydration number of glucose fructose and maltose in function of mass concentration, at 20°C comparison between (Cooke, Jónsdóttir and Westh 2002) and (Gharsallaoui, et al. 2008) literature data.

However it is difficult to observe differences between the hydration phenomena of isomers (see Dextrose and Fructose), although it is possible to observe that D-fructose shows higher hydration than D-glucose at all concentrations and a better compatibility with water structure.

2.2.2 “Salting out” effect

Dehydration experimentally occurs when a salt is added to the solution. The salting out technique is well known in the field of protein separation where the protein hydrophilic

property is overridden by the introduction of a salt which causes the protein to precipitate. Similarly, the addition of salt to an aqueous organic solution can be used to enhance the extraction of organic compounds by reducing their solubility in water. The contribution of salting out, to the negative rejection of neutral solutes was studied by (Mandale and Jones 2010). Hofmeister firstly observed in his work on the influence of the nature of the background salt on the precipitation of hen-egg-white protein (Kunz, Henle and Ninham 2004):



Increasing in molar volume of sugars in salt solution can be interpreted as a dehydration of the sugars. The addition of the salt (NaCl or LiCl) to the water decreased the average molar volumes of the sugars (Seuvre and Mathlouthi 2010). The apparent size of neutral solutes, like carbohydrates, is expected to be influenced by the ionic composition. Indeed, it was established that glucose is less hydrated when NaCl is added to the solution (Zhuo, et al. 1998). Since this release of water makes the apparent size of the solute smaller, a lower retention can be expected.

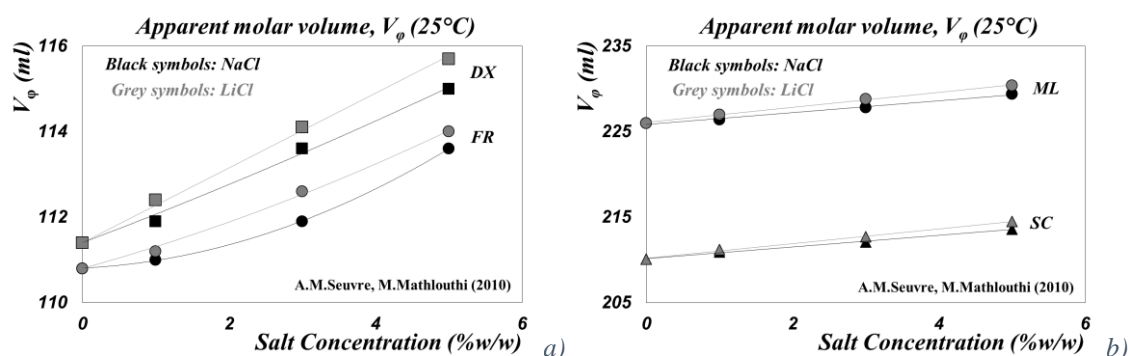


Figure 2.5: Apparent Molar volumes of carbohydrates in pure water and in salt aqueous solutions at 25 °C; (a) glucose and fructose, (b) maltose and sucrose (Seuvre and Mathlouthi 2010)

In conclusion, despite the attempts for study water-sugar interactions, it remains very difficult to accurately identify the number of water molecules that hydrate sugar molecules: thermodynamic methods give one value in the equilibrium state, whereas perturbation methods give numbers which depend on the magnitude of the perturbation (Ben Gaida, Dussap and Gros 2006).

2.2.3 Sweetness and sweetener

The sense of sweetness in a food product is the subjective evaluation of the interaction of sugars, total acidity, pH level, and other constituents when tasted under a given set of conditions.

An extensive amount of research has been directed about sweetener chemistry. Sucrose is the standard sweetener to which all other sweeteners are compared. The relative sweetness of sucrose is set to 1 or 100% (See Fig. 2.6)

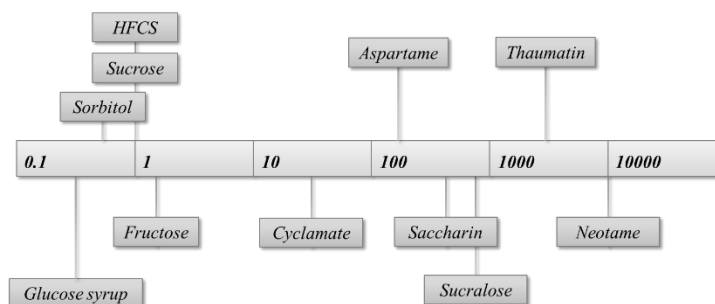


Figure 2.6: Approximate sweetness of selected sweeteners.

The only way to measure the sweetness of a substance is to taste it. When a substance is placed on the tongue, the taste buds decipher the chemical configuration of the substance and a signal of the taste is sent to the brain. A growing number of alternative sweeteners exist on the market all with somewhat different sweetness compared to sucrose, except for HFS. The literature offers figures for the sweetness of the various sweeteners but in most cases these figures are related to just one application.

It is necessary to know in what medium the product was tested because the sweetness of many sweeteners depends on concentration, pH, temperature and the use of other ingredients, for example other sweeteners or flavors. In some cases, psychological effects also influence the taste sensation: green jelly is perceived as less sweet than red jelly although they contain exactly the same amount of sweetener.

Figure 2.6 shows some of the sweeteners available today and their approximate level of sweetness. Sweeteners are divided into two main groups: bulk sweeteners, with a relative sweetness lower or slightly higher than sucrose, and high intensity sweeteners (HIS) with a relative sweetness considerably above 1.

Sucrose, glucose and fructose are the most common sweeteners in nature. Glucose is always less sweet than sucrose, whereas the sweetness of fructose is highly dependent on temperature. Fructose is sweeter than sucrose at low temperatures, whereas the sweetening effect decreases as the temperature rises (Shallenberger and Birch 1975).

Sweetness decreases as temperature, concentration, and acidity increase. The effect of temperature and concentration was established by (Tsuzuki and Yamasaki 1953).

2.2.4 Solubility

Solubility represent another peculiar feature of oligosaccharides. Solubility characteristics of sugars in water are determined by their molecular structure, as well as by their molecular size. Basically, temperature and the chemical interaction between a given component and the water molecule determine the component's solubility in water [(Pancoast and Junk 1980), (Bubnik, et al. 1995)].

The solubility of saccharide molecules is directly determined by the chemical structure, and the oligosaccharide solubility has a major impact on membrane separation (Pinelo, Jonsson and Meyer 2009).

The solubility of sucrose in water has been widely studied in literature. Dextrose has a lower solubility in water than sucrose. For example, at 30°C dextrose has a solubility of 54.6%, whereas at the same temperature the value for sucrose is 68.2%. This difference in solubility becomes important in the storage of dextrose solutions.

The relatively high solubility of sucrose is an important parameter for its bulking effect in many foods and beverages. The dissolved sugar increases the viscosity of water-based solutions or mixtures, resulting in enhanced mouth feel.

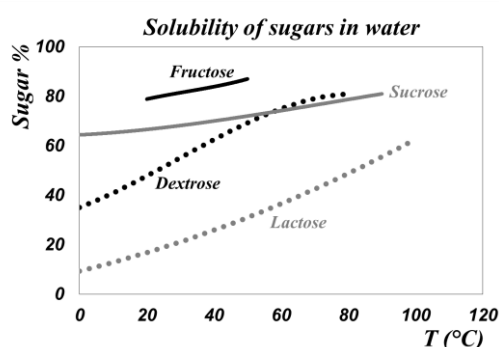


Figure 2.7: Solubility of selected sugars as a function of temperature, from (Pancoast and Junk 1980)

The solubility of sucrose is lower than fructose but higher than glucose, as shown in figure 2.7. The presence of other ingredients in the solution or product affects the solubility and the potential crystallization. Glucose syrups and invert sugar are typically used to avoid crystallization of sucrose, but other ingredients such as proteins, texturisers and stabilisers also influence crystallization process, for instance the solubility of dextrose limits the total solids for each type of *HFCS* when stored for a given temperature.

2.3 Sugar fractionation: state of the art

2.3.1 Conventional techniques: the isomer separation case

Glucose and fructose are the most applicable sugars in the food industry. Not to mention the importance of sucrose, fructose is the second important bulk sugar in food industry. It is a popular dietary sugar because it is 1.3-1.8 sweeter than sugar, depending on its anomeric form in aqueous solution, moreover, unlike dextrose, it does not require insulin in its metabolic pathway. Fructose is strongly soluble in water (79% w/w at 20°C), is more soluble than glucose in water, and is the sweetest natural sugar in the world and it is 30% sweeter than sucrose, while glucose has 70% of the sweetness of sucrose; not to mention that fructose can be produced from starch (substrate available in food material) at lower cost (Hanover and White 1993).

Nowadays fructose is produced by separation from the enzymatically isomerised mixture containing fructose and glucose from corn starch [(Zhang, Hidajat and Ray 2004), (Azavedo and Rodrigues 2001)]. The research and commercial production of high fructose corn syrup (*HFCS*) is the most important development that has occurred in the corn refining industry in the last years

The isomerized fructose corn syrup typically contains 42% fructose, 50% glucose and 8% oligosaccharides on a dry-weight basis; actually fructose is available on the market in the following types: high-fructose corn syrups with 42% fructose (*HFS42*), 55% (*HFS55*) and 85-90% (*HFS90*) of total sugars.

The basic difference among the various types of *HFCS* is the dextrose-fructose ratio. Table 2.3 summarizes the saccharide composition of a number of commercially available type of *HFCS*.

Table 2.3: Typical carbohydrate composition of commercially produced High Fructose Corn Syrup

	<i>HFCS42</i>	<i>HFCS55</i>	<i>HFCS60</i>	<i>HFCS90</i>
<i>Dextrose</i>	50-52	41	36	7
<i>Fructose</i>	42-43	55	60	90
<i>Other saccharides</i>	5-8	4	4	3

All of them are used extensively in the food and pharmaceutical industries. In order to produce high fructose corn syrup (*HFCS*) containing 90% fructose, the fructose should be removed continuously as the conversion rate decreases sharply from about 50% fructose.

The trend in the commercial production of *HFCS* is to increase the concentration of fructose with a corresponding decrease in dextrose concentration. There are two advantages in the higher fructose syrup:

- i)* the first is a gain in sweetness values, this allow the use of lower concentrations of the syrup to obtain sweetness values equal to those of syrups of lower fructose concentrations;
- ii)* the second advantage is the gain in total solids because of the higher solubility of fructose when compared with dextrose;
- iii)* lastly, high osmotic pressure: the average molecular weight is lower than in the other corn syrups, so that the osmotic pressure inhibits the growth of microorganism.

The method of producing *HFCS* consists essentially of an initial step of hydrolyzing the corn starch to obtain dextrose or solutions containing high concentrations of dextrose. In the second step, an isomerizing enzyme (glucose isomerase from a *Streptomyces sp.*) is used to convert part of the dextrose to fructose.

The conversion is equilibrium limited and with the current enzymatic isomerization technology, the conversion of glucose to fructose is economically limited to 42% fructose. Since soft drink industries require *HFS55* product, *SMB* separation is used to concentrate the fructose to 90%, which is blended with *HFS42* to produce *HFS55*. The same approach is used to produce *HFS60*, however the amount of fructose in *HFCS* is governed by the degree of isomerization of the *D-glucose* (Zhang, Hidajat and Ray 2004).

Because of the similarity of these two sugars in physical and chemical properties (fructose is glucose isomer), they are not separable by conventional methods. Glucose and fructose have very similar structures and are hard to isolate, and separation is rather complex on an industrial scale.

Complex separations of monosaccharides from each other are commercially carried out by chromatographic methods. The state of the art for industrial sugar purification (i.e. raffinose-sucrose, fructose-glucose and xylose-glucose) is Simulated Moving Bed (*SMB*) chromatography on a commercial scale (Vanneste, et al. 2011).

A wide literature production is available for chromatographic separation (Khosravanipour Mostafazadeh, et al. 2011), and many articles have been published about carbohydrate separation by *SMB*, as mentioned by (Azavedo and Rodrigues 2001).

Resin chromatographic method is a suitable method for the separation of fructose in sugar mixtures. The literature survey shows that there are many scientific researches on the separation of fructose and glucose by resin chromatography. In order to separate fructose from glucose, the following approaches have been studied in literature:

- Exploit the solubility differences between the two sugars by adding solvents such as ethanol or propanol;
- By adding salts (NaCl, CaCl₂) which preferentially complex one of these monosaccharides;
- By adding salts and solvents together;
- By Chromatography;
- By Ionic exchange membranes (Kalyanasundram Venkatasubramanian 1980);
- By Ionic liquid membranes (Di Luccio, et al. 2000).

Chromatographic systems for the separation of sugars are very impressive and feasible methods, moreover allow to reach very high purities (~95% in fructose).

In chromatography the mechanism and quality of separation depend on several parameters such as the characteristics of the mixture and resin, but the more influencing parameters in the separation of the two mentioned components in their mixtures are the size exclusion and the ligand exchange, in fact gel-type calcinate (Ca²⁺ form) resins make strong complexes with fructose rather than glucose. The fructose is absorbed by the calcinate resin stronger than glucose, and left the column later than glucose, thus a fructose rich fraction can be obtained. Affinity of calcium ions towards specific sugar molecules is also evident in some of the mechanisms of cellular recognition, for which glycoproteins have an important role, through the binding specificity of their oligosaccharide portions (Hosoi, Imai and Irimura 1998).

(Azavedo and Rodrigues 2001) separated glucose from fructose experimentally using a simulated moving bed (SMB) adsorber in a pilot unit. Some years later (Borges de Silva, et al. 2006) produced high-fructose syrup using a simulated moving bed reactor (SMBR) with immobilized enzyme glucose isomerase: in this study reaction and separation processes have been coupled to achieve complete reactant conversion, reaching a separation factor of 1.52 for resin in the form Ca²⁺.

However, such chromatographic separations are essentially batch processes and normally imply expensive installations, low productivity and low yields of the desired product; it is natural to look at new methods of separation.

Membrane technology has a number of advantages as compared to chromatographic purification techniques. These advantages include low energy requirements, hence sustainable processing, easy modification of the critical operational variables such as pressure, temperature, feed flow rate, and relatively easy scale-up.

The membrane separation of fructose and glucose has not been reported except some work, including (Kim, Chang and Ghim 1985).

(Aydogan, Gurka and Yilmaz 1998) stated that NF separations of sugars, with differences in their molecular size in the range of a few glucosyl units are not feasible due to poor selectivity. The possibility of separating through NF a pentose sugar (xylose) from a hexose sugar (dextrose) was documented by (Sjoman, et al. 2007), who reported a higher xylose separation factor when the proportion of xylose in the feed was increased.

The molar mass of a hexose sugar is only about 20% higher than the molar mass of a pentose sugar. The difference in molecular radius is smaller than a 10th of a nanometer, thus, the demand for selectivity is great. Separation of uncharged substances is mostly based on differences in molecular sizes and diffusivities. The possibility for a partial separation of disaccharides (maltose MW=342.3 g/mol) from monosaccharides (~150-180 g/mol) is documented in results of (Pontalier, Ismail and Ghoul 1997), (Goulas, Grandison and Rastall 2002), (Bandini and Nataloni 2015)]. (Morthensen, et al. 2015) proposed an integrated system for the separation of mixtures of xylose and glucose, presenting an enzymatic process for converting glucose to gluconic acid (MW 196.16 g/mol) followed by a nanofiltration, achieving a separation factor of 34, in comparison, the separation factor was only 1.4 for solutions of xylose and glucose.

However, except for these application chromatographic methods are still the basic technology for isomer separation.

2.3.2 Nanofiltration

A wide literature concern with Nanofiltration of oligosaccharide solutions and many authors have dealt with NF recovery/separation of sugars.

Table 2.4 shows a brief summary of the remarkable sugar NF studies documented in literature.

Table 2.4: Sugar Nanofiltration: State of the art. Membranes, configurations, test conditions and sugar tested

References	Membranes	Materials	Configuration	Application	Test Conditions
(Aydogan, Gurka and Yilmaz 1998)	BM5 Berghof (500 MWCO) BM2 Berghof (200 MWCO)	PA ⁴	Flat cell, A=0.0045 m ²	Glucose + sucrose	T=25°C P=10-50 bar
(Bargeman, et al. 2005)	Desal 5 DK (200 MWCO), 5DL (400 MWCO), G5 (1000 MWCO) NF (<200MWCO) (Dow Chemicals) NTR-7450 (1000 MWCO) (Nitto)	PA (top layer) on PS ⁵ PIP ⁶ (top-layer) on PS sulfonated PES	Flat cell, A=0.036 m ²	glucose , glycerin + NaCl, KCl, CaCl ₂	T=20°C P= 2 -30 bar v= 0.9 m/s
(Bouchoux, Roux-de Balmann and Lutin 2005)	DK (Desal)	PA/PS	Flat cell , A=0.014 m ²	glucose + Sodium Lactate	T=25°C P=2-20 bar
(Bouranene, et al. 2007)	Tami Industries	TiO ₂ (Ceramic)	Tubular, (L=604 m, A=0.022 m ²	PEG + KCl, LiCl, MgCl ₂	T=25°C P=5-60 bar
(Boy, Roux-de Balmann and Galier 2012)	Dow Filmtec NF membrane	TFC ⁷ (negative charged)	Flat cell, A=0.012 m ²	xylose, glucose, sucrose + NaCl, Na ₂ SO ₄ , CaCl ₂ , MgCl ₂	T=25°C
(Catarino, et al. 2008)	CA, CA77.5, CA80, CA82.5, CA85, CA87.5 (self made)	CA ⁸	Flat cell, A=0.00132 m ²	glucose, sucrose, lactose, raffinose, melezitose + CaCl ₂	T=25°C P=15 bar
(de Pinho, et al. 1988)	CA	CA	Flat cell, A=0.00141 m ²	Glucose (2000-75000 ppm)/ethanol (1/5 -1/2 of glucose)	T=23-26°C P=70 bar
(Escoda, et al. 2010)	Desal GH (GE Osmonics)	PA (top layer) supported on a polyester layer	Flat cell, A=0.014 m ²	PEG +	T=20°C P= 2-20 bar

⁴ Polyamide;⁵ Polysulfone;⁶ poly(piperazine)⁷ Thin Film Composite;⁸ Cellulose Acetate;

				KCl, LiCl, MgCl ₂ , K ₂ SO ₄	
(Kim, Chang and Ghim 1985)	CA10-60, CA10-90 (self made) PVA (self made)	CA Poly(vinyl alcohol)	n.2 Flat cell, A=0.00181 m ² ×2	Glucose + Fructose + NaCl or Na ₂ CO ₃ or NaHSO ₃ or CaCl ₂	room T, P=100 atm
(Kuhn, et al. 2010)	NP010, NP030 (Microdyn-Nadir) NF270 (Dow Filmtec) DL, HL, DK (Desal)	PES ⁹ - PA	stirred cell STERLITECH, A=0.00146 m ² flat cell, A=0.0066m ² spiral wound NP030, A=1.8 m ²	FOS + glucose + sucrose + fructose	P=18 bar
(Goulas, Grandison and Rastall 2002)	NF-CA-50, UF-CA-1 (Intersep) DS-5-DL, DS-51-HL, DS-GE (Desal)	CA TFC	n.2 flat cells, in parallel A=0.0081 m ²	galacto- oligosaccharides (raffinose, sucrose, fructose)	T= 25°C, P=13.8 bar T=60°C P=13.8 bar
(Mandale and Jones 2010)	XN45 (Trisep), LFC1 (Hydranautics), NF90, NF200 (Dow-Filmtec), DK (Gewater), NTR7450 (Nitto Denko)	-	Flat cell, A=0.0109 m ²	glycerol, benzyl alcohol, sodium benzoate, glucose, caffeine, raffinose + NaCl, Na ₂ SO ₄ , Na ₂ HPO ₄	P _{max} 7.5 bar, v = 0.5 m/s
(Manttari, Pihlajamaki and Kaipainem, et al. 2002)	5 DK, 5 DL, G10, 11AG, (Desal), TS-80, XN-40 (Trisep), NF2xx, NF200, NF70, NF45 (Dow), PVD-1 (Hydranautics), SR-1 (Koch), NTR-7540 (Nitto Denko), NF-PES- 10 (Celgard)	-	plate and frame DSS Labstak in serie	glucose	T=25- 65°C
(Manttari, Pihlajamaki and Nystrom 2006)	NTR 7450 (Nitto Denko) NF 200, NF 270 (Dow Deutschkand)	suphonated PES (skin layer) on PS PA (skin layer) on PS	n.3 flat sheet modules in parallel, A=0.046 m ²	Glucose + NaCl	T=40°C P=8 bar

⁹ Polyethersulfone

	OPMN-K, OPMN-P70 (Vladipor)	PA (skin layer) on PP ¹⁰ support			
	NF PES-10 (Nadir)	PES (skin layer)			
	5DL (Desal)	PA (skin layer) on PS			
(Mohammad, Basha and Leo 2010)	DK (Osmonic)	PA (skin layer) on PS	Flat cell , A=0.00152 m ²	glucose, sucrose, raffinose + NaCl, MgCl ₂ , Na ₂ SO ₄	T=25°C
	CK (Osmonic)	CA			
(Nilsson, Tragardh and Ostergren 2006)	NFT-50 (Alfa Laval)	active layer of aromatic/aliphatic PA	plate and frame DSS Labstak (A=0.036 m ²)	glucose + NaCl	T=20-30- 40-50 °C P=6 bar
(Rodrigues, et al. 2010)	NF90 , NF 200, NF 270 (Filmtec, Dow Chemicals)	PA TFC	plate and frame module, A=0.036 m ²	Glucose + sucrose + Na ₂ SO ₄	T=22°C P=10-60 bar
(Umpuch, et al. 2010)	Desal 5DK	PA (skin layer) on PS	Flat cell , A=0.0137 m ²	glucose, NaLac + NaCl or Na ₂ SO ₄	T=25°C P=2-18 bar
(Vellenga and Tragardh 1998)	DS-5 (Desalination System)	–	Flat cell, A=0.00188 m ²	Sucrose + NaCl	T=23.5°C P=8-21 bar
(Wang, Zhang and Ouyang 2002)	NF45	aromatic PA/PS	Flat cell , A=0.0035 m ²	glucose, glycerin, sucrose, raffinose + NaCl, KCl, MgCl ₂ , Na ₂ SO ₄ , MgSO ₄	T= 32°C P= 2.5-15 bar

Initial studies about sugar *NF* were performed mainly on cellulose acetate membranes (Kimura and Sourirajan 1968); (de Pinho, et al. 1988) investigated separation performance of such membranes with a binary mixture of glucose and ethanol, focusing on a reverse osmosis unit connected to a yeast cell reactor.

Many authors studied firstly sucrose-glucose systems: (Nabetani 1992) focused on the separation capacity of a binary solution containing glucose and sucrose at high concentration (5-25 wt.%), (Aydogan, Gurka and Yilmaz 1998) observed that for binary solutions of sucrose and glucose the separation factor slightly decreased, probably due to a glucose-sucrose interaction; results indicate that some glucose is retained together with

¹⁰ Polypropylene

sucrose, therefore glucose retentions are increased relative to single-component experiments. This reduction in selectivity was less significant at higher fluxes, when total rejection is reached for both solutes.

Some year later (Goulas, Grandison and Rastall 2002) studied the total sugar concentration effect on the retentions of single sugars with two membranes of different cut-off: the increase of total sugar concentration caused a decrease on the observed rejection of sugars and this effect was more intense as the molecular weight of sugar decreased and the membrane molecular weight cut-off increased.

All these studies showed that solutes in the solution may affect separation performances: interactions of these compounds with each other and with the membrane can modify the separation efficiency and should be investigated.

Sugars are very soluble in water: water molecules surround the sugar structure, the so-called hydration layer is not constant under varying operating conditions. The hydration number is a parameter calculated at infinite dilution, but it is affected by temperature, total solute concentration and presence of electrolyte in solution, therefore the variation of these parameters can alter separation performance, particularly when the mass transfer is mainly diffusive (predominantly).

The role of the hydration layer of carbohydrate in NF is not well studied. When the solute molecules can hydrate, the solute transport through the membrane will depend on hydration number (n_h), therefore, the hydrated molecules are subjected to more complex interactions with other solution components and the membrane. Interactions between solution components with each other and with the membrane depend on the hydration number of solutes (Slezak, Grzegorzczyn and Wasik 2004).

However, when the solute molecular weights are almost the same (for instance is the case of glucose -180.16 g/mol -and xylose -150.13 g/mol-) hydration could play an important role and emphasizing size differences (Sjoman, et al. 2007); on the contrary when sugars in solution have different molecular weight the size difference is playing a big role in retention, compared to hydration phenomena which are negligible.

Dehydration of neutral solute always occurs when neutral solute solutions are processed: the higher the concentration and the temperature, the lower the hydration of neutral solutes, in fact as concentration increases, sugar-sugar interactions become preponderant, these complexes are more stable in the solution, and n_h decreases [(Gharsallaoui, et al. 2008) , (Seuvre and Mathlouthi 2010), (Branca, Magazù, et al. 2001), (Banipal, Gautam, et al. 2006), (Banipal, Singh, et al. 2015), (Sjoman, et al. 2007)].

Therefore, when sugar mixtures are processed, at least three elementary types of molecular interactions take place in sugar solutions:

- i)* water-water;
- ii)* sugar-water; and
- iii)* sugar-sugar,

all resulting in the formation of intermolecular hydrogen bonds (Gharsallaoui, et al. 2008). The stability of these mechanisms is altered when a salt is added to the solution: the introduction of salts to the solution induces perturbations in the carbohydrate-water interactions: when an electrolyte is added to the solution it can: (*a*) create interaction sugar-electrolyte, (*b*) dehydrate the sugar.

For this reason sugar-electrolyte interaction are widely documented in literature, specially in sugar *NF* applications, where these phenomena compete with electrolyte-membrane interaction.

In the first case (*a*), if sugars form a selective complex with a salt the permeability of the sugar-salt complex will decrease accordingly, and this will increase separation. For sugar/electrolyte systems, interactions between the hydrophilic sites of the sugar (-OH) and the ions are possible, and depend on the number of -OH site of the sugar (Boy, Roux-de Balmann and Galier 2012). This type of interactions are exploited in chromatography in order to separate sugars: for instance fructose is known to form complexes with calcium ions, in the form Ca^{2+} , and glucose with NaCl, NaHSO₃, and Na₂CO₃. The mechanism of complexing is not yet well known; the ionic form of these salts such as Ca^{2+} , SO_3H^- , and CO_3^{2-} are used as the counterions in resin chromatography in separating sugars; the stability of these complexes is the basis for chromatographic separation of sugar.

In a binary solution of sugar-salt complexes formation is limited by the ratio between sugar and salt, operating next to an equimolar ratio in order to promote complexation; the higher the sugar concentration, the higher must be the concentration of the salt (Kim, Chang and Ghim 1985).

Studies of (de Pinho, et al. 1988) investigate the fractionation of low molecular weight saccharide-ethanol mixtures by CA membranes and the dependence on the presence of calcium chloride in solution. (Catarino, et al. 2008) obtained an increase in the fractionation of glucose and raffinose in the presence of calcium ions; the presence of calcium ions leads to an increase on the sugar retention, related to the formation and stability of sugar-calcium complexes with the membrane matrix. The same results are provided by (Ribeiro 2006) trough diffusivity measurements: sugars like sucrose, glucose and fructose play a role on

the behavior of the diffusion of calcium chloride in aqueous solutions, the decrease of CaCl_2 diffusion coefficients can be explained by aggregate formation of 1:1 between calcium ions and sugar

Contrarily to complexation, dehydration is a severe phenomenon when electrolyte is added to sugar solutions. (Bouchoux, Roux-de Balmann and Lutin 2005) proposed a correlation, only qualitative, between the hydration scale of ions and the increase of organic solute transfer through *NF* membranes; (Seuvre and Mathlouthi 2010) observed the most important perturbations in LiCl solutions compared to the NaCl ones: this behavior was attributed to the fact that LiCl is surrounded with more water molecules.

(Banipal, Gautam, et al. 2006) studied the effect of ammonium salts on the volumetric and viscometric behavior of D-glucose, D-fructose and sucrose, pointing out that alkylammonium ions ($-\text{R}-\text{NH}_3^+$: hydrophobic) induced structural effects different from that of hydrophilic ions. (Zhuo, et al. 1998) established that glucose is less hydrated when NaCl is added to the solution; in particular more hydrated salts in solution means less hydrated sugar in solution, and thus a lower size and a lower retention of the sugar is expected.

(Mandale and Jones 2010) proposed weak negative retention of neutral solutes in presence of phosphate ions can be due to the polarisability of the molecule leading to interactions with the negatively charged membranes.

Many authors (Boy, Roux-de Balmann and Galier 2012) studied the effect of electrolyte on neutral solute in combination with the effect on membrane: the presence of the electrolyte can change the mass transfer of a neutral specie, and this effect depends on nature and concentration of the electrolyte [(Bouchoux, Roux-de Balmann and Lutin 2005), (Bouranene, et al. 2007), (Umpuch, et al. 2010), (Escoda, et al. 2010)] but the electrolyte can introduce modifications of the membrane properties (“Pore swelling”).

Only (Boy, Roux-de Balmann and Galier 2012) concluded that the influence of the electrolyte is mainly due to the resulting change of the saccharide properties, since only weak influence was observed on the membrane properties.

The mass transfer of a neutral solute increases, and so the retention decreases, when (i) membrane pore radius increases; (ii) solute radius decreases; (iii) a combination of both phenomena. In other words, a lower retention when a salt is added to the solution can be ascribed to an increase of the pore radius, to a decrease of the solute hydrodynamic radius, or to a combination of both. On the other hand, an increase of solute retention is due to complex formation in solution.

(Escoda, et al. 2010) and (Bouranene, et al. 2007) dissociated both contributions: the pore swelling was evaluated with polymeric NF membranes, while the dehydration of a neutral solute has been studied through ceramic membranes

Such an effect of the presence of charged species on the retention of neutral ones was summarized by (Umpuch, et al. 2010) (see Tab. 2.5):

Table 2.5: Influence of salt on retention of neutral compound (Umpuch, et al. 2010)

Neutral Compound	Concentration Neutral Compound	Electrolyte	Electrolyte Concentration	NF membrane	Neutral solute Reduction *	Reference
Dextrose	1 mM	NaCl	0.01-0.1 M	NF 45 (Dow Chemical)	25%	(Wang, Zhang and Ouyang 2002)
Sucrose	0.6 mM				<8%	
Dextrose	0.01 M	NaCl	0.01-0.1 M	NF 45 (Dow Chemical)	15%	(Bargeman, et al. 2005)
	0.1 M	NaCl	0.5 and 1 M	Desal 5 DK (Osmonics)	20%	(Bouchoux, Roux-de Balmann and Lutin 2005)
		NaLac	0.5 M		75%	
Lactose in UF whey	0.1-0.15 M	Mineral salt in UF whey	0.05-0.10 M	Desal 5 DL(Osmonics)	<5%	(Cuartas-Uribe, et al. 2007)
Dextrose		NaCl	0.01-0.1 M	XN45 (Trisep)	Retention reduction (data not given);	(Mandale and Jones 2008)
		Na ₂ SO ₄	0.01-0.1 M		Negative retentions for	
		Na ₂ HPO ₄	0.01-0.1 M		Na ₂ HPO ₄ >0.03 M	
PEG (600 g/mol)	~3 mM	KCl	0.1-1 M	NF ceramic membrane	30% **	(Bouranene, et al. 2007)
		LiCl	0.1-1 M	Filtanium®	60% **	
		MgCl ₂	0.1-1 M	(Tami Industries)	70% **	

* The Retention reduction is calculated from $[(R(\text{without salt})-R(\text{with salt}))/R(\text{without salt})] \times 10$; ** only salting out effect for these data

Typically a lower sugar retention is observed when electrolyte is added to the solutions: an increase in salt concentration results in lowering the neutral solute retention and that this decrease depend on the nature of the added salt. (Umpuch, et al. 2010) studied the effect of NaCl and Na₂SO₄ on the sodium lactate/glucose separation by NF, and saw that the glucose retention remain constant when adding a completely retained anion, in this case Na₂SO₄, while decreases in presence of NaCl as NaCl concentration increases.

Retention of glucose decreases more with the addiction of sodium lactate than with that of sodium chloride, at the same concentration (Bouchoux, Roux-de Balmann and Lutin 2005), and reaches negative retentions in the presence of increased concentrations of Na₂HPO₄ (Mandale and Jones 2010).

(Bouchoux, Roux-de Balmann and Lutin 2005) explained the dehydration of neutral solute in presence of electrolyte; in mixed solution containing neutral solute and electrolyte, water preferentially solvate the ions compared to neutral solute, that it to say that neutral solute transfer increases in presence of ions in solution.

(Bargeman, et al. 2005) pointed out that, relating to the addiction of an inorganic salt (NaCl, KCl or CaCl₂) the lowest the salt retention the deep the influence on the glucose retention, moreover increasing NaCl concentrations decreased the retention of glucose

Other authors (Vellenga and Tragardh 1998) reported that the sugar retention by a thin film NF membrane was unaffected by the salt concentration, however the extremely high retention of sugar (sucrose in thus study) could hide a dependency: the effect of salt on sugar is not discernable when sugar rejections are very high (>99%) (Mandale and Jones 2008). (Wang, Zhang and Ouyang 2002) reported a slight fall in the sugar retention with sodium chloride concentration, and this effect was smaller for sucrose than for glucose.

In contrast to the sugar retention, (Vellenga and Tragardh 1998) observed that NaCl retention was dependent on the sugar concentration, probably due to viscosity effect.

The pH has a clear effect on the ion retentions of *NF* membranes, and it also affects reversibly the permeability and the neutral solute retention. (Manttari, Pihlajamaki and Nystrom 2006) saw that when the flux increases with the increase of pH the retention of uncharged molecules tends to decrease; in this case at high pH the membrane matrix would be in a more expanded state due to the greater intra-membrane electrostatic repulsion, therefore the membrane pore size is slightly larger causing lower retention of neutral glucose, excluding membranes stable in a wide pH range (e.g GE-DL shows a 2-11 pH range). For these authors decreasing glucose retention is not imputable to the salt, but only to the pH effect. According to (Sharma, Agrawal and Chellam 2003) increases in

temperature at the same time lead to a changes in the membrane structure, resulting in larger pore sizes which additionally contribute to reducing the solute retention.

In conclusion, a wide literature about sugar *NF* is available, and some conclusion can be drawn, typically:

- i)* small samples of polymeric membranes (such as Polyamide) have been study in small range of temperature and concentration;
- ii)* sugar-sugar interactions may occur at high concentrations, affecting separation factor, depending on the type of sugar mixture;
- iii)* sugar-electrolyte in solution are quite complex, depending on the type of salt added to the solution: a decrease in sugar retention is generally observed when a salt is added to the solution, and most of author attribute this behavior to membrane pore swelling instead of sugar dehydration.

Nowadays, since a lot of studies focused on particular applications, there is a lack of overview about sugar *NF*.

In view of such phenomena, the aim of this work is to provide a critical and general method to processing experimental data, in order to understand which kind of interactions take place when sugar solutions are processed, or which mainly affect membrane performances during *NF*.

References

- Akhumov, E.I. "Hydration of sucrose in solutions." *Zhurnal Fizicheskoi Khimii* 55 (1981): 1496–1499.
- Aydogan, N., T. Gurka, and L. Yilmaz. "Effect of operating parameters on the separation of sugars by nanofiltration." *Separation Science Technology* 33, no. 12 (1998): 1767-1785.
- Azavedo, D.C.S., and A.E. Rodrigues. "Fructose-glucose separation in a SMB pilot unit: modeling simulation design and operation." *AIChE Journal* 47 (2001): 2042-2051.
- Bandini, S., and L. Nataloni. "Nanofiltration for dextrose recovery from crystallization mother liquors: A feasibility study." *Separation and Purification Technology* 139 (2015): 53-62.
- Banipal, P.K., S. Gautam, S. Dua, and Banipal. "Effect of ammonium salts on the volumetric and viscometric behaviour of D(+)-glucose, D(-)-fructose and sucrose in aqueous solutions at 25°C." *Journal of Solution Chemistry* 35 (2006): 815-844.
- Banipal, P.K., V. Singh, N. Aggarwal, S. Tarlok, and Banipal. "Hydration behaviour of some mono-, di-, and tri-saccharides in aqueous sodium gluconate solutions at (288.15, 298.15, 308.15 and 318.15) K: volumetric and rheological approach." *Food Chemistry* 168 (2015): 142-150.

- Bargeman, G., J.M. Vollenbroek, J. Straatsma, and C.G.P.H. Schroen. "Nanofiltration of multicomponent feeds. Interactions between neutral and charged components and their effect on retention." *Journal of Membrane Science* 247 (2005): 11-20.
- Ben Gaida, L., C.G. Dussap, and J.B. Gros. "Variable hydration of small carbohydrates for predicting equilibrium properties in diluted and concentrated solutions." *Food Chemistry* 96 (2006): 387-401.
- Bhattacharyya, L., and Jeffrey S. Roherer. *Applications of ion chromatography for pharmaceutical and biological products*. 1. John Wiley & Sons, 2012.
- Borges de Silva, E.A., A.A. Ulson de Souza, S.G.U. de Souza, and A.E. Rodrigues. "Analysis of the high-fructose syrup production using reactive SMB technology." *Chemical Engineering Journal* 118 (2006): 167-181.
- Bouchoux, A., H Roux-de Balman, and F. Lutin. "Nanofiltration of glucose and sodium lactate solutions variations of retention between single- and mixed- solute solutions." *Journal of Membrane Science* 258 (2005): 123-132.
- Bouranene, S., A. Szymczyk, P. Fievet, and A. Vidonne. "Influence of inorganic electrolytes on the retention of polyethylenglycol by nanofiltration ceramic membranes." *Journal of Membrane Science* 290 (2007): 216-221.
- Boy, V., H. Roux-de Balman, and S. Galier. "Relationship between volumetric properties and mass transfer through NF membrane for saccharide/electrolyte systems." *Journal of Membrane Science* 390-391 (2012): 254-262.
- Branca, C., S. Magazù, G. Maisano, F. Migliardo, P. Migliardo, and G. Romeo. "a,a-Trehalose/Water solutions.5. Hydration and viscosity in dilute and semi dilute disaccharide solutions." *Journal of Physics Chemistry B*. 105 (2001): 10140-10145.
- Branca, C., S. Magazù, G. Maisano, F. Migliardo, P. Migliardo, and G. Romeo. "a,a-Trehalose/Water solutions.5. Hydration and viscosity in dilute and semi dilute disaccharide solutions." *Journal of Physics Chemistry B*. 105 (2001): 10140-10145.
- Bubnik, Z., P. Kadlec, D. Urban, and M. Bruhns. In *Sugar Technologist's Manual*, 175-176. Berlin: Verlag Bartens, 1995.
- Catarino, I., M. Minhalma, L. L. Beal, M. Mateus, and M.N. de Pinho. "Assessment of saccharide fractionation by ultrafiltration and nanofiltration." *Journal of Membrane Science* 312 (2008): 34-40.
- Cooke, S.A., S.O. Jónsdóttir, and P. Westh. "The vapour pressure of water as a function of solute concentration above aqueous solutions of fructose, sucrose, raffinose, erythritol, xylitol, and sorbitol." *Journal of Chemical Thermodynamics* 34 (2002): 1545-1555.
- Cuartas-Urbe, B., M.C. Vincent-Vela, S. Alvarez-Blanco, M.I. Alcaina-Miranda, and E. Soriano-Costa. "Nanofiltration of sweet whey and prediction of lactose retention as a function of permeate flux using the Kedem-Spiegler and Donnan Steric Partitioning models." *Separation and Purification Technology* 56 (2007): 38-46.
- de Pinho, M.N., T. Matsuura, T.D. Nguyen, and S. Sourirajan. "Reverse Osmosis separation of glucose-ethanol-water system by cellulose acetate membranes." *Chemical Engineering Comm.*, 1988: 113-123.

- Di Luccio, M., B.D. Smith, T. Kida, C.P. Borges, and T.L.M. Alves. "Separation of fructose from a mixture of sugars using supported liquid membranes." *Journal of Membrane Science* 174, no. 2 (2000): 217-224.
- Escoda, A., P. Fievet, S. Lakard, A. Szymczyk, and S. Deon. "Influence of salts on the rejection of polyethyleneglycol by a NF organic membrane: pore swelling and salting-out effects." *Journal of Membrane Science* 347 (2010): 174-182.
- Franks, F. "Properties of water in foods." In *Water and aqueous solutions: Recent advances*, by D. Simatos and J.L. Multon, 1-21. 1985.
- Galema, S.A., and H. Høiland. "Stereochemical aspects of hydration of carbohydrates in aqueous solutions. 3. Density and ultrasound measurements." *Journal of Physical Chemistry* 95 (1991): 5321-5326.
- Geankoplis, C.J., and P.R. Toliver. "Membrane separation processes." In *Transport Processes and Separation Process Principles*. Prentice Hall PTR, 2003.
- Gharsallaoui, A., B. Rogé, Jean Génotelle, and M. Mathlouthi. "Relationships between hydration number, water activity and density of aqueous sugar solutions." *Food Chemistry* 106 (2008): 1443-1453.
- Goulas, A., A.S. Grandison, and R. A. Rastall. "Fractionation of oligosaccharides by NF." *Journal of Membrane Science* 209 (2002): 321-335.
- Hanover, L.M., and J.S. White. "Manufacturing, composition, and applications of fructose." *Am. J. Clin. Nutr.* 58, no. 3 (1993): 724-732.
- Hosoi, T., Y. Imai, and T. Irimura. "Coordinated binding of sugar, calcium, and antibody to macrophage C-type lectin." *Glycobiology* 8 (1998): 791.
- Kalyanasundaram Venkatasubramanian, Surendar M. Jain, Anthony J. Giuffrida. Patent US4299677 A. 1980.
- Khosravanipour Mostafazadeh, A., M. Sarshar, Sh. Javadian, M.R. Zarefard, and Z. Amirifard Haghghi. "Separation of fructose and glucose from date syrup using resin chromatographic method: Experimental data and mathematical modeling." *Separation and Purification Technology* 79 (2011): 72-78.
- Kim, S.S., H.N. Chang, and Y.S. Ghim. "Separation of fructose and glucose by reverse osmosis." *Ind. Eng. Fundam.* 24 (1985): 409-412.
- Kimura, S., and S. Sourirajan. *Ind. Eng. Chem. Process Des. Dev.* 7 (1968): 539-547.
- Kuhn, R.C., F. Mauger Filho, L. Palacio, A. Hernandez, and P. Pradanos. "Mass transfer and transport during purification of fructo oligosaccharides by nanofiltration." *Journal of Membrane Science* 365 (2010): 356-365.
- Kunz, W., J. Henle, and B.W. Ninham. "Zur Lehre von der Wirkung der Salze (about the science of the effect of salts) Franza Hofmeister's historical papers." *Curr. Opin. Colloid. Interface Sci.* 9 (2004): 19-37.
- Mah, K.H., H.W. Yussof, N.A. Jalanni, M.N.A. Seman, and N. Zainol. "Separation of xylose from glucose using thin film composite (TFC) nanofiltration membrane: effect of pressure, total sugar concentration and xylose/glucose ratio." *J. Teknol.* 1 (2014): 93-98.
- Mandale, S., and M. Jones. "Interactions of electrolytes and non-electrolytes in NF." *Desalination* 219 (2008): 262-271.
- Mandale, S., and M. Jones. "Membrane transport theory and the interactions between electrolytes and non electrolytes." *Desalination* 252 (2010): 17-26.

- Manttari, M., A. Pihlajamaki, and M. Nystrom. "Effect of pH on hydrophilicity and charge and their effect on the filtration efficiency of NF membranes at different pH." *Journal of Membrane Science* 280 (2006): 311-320.
- Manttari, M., A. Pihlajamaki, E. Kaipainem, and M. Nystrom. "Effect of temperature and membrane pretreatment by pressure on the filtration properties of nanofiltration membranes." *Desalination* 145 (2002): 81.
- Mathlouti, M., and J. Génétolle. "Sucrose, Blackie Academic and Professional." By M. Mathlouti, 127–154. P. Reiser (Eds.), 1994.
- McGee, Harold. *On food and cooking: the science and lore of the kitchen*. 1984.
- Mohammad, A.W., R.K. Basha, and C.P. Leo. "Nanofiltration of glucose solution containing salts: effects of membrane characteristics, organic component and salt on retention." *Journal of Food Engineering* 97 (2010): 510-518.
- Moreno-Vilet, L., et al. "Sugars and fructans separation by nanofiltration from model sugar solution and comparative study with natural agave juice." *Separation Science and Technology* 48 (2013): 1768-1776.
- Morthensen, Sofie T., J. Luo, Anne S. Meyer, H. Jørgensen, and M. Pinelo. "High performance separation of xylose and glucose by enzyme assisted nanofiltration." *Journal of Membrane Science* 492 (2015): 107-115.
- Nabetani, H. "Prediction of the flux for reverse osmosis of a solution containing sucrose and glucose." *Journal of Chemical Engineering Jpn.* 25 (1992): 575.
- Nilsson, M., Gun Tragardh, and K. Ostergren. "The influence of sodium chloride on mass transfer in a polyamide nanofiltration membrane at elevated temperatures." *Journal of Membrane Science* 280 (2006): 928-936.
- P.M. Olinger, T. Pepper. "Xylitol." In *Alternative Sweeteners*, by T. Pepper P.M. Olinger, 335-365. New York: L. O'Brien Nabors, 2001.
- Pancoast, H.M., and W.R. Junk. *Handbook of sugars*. 2nd. AVI Publishing Company Inc., 1980.
- Pinelo, M., G. Jonsson, and A.S. Meyer. "Membrane Technology for purification of enzymatically produced oligosaccharides: Molecular and operational features affecting performance." *Separation and Purification Technology* 70 (2009): 1-11.
- Pontalier, P.-Y., A. Ismail, and M. Ghoul. "Mechanism for the selective rejection of solutes in nanofiltration membranes." *Separation and Purification Technology* 12 (1997): 175-181.
- Ribeiro, Ana C.F. "Binary mutual diffusion coefficients of aqueous solutions of sucrose, lactose, glucose and fructose." *Journal of Chemical Engineer Data* 51, no. 5 (2006): 1836-1840.
- Rodrigues, C., A.I. Cavaco Morao, M.N. de Pinho, and V. Geraldes. "On the prediction of permeate flux for nanofiltration of concentrated aqueous solutions with thin-film composite polyamide membranes." *Journal of Membrane Science* 346 (2010): 1-7.
- Seuvre, A. M., and M. Mathlouthi. "Solution properties and solute-solvent interactions in ternary sugar-salt-water solutions." *Food Chemistry* 122 (2010): 455-461.
- Shallenberger. *Taste Chemistry*. Springer Science & Business, 1993.
- Shallenberger, R.S., and G.G. Birch. *Sugar Chemistry*. Westport: AVI Publishing Co., 1975.

- Sharma, R.R., R. Agrawal, and S. Chellam. "Temperature effects on sieving characteristics of thin-film composite nanofiltration membranes: pore size distributions and transport parameters." *Journal of Membrane Science* 223 (2003): 69-87.
- Shibusawa, T., and Sen'i Gakkaishi. 43, no. 8 (1987): 401-415.
- Sjoman, E., M. Manttari, M. Nystrom, H. Koivikko, and H. Heikkila. "Separation of xylose from glucose by nanofiltration from concentrated monosaccharide solutions." *Journal of Membrane Science* 292 (2007): 106-115.
- Slezak, A., S. Grzegorzyn, and J. Wasik. "Model Equations for interactions of hydrated species in transmembrane transport." *Desalination* 163 (2004): 177-192.
- Taylor, and Francis. *CRC HandBook of Chemistry and Physics*. D.R. Lide, 2006.
- Tsuzuki, Y., and J. Yamasaki. "On the sweetness of fructose and some other sugars, especially its variation with temperature." *Bioche.* 323 (1953): 525-531.
- Umpuch, C., S. Galier, S. Kanchanatawee, and H. Roux de Balmann. "Nanofiltration as a purification step in production process of organic acids: selectivity improvement by addition of an inorganic salt." 2010: 1763-1768.
- Van der Linden, T. "Solubility of sucrose and invert sugar." *Arch. Suikerind.*, 1919: 591.
- Vanneste, Johan, Stijn De Ron, Steven Vandecruys, Sandra Adina Soare, Siavash Darvishmanesh, and Bart Van der Bruggen. "Techno-economic evaluation of membrane cascades relative to simulated moving bed chromatography for the purification of mono- and oligosaccharides." *Separation and purification technology* 80 (2011): 600-609.
- Vellenga, E., and G. Tragardh. "Nanofiltration of combined salt and sugar solutions: coupling between retentions." *Desalination* 120 (1998): 211.
- Wang, Xiao-Ling, C. Zhang, and P. Ouyang. "The possibility of separating saccharides from a NaCl solution by using NF in diafiltration mode." *Journal of Membrane Science* 204 (2002): 271-281.
- Zhang, Y., K. Hidajat, and A.K. Ray. "Optimal design and operation of SMB bioreactor: production of high fructose syrup by isomerization of glucose." *Biochem. Eng. J.* 21 (2004): 111-121.
- Zhuo, K., J. Wang, Y. Cao, and J. Lu. "Thermodynamics of the interaction of HCl with D-Fructose in water at 298.15-318.15 K." *J. Phys. Chem. B* 102 (1998): 3574-3577.

3. Separation of oligosaccharide mixtures in Nanofiltration: Experimental study

3.0 Introduction.....	61
3.1 Hydraulic permeability	62
3.2 Experimental data as it is	66
3.2.1 Single solutes	66
3.2.2 Mixtures (Temperature and Electrolyte effect).....	70
3.2.3 Isomers Separation (T, pH and Electrolyte effect on separation).....	74
3.3 Intrinsic membrane performances.....	77
3.3.1 Single solutes	78
3.3.2 Mixtures	82
3.4 Discussions and Conclusions	84
References.....	85

List of symbols

<i>Symbol</i>	<i>Units</i>	<i>Quantity</i>			
$L_{p,w}$	[dm ³ /(hm ² bar)]	hydraulic permeability	S_{factor}	-	separation factor
L_{p0}	[dm ³ /(hm ² bar)]	hydraulic Permeability, in Arrhenius type law	k_L	[m/s]	mass transfer coefficient
L_p	[dm ³ /(hm ² bar)]	membrane Permeability	k_L^0	[m/s]	mass transfer coefficient in the bulk phase
E_a	[J/mol]	activation energy	Sh	-	Sherwood number
R	[J/(mol K)]	Universal Gas constant (8.314 J/(mol K))	Re	-	Reynolds number
T	[K]	temperature	Sc	-	Schmidt number
η	[Pa/s]	dynamic viscosity	R_c	[m]	radial flow test cell radius
c	[g/dm ³]	concentration	b	[m]	radial flow test cell height
P	[bar]	pressure	<i>Subscript</i>		
π	[bar]	osmotic pressure	w	water	
ΔP	[bar]	trans membrane pressure	i, j	solutes/components	
ΔP_{eff}	[bar]	effective driving force	$bulk$	bulk side	
$\Delta\pi_{real}$	[bar]	osmotic pressure difference	I	feed/membrane interface	
R_{obs}	-	observed rejection	F	feed	
R_{real}	-	real rejection	P	permeate	
R_{real}^{∞}	-	asymptotic real rejection	R	retentate	
σ_v	-	Staverman reflection coefficient	exp	experimental data	
Q	[dm ³ /h]	flow rate	DX	dextrose (glucose)	
J_v	[dm ³ /(hm ²)]	permeate flux	FR	fructose (levulose)	
A	[m ²]	membrane area	XY	xylose	
Δ	-	difference	ML	maltose	

3.0 Introduction

Nanofiltration appears to be a potential industrial scale method for purification and concentration of oligosaccharide mixtures. The potential of NF to fractionate oligosaccharide mixtures has been widely evaluated and documented in literature (*Chapter 2*), as an alternative to more expensive chromatographic techniques.

However, from literature overview some critical drawbacks have been put in evidence: typically sugar mixtures are investigated at low concentration ranges and temperatures (conditions far from industrial applications), and above all a lack of systematic investigation prevents to understand main aspects affecting sugar NF.

The aim of the work is to investigate the role of operating parameters (temperature, pH, composition) on membrane performance, as well as interactions between sugars in multicomponent mixtures and electrolyte effect on sugar (mass-transfer) properties, in order to achieve the best separation performances.

In this section separation performance of commercial Nanofiltration membranes are investigated in a wide range of test conditions: model solutions containing single and mixed solutes (such as xylose, dextrose, fructose and maltose) were mixed in demineralized water (conductivity $< 10 \mu\text{Scm}^{-1}$, pH 5.6) from pure crystalline substances. Experimentation was performed with total concentration for single solute model solutions ranging from 5 to 300 g/dm³. Tests were carried out from 30° to 50°C, the pH was adjusted to 4 and 6 with concentrated drops of HCl and NaOH. The filtration pressures used were from 4 to 30 bar, depending on membrane and module type. Electrolyte effect was study both on single oligosaccharide and on mixture of oligosaccharide too: NaCl, CaCl₂ and Na₂SO₄ were added to neutral solute solutions at different salt concentrations (ranging from the lower to the higher concentrations).

All experiments were performed in a bench-scale plant, with small flat membranes housed in radial flow cell ($39.6 \times 10^{-4} \text{ m}^2$ membrane area) or small commercial spiral wound modules (0.32 m^2 membrane area), in total recirculation mode of retentate (*R*) and permeate (*P*). Commercial thin-film composite membranes were tested, in particular GE-DL and GE-DK Nanofiltration membranes, and GE-AG GE-AK “Brackish water” membranes. *NF* membranes and filtration apparatus are described in detail in *Appendix A: Materials & Methods*.

In the following sections a critical summary of the experimental investigation is reported. All the results obtained, performed with both module configurations, have been organized in three main sections:

- 1) Hydraulic permeability (*Section 3.2*);
- 2) Experimental investigation as it is (*Section 3.3*);
- 3) Intrinsic membrane performances (*Section 3.4*).

Firstly hydraulic permeability of the membranes and their dependence on temperature is documented.

In *Section 3.3* data are reported in terms of observed rejection (R_{obs}) and Separation factor ($S_{factor,obs}$) as a function of experimental permeate flux ($J_{v,exp}$).

In *Section 3.4* data are reported as intrinsic rejection (R_{real}) and Separation factor ($S_{factor,real}$) as a function of experimental permeate flux, according to the data reduction procedure tabled.

This pathway gives an overview about operating conditions that greatly affect separation performances.

3.1 Hydraulic permeability

Hydraulic permeability ($L_{p,w}$) of all the membrane used (see *Appendix A*) is calculated by water flux measurements (with demi water) according to Eq. 3.1:

$$J_v = L_{p,w} \Delta P \quad (3.1)$$

In which J_v and ΔP stand for permeate flux and pressure difference across the membrane respectively.

Water fluxes were performed at three different operating temperatures, 30°, 40° and 50°C, in a pressure inlet range varying from 3 to 30 bar for flat sheet membranes, and from 4 to 25 bar for spiral wound modules. Flow rate and feed pH are set at 400 dm³/h and 4 respectively.

The hydraulic permeability of “virgin membranes” is used as a comparison in order to monitor the state of the membranes and to perform washing procedure (*Appendix A*).

Hydraulic permeability are collected in Table 3.1 for all the membrane tested.

Table 3.1: Hydraulic Permeability, $L_{p,w}(T)$. Permeability was measured at 30°, 40° and 50°C, pH 4 (conductivity < 10 μScm^{-1}), 400 dm^3/h (values shown as average \pm standard deviation)

Membrane	Configuration	$L_{p,w}(30^\circ\text{C})$ ($\text{dm}^3/(\text{hm}^2\text{bar})$)	$L_{p,w}(40^\circ\text{C})$ ($\text{dm}^3/(\text{hm}^2\text{bar})$)	$L_{p,w}(50^\circ\text{C})$ ($\text{dm}^3/(\text{hm}^2\text{bar})$)
GE-DL	flat sheet	10.7 \pm 0.1	13.3	15.2 \pm 0.9
	Spiral Wound	7.8 \pm 0.4	9.2 \pm 0.8	10.7 \pm 0.9
GE-DK	flat sheet	6.9 \pm 0.6	–	10.3 \pm 0.8
	Spiral Wound	8.8 \pm 0.8	11.2 \pm 0.9	12.7 \pm 0.4
GE-AG	flat sheet	2.5	–	3.29
GE-AK	flat sheet	3.7	–	5.63

The data obtained are comparable with most of data found in literature for membranes of the same kind (Tab. 3.2).

Table 3.2: Hydraulic Permeability, experimental data from Literature, Desal GE-DK and GE-DL membranes

Test Condition	$L_{p,w}(GE-DL)$ ($\text{dm}^3/(\text{hm}^2\text{bar})$)	$L_{p,w}(GE-DK)$ ($\text{dm}^3/(\text{hm}^2\text{bar})$)	Ref.
25°C	7.56 *	5.4*	(Bowen and Mohammad 1998)
20°C, 5-40 bar, flat sheet, A=0.036 m ²	-	4.7	(Straatsma, et al. 2002)
20°C, P _{in} = 2-40 bar, plate & frame A=0.036 m ²	5.76	5.4	(Bargeman, Vollenbroek, et al. 2005)
25°C	7.6*	–	(Manttari, Pihlajamaki and Nystrom 2006)
45°C, P _{in} 10 and 20 bar, plate and frame A=0.18 m ² (used cleaned membrane)	7.6 \pm 0.5	6.4 \pm 0.94	(Sjoman, et al. 2007)
20°C, Spiral Wound 2540, A=2.51 m ²	3.96	–	(Cuartas-Uribe, et al. 2007)
15°C, P _{in} =6-40 bar, plate and frame A=0.072 m ²	–	3.49	(Cavaco Morao, et al. 2008)

25°C, P _{in} 4-20 bar, cross flow A=0.0137m ²	–	5.0±0.25	(Umpuch, et al. 2010)
25°C, dead-end stirred cell, A=0.00146 m ²	7.6*	5.4*	(Kuhn, et al. 2010)
25°C, dead-end stirred cell, A=0.00152 m ²	–	3.05	(Mohammad, Basha and Leo 2010)
25°C, P _{in} 2-20 bar, flat sheet membranes, A=0.014 m ²	–	7.5	(Escoda, Déon and Fievet 2011)
25°C	6.0*	5.1*	(Bandini and Nataloni 2015)

* from technical sheet

Since hydraulic permeability increases with temperature according to an Arrhenius type law:

$$L_{p,w} = L_{p0} \exp\left(-\frac{E_a}{RT}\right) \quad (3.2)$$

Where L_{p0} and E_a show the meaning of a frequency factor and activation energy respectively (Tab. 3.3).

Table 3.3: Arrhenius type law describing the dependency of hydraulic permeability from temperature (Eq. 3.2)

	GE-DK		GE-DL		GE-AG	GE-AK
	Flat sheet	SW1812	Flat sheet	SW1812	Flat sheet	Flat sheet
L_{p0} (dm ³ /(hm ² bar))	8.27	8.46	8.66	8.38	7.11	7.64
E_a (J/mol)	229.93					

Validation of Eq. (3.2) can be observed in Fig. 3.1, in which a comparison among experimental data from this work and data from literature, including data sheets values, are reported.

Hydraulic permeability data have been elaborated as a function of temperature in order to underline the dependence on viscosity, according to the equation:

$$L_{p,w}(T)\eta_w(T) = L_{p,w}(T^0)\eta_w(T^0) \quad (3.3)$$

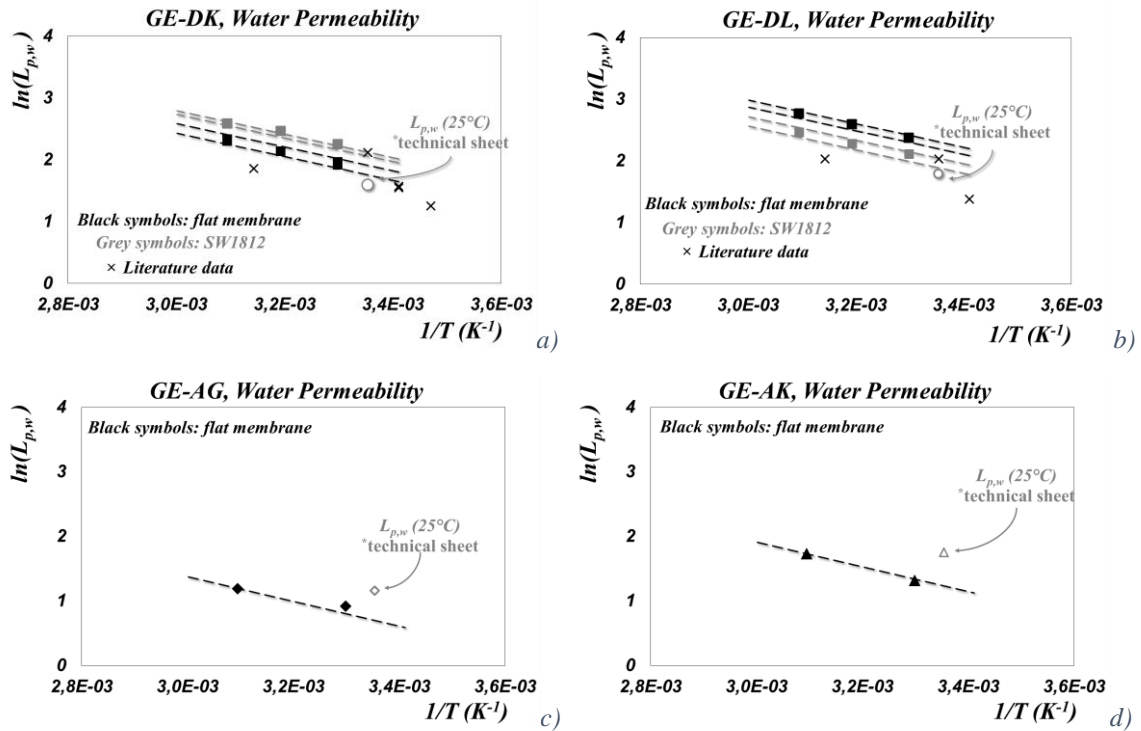


Figure 3.1 Arrhenius plot. Hydraulic Permeability as a function of temperature for both module configurations: flat sheet (black symbols and lines) and spiral wound (grey symbols and lines). Comparison between data from this work (closed symbols), data from literature (\times symbols) and prediction according to Eq. 3.3 (lines) for GE-DK (a), GE-DL (b), GE-AG (c) and GE-AK (d) membranes.

Many authors documented hydraulic permeability from technical sheet [(Bowen and Mohammad 1998), (Manttari, Pihlajamaki and Nystrom 2006), (Kuhn, et al. 2010), (Bandini and Nataloni 2015)], however datasheet reduction gives only $L_{p,w}(T)$ values approximately, as shown in Fig. 3.1 a-d.

The dispersion of experimental data compared to literature data is probably due to the diversity of membrane configuration or to the different procedures as well as pressure for membrane stabilization, as suggested by (Mohammad, Basha and Leo 2010).

On the contrary, deviations between experimental data and prediction (according to Eq. (3.3)) are less than 6.5% and 7.6% for GE-DK and GE-DL membranes respectively.

These results put in evidence that one experimental permeability data is necessary in order to predict membrane performance in a wide range of operating temperature, applying Eq. (3.3).

Finally, it can be observed a very good reproducibility of the results documented by a wide number of samples.

3.2 Experimental data as it is

A report is given of the results obtained in all the experiments performed first with the radial flow test cell and then with the “lab-scale” spiral wound module, in total recirculation mode of retentate and permeate (details are reported in *Appendix A*).

Temperature, pH, composition as well as concentration effects were tested, in a wide range of operative conditions.

Notation used in this section is explained in the list of symbols.

For clarity sake, definition of observed Rejection is reminded, referred to a general solute i :

$$R_{obs,i} = 1 - \frac{c_{P,i}}{c_{bulk,i}} \quad (3.4)$$

In which $c_{P,i}$ and $c_{bulk,i}$ are the concentration of the solute i in the permeate and in the feed side, respectively.

In addition, with regards to mixtures, separation factor was defined as:

$$S_{factor,i-j} = \frac{c_{P,i}/c_{P,j}}{c_{F,i}/c_{F,j}} = \frac{1-R_{obs,i}}{1-R_{obs,j}} \quad (3.5)$$

This factor indicates the change in the permeate composition compared to the original ration of i to j in the feed.

3.2.1 Single solutes

Experiments were carried out using model solution of approximately 5-300 g/dm³ of one sugar in aqueous solution. Xylose, Dextrose, Fructose and Maltose were tested at pressures and temperatures ranging from 4 to 30 bar and from 30 to 50°C respectively. Results are reported in Figures 3.2 to 3.4

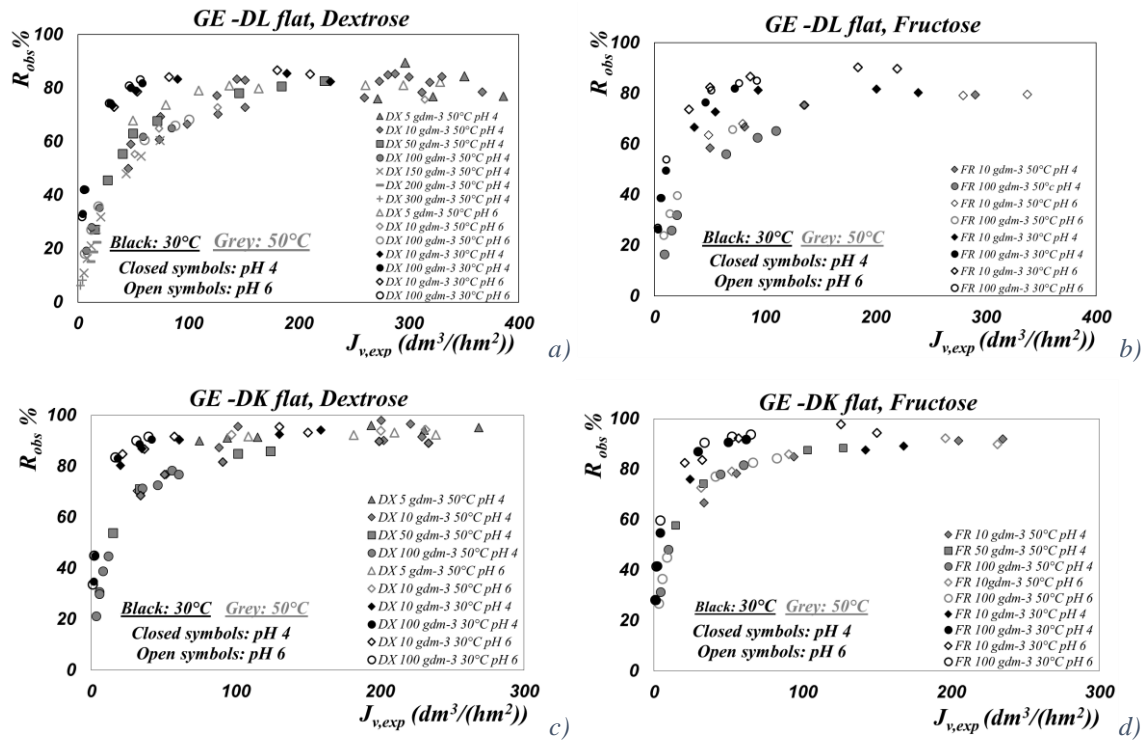


Figure 3.2: Observed Rejection vs. Experimental Permeate flux, radial flow test cell, GE-DL and GE-DK, dextrose (a,c), fructose (b,d), model solutions, 30° and 50°C, pH 4 6, flow rate 400 dm³/h, total recirculation of R and P

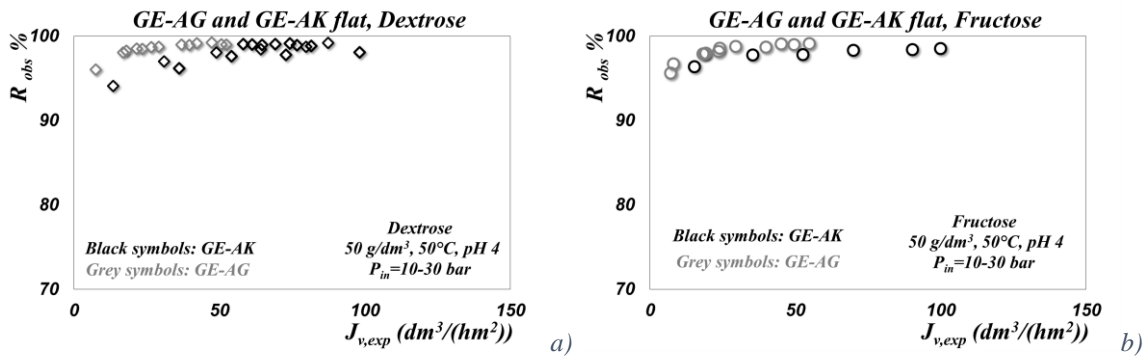


Figure 3.3: Observed Rejection vs. Experimental Permeate flux, radial flow test cell, GE-AG and GE-AK, dextrose (a) and fructose (b), model solutions, 50°C, pH 4, flow rate 400 dm³/h, total recirculation of R and P

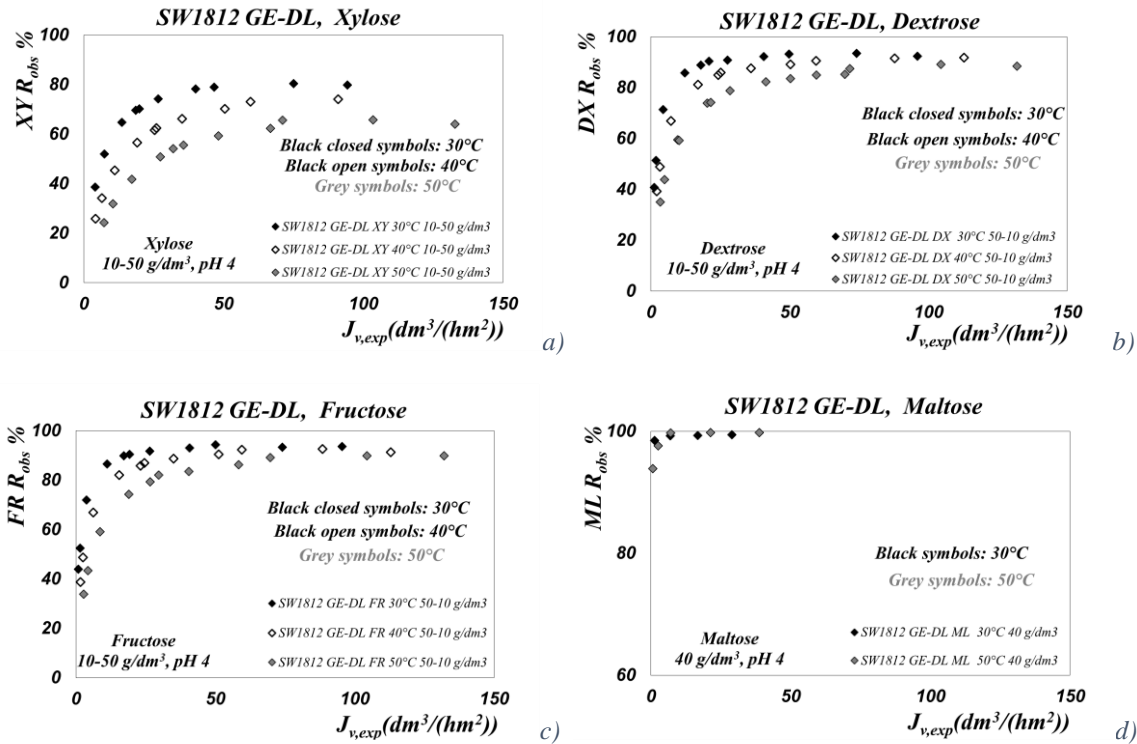


Figure 3.4: SW1812 GE-DL Module. Observed Rejection (R_{obs}) as a function of experimental permeate flux ($J_{v,exp}$), Xylose (a), Dextrose (c), Fructose (d) and Maltose (e). NF of model solution of dextrose (10 and 50 g/dm³), fructose (10 and 50 g/dm³), xylose (10 and 50 g/dm³) and maltose (40 g/dm³), in total recirculation mode of R and P, 30°, 40° and 50°C, pH 4, Q_F 400 dm³/h, inlet pressure ranging from 4 to 20 bar.

The results show similar trends: experimental curves of observed rejection range from the lowest to the highest fluxes, with high reproducibility.

Oligosaccharide retentions obtained for Desal GE-DK, GE-AG and GE-AK are significantly higher than those for GE-DL, and these results are in agreement with information from membrane technical sheet. From permeate fluxes higher than 300 dm³/(hm²) monosaccharide retentions started to decrease with increasing flux. This behavior indicates that concentration polarization clearly affected GE-DK and GE-DL membranes, particularly at higher permeate fluxes. Concentration polarization will be taken into account in the next section.

For all membrane tested, increasing temperature caused the sugar rejections to decrease, but the effect is quite different for each compound. The monosaccharides, first of all xylose (C5), followed by dextrose and fructose (both C6), showed the greatest change in rejection values, followed by maltose (C12), which totally rejected with GE-DK and GE-DL membranes at permeate fluxes higher than 100 dm³/(hm²).

The observed retentions are stable above fluxes of 200 dm³/hm² for both membranes in the case of monosaccharides. Glucose and fructose have the same retentions, which are strongly affected by sieving effect.

The rejections of the sugar decrease as the total sugar concentration of the solution increases. Viscosity and osmotic pressure are very strong for these solutions, not to mention concentration polarization, which is a sever phenomenon particularly for GE-DL and DK membranes.

When a sugar is completely rejected, such as maltose, depending on the ratio solute to pore size, temperature effect on rejection became negligible, and rejection reaches asymptotic values since the lowest fluxes. This is confirmed by dextrose and fructose with GE-AG and GE-AK membranes (Fig. 3.3 *a, b*).

Besides the different configuration, the same trend was observed when experimentation was performed on lab-scale spiral wound modules.

As a matter of fact temperature is a critical factor affecting *NF* separation. A stepwise increase in temperature from 30° to 50°C was reported to decrease retentions, however maximum deviation with temperature is in the low flux range that it should corrensponf to the diffusive transport zone (as documented in Fig. 3.5 *a, b*)

By comparison of Fig. 3.4 it was also found that the effect of temperature on rejection is negligible for maltose, compared to dextrose or fructose, and xylose. We expect that molecular size of maltose is much contiguous to the pore radius of GE-DL and GE-DK membranes, compared to xylose.

In order to quantify the temperature effect on rejection from 30° to 50°C, the following difference has been introduced, once fixed permeate flux:

$$\Delta R_{obs,30^{\circ}-50^{\circ}C,\bar{J}_v} = \frac{R_{obs,30^{\circ}C,\bar{J}_v} - R_{obs,50^{\circ}C,\bar{J}_v}}{R_{obs,50^{\circ}C,\bar{J}_v}} \quad (3.6)$$

Results are shown graphically in Fig. 3.5 *a* and *b*. Temperature effect depends both on:

- (i) Mass transport zone (diffusive vs. convective);
- (ii) Solute to pore size ratio.

In particular the lower the fluxes (i.e. transport is mainly diffusive), the higher the difference in retention, in particular for monosaccharides.

This behavior is intrinsic of the type of membrane and solutes, while is independent from module geometry, confirming the dependence from solute.

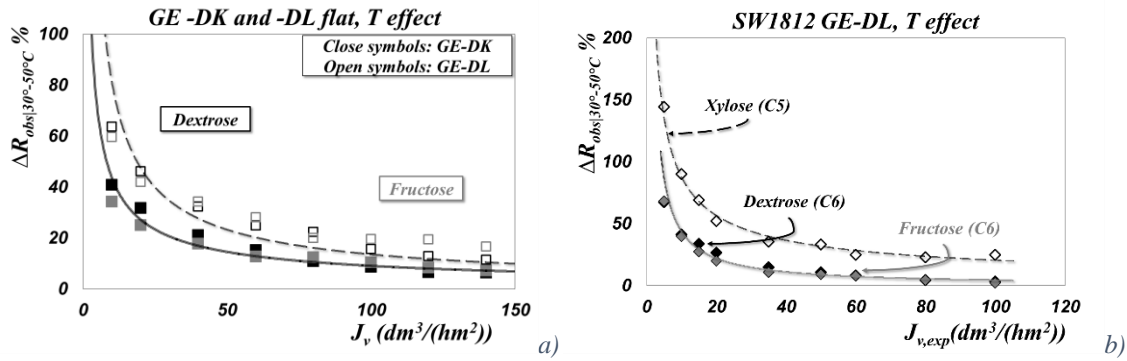


Figure 3.5: Temperature effect on difference in rejections for Xylose, dextrose and fructose as a function of permeate flux. GE-DK and GE-DL flat membranes (a), and GE-DL SW1812 membrane (b). Difference in observed rejection defined according to Eq. (3.6).

Increased temperature caused the sugar rejections to decrease, but the effect is quite different for the sugars in the model solutions. The monosaccharides, xylose in particular, showed the greatest change in rejection values, followed by fructose and dextrose. The rejection of maltose, which is totally rejected, remained constant.

These results are in agreement with the results reported from (Goulas, Grandison and Rastall 2002) and (Tsuru, et al. 2000) with regard to the effect of temperature on the transport performances of organic and inorganic membranes respectively. (Pontalier, Ismail and Ghoul 1997) reported that diffusive transport of sugars depends on the concentration gradient and remains pressure independent, whereas convective transport increases with pressure. This behavior is observed in particular for GE-DK and GE-DL membranes, for which monosaccharide rejection ranges widely from 5% to 90% approximately, and highlights the importance of temperature in sugar NF.

3.2.2 Mixtures (Temperature and Electrolyte effect)

In this section (i) sugar-electrolyte, and (ii) sugar-sugar interactions have been investigated in a wide range of composition.

Literature widely documented electrolyte effect on neutral solutes, already. Typically low concentration have been studied. Electrolyte effect was firstly studied on dextrose retention, at very low Sodium Chloride concentrations (ranging from 0.5 to 1.1 g/dm^3) at 50°C.

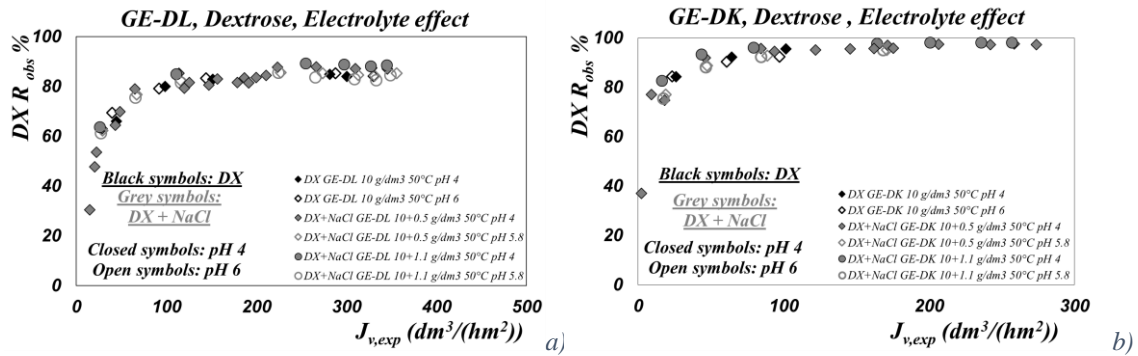


Figure 3.6: Radial flow test cell, Observed Rejection (R_{obs}) as a function of Permeate flux ($J_{v,exp}$) for Binary mixtures of Dextrose (10 g/dm^3) and Sodium Chloride ($0.5\text{-}1.1\text{ g/dm}^3$), GE-DL (a) and GE-DK (b). NF of model binary solution performed in total recirculation mode of R and P, 50°C , pH 4, Q_F $400\text{ dm}^3/\text{h}$, inlet pressure ranging from 4 to 20 bar.

In the whole range of permeate flux, dextrose retention was unaffected by the presence of the electrolyte, for both GE-DK and GE-DL membranes, as shown in Fig. 3.6 a,b.

Increasing electrolyte concentration, GE-AK (a more selective membrane compared to GE-DK and GE-DL) shown the same behavior for dextrose and fructose rejection in presence of sodium chloride and calcium chloride at concentration of 10 g/dm^3 . In view of the higher osmotic pressures in presence of electrolytes, permeate flux decreases.

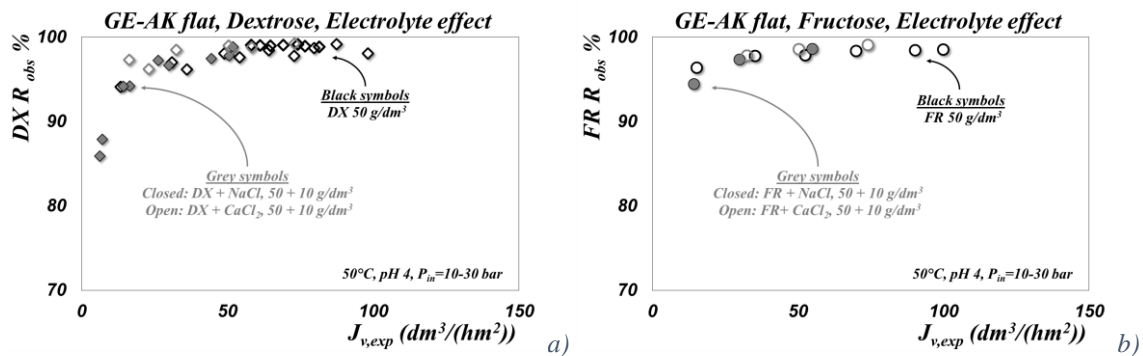


Figure 3.7: Radial flow test cell, Observed Rejection (R_{obs}) as a function of Permeate flux ($J_{v,exp}$) for Binary mixture of Dextrose (a) or Fructose (b) (50 g/dm^3) and Sodium Chloride or Calcium Chloride (10 g/dm^3), GE-AK membrane. NF of model binary solution performed in total recirculation mode of R and P, 50°C , pH 4, Q_F $400\text{ dm}^3/\text{h}$, inlet pressure ranging from 10 to 30 bar.

When sugar mixtures are tested, sugar-sugar interaction may increase sugar retention. Experiments were carried out with model solutions containing mono- and disaccharide at high concentrations, resembling those of commercial applications.

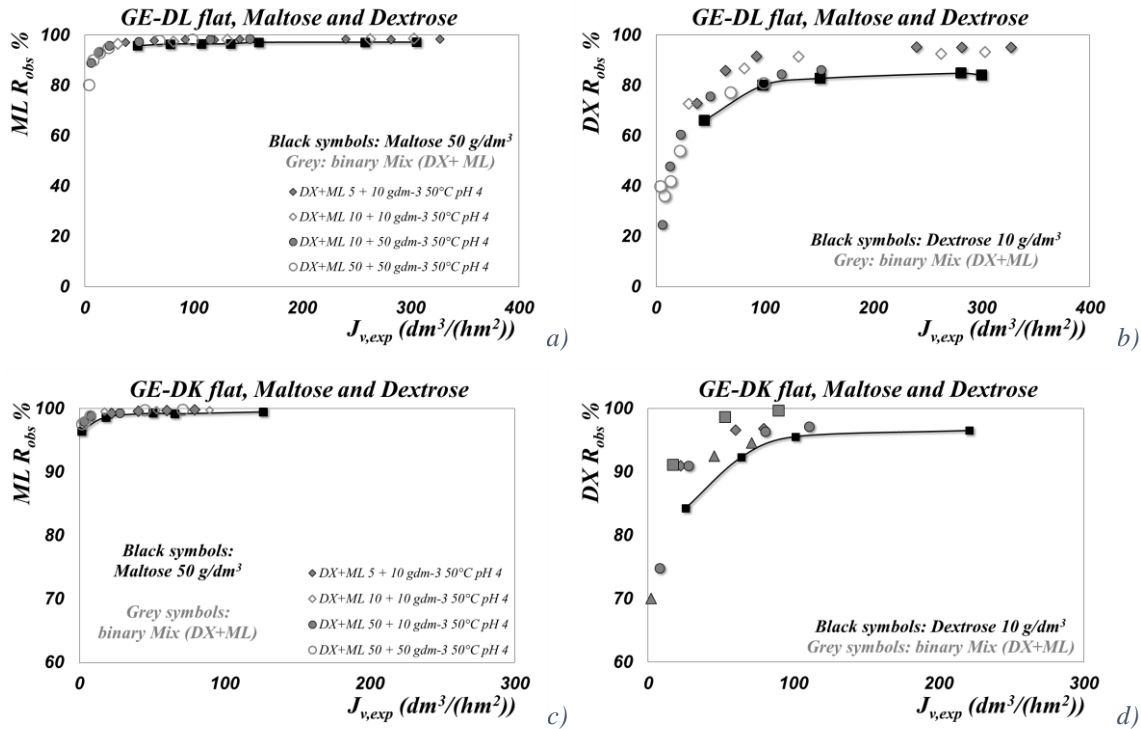


Figure 3.8: Radial flow test cell, Observed Rejection (R_{obs}) as a function of Permeate flux ($J_{v,exp}$) for Binary mixture (grey symbols) of Dextrose and Maltose, compared with pure compound (black symbols + line), GE-DL (a-b) and GE-DK (c-d). NF of model binary solution performed in total recirculation mode of R and P, 50°C, pH 4, Q_F 400 dm³/h, inlet pressure ranging from 10 to 30 bar.

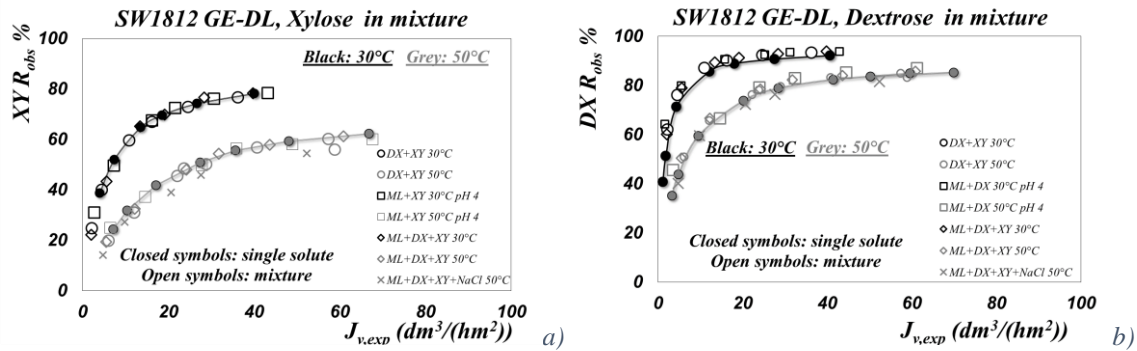


Fig. 3.9: Observed rejection (R_{obs}) as a function of experimental permeate ($J_{v,exp}$). Comparison between single sugar (closed symbols + lines) and mixtures (open symbols). SW1812 GE-DL, Xylose (a) and Dextrose (b), 30°-50°C, pH 4, total concentration 50 g/dm³. Total recirculation mode of R and P.

Differently from flat membranes, where dextrose rejection increases when maltose is added to the solution (whereas no effect was observed on maltose), experiments performed on SW1812 GE-DL shown the same behavior for single solutes and mixtures, in the whole range investigated: it is clear that no sugar-sugar interaction occurs in solution; only a slight increase in dextrose retention was observed, anyhow not comparable with those observed in Fig. 3.8 b and d.

When mixtures are processed, separation factor become a key parameter in order to evaluate separation efficiency. In Fig. 3.10 separation factor is presented as a function of experimental permeate flux, since difference in retention is not a representative parameter. The separation between two solutes is achieved if the separation factor differs from unit. As illustrated in Fig. 3.10, for the same membrane, Separation factor depends mainly on: (i) type of solutes, (ii) operating conditions (T, and P), and (iii) may be affected by the presence of electrolyte in solution.

Increased temperature, in all cases, caused the differences between the rejections of the sugars to decrease, indicating a less effective separation.

The nanofiltration membranes used in this study are able to separate xylose from dextrose, in agreement with the observations of (Sjoman, et al. 2007). However separation efficiency is affected by permeate flux and, even further by temperature. Temperature effect on separation was not documented in literature yet.

The results indicate that higher separation factors are gained at higher permeate fluxes and lower temperatures. In this study maximum separation factor (about 3.5) is achieved at 30°C and permeate flux higher than 20 dm³/(hm²).

The trend observed at 50°C is however in accordance with results from (Sjoman, et al. 2007), who obtained xylose separation factors up to around 3.3 with the Desal 5 DK membrane. (Morthensen, et al. 2015) achieved a xylose separation factor of 34 (corresponding to a throughput of 18.7 l/(hm²)) converting enzymatically glucose to gluconic acid, followed by a nanofiltration separation step.

Differently from Xylose-Dextrose separation, Xylose-Maltose and Dextrose-Maltose show a dependence of Separation factor from mixture composition. The separation factor reaches the maximum value in the ternary mixture, compared to binary mixture. The separation efficiency of xylose-maltose as well as dextrose-maltose separation is promoted when a third neutral solute is added to the solution, at the same total solution concentration. The significance of concentration, pressure, temperature, as well as electrolyte in solution were studied to optimize the separation.

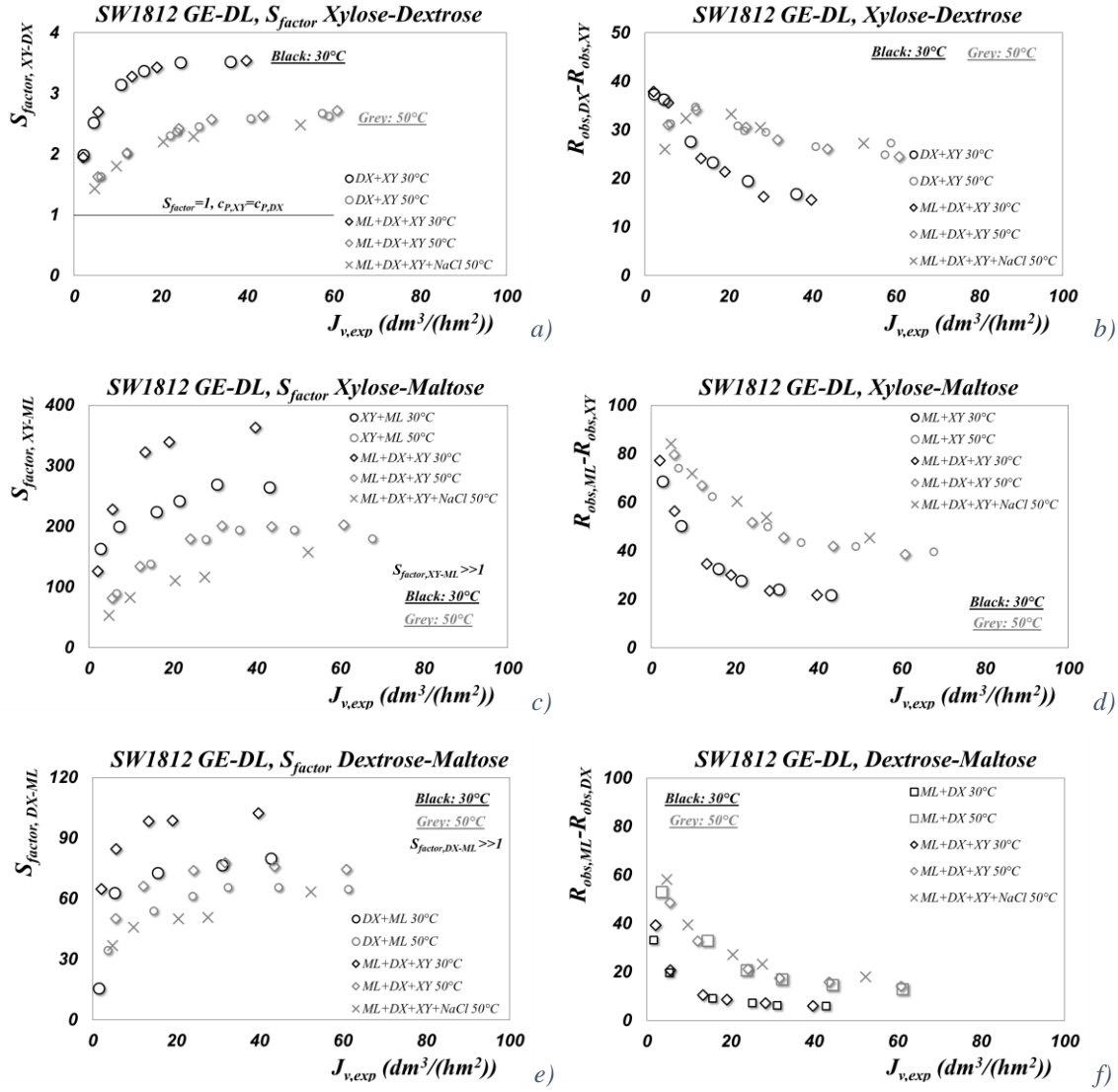


Fig. 3.10: Separation factor and difference in observed retention as a function of permeate flux for xylose-dextrose (a, b), xylose-maltose (d, e), dextrose-maltose (e, f). 1812C-34D GE-DL module, 30° and 50°C, pH 4, total recirculation of R and P, $Q_F=400 dm^3/h$

3.2.3 Isomers Separation (T, pH and Electrolyte effect on separation)

One of the objectives of this study is to evaluate to what extent operating conditions (i.e. pH of the feed solution, composition and the addition of an electrolyte) can improve the selectivity of isomer separation. Indeed, until now, previous studies has shown that this separation is hardly achievable because these sugars are isomers, and on an industrial scale, these separations are achievable only with chromatographic methods.

The influence of pH on both dextrose and fructose rejection was firstly studied, both on GE-DK and GE-DL membranes.

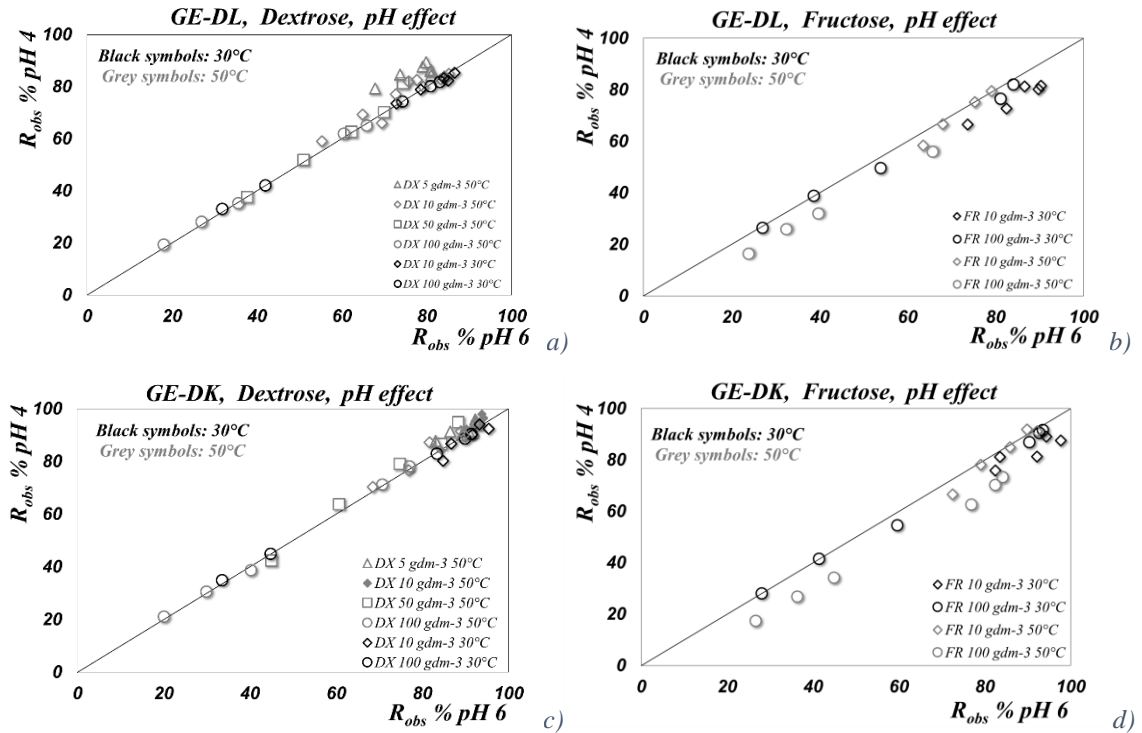


Figure 3.11: pH effect on neutral solute rejection, radial flow test cell, GE-DL and GE-DK, dextrose (a and c), fructose (b and d), model solutions, 30° and 50°C, pH 4 and 6, flow rate 400 dm³/h, total recirculation of R and P.

Experimentally a slight pH effect was observed on fructose rejection. Overall, the results obtained at pH 6 are compared with those at pH 4 (which represent approximately the Isoelectric Point of these membrane).

Electrolyte effect was then investigated on isomer separation. Results are shown in Fig. 3.12.

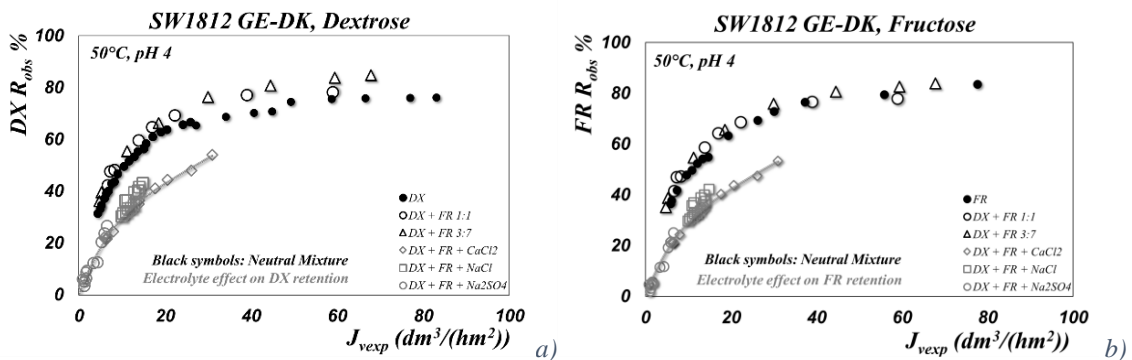


Fig. 3.12: Electrolyte Effect on Dextrose (a) and Fructose (b) rejections. SW1812 GE-DK, 50°C, $Q_F=400$ dm³/h, total recirculation mode of R and P

Electrolyte in dextrose-fructose mixture strongly affects the sugar retentions. This is illustrated for 1812C-34D GE-DK membrane, where dextrose and fructose rejections are shown as a function of permeate flux. The observed reduction in dextrose as well as fructose

rejection is not only due to the reduction in flux at higher electrolyte concentration (as shown in Fig. 3.6-3.7 a and b), but is clearly attributed to electrolyte.

For operation at flux of $20 \text{ dm}^3/(\text{hm}^2)$ dextrose and fructose rejection reduction is about 50% (from 60% to 40% approximately). The sugar retention obtained with mixed solute solutions is systematically lower than that obtained with “neutral” solutions. These decrease is more or less important depending on the nature of the salt and its concentration. Nevertheless, the reduction in retention does not result in a change in separation factor, as shown in Fig. 3.13 and 3.14 a and b.

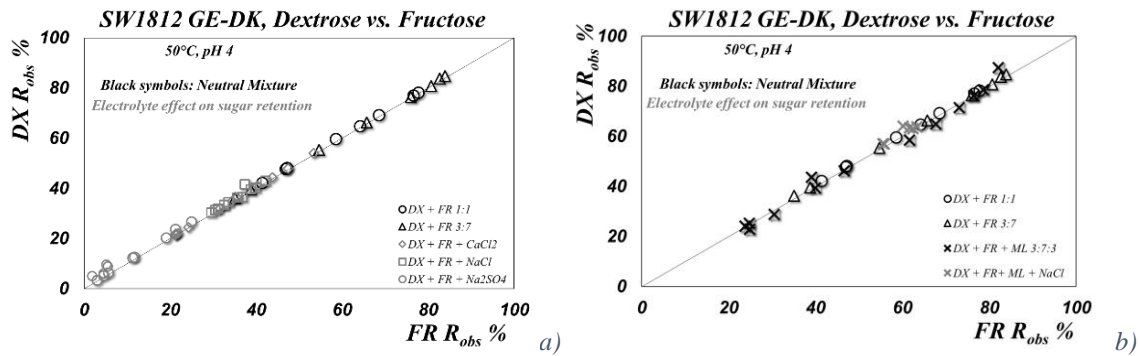


Fig. 3.13: Electrolyte effect on Dextrose-fructose separation, by NF at 50°C . Comparison between observed rejections, of dextrose and fructose. 1812C-34D GE-DK, pH 4, $Q_F=400 \text{ dm}^3/\text{h}$, total recirculation mode of R and P.

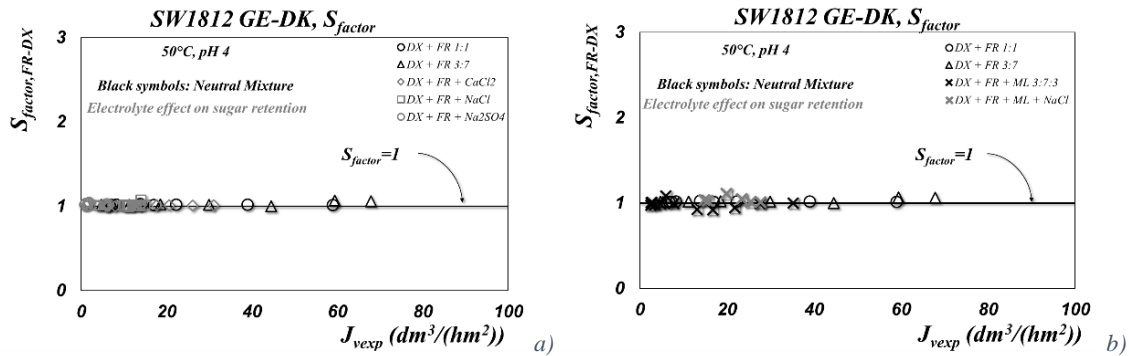


Fig. 3.14: Electrolyte effect on Dextrose-fructose separation factor as a function of permeate flux, by NF at 50°C . 1812C-34D GE-DK, pH 4, $Q_F=400 \text{ dm}^3/\text{h}$, total recirculation mode of R and P.

Membrane tested is not able to fractionate isomer oligosaccharide, confirming that chromatographic methods are suitable for these kinds of separations.

Overall, experimental data as it is shown that:

- i) Sugars shown approximately the same behavior with operating conditions (T, P, concentration), except for totally rejected solutes;

- ii) Electrolyte at high concentration may affect sugar retention, and reduce separation factor;
- iii) No separation is achievable by NF when isomers are processed.

These results are in agreement with literature study [(Wang, Zhang and Ouyang 2002), (Bargeman, Vollenbroek, et al. 2005), (Bouchoux, Roux-de Balmann and Lutin 2005) (Cuartas-Uribe, et al. 2007), (Mohammad, Basha and Leo 2010) , (Mandale and Jones 2008) , (Bouchoux, Roux-de Balmann and Lutin 2005), (Wang, Zhang and Ouyang 2002), (Freger, Arnot and Howell 2000), (Vellenga and Tragardh 1998), (Bargeman, Westerink, et al. 2014)].

Electrolyte effect on oligosaccharide rejection is a key phenomenon that affect NF performances.

3.3 Intrinsic membrane performances

Intrinsic membrane performances have been investigated for all the experimental data documented in the previous section.

Effective Driving force of the process and real Rejection are evaluated by using the film theory model in order to calculate the feed-membrane interface concentration of i specie. Effective driving force takes into account a Staverman coefficient, which can be assumed (in first approximation) to be equal to the asymptotic real Rejection of i specie, $R_{real,i}$, defined as:

$$J_v = L_p \Delta P_{eff} = L_p (\Delta P - \sum_{i=1}^n \sigma_{v,i} \Delta \pi_{real,i}) \quad (3.7)$$

$$\Delta \pi_{real,i} = \pi(c_{I,i}) - \pi(c_{P,i}) \quad (3.8)$$

$$R_{real,i} = 1 - \frac{c_{P,i}}{c_{I,i}} \quad (3.9)$$

$$\sigma_{v,i} = R_{real,i}^{\infty} = \lim_{J_{v,exp} \rightarrow \infty} R_{real,i} \quad (3.10)$$

Where $c_{I,i}$ is the solute concentration at feed-membrane interface, which is described by the Film-Theory:

$$\frac{J_v}{k_L} = \ln \frac{c_{I,i} - c_{P,i}}{c_{bulk,i} - c_{P,i}} \quad (3.11)$$

The mass transfer coefficient, k_L , can be evaluated by means of an appropriate correlation of dimensionless numbers for the system and process conditions. Typically, it is necessary to account of the role of viscosity. To that purpose (Aimar e Field 1992) proposed:

$$k_L = k_L^0 \left(\frac{\eta_{bulk,i}}{\eta_{l,i}} \right)^{0.27} \quad (3.12)$$

For the radial flow test cell a correlation identified in a previous work (Camera-Roda, Saavedra and G.C. Sarti 1993) was used:

$$Sh = 1.61 Re^{0.35} Sc^{\frac{1}{3}} \left(\frac{R_c}{b} \right)^{\frac{1}{3}} \quad (3.13)$$

$$500 < Re < 5000$$

Where R_c and b are the cell radius and height respectively.

With regard to the 1812 spiral wound modules an appropriate relationship was elaborated and discussed in *Appendix B*. The experimental relationship is:

$$Sh = 0.023 Re^{0.8} Sc^{\frac{1}{3}} \quad (3.14)$$

$$200 < Re < 800$$

These relationships have been applied in order to evaluate intrinsic performances of the membranes.

In this section intrinsic separation factor ($S_{factor,real}$) has been defined according the following relationship:

$$S_{factor,i-j} = \frac{c_{P,i}/c_{P,j}}{c_{I,i}/c_{I,j}} = \frac{1-R_{real,i}}{1-R_{real,j}} \quad (3.5)$$

Where $c_{F,i}$ and $R_{obs,i}$ in Eq. (3.5) has been replaced by $c_{I,i}$ and $R_{real,i}$ respectively.

3.3.1 Single solutes

When concentration polarization affects membrane performances, real rejection ($R_{real,i}$) is a key parameters which describes the intrinsic behavior of the membrane.

All experimental data presented and discussed in previous section, now are documented in terms of intrinsic performances of the membrane. Results are reported from Figures 3.15 to 3.17.

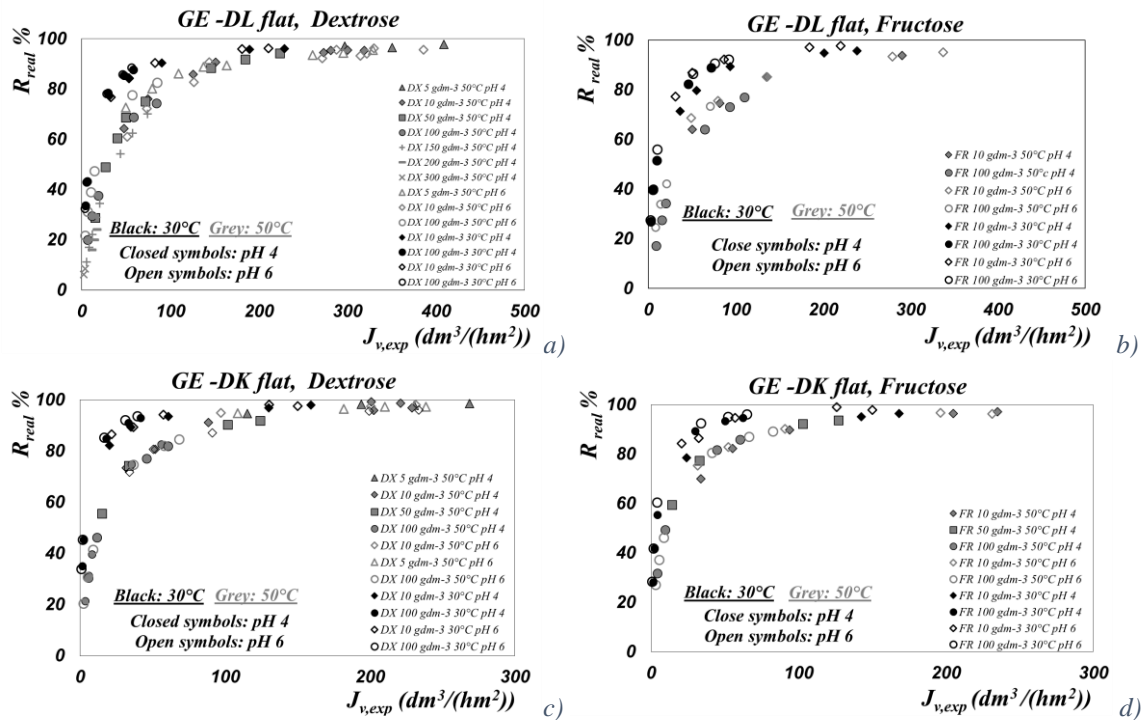


Figure 3.15: Real Rejection vs. experimental Permeate flux, radial flow test cell, GE-DL and GE-DK, dextrose (a, c), and fructose (b, d), model solutions, 30 and 50°C, pH 4 6, flow rate 400 dm³/h, total recirculation of R and P

Intrinsic rejections show the same trend with temperature, concentration and pressure of observed rejection, however values are slightly higher than “observed” results.

Fig. 3.15 a-c show the variations of the real retention of dextrose and fructose versus J_v for different concentrations (ranging from 1 to 300 g/dm³). It can be observed that the intrinsic retention is quite independent of the sugar concentration.

Comparison between intrinsic (R_{real}) and observed rejection (R_{obs}) (Fig. 3.16 a-c) quantifies the extent of concentration polarization in the test conditions investigated.

Concentration polarization is a key phenomenon especially at high permeate fluxes and it is not negligible for GE-DL membranes

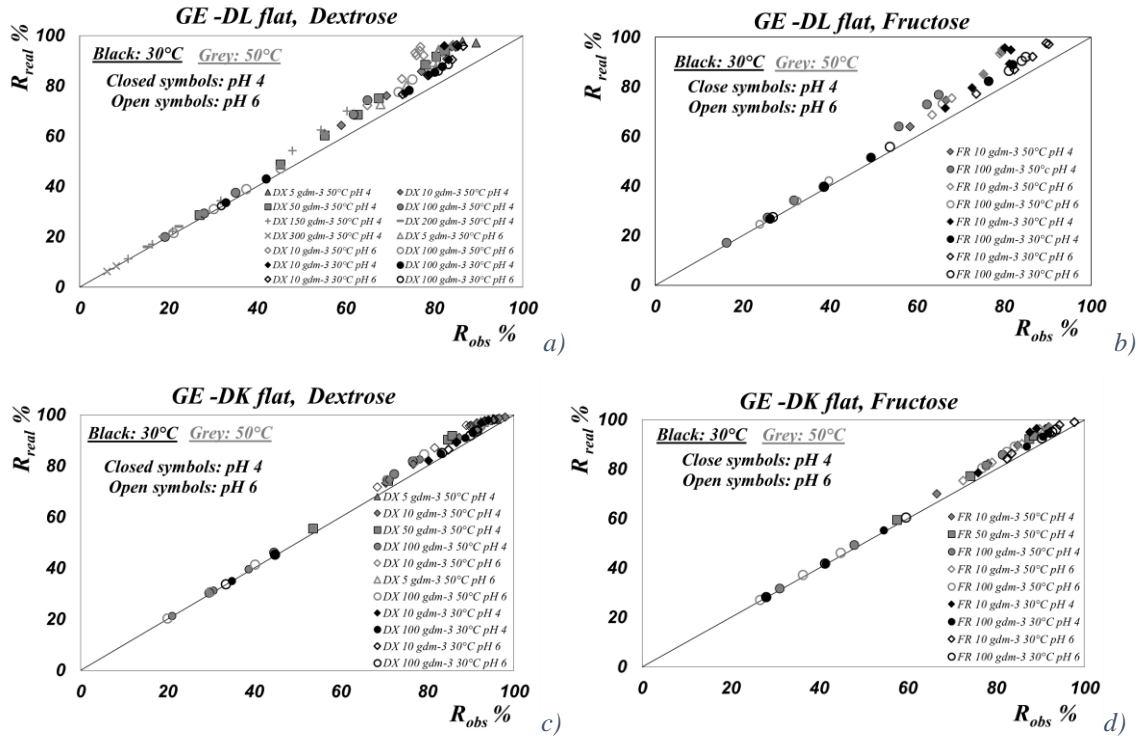


Figure 3.16: Comparison between intrinsic (R_{real}) and observed rejection (R_{obs}). Radial flow test cell, GE-DL and GE-DK, dextrose (a, c), and fructose (b, d), model solutions, 30 and 50°C, pH 4 6, flow rate 400 dm^3/h , total recirculation of R and P

These results have been confirmed in spiral wound module (Fig. 3.17 and 3.18 a-c).

Temperature is an operating parameter that affects mainly:

- i) Intrinsic rejection, and
- ii) Concentration polarization

Depending on the type of solute.

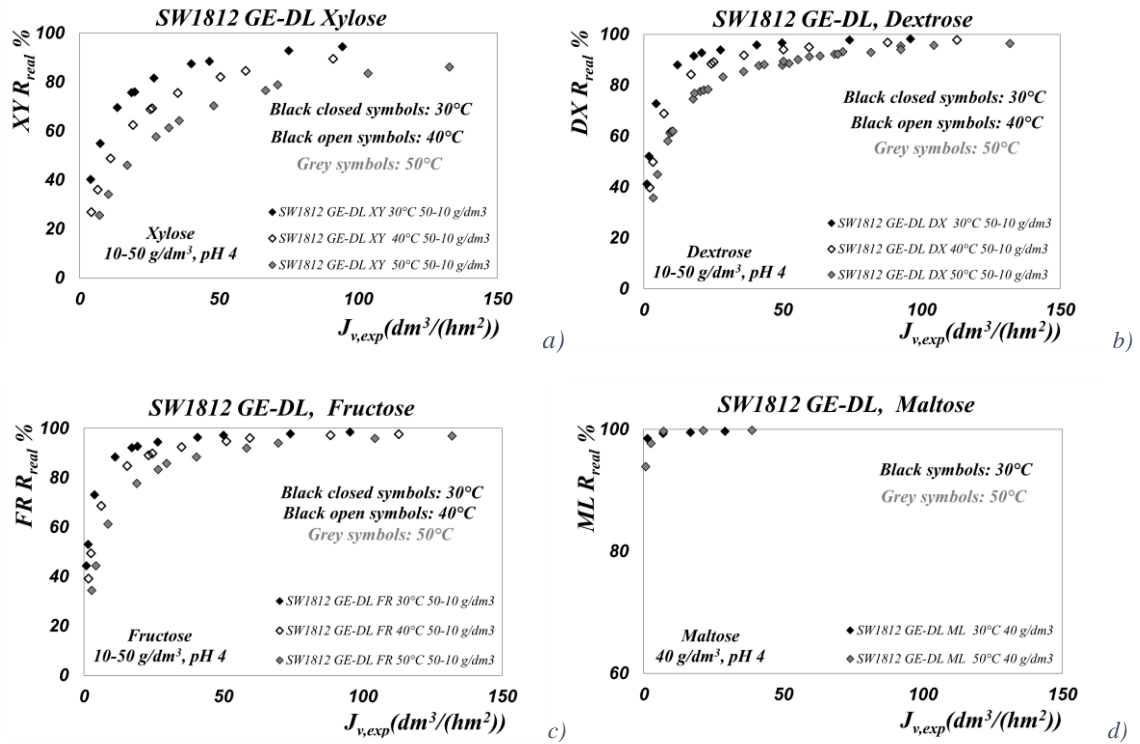


Figure 3.17: SW1812 GE-DL module, Data Reduction: real Rejection (R_{real}) as a function of Permeate flux ($J_{v,exp}$) for Xylose (a), Dextrose (b), Fructose (c), Maltose (d). NF of model solution of Xylose, Dextrose or Fructose (10 and 50 g/dm^3) and maltose (40 g/dm^3), in total recirculation mode of R and P, 30°, 40° and 50°C, pH 4, Q_F 400 dm^3/h , inlet pressure ranging from 4 to 20 bar.

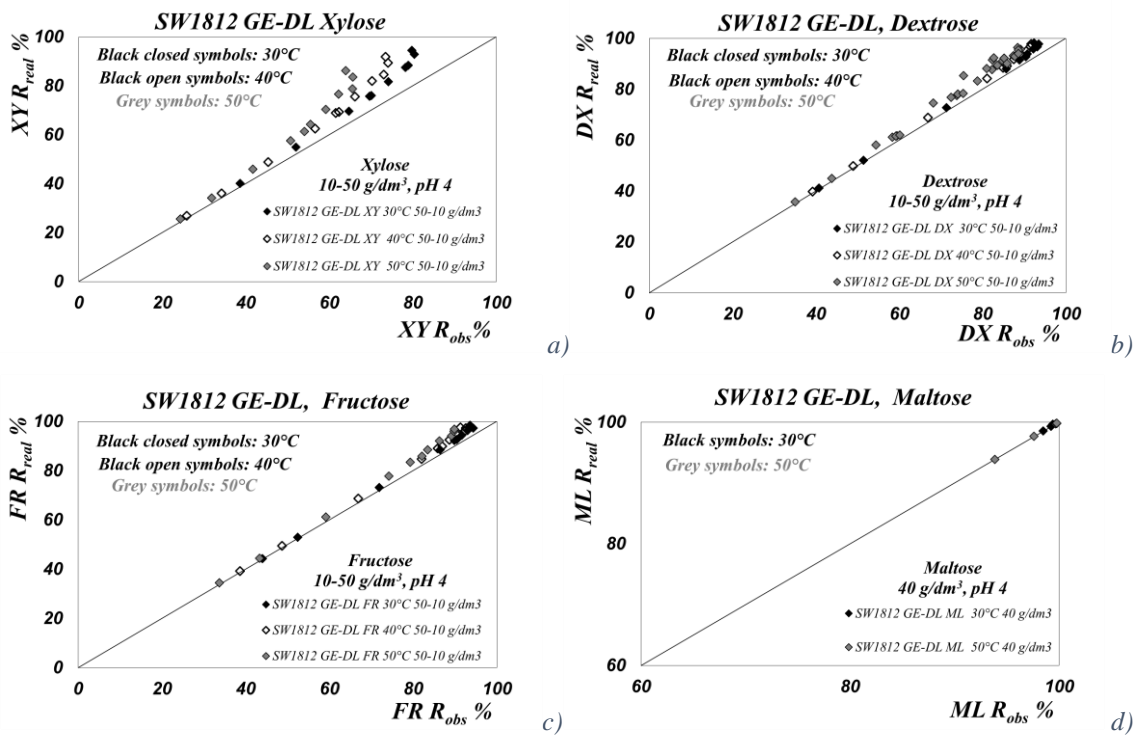


Figure 3.18: Comparison between intrinsic (R_{real}) and observed rejection (R_{obs}). SW1812 GE-DL module, Xylose (a), Dextrose (b), Fructose (c), Maltose (d). NF of model solution of Xylose, Dextrose or Fructose (10 and 50 g/dm^3) and maltose (40 g/dm^3), in total recirculation mode of R and P, 30°, 40° and 50°C, pH 4, Q_F 400 dm^3/h , inlet pressure ranging from 4 to 20 bar.

Concentration polarization is a key phenomenon affecting *NF* membranes, especially at high permeate fluxes (corresponding to low concentrations and high temperatures) and low molecular weight solutes, like xylose, dextrose and fructose.

3.3.2 Mixtures

As illustrated in the previous section, electrolyte at low concentration does not affect solute rejection. The trend has been confirmed in terms of intrinsic membrane performances.

This is illustrated for Desal GE-DK and GE-DL in Fig. 3.19, where dextrose real retention is shown as a function of permeate flux for a 10 g/dm³ dextrose solution containing different NaCl concentrations, ranging from 0.5 to 1.1 g/dm³. In this case concentration polarization is negligible, especially for GE-DK membrane (Fig. 3.20).

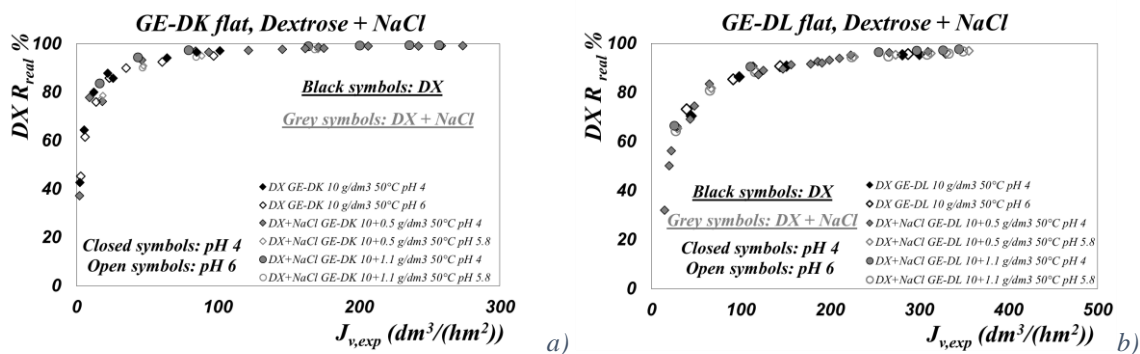


Figure 3.19: Radial flow test cell, data Reduction: real Rejection (R_{real}) as a function of Permeate flux ($J_{v,exp}$), for Binary mixture of Dextrose (10 g/dm³) and Sodium Chloride (0.5-1.1 g/dm³), GE-DK (a) and GE-DL (b). NF of model binary solution performed in total recirculation mode of R and P, 50°C, pH 4, Q_F 400 dm³/h, inlet pressure ranging from 4 to 20 bar.

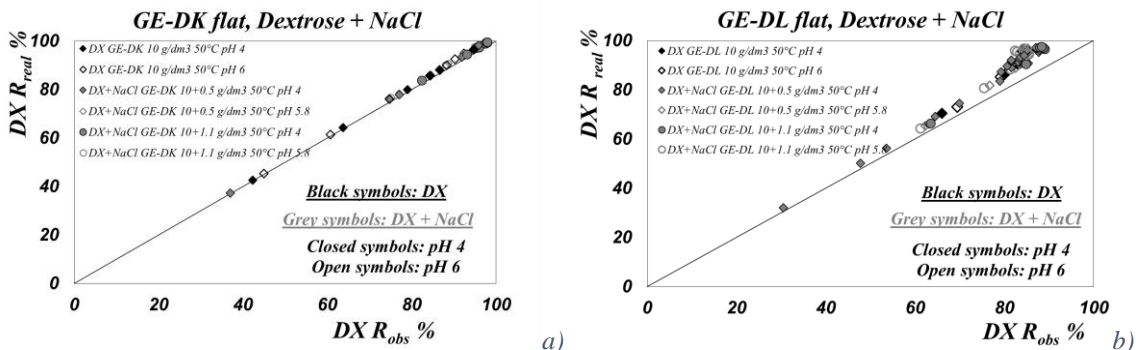


Figure 3.20: Radial flow test cell, data Reduction: real Rejection (R_{real}) as a function of observed rejection (R_{obs}), for Binary mixture of Dextrose (10 g/dm³) and Sodium Chloride (0.5-1.1 g/dm³), GE-DK (a-b) and GE-DL (c-d). NF of model binary solution performed in total recirculation mode of R and P, 50°C, pH 4, Q_F 400 dm³/h, inlet pressure ranging from 4 to 20 bar.

Studying complex mixtures, no complexation was found in terms of intrinsic performances, although concentration polarization is not negligible, as illustrated in Fig. 3.21 *c* and *d*.

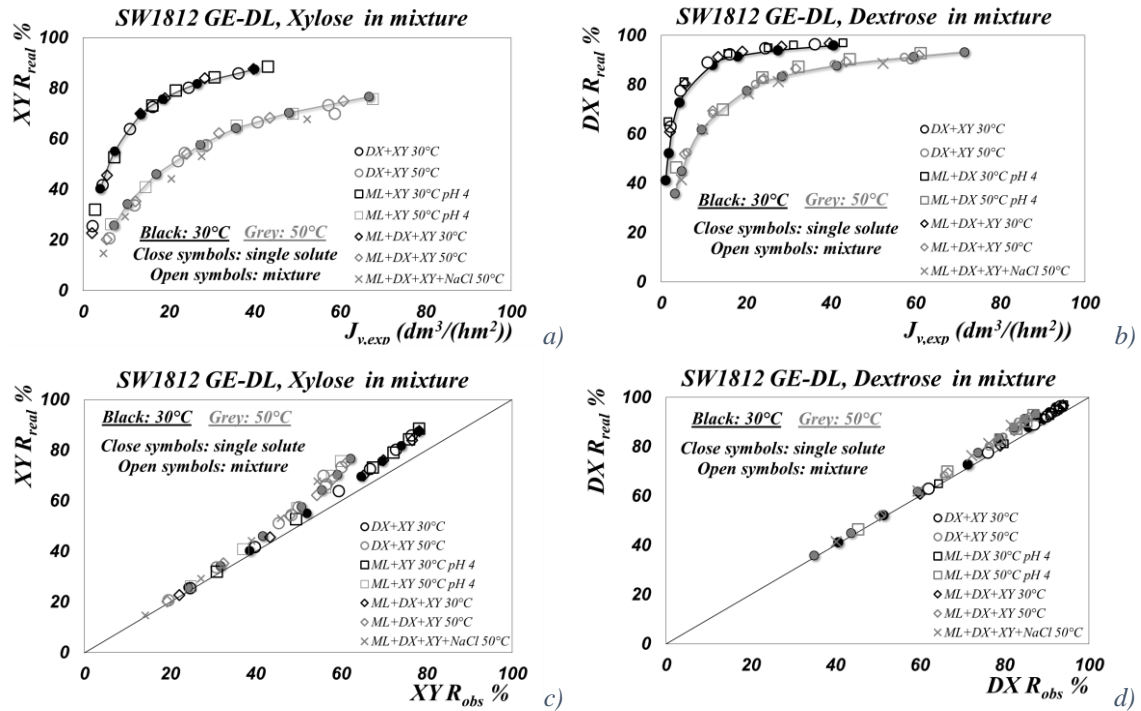


Figure 3.21: SW1812 GE-DL module, Data Reduction: Xylose and Dextrose real Rejection (R_{real}) as a function of Permeate flux ($J_{v,exp}$) (a, b) and as a function of observed rejection (R_{obs}) for Binary and Ternary mixture of Xylose, Dextrose, and Maltose. NF of model binary and ternary solution of Xylose, Dextrose and maltose (total concentration 50 g/dm³), in total recirculation mode of R and P, 30° and 50°C, pH 4, Q_F 400 dm³/h, inlet pressure ranging from 4 to 20 bar.

Since intrinsic rejection is on average higher than observed rejection, also the real separation factor deviates from the observed one, although the trend is the same.

Experimentally, (Fig.3.22) a slight increase in separation factor compared to observed separation factor is observed at high permeate fluxes.

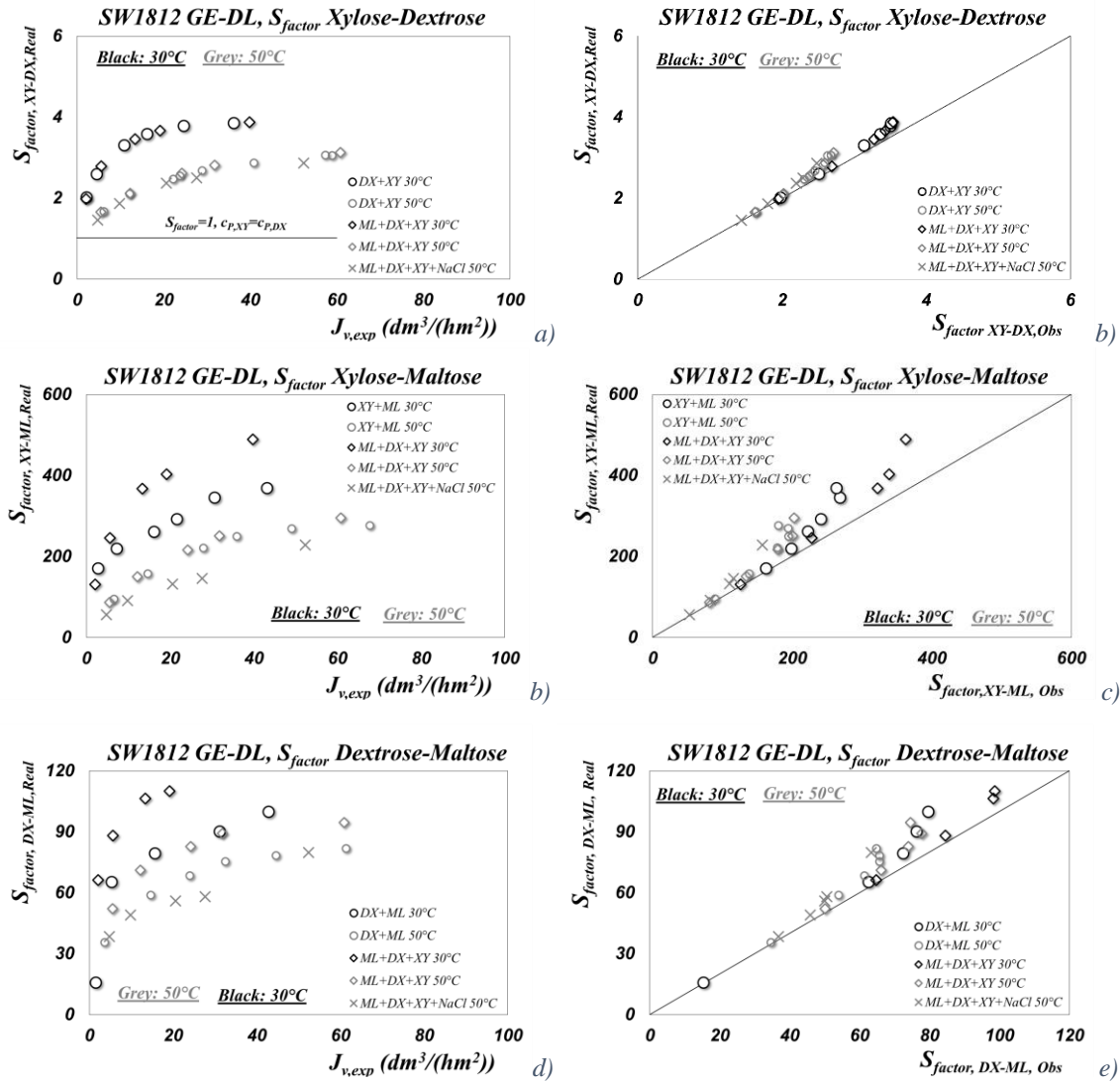


Figure 3.22: Intrinsic S_{factor} as a function of experimental permeate flux and Observed S_{factor} (defined in Eq. (3.5)). Xylose-Dextrose (a-b), Xylose-Maltose (c-d), Dextrose-Maltose (d-e). SW1812 GE-DL, Binary and ternary mixtures, 30°C and 50°C, pH 4, $Q_F=400 \text{ dm}^3/\text{h}$, total recirculation mode of R and P.

3.4 Discussions and Conclusions

A wide experimentation was carried out to test performances of commercial polyamide membranes for oligosaccharide Nanofiltration. Tests were carried out by using synthetic sugar solutions in a wide range of concentrations, composition, pressures and temperatures. A lot of experimental data are available, and some interesting general conclusions can be drawn.

- i) All the membrane tested, in two configurations (flat sheet and spiral wound membranes) show remarkable analogies in their behavior as a function of operative conditions;
- ii) Experimental data are highly reproducibly;
- iii) A general trend is observed in which membrane/module performances can be described by using few simple quantities, in a wide range of confidence.
- iv) Differently from literature, whole curves R_{obs} vs. $J_{v,exp}$ and R_{real} vs. $J_{v,exp}$ are available in a wide range of operative conditions;
- v) Concentration polarization affects membrane performances, especially at high permeate fluxes;
- vi) remarkable effects of pressure and temperature on flux and rejection is quite typical Nanofiltration processes: (i) flux increases with pressure and temperature; (ii) rejection decrease as temperature increases.
- vii) The retention of monosaccharides (pentose and hexose sugars) strongly depends on temperature, and is altered by the presence of electrolyte at high concentrations in solution;
- viii) Solute-solute interactions are negligible as well as solute-salt interactions.

Temperature effect on neutral solute rejection will be further investigated in the next chapter, with the transport model support. At the moment we limit to observe a different temperature effect depending on the sugar tested, while pH effect on sugar retention is not yet well understood. Temperature also affects separation efficiency: can be observed that separation factor increase as temperature decreases from 50° to 30°C.

As well as the interactions between different components and the membrane, and their effect on the separation of NF membrane are negligible in the conditions tested.

Data reported in this chapter are the experimental basis for the critical assessment of the Model that will be discussed in the next section.

References

- Aimar, P., and R. Field. "Limiting flux in membrane separations: a model bases on the viscosity dependency of the mass transfer coefficient." *Chemical Engineering Science* 47, no. 3 (1992): 579-586.
- Bandini, S., and L. Nataloni. "Nanofiltration for dextrose recovery from crystallization mother liquors: A feasibility study." *Separation and Purification Technology* 139 (2015): 53-62.

- Bargeman, G., J.B. Westerink, O. Guerra Miguez, and M. Wessling. "The effect of NaCl and glucose concentration on retentions for nanofiltration membranes processing concentrated solutions." *Separation and Purification Technology* 134 (2014): 46-57.
- Bargeman, G., J.M. Vollenbroek, J. Straatsma, and C.G.P.H. Schroen. "Nanofiltration of multicomponent feeds. Interactions between neutral and charged components and their effect on retention." *Journal of Membrane Science* 247 (2005): 11-20.
- Bouchoux, A., H Roux-de Balman, and F. Lutin. "Nanofiltration of glucose and sodium lactate solutions variations of retention between single- and mixed- solute solutions." *Journal of Membrane Science* 258 (2005): 123-132.
- Bouranene, S., A. Szymczyk, P. Fievet, and A. Vidonne. "Effects of salts on the retention of polyethyleneglycol by a nanofiltration ceramic membrane." 240 (2009): 94-98.
- Bouranene, S., A. Szymczyk, P. Fievet, and A. Vidonne. "Influence of inorganic electrolytes on the retention of polyethyleneglycol by nanofiltration ceramic membranes." *Journal of Membrane Science* 290 (2007): 216-221.
- Bowen, W.R., and A.W. Mohammad. "Characterization and prediction of nanofiltration membrane performance- a general assessment." *Trans. IChemE* 76A (1998): 885.
- Bowen, W.R., and J.S. Welfoot. "Modeling of membrane nanofiltration-pore size distribution effects." *Chem. Eng. Sci.* 57 (2002): 1393-1407.
- Camera-Roda, G., A.I. Saavedra, and G.C. Sarti. "Heat and Mass Transfer in Radial Flow Boundary Layer." *Proc. First Conference on Chemical and Process Eng.* Firenze, 1993. 65-70.
- Cavaco Morao, A.I., A. Szymczyk, P. Fievet, and A.M. Brites Alves. "Modelling the separation by nanofiltration of multi-ionic solution relevant to an industrial process." *Journal of Membrane Science* 322 (2008): 320-330.
- Cuartas-Uribe, B., M.C. Vincent-Vela, S. Alvarez-Blanco, M.I. Alcaina-Miranda, and E. Soriano-Costa. "Nanofiltration of sweet whey and prediction of lactose retention as a function of permeate flux using the Kedem-Spiegler and Donnan Steric Partitioning models." *Separation and Purification Technology* 56 (2007): 38-46.
- Escoda, A., S. Déon, and P. Fievet. "Assessment of dielectric contribution in the modeling of multi-ionic transport through nanofiltration membranes." *Journal of Membrane Science* 378 (2011): 214-223.
- Freger, V., T.C. Arnot, and J.A. Howell. "Separation of concentrated organic/inorganic salt mixtures by nanofiltration." *Journal of Membrane Science* 178 (2000): 185-193.
- Goulas, A., A.S. Grandison, and R. A. Rastall. "Fractionation of oligosaccharides by NF." *Journal of Membrane Science* 209 (2002): 321-335.
- Kimura, S., H. Nabetani, M. Nakajima, S.-i Nakao, and A. Watanabe. "Prediction of the flux for the reverse osmosis of a solution containing sucrose and glucose." *Journal of Chemical Engineering of Japan* 25, no. 5 (1992): 575-580.
- Kuhn, R.C., F. Mauger Filho, L. Palacio, A. Hernandez, and P. Pradanos. "Mass transfer and transport during purification of fructo oligosaccharides by nanofiltration." *Journal of Membrane Science* 365 (2010): 356-365.
- Lide, D.R., and H. Frederikse. *CRC Handbook of Chemistry and Physics*. CRC Press, 1990.

- Lopez Leiva, M.H., and M. Guzman. "Formation of oligosaccharides during enzymatic hydrolysis of milk whey permeates." *Pro. Biochem.* 30 (1995): 757.
- Luo, J., and Y. Wan. "Effect of highly concentrated salt on retention of organic solutes by nanofiltration polymeric membranes." *Journal of Membrane Science* 372 (2011): 145-153.
- Mandale, S., and M. Jones. "Interactions of electrolytes and non-electrolytes in NF." *Desalination* 219 (2008): 262-271.
- Mandale, S., and M. Jones. "Membrane transport theory and the interactions between electrolytes and non electrolytes." *Desalination* 252 (2010): 17-26.
- Manttari, M., A. Pihlajamaki, and M. Nystrom. "Effect of pH on hydrophilicity and charge and their effect on the filtration efficiency of NF membranes at different pH." *Journal of Membrane Science* 280 (2006): 311-320.
- Manttari, M., A. Pihlajamaki, E. Kaipainen, and M. Nystrom. "Effect of temperature and membrane pretreatment by pressure on the filtration properties of nanofiltration membranes." *Desalination* 145 (2002): 81.
- Mazzoni, C., L. Bruni, and S. Bandini. "Nanofiltration: Role of the electrolyte and pH on Desal DK performances." *Industrial & Engineering Chemistry Research* 46 (2007): 2254-2262.
- Mohammad, A.W., R.K. Basha, and C.P. Leo. "Nanofiltration of glucose solution containing salts: effects of membrane characteristics, organic component and salt on retention." *Journal of Food Engineering* 97 (2010): 510-518.
- Morthensen, Sofie T., J. Luo, Anne S. Meyer, H. Jørgensen, and M. Pinelo. "High performance separation of xylose and glucose by enzyme assisted nanofiltration." *Journal of Membrane Science* 492 (2015): 107-115.
- Nilsson, M., Gun Tragardh, and K. Ostergren. "The influence of sodium chloride on mass transfer in a polyamide nanofiltration membrane at elevated temperatures." *Journal of Membrane Science* 280 (2006): 928-936.
- Nilsson, M., T. Tragardh, and K. Ostergren. "The influence of pH, salt and temperature on nanofiltration performance." *Journal of Membrane Science* 312 (2008): 97-106.
- Pontalier, P.-Y., A. Ismail, and M. Ghoul. "Mechanism for the selective rejection of solutes in nanofiltration membranes." *Separation and Purification Technology* 12 (1997): 175-181.
- Sharma, R.R., R. Agrawal, and S. Chellam. "Temperature effects on sieving characteristics of thin-film composite nanofiltration membranes: pore size distributions and transport parameters." *Journal of Membrane Science* 223 (2003): 69-87.
- Sjoman, E., M. Manttari, M. Nystrom, H. Koivikko, and H. Heikkila. "Separation of xylose from glucose by nanofiltration from concentrated monosaccharide solutions." *Journal of Membrane Science* 292 (2007): 106-115.
- Slezak, A., S. Grzegorzczyn, and J. Wasik. "Model Equations for interactions of hydrated species in transmembrane transport." *Desalination* 163 (2004): 177-192.
- Straatsma, J., G. Bargeman, H.C. Van der Host, and J.A. Wesslingh. "Can nanofiltration be fully predicted by a model?" *Journal of Membrane Science*, no. 198 (2002): 273-284.

- Tsuru, T., S. Izumi, T. Yoshioka, and M. Asaeda. "Temperature effect on transport performance by inorganic nanofiltration membranes." *AIChE Journal* 46 (2000): 565.
- Umpuch, C., S. Galier, S. Kanchanatawee, and H. Roux de Balman. "Nanofiltration as a purification step in production process of organic acids: selectivity improvement by addition of an inorganic salt." 2010: 1763-1768.
- Vellenga, E., and G. Tragardh. "Nanofiltration of combined salt and sugar solutions: coupling between retentions." *Desalination* 120 (1998): 211.
- Wang, Xiao-Ling, C. Zhang, and P. Ouyang. "The possibility of separating saccharides from a NaCl solution by using NF in diafiltration mode." *Journal of Membrane Science* 204 (2002): 271-281.

4. Separation of oligosaccharide mixtures in Nanofiltration: Modelling and critical assessment

4.0	Introduction.....	91
4.1	Introduction to <i>NF</i> modelling	92
4.2	The revised DSP&DE Model: Theoretical Background.....	94
4.2.1	The general Physical Problem	94
4.2.2	Solute partitioning.....	97
4.2.3	Total flux.....	98
4.2.4	Hydraulic and Membrane permeability: $L_{p,w}$ and L_p	100
4.2.5	Solute flux.....	102
4.2.6	Rejection of neutral solutes.....	105
4.2.7	Dependence of revised model parameters from pore geometry	105
4.3	The problem of parameters calculation: critical analysis of current approach	108
4.3.1	Parameter calculation: state of art.....	108
4.3.2	Molecular shape of mono- and disaccharides.....	115
4.3.3	Calculation of model parameters: a new approach.....	118
4.4	Calculation of model parameters: Results	120
4.4.1	Check of Membrane permeability	120
4.4.2	Calculation of model parameters (λ_i , δ) and sensitivity from pore geometry.....	122
4.5	Revised DSP&DE model Validation.....	127
4.6	Conclusions.....	132
	References.....	132

List of symbols

<i>Symbol</i>	<i>Units</i>	<i>Quantity</i>	<i>K_{ic}</i>	-	
			<i>K_{ic}</i>	-	convective hindrance factor
x	[m]	axial coordinate in the membrane	<i>K_{id}</i>	-	diffusive hindrance factor
0^-	-	feed/membrane interface, feed side	<i>Pe</i>	-	hindered Peclet number
0^+	-	feed/membrane interface, membrane side	\bar{V}	[m ³ /mol]	partial molar volume
δ^-	-	membrane/permeate interface, membrane side	<i>R_{real}</i>	-	real Rejection

δ^+	-	membrane/permeate interface, permeate side	γ	-	activity coefficient
r_p	[m]	average pore radius	$\tilde{\mu}$	[J/mol]	electrochemical potential
r_s	[m]	Stokes radius	ψ	-	dimensionless electrostatic potential
λ	-	hydrodynamic coefficient ($=r_s/r_p$)	Ψ	[V]	electrostatic potential
ϕ	-	steric partitioning coefficient			
δ	[m]	effective membrane thickness accounting for tortuosity and porosity	F	[C/mol]	Faraday constant (=98485)
δ^*	[m]	effective membrane thickness accounting for tortuosity and porosity, according Hagen-Poiseuille	z	-	ionic valence
c	[mol/dm ³]	mole concentration	ΔW_{DE}	-	excess energy due to dielectric exclusion
j	[mol/(m ² s)]	mole solute flux	$\Delta \psi_D$	-	Donnan potential
J_v	[dm ³ /(hm ²)]	total volume flux	k_L	[m/s]	Mass transfer coefficient
J_s		solute flux	k_L^0	[m/s]	Mass transfer coefficient in the bulk phase
L_p	[dm ³ /(hm ² bar)]	membrane Permeability			
Δ	-	difference			
P	[bar]	pressure	<i>Subscript</i>		
π	[bar]	osmotic pressure	i, j	solute/components	
ΔP	[bar]	trans membrane pressure	0	at the feed/membrane interface	
ΔP_{eff}	[bar]	effective driving force	δ	At the membrane/permeate interface	
$\Delta \pi_{real}$	[bar]	effective osmotic pressure difference	$bulk$	bulk side	
σ_v	-	Staverman reflection coefficient	I	feed/membrane interface	
$L_{p,w}$	[dm ³ /(hm ² bar)]	hydraulic permeability	$inside$	inside the pore	
R	[J/(mol K)]	Universal gas constant (=8.314 J/(mol K))	F	feed	
T	[K]	temperature	P	permeate	

η	[Pa/s]	water dynamic viscosity inside the pore	R	retentate
η_0	[Pa/s]	water dynamic viscosity in the external bulk	exp	Experimental data
R_{obs}	-	Observed rejection	w	water
R_{real}^∞	-	Asymptotic Real Rejection	DX	Dextrose
D_∞	[m ² /s]	bulk diffusivity at infinite dilution	FR	Fructose
D_{ip}	[m ² /s]	hindered diffusivity inside the pore	XY	Xylose
k_B	[J/K]	Boltzmann constant (=1.381 × 10 ⁻²³)	ML	Maltose

4.0 Introduction

Since the beginning of membrane technology a substantial amount of research focused on the description of the transport mechanism through the membranes, with the aim of process understanding and development. Most of these studies used flat sheet membranes; on the other hand many researchers studied fluid dynamics and mass transfer in spiral wound membrane modules, mainly in aqueous solutions.

The development of membrane processes usually involves several steps, starting from feasibility tests at laboratory scale (typically small flat sheet membranes), passing through bench scale as well as pilot plant tests and finishing with large industrial scale processes.

Across the different steps, modelling can be applied for two purposes:

- a) Modeling mass transfer across the membrane: it requires the description of partitioning and transport phenomena across the membranes. Typically it is accomplished by the determining of adjustable parameters which characterize the membrane behavior.
- b) Simulation of module and process performances at different scales

Modelling is a key aspect of *NF* for food applications.

In this study firstly an overview about *NF* modelling is documented, highlighting criticalities and issues not solved yet. Afterwards a revised transport model is presented, identifying and discussing the key aspects and criticalities.

Finally a validation of the model presented is performed by using all the experimental investigation reported in *Chapter 3*.

4.1 Introduction to NF modelling

Polymeric NF membranes show characteristics which are intermediate between Ultrafiltration and RO. The development of mathematical models describing transport mechanism through the membrane is essential to predict and optimize membrane performances, in the case of both simple and multicomponent systems containing neutral solutes, as well as electrolytes. Of course a good modelling allows to reduce the number of tests required to perform process scale up.

The question about the mathematical modeling of neutral solute and electrolyte transport through NF membranes is well known [(Spiegler and Kedem 1966), (Bowen, Mohammad and Hilal 1997), (Bandini and Vezzani 2003), (Szymczyk and Fievet 2005), (Bandini and Bruni 2010)]. The key points of the problem can be basically identify both in the characterization of the membrane (which can be seen as a homogeneous or as a porous medium) and in the understanding of the phenomena giving rise to partitioning and transport of the species across the membrane.

Transport of uncharged solutes has been firstly described by continuous hydrodynamic models; later porous membranes were modeled as bundles of straight cylindrical pores and solute transport was corrected on account of hindered diffusion and convection cause by solute-membrane interactions, owing to the moving of a species in a confined spaces.

Nowadays, it is recognized that the separation mechanism of the process is remarkably related to the steric and electrostatic partitioning effects between the membrane and the external solutions.

In the case of neutral solutes, partitioning between feed and membrane is mainly related to size exclusion effects, and molecular weight cutoff is generally sufficient to describe the separation efficiency of the membrane. In the case of electrolyte solutions, rejection properties of NF membrane are remarkably affected by type and valence of the ionic species as well as by the type of membrane material and strongly depend on operative conditions such as pH and ionic strength values existing in the feed side.

There are several models describing the mass transfer in a NF membrane: the solution-diffusion model (Lonsdale 1965), the irreversible thermodynamics model described by Kedem and Katchalsky (1958), Maxwell-Stefan equation (Mason and Lonsdale 1990), and

recent structural models [(Spiegler and Kedem 1966), (Bowen, Mohammad and Hilal 1997), (Bandini and Vezzani 2003), (Szymczyk and Fievet 2005), (Bandini and Bruni 2010)].

Most of the recently developed models accept a porous vision of the membrane and describe mass transfer through the extended Nernst-Planck (*ENP*) equation. In addition, *ENP* equation is appropriately modified by some authors for taking into account of the hindered transport through narrow pores comparable with the molecular dimensions of the permeating species.

All the models make use of several parameters to characterize the membrane: there are structural parameters, such as average pore radius, membrane thickness, tortuosity, and porosity; electrical parameters, such as surface or volume membrane charge; and electrochemical parameters, such as the dielectric constants of the membrane and of the solution inside/outside the pores. In addition, depending on the authors, all the parameters are considered as adjustable parameters or, alternatively, some of them can be obtained by independent measurements, such as tangential streaming potential as well as atomic force microscopy.

The more advanced models describe: (*i*) Solute partitioning at the interfaces between the membrane and the external phases; (*ii*) solute transport across the membrane; and (*iii*) water or total flux across the membrane.

Typically solute and membrane properties are identified by several parameters: *Stokes* radius (r_s) is used to describe the solute size, as well as average pore radius (r_p), effective membrane thickness (δ) and pore geometry (usually cylindrical) are used to characterize membrane itself. The most common procedure used for parameters calculation involves several steps:

- a) Calculation of Stokes radius of the solute;
- b) Calculation of pore radius from asymptotic rejection data;
- c) Application of a porous viscous vision, accounting of Hagen-Poiseuille equation, for the calculation of the effective membrane thickness, by using hydraulic permeability data.

The critical aspects of this procedure are manifold:

- i) Membrane parameters are fitted from time to time for each solute; thus each solute is associated with a defined couple of parameter (r_p , δ), although the membrane is the same;

- ii) Both parameters are validated by comparing model predictions with experimental rejection data, generally available at conditions very close to asymptotic rejections. Lack of well-defined data in the low flux region, hinders determination of the δ which is significant in the diffusive transfer zone;
- iii) Stokes radius is not a representative parameter for solute size, because it does not account for the orientation of non-spherical molecules, of phenomena that take place in solution, such as dehydration or complexation effects, as well as of membrane-solute interactions.

In this work *Donnan Steric Pore and Dielectric Exclusion Model (DSP&DE)* is used as basic tool for data elaboration. The numerous experimental data available in *Chapter 3* and their high reproducibility allow us to revise the basic DSP&DE model. In addition, the availability of a good modelling allows to interpret the experimental results.

Key points of modelling are:

- a) Identification of the suitable parameters;
- b) Evaluation of a proper procedure for membrane characterization;
- c) Model validation in the case of aqueous mixtures containing sugars;
- d) Module and process simulation.

4.2 The revised DSP&DE Model: Theoretical Background

4.2.1 The general Physical Problem

In this section, basic elements of the revised *DSP&DE* model for food *NF* applications are reported. The standard *DSP&DE* (Bandini and Bruni 2010) is an extension of the original *DSPM* developed by (Bowen and Mukhtar 1996).

With reference to the scheme reported in Fig. 4.1, *NF* membrane separates two aqueous liquid phases (the feed, and the permeate) kept at different pressure value (ΔP); the main operative variables are related to the feed conditions (kind of solutes, concentration, pH, temperature, pressure, and flow rate) and to the permeate conditions (the pressure downstream the membrane). Depending on the membrane material as well as on the feed conditions, the membrane generally assumes a surface charge located at each interface existing between a liquid phase and the polymeric material.

In order to characterize the membrane performances the solute flux (J_s) as well as the water flux ($J_{v,w}$) through the membrane should be calculated in order to evaluate real rejection, R_{real} , and total transmembrane flux, (J_v). With reference to a generic section of the membrane, (Fig. 4.1) the problem can be considered in a plane geometry:

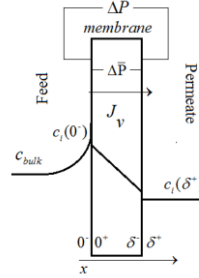


Figure 4.1 Scheme of a generic membrane section, referring to a plane geometry

The membrane is considered as a bundle of identical pores whose length is much larger than their diameter and the motion of the species is assumed as unidirectional through the membrane.

The set of basic equations of the revised *DSP&DE* model for neutral solutes is summarized in Table 4.1:

Table 4.1: Basic equations of the revised *DSP&DE* model

<i>DSP&DE: Model equation ($i=1, \dots, n$ solutes)</i>		
Total flux	$J_v = L_p (\Delta P - \sum_{i=1}^n \sigma_{v,i} \Delta \pi_i)$	(4.1)
Hydraulic Permeability	$L_{p,w}(T) \eta_w(T) = L_{p,w}(T^0) \eta_w(T^0)$	(4.2)
Membrane Permeability	$L_p(T) \eta(c_{inside}, T) = L_{p,w}(T) \eta_w(T)$	(4.3)
Osmotic Pressure difference	$\Delta \pi_i = \pi(c_{I,i}) - \pi(c_{P,i})$	(4.4)
Diffusivity	$D_{S,i}(T) = D_i^0(T) \cdot \left(\frac{\eta_w(T)}{\eta_{bulk,i}(T)} \right)^{0.45}$	(4.5)
Hindered diffusivity	$D_{ip} = K_{id} D_i^0(T) \left(\frac{\eta_w(T)}{\eta(c_{inside}, T)} \right)^{0.45}$	(4.6)
Concentration inside pore	$c_{inside} = \sum_{i=1}^n \phi_i \frac{c_{I,i} + c_{P,i}}{2}$	(4.7)

<i>Peclét number</i>	$Pe_i = \frac{J_v K_{ic} \delta}{D_{ip}} \quad (4.8)$	
<i>Real rejection</i>	$R_{real,i} = 1 - \frac{K_{ic} \phi_i}{1 - (1 - K_{ic} \phi_i) \exp(-Pe_i)} = 1 - \frac{c_{P,i}}{c_{I,i}} \quad (4.9)$	
<i>Observed rejection</i>	$R_{obs,i} = 1 - \frac{c_{P,i}}{c_{bulk,i}} \quad (4.10)$	
<i>Staverman reflection coefficient</i>	$\sigma_{v,i} = 1 - \phi_i \quad (4.11)$	
<i>Asymptotic rejection</i>	$\sigma_{S,i} = \lim_{Pe_i \rightarrow \infty} R_{real,i} = 1 - K_{ic} \phi_i \quad (4.12)$	
<i>Slit-like pore geometry</i> (Deen 1987), (Faxen 1922), $0 \leq \lambda_i < 1$		
<i>Steric partitioning</i>	$\phi_i = (1 - \lambda_i) \quad (4.13)$	
<i>Hindrance factor to convection</i>	$K_{ic} = \frac{1}{2} (3 - \phi_i^2) (1 - \frac{\lambda_i^2}{3} + O(\lambda_i^3)) \quad (4.14)$	
<i>Hindrance factor to diffusion</i>	$K_{id} = 1 - 1.004\lambda_i + 0.418\lambda_i^3 + 0.21\lambda_i^4 - 0.169\lambda_i^5 + O(\lambda_i^6) \quad (4.15)$	
<i>Cylindrical pore geometry</i> , (Bungay and Brenner 1973), $0 \leq \lambda_i < 1$		
<i>Steric partitioning</i>	$\phi_i = (1 - \lambda_i)^2 \quad (4.16)$	
<i>Hindrance factor to convection</i>	$K_{ic} = (2 - \phi_i) \frac{K_{i,s}}{2K_{i,t}} \quad (4.17)$	
<i>Hindrance factor to diffusion</i>	$K_{id} = \frac{6\pi}{K_{i,t}} \quad (4.18)$	
	$K_{i,t} = \frac{9}{4} \pi^2 \sqrt{2} (1 - \lambda_i)^{-\frac{5}{2}} \left[1 + \sum_{n=1}^2 a_n (1 - \lambda_i)^n \right] + \sum_{n=0}^4 a_{n+3} \lambda_i^n \quad (4.19)$	
	$a_1 = -73/60, a_2 = 77.293/50.400, a_3 = -22.5083, a_4 = -5.6117$	
	$a_5 = -0.3363, a_6 = -1.216, a_7 = 1.647$	
	$K_{i,s} = \frac{9}{4} \pi^2 \sqrt{2} (1 - \lambda_i)^{-\frac{5}{2}} \left[1 + \sum_{n=1}^2 b_n (1 - \lambda_i)^n \right] + \sum_{n=0}^4 b_{n+3} \lambda_i^n \quad (4.20)$	
	$b_1 = 7/60, b_2 = -2.227/50.400, b_3 = 4.0180, b_4 = -3.9788$	

$$b_5 = -1.9215, b_6 = 4.392, b_7 = 5.006$$

The revised model contains the dependence from several parameters, particularly from:

- i) Hydraulic permeability, $L_{p,w}$;
- ii) Hydrodynamic coefficient, λ_i ;
- iii) Effective membrane thickness, δ .

Assuming a pore geometry, in the case in which the model parameters are known, equations in Tab. 4.1 can be solved in order to characterize membrane performances. The model then can be used for the simulation of a membrane module in a *NF* process. Alternatively, the same set of equations can be used to calculate all the model parameters, or any of them, as adjustable parameters.

In order to predict the *NF* performance of single solutes, but especially for better understand multicomponent mixtures behavior, it is necessary to consider the mass transfer both across the membrane and within the film layer at the interface of feed solution/membrane.

4.2.2 Solute partitioning

Partitioning of the specie i at the interfaces between the membrane and the external solutions is described through the general following equations:

$$\frac{c_i(0^+)}{c_i(0^-)} = \phi_i \frac{\gamma_i(0^-)}{\gamma_i(0^+)} \exp(-z_i \Delta \psi_{D0}) \exp(-z_i^2 \Delta W_{DE0}) \quad (4.21a)$$

$$\frac{c_i(\delta^-)}{c_i(\delta^+)} = \phi_i \frac{\gamma_i(\delta^+)}{\gamma_i(\delta^-)} \exp(-z_i \Delta \psi_{D\delta}) \exp(-z_i^2 \Delta W_{DE\delta}) \quad (4.21b)$$

With reference to charged solutes, the ion partitioning coefficient at each interface takes into account of four contributions: steric exclusion, through ϕ_i , nonideality of the solutions, through activity coefficients γ_i , Donnan equilibrium, through $\Delta \psi_D$, and Dielectric Exclusion, through ΔW_{DE} , which are widely discussed in literature [(Bowen, Mohammad and Hilal 1997), (Szymczyk and Fievet 2005), (Bandini and Vezzani 2003), (Bandini and Bruni 2010)].

In the case of neutral solutes, steric exclusion and activity coefficients are the only partitioning effects existing. Steric exclusion accounts for the sieve effect, due to the intrinsic porosity of the membrane; it depends on the pore geometry and ranges from 0 (for

solutes larger than the pore radius) to 1 (for point solutes). In the case of neutral solutes, activity coefficients can be expressed making use of the typical models used in thermodynamics.

In this work, in view of the low values of molar concentrations of sugars, the ratio between activity coefficients is assumed to be equal to 1, so doing the following relationships for partitioning coefficients:

$$\frac{c_i(0^+)}{c_i(0^-)} = \phi_i \quad (4.22a)$$

$$\frac{c_i(\delta^-)}{c_i(\delta^+)} = \phi_i \quad (4.22b)$$

Solute partitioning coefficient at both membrane/solution interfaces is thus given once pore geometry and λ_i have been fixed, in view of the corresponding relations for ϕ_i (Eq. (4.13) and Eq. (4.16)).

4.2.3 Total flux

Experimental data performed on *NF* of pure water, as well as of aqueous solutions containing electrolytes and/or neutral solutes clearly put in evidence that there is a linear proportionality between the total trans-membrane flux, $J_{v,exp}$, and the driving force maintained across the membrane, ΔP_{eff} . As a consequence, the standard relationships, typically used for *RO*, can be considered in which the total volume flux, J_v , linearly depends on the effective pressure difference across the membrane, ΔP_{eff} , through the membrane permeability L_p , according to the following equation:

$$J_v = L_p \Delta P_{eff} = L_p (\Delta P - \sigma_v \Delta \pi) \quad (4.1)$$

$$\Delta \pi = \pi(0^-) - \pi(\delta^+) \quad (4.4)$$

In which $\Delta \pi$ is the osmotic pressure difference across the membrane, which must be calculated at the composition values existing at the membrane/external phases interfaces, in the case in which concentration polarization occurs.

Eq. (4.1) can be developed both from irreversible process thermodynamics and from a theoretical statistical approach.

From a *Phenomenological approach* [(Kedem-Spiegler), (Mason and Lonsdale 1990)], σ_v can be related to the asymptotic rejection:

$$\sigma_{V,i} = \lim_{\Delta P \rightarrow \infty} R_{real,i} = R_{real,i}^{\infty} \quad (4.23)$$

For water, Eq. (4.23) can be rewritten in a simplest form:

$$J_{v,w} = L_{p,w} \Delta P \quad (4.24)$$

Where $L_{p,w}$ and ΔP are the hydraulic permeability and difference across the membrane respectively.

Parallel to the *Phenomenological approach*, a *Structural approach* is here developed, applying a porous vision of the membrane.

On the basis of a generic membrane section in plane geometry (Fig. 4.1), permeate flux through the membrane can be expressed as:

$$J_v = L_p \Delta \bar{P} \quad (4.25)$$

Where the term $\Delta \bar{P}$ represents the pressure difference inside the membrane. The definition of $\Delta \bar{P}$ in Eq. (4.25) differs from that based on irreversible thermodynamics where an osmotic (Staverman) reflection coefficient, σ_v , is included, as suggested by (Bowen and Welfoot 2002).

In view of the partitioning phenomena occurring at the solution-membrane interfaces, this quantity can be presented in an explicit form, as follows:

$$\Delta \bar{P} = \Delta P - (\Delta \pi_0 - \Delta \pi_{\delta}) \quad (4.26)$$

$$\Delta \pi_0 = \pi(0^-) - \pi(0^+) \quad (4.27a)$$

$$\Delta \pi_{\delta} = \pi(\delta^-) - \pi(\delta^+) \quad (4.27b)$$

Comparing *Phenomenological* (Eq. (4.1)) to *Structural* (Eq. (4.26)) approaches, the following equation is obtained:

$$(\Delta P - \sigma_v \Delta \pi) = (\Delta P - (\Delta \pi_0 - \Delta \pi_{\delta})) \quad (4.28)$$

The Staverman reflection coefficient assumes the following form:

$$\sigma_v = \frac{\Delta \pi_0 - \Delta \pi_{\delta}}{\Delta \pi} \quad (4.29)$$

Under some simple hypothesis:

- Single solute (i.e. Dextrose)
- Osmotic pressure calculated from *Van 't Hoff law*

$$\Delta\pi_0 = RT \left[c(0^-) - c(0^+) \right] \quad (4.30a)$$

$$\Delta\pi_\delta = RT \left[c(\delta^-) - c(\delta^+) \right] \quad (4.30b)$$

$$\Delta\pi = RT \left[c(0^-) - c(\delta^+) \right] \quad (4.31)$$

- Partitioning coefficient (Eq. (4.22a), (4.22b))

Staverman reflection coefficient can be rewritten according the following equation:

$$\sigma_v = 1 - \frac{\phi \left[\pi(0^-) - \pi(\delta^+) \right]}{\Delta\pi} = 1 - \phi \quad (4.32)$$

Table 4.2: Comparison between Phenomenological and structural models, in order to identify the Staverman reflection coefficient, in Eq. 4.x, in the case of neutral solute

$$\sigma_v = \frac{\Delta\pi_0 - \Delta\pi_\delta}{RT} = [c(0^-)(1 - \phi_0)] - [c(\delta^+)(1 - \phi_\delta)] \quad (4.33)$$

$$\Delta\pi_0 - \Delta\pi_\delta = (1 - \phi_0)\pi(0^-) - (1 - \phi_\delta)\pi(\delta^+) \quad (4.34)$$

$$J_v = L_p [\Delta P - [(1 - \phi_0)\pi(0^-) - (1 - \phi_\delta)\pi(\delta^+)]] = L_p [\Delta P - \sigma_v \Delta\pi] \quad (4.35)$$

$$\sigma_v = 1 - \frac{\phi_0\pi(0^-) - \phi_\delta\pi(\delta^+)}{\Delta\pi} \quad (4.36)$$

$$\sigma_v = 1 - \phi \frac{[\pi(0^-) - \pi(\delta^+)]}{\Delta\pi} = 1 - \phi \quad (4.32)$$

Comparing *Phenomenological* and *Structural* model, Staverman reflection coefficient, σ_v , defined in Eq. (4.32), deviates from the asymptotic rejection, as assumed in Eq. (4.12) (see Tab. 4.1). The deviation depends on both λ_i value and pore geometry.

A comparison between σ_S and σ_V behavior as a function of pore geometry and hydrodynamic coefficient is proposed *Section 4.1.7*.

4.2.4 Hydraulic and Membrane permeability: $L_{p,w}$ and L_p

Both hydraulic and membrane permeability are key parameters in the revised *DSP&DE* model. Typically hydraulic permeability values can be obtained from membrane technical sheet, however as shown in the previous chapter only qualitative behavior can be drawn, thus it is recommended to get an experimental value.

In several studies permeability value changes processing strong electrolyte and it can be function of pH. Typically alkaline cleaning increase the membrane water flux and decrease

the retention of dextrose (Manttari, Pihlajamaki and Kaipainem, et al. 2002) A decrease in permeability can be attributed to elevated operating temperatures (above the recommended temperature, typically 55°C): high temperature as well as high operating pressures could lead to a membrane compaction, resulting in permanent loss of permeability. A relation between membrane swelling and an increase in the intrinsic membrane permeability with salinity and pH was already found with *AFM*¹ measurements (Freger 2004).

Hydraulic permeability in dense membranes generally depends on temperature according to Arrhenius type equation, which has been confirmed by experiments in *Chapter 3*.

Dependence of hydraulic permeability on temperature can be also described by a porous viscous vision of the membrane, according Hagen-Poiseuille equation: Under the hypothesis of constant pressure gradient along the membrane pore, the Hagen-Poiseuille flow can be considered according to:

$$J_v = \frac{r_p^2}{c\eta\delta} \Delta P_{eff} \quad (4.37)$$

In which c is a constant that depends on pore geometry. Pore geometry is somewhat critical to describe, typically it varies from slit-like to cylindrical. As a consequence the c value ranges from 3 for slit-like pore to 8 for cylindrical pore geometry.

Hagen-Poiseuille equation correlates the membrane permeability, L_p , to the effective membrane thickness, δ , consisting of tortuosity and porosity, through the mean pore radius, r_p .

When *NF* is performed with pure water, L_p represents the hydraulic permeability, $L_{p,w}$, as a consequence, the viscosity of the solution inside the pore corresponds to the water viscosity inside the pore.

L_p at fixed pore geometry, is a constant which depends on membrane parameters (r_p , δ) and solution viscosity inside pores, which contains the temperature dependence.

Unfortunately, there is a certain level of uncertainty in determining that quantity, since the assumption of bulk solvent properties may not be valid within narrow pores: the use of bulk water viscosity η_0 may lead to an overestimation of $L_{p,w}$, since the actual viscosity η may be increased with respect to η_0 by interactions of water dipole with the charge pore walls. The problem has been studied in detail by (Bowen and Welfoot 2002), and it was recognized that the ratio η/η_0 can be assumed closed to 10.

¹ *Atomic Force Microscopy*

Equation (4.37), under the hypothesis of constant membrane parameters (r_p , δ) in the whole range of temperature, leads to Eq. (4.38):

$$L_{p,w}(T)\eta_w(T) = \text{const} \quad (4.38)$$

Experimental evidence of it was obtained in *Chapter 3*, in which:

$$L_{p,w}(T)\eta_w(T) = L_{p,w}(T^0)\eta_w(T^0) \quad (4.39)$$

Where T^0 is a reference temperature, thus confirming that no swelling is observed.

When sugar solutions are processed, membrane permeability is a function of temperature and concentration inside the pore, c_{inside} , and Eq. (4.38) is revised to account for concentration inside the pore, according Eq. (4.40):

$$L_p(T)\eta(c_{\text{inside}}, T) = L_{p,w}(T)\eta_w(T) \quad (4.40)$$

In order to understand the right c_{inside} value, experimental data have been compared with model prediction at different pore concentration. The best correlation that describe concentration inside the pore and fits experimental data shows the following for (Eq. 4.7):

$$c_{\text{inside},i} = \phi_i \frac{c_i(0^-) + c_i(\delta^+)}{2} \quad (4.7)$$

The equation contains inside it the dependence from pore geometry selected, through the steric partitioning coefficient, ϕ_i . The composition inside the pore is given by the theory of solute partitioning. This value is confirmed by experimental data and depend on pore geometry (through ϕ_i), type of solute (for high values of λ_i , $\phi_i \approx 0$) and is a function of feed/permeate concentrations.

4.2.5 Solute flux

The basic equation for the description of mass transfer of a generic specie across the membrane is the extended Nerst-Planck equation (*ENP*). Since in *NF* dilute aqueous solutions are processed, under the approximation of no direct coupling between solutes the flux of each species, j_i , can be written as a function of the electrochemical potential:

$$j_i = K_{ic}c_iJ_v - \frac{c_iD_{ip}}{RT} \frac{d\tilde{\mu}_i}{dx} \quad (4.41)$$

In which D_{ip} is the hindered diffusivity of the specie inside the pore, defined as:

$$D_{ip}\eta = K_{id}D_{i,\infty}\eta_0 \quad (4.42)$$

Where $D_{i\infty}$ is the diffusivity of the specie i in water at infinite dilution, and K_{ic} and K_{id} are the hindrance actors for convection and diffusion, respectively. It must be observed that the axial coordinate x accounts for both tortuosity and the porosity of the membrane; the membrane thickness resulting from the integration of Equation (4.41) is defined as the effective membrane thickness, δ .

Equation (4.41) can be rewritten in an explicit form, accounting for the dependence of the electrochemical potential on activity, pressure, as well as on the electrostatic potential, according to Equation 4.43:

$$j_i = K_{ic}c_iJ_v - c_iD_{ip} \frac{d \ln \gamma_i}{dx} - D_{ip} \frac{dc_i}{dx} - \frac{c_iD_{ip}\bar{V}_i}{RT} \frac{dP}{dx} - z_i c_i D_{ip} \frac{F}{RT} \frac{d\Psi}{dx} \quad (4.43)$$

Which can be easily simplified into Eq. (4.44) neglecting the contributions of the gradient of $\ln\gamma_i$ as well as of the pressure gradient on the solute flux.

$$j_i = K_{ic}c_iJ_v - D_{ip} \frac{dc_i}{dx} - z_i c_i D_{ip} \frac{F}{RT} \frac{d\Psi}{dx} \quad (4.44)$$

Equation (4.44) is a simplified form of the *ENP* equation accounting for convection, diffusion, and electromigration (in the case of charged solutes) through the membrane pores; it is appropriately modified to account for the hindered transport of the permeating species through narrow pores comparable with the molecular dimensions. The meaning and relevance of hindrance factors K_{ic} and K_{id} have been widely (extensively) documented by (Deen 1987) as well as by many authors, as reported by (Bandini and Bruni 2010).

Solutes moving in free solution experience a drag force exerted by the solvent; when solutes move in confined spaces, such as membrane pores the drag is altered and the transport may be considered to be hindered (Bowen and Mukhtar 1996).

K_{ic} is a drag factor accounting for the effects of the pore walls on the specie transfer; K_{id} represents the effect of the pore to reduce the solute-solvent diffusivity below the value in the free bulk solution, $D_{i,\infty}$. Hindrance factors are related to hydrodynamic coefficients calculated from the solution of the motion problem of a spherical specie inside cylindrical as well as slit-like pores of infinite length; they depend on the solute to pore-size ratio, λ_i . Many relationships have been proposed in order to calculate the proper hindrance factor.

In Table 4.1 a couple of representing relationship is proposed to calculate hindrance factors for cylindrical as well as for slit geometry. Equations listed are considered suitable for sugar, since λ_i in case of mono- and di-saccharides, is very close to 1.

It should be noted that hindrance factors depend not only on λ_i but also on pore geometry, as well as on the radial position within the pore; in these equations the solute particle is located at centerline radial coordinate of the pore (Centerline approximation), according to other solutions the solute particle is located at different radial coordinates of the pore, like cross-sectional average, solvent velocity parabolic profile, etc.)

With reference to the generic section of the membrane (Fig. 4.1), for uncharged solutes the transport inside the pores can be simplified in the form of:

$$j_i = K_{ic}c_iJ_v - D_{ip} \frac{dc_i}{dx} \quad (4.45)$$

Transport of uncharged solutes happens by convection due to the applied pressure difference and by diffusion due to the concentration gradient that appears across the membrane. At low pressures, both terms contribute to the transport of solutes through the membrane. Close to the infinite pressure, diffusion term is negligible, compared to the infinite convective flux.

The ENP equation (Eq. (4.45)) can be rewritten to obtain a relationship for the concentration gradient of each specie; in addition it can be rearranged into equation:

$$\frac{dc_i}{dx} = \frac{J_v}{D_{ip}} [K_{ic}c_i - c_i(\delta^+)] = \frac{Pe_i}{\delta} \left[c_i \frac{(\delta^+)}{K_{ic}} \right] \quad (4.46)$$

in which the parameter Pe_i is defined in a straightforward manner (Tab. 4.1):

$$Pe_i = \frac{J_v K_{ic} \delta}{D_{ip}} \quad (4.8)$$

It can be observed that Pe_i is independent of the membrane thickness, since membrane permeability can be considered inversely proportional to δ . In view of the porous nature of the membrane, by applying Hagen-Poiseuille flow type, the following relationships can be also obtained to calculate Pe_i :

$$Pe_i = \frac{J_v K_{ic} \delta}{D_{ip}} = \frac{L'_p \Delta P_{eff} K_{ic}}{D_{ip}} = \frac{r_p^2 \Delta P_{eff} K_{ic}}{c \eta D_{ip}} = \frac{r_p^2 \Delta P_{eff} K_{ic}}{c \eta_0 K_{id} D_{i,\infty}} = \frac{J_v r_p^2 K_{ic}}{L_p c \eta_0 K_{id} D_{i,\infty}} \propto J_v r_p^2 \quad (4.47)$$

In which L'_p represents a kind of permeability coefficient including all the membrane characteristics with the exception of the effective thickness. Apparently, independently of

the pore geometry (c is a constant depending on pore geometry), Pe_i can be assumed related to r_p^2 , approximately.

When we are faced with the problem of calculating the membrane parameters, r_p calculation can be performed separately from the determination of the effective membrane thickness.

As a consequence the concentration gradient is inversely proportional to the membrane thickness. Therefore, the concentration difference across the membrane thickness and the rejection of each solute will be independent of δ as well. However this conclusion does not mean that one can calculate rejection assuming an arbitrary membrane thickness, rather that, after the right calculation of Pe_i any membrane thickness can give the right retention. The problem is then transferred into the determination of the parameter Pe_i which can be expressed according to one of the relationships reported in Eq. (4.47), depending on which parameters are known with a better precision. The knowledge of δ is, however, required for the calculation of concentration profiles.

4.2.6 Rejection of neutral solutes

In the case of neutral solutes, the integration of Eq. (4.46) over the membrane thickness, δ , leads to a simple analytical relationship for the solute rejection:

$$R_{real,i} = 1 - \frac{K_{ic}\phi_i}{1 - (1 - K_{ic}\phi_i)e^{-Pe_i}} \quad (4.9)$$

The asymptotic retention is reached at infinite *Peclet* number:

$$R_{real,i}^\infty = \lim_{Pe_i \rightarrow \infty} R_{real,i} = 1 - K_{ic}\phi_i \quad (4.12)$$

In this case Pe_i assumes the meaning of a hindered *Peclet* number of the uncharged solute. Apparently, the solute rejection depends on the pore geometry, and on λ_i , through ϕ_i , K_{ic} and K_{id} contained in Pe_i . At very high volume fluxes, the asymptotic rejection is obtained in the limiting case of $Pe_i \rightarrow \infty$; apparently, asymptotic rejection depends on the pore geometry and λ_i , as well as on the partitioning at the feed/membrane interface only.

4.2.7 Dependence of revised model parameters from pore geometry

The revised *DSP&DE* model discussed contains the dependence from pore geometry, particularly for:

- Steric partitioning coefficient, ϕ_i
- Hindrance factors for convection and diffusion, K_{ic} and K_{id} respectively;
- Staverman reflection coefficient, σ_V and asymptotic rejection, σ_S .

Most of authors assume a cylindrical pore geometry for calculating these parameters [(Mohammad, Basha and Leo 2010), (Otero, Lena, et al. 2006), (Kuhn, et al. 2010)].

Just a few authors state that the best description of experimental data was obtained assuming slit-like pores [(Bandini and Vezzani 2003), (Bandini and Bruni 2010)], others (Cavaco Morao, et al. 2008) verified both pore geometries.

As a rule of thumb, the Staverman reflection coefficient, σ_V , is determined experimentally, and assumed equal to the asymptotic rejection (Cuartas-Uribe, et al. 2007), however by using phenomenological equation [(Van der Bruggen, Schaep, et al. 2000), (Van der Bruggen and Vandecasteele 2002)] became possible to predict rejections based on two key parameters: solute size and mean pore radius, describing a pore radius distribution.

In this work, as suggested before, both pore geometries have been analyzed in order to determine the best geometry describing experimental data, further it has proved that Staverman reflection coefficient differs from asymptotic rejection.

In Table 4.1 the list of correlations is proposed for both geometries. Hindrance factor equations have been selected on the basis of the range of validity for λ_i , which in the case of sugars is next to one.

Correlations put in evidence the dependence of the main parameters of the model (i.e. steric partition coefficient, Staverman reflection coefficient, asymptotic rejection, as well as hindered coefficients) from hydrodynamic coefficient (λ_i) and pore geometry.

A comparison between model parameter, as a function of hydrodynamic coefficient, is depicted in Fig. 4.2 for both pore geometries.

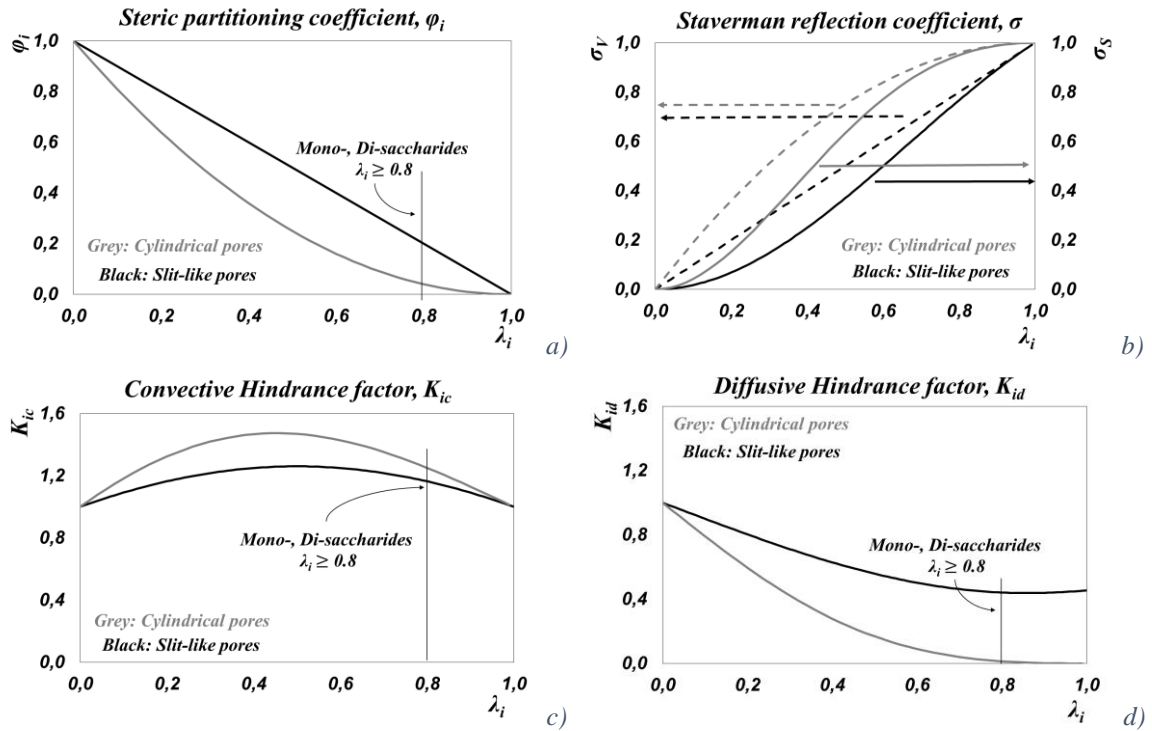


Figure 4.2: Model parameter as a function of solute to pore-size ratio (λ_i): Steric partitioning coefficient (a), Staverman reflection coefficient and asymptotic rejection (b), Hindrance factors for convection (c) and Diffusion (d). Comparison between Slit-like pore geometry (black lines) (Deen 1987) (Faxen 1922) and Cylindrical pore geometry (grey lines) (Bungay and Brenner 1973)

Differences between σ coefficients are related to both pore geometry ($\sigma_{cyl}(\lambda_i) > \sigma_{slit}$) and solute to pore-size ratio, λ_i : when oligosaccharide are processed in NF membranes (typically $\lambda_i \geq 0.8$) coefficients are very similar to each other, for both pore geometries, thus Staverman reflection coefficient is very close to asymptotic rejection value. In the cases in which totally rejected solutes are processed, its contribution is clearly negligible, however, since sugars (in this study mono- and disaccharides) present rejection values ranging from 0.2 to 0.95 this term must be taken into account.

When the neutral solute is a mono- or a disaccharide the solute to pore size ratio, λ_i , will be greater than 0.8. In this proper case Fig.(4.2) put in evidence that if on one side convective hindrance factor is equal for both pore geometries ($K_{ic,slit} \approx K_{ic,cyl}$, when $\lambda_i \geq 0.8$), on the other side diffusive hindrance factor assumes different values depending on the pore geometry ($K_{id,slit} > K_{id,cyl}$, $K_{id,cyl} \rightarrow 0$, when $\lambda_i \geq 0.8$).

Particularly for a cylindrical pore geometry, when K_{id} parameter approaches zero ($\lambda_i \geq 0.8$), *Peclét* number tends to infinite values.

As will be shown later, a cylindrical pore geometry gives very low values for the effective membrane thickness, which are typical of high permeate flux. In this flow regime, the diffusion is not a prevalent, and the mass transport is governed mainly by convection.

Tab.4.2: Sugar and Ionic properties and hydrodynamic coefficient λ_i , for $r_p = 0.380$ nm

	<i>Oligosaccharides</i>			<i>Electrolytes (Bowen & Mukhtar (1996))</i>		
	<i>DX</i>	<i>FR</i>	<i>ML</i>	<i>Na⁺</i>	<i>Cl⁻</i>	<i>SO₄²⁻</i>
<i>D_{i,∞} × 10⁹ [m²/s] @ 25°C</i>	0.679	0.686	0.480	1.333	2.031	1.062
<i>r_s × 10⁹ [m²/s]</i>	0.361	0.357	0.470	0.184	0.121	0.231
<i>λ</i>	0.940	0.930	1	0.470	0.310	0.600

Calculation of all these parameters requires *a priori* the knowledge of the hydrodynamic coefficient (λ_i), that in turn requires the knowledge of molecule (r_s) and pore radii (r_p). In Tab. 4.2 molecule radii derive from Stokes-Einstein equation, and pore radius is assumed to be equal to 0.380 nm. This procedure allow to obtain a range of λ_i values, just to compare sugars and electrolytes.

It should be noted in Fig.4.2 that the correction for hindered diffusion is substantially greater than the correction for hindered convection.

4.3 The problem of parameters calculation: critical analysis of current approach

4.3.1 Parameter calculation: state of art

Contemporary to development of the various *DSP&DE* model versions, many procedures have been proposed for the calculation of the membrane parameters.

The information supplied by manufacturers is limited to the molecular weight cut-off of the membrane, permeate flux and retention of given molecules (typically electrolytes), at fixed operating conditions; however datasheet reduction gives only indications on hydraulic permeability values.

To overcome the lack of information, membrane properties should be obtained from a limited number of experiments with model liquids. The advantage of tools able to predict membrane performances is that costs can be saved by reducing the number of these experiments (Straatsma, et al. 2002).

In case of neutral solutes, from the application of Donnan-Steric models, the mean pore radius (r_p) and the effective membrane thickness (δ) are the parameters required to describe retention behavior on the basis of the sieving effect during transport.

These “model” parameters are usually obtained by fitting the model to solute retentions and membrane fluxes measured in membrane characterization experiments using pure water and single sugar solutions (Straatsma, et al. 2002).

Many authors express the parameter λ_i as the ratio between the Stokes radius of the i -th molecule ($r_{S,i}(25^\circ C)$) and the pore radius of the membrane (r_p), assuming that: *i*) molecules are spherical (no orientation is taken into account); *ii*) solute properties are constant in the whole range of operative conditions (no hydration, complex formation or salting out effect occurs), according Eq. (4.48),

$$\lambda_i = \frac{r_{S,i}(25^\circ C)}{r_p} \quad (4.48)$$

The Stokes radius, $r_{S,i}$, of a solute i is calculated by using the well-known Stokes-Einstein equation, derived for the motion of spherical solutes in liquid:

$$r_{S,i} = \frac{k_B T}{6\pi\eta D_{i,\infty}} \quad (4.49)$$

Where k_B is the Boltzmann constant, T the absolute temperature, η the solvent bulk viscosity, and $D_{i,\infty}$ the bulk diffusivity at infinite dilution. In this equation molecular dimension is strongly related to diffusion coefficient as well as it is an important parameter that affects solute transport properties in the pore.

Based on the asymptotic limiting rejection, the effective pore radius, r_p , can be fitted by using Eq. (4.12). Typical values from literature (Table 4.3) shows how pore radius defined from Eq. (4.48) is strictly dependent from the solute on which the parameter is fitted.

Once pore radius has been fitted, most of authors [(Otero, Mazarrasa, et al. 2008), (Bargeman 2014), (Kuhn, et al. 2010), (Labbez, Flevet, et al. 2003), (Mohammad, Basha and Leo 2010)] correlate pore radius (r_p), effective membrane thickness (δ) and hydraulic permeability ($L_{p,w}$), by assuming cylindrical pore geometry, according the following Hagen-Poiseuille equation:

$$L_{p,w} = \frac{r_p^2}{8\eta\delta^*} \quad (4.50)$$

In which δ^* stands for membrane thickness and water viscosity inside the pore is calculated as the bulk value. A schematic representation of this procedure is depicted in Fig. 4.3.

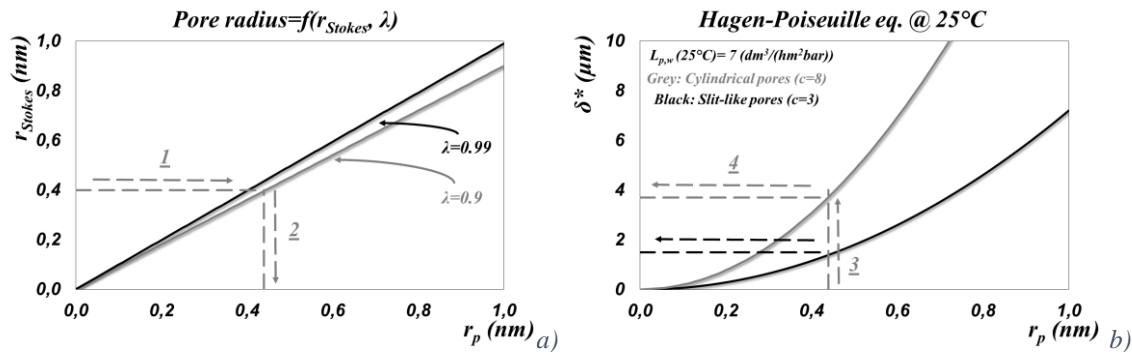


Fig.4.3. Schematic procedure for the calculation of membrane parameters (r_p , δ) documented in literature. (a) Pore radius related to Stokes radius and hydrodynamic coefficient (b) relationship between effective membrane thickness (δ^*) and pore radius (r_p) according Hagen-Poiseuille equation, obtained from pure water Permeability ($7 \text{ dm}^3/(\text{hm}^2\text{bar})$) at 25°C) for both pore geometries, cylindrical pores (grey lines) and slit-like pores (black lines);. Dashed lines represent the calculation procedure, from stokes radius to pore radius (1-2), and from pore radius to effective membrane thickness (3-4).

The limit of this procedure is that for the same membrane, different solutes tested identify different membrane pore radii. Some authors justify it talking about a pore size distribution [(Kuhn, et al. 2010), (Van der Bruggen and Vandecasteele 2002)]. The starting point for this approach is the log-normal distribution used for the calculation of the reflection coefficient as a function of the effective molecular diameter, however by the application of this method an effective membrane thickness distribution is achieved yet. (Nakao and Kimura 1981) showed a relationship between effective membrane thickness and solute size, in particular δ decrease with increasing solute size; however the δ^* value obtained from the pure water permeability was much larger than those obtained from the fitting of rejection data. (Kuhn, et al. 2010), (Van der Bruggen and Vandecasteele 2002) argue that the membrane has a pore size distribution, and when multi-component mixtures are processed each solute will provide a pore radius proportional to its own size. (Kuhn, et al. 2010) processing a fructooligosaccharide mixture, fitted experimental data to a Gaussian function which leads to a mean pore size of 0.52 nm and standard deviation of 0.08 nm

In parallel of these studies, others researchers have proposed to estimate the mean pore radius, r_p , by atomic force microscopy (AFM^2), or rejection of neutral solutes [(Bowen, Mohammad and Hilal 1997), (Bowen, Welfoot and Williams 2002)]. (Otero, Lena, et al. 2006) compared the pore radius fitted from Nanofiltration experiments with the detailed

² Atomic Force Microscopy

pore size distribution obtained from topographic AFM images, and then compared the thickness of the active layer with one obtained from the fitting procedure.

(Déon, et al. 2013) compared the effective membrane thickness obtained from the mean pore radius and the membrane hydraulic permeability with experimental thickness observed with SEM³ + FIB⁴ images. For a GE-DK membrane, the Hagen-Poiseuille equation gives value ($\delta^* \sim 1.2 \mu\text{m}$), while the thickness measured with SEM images of the membrane cross section was found to be $0.095 \pm 0.01 \mu\text{m}$. The discrepancy between the two methods could be attributed to a partial contribution of the membrane support in the membrane overall permeability. In this case, the effective membrane thickness should be considered as a parameter describing both active and a part of support layer, and can't be deduced by SEM images. Although the values obtained are quite similar, the same authors state that the effective membrane thickness cannot be deduced from microscopic images, but has to be deduced from measurements of water flux and neutral solutes rejection. SEM images could not be used for a model parameter assessment, anyhow they can give interesting information.

According to [(Cuartas-Uribe, et al. 2007), (Bargeman, Vollenbroek, et al. 2005), (Bargeman 2014)] the viscosity term in Hagen-Poiseuille equation represents the dynamic viscosity of the solution; thus both the mean pore radius as well as the effective membrane thickness depend on the composition of the solution, and are different from values obtained for pure water, moreover osmotic pressure is taken into account in order to calculate the effective membrane thickness δ^* :

In their study the determination of membrane parameters (r_p, δ^*) is obtained for a solution containing 1 g/dm^3 of dextrose (in this case $L_p=L_{p,w}$ and $\eta=\eta_w$).

Other authors (Rodrigues, et al. 2010) assert that the solvent pore viscosity is equal to one of the aqueous solution adjacent to the membrane surface, this correction according to the authors strongly improves the prediction of the permeate flux, in any case permeate flux predicted by the model overestimate the experimental flux.

(Bowen, Mohammad and Hilal 1997) used two approaches to obtain membrane parameters: (a) independent fitting of experimental data to obtain both parameters (r_p and δ); and then (b) only r_p was fitted while δ was obtained from the permeability data. However the author demonstrated that the permeability data should not to be used to estimate the value of δ for

³ Scanning Electron Microscope

⁴ Focused Ion Beam

membrane having nanometer dimension. (Rosa and de Pinho 1994) tried the same approach, however obtained quite larger standard deviation.

One of the few studies in which Hagen Poiseuille correlation is not used has been published by (Luo and Wan 2011) : they solved equations () by fitting both membrane parameters (r_p , δ) independently.

(Bowen and Welfoot 2002) developed firstly a one-parameter model for uncharged solute rejection as a function of effective pressure difference based on a hydrodynamic description with hindered solute transport within the pores. The only parameter in the model is r_p . However this approach might be right for high permeate flux, that is in convective transport, when $Pe_{cl\grave{e}t}$ number tends to infinite value. In fact in convective transport region, membrane thickness is negligible. A more rigorous analysis shows that rejection is independent of membrane thickness only at high fluxes (unlike supported by (Bowen and Welfoot 2002))

Just few authors (Bargeman, Vollenbroek, et al. 2005) proposed the calculation of both r_p and δ through fitting of the experimental flux and retention, neglecting the effect of the membrane charge and the electrical forces on the transport of neutral solutes.

While (Cavaco Morao, et al. 2008) proposed the calculation of model adjustable parameters for both geometries, however in this case instead of λ_i , they calculated the effective pore size, r_p , from asymptotic retention, while the effective membrane thickness was evaluated from Hagen-Poiseuille equation, for both geometries.

Table 4.3 summarize the main adjustable parameters obtained for commercial *NF* membranes and documented in literature, by applying different methods.

Table 4.3: Membrane Characterization: main results from literature

<i>Membrane</i>	<i>Pore geometry</i>	<i>Test conditions</i>	<i>Solute</i>	<i>Pore radius, r_p (nm)</i>	<i>Effective thickness, δ^* (μm)</i>	<i>Ref.</i>
Desal 5 DL	-	20°C	Glucose	0.45	2.54	(Bargeman, Vollenbroek, et al. 2005)
Desal 5 DK			Glucose	0.42	2.59	
			Glycerine	0.44	2.62	
Desal 5 DK	Cylindrical (Bowen e Sharif 1994)	20°C	Glucose	0.44	2.30	(Bargeman 2014)

TiO ₂ – Tami Industries	Cylindrical (Bungay and Brenner 1973)	25°C	PEG 400	1.22	7.00	(Bouranene, Szymczyk, et al. 2007)
			PEG 600	1.14	3.75	
			PEG 1000	1.17	1.00	
Desal 5 DK	Cylindrical	25°C	Glucose	0.43	-	(Bowen and Welfoot 2002)
			Glycerol	0.45	-	
Desal 5 DL, Spiral Wound 2540	Cylindrical (Bowen & Sharif, (1994))	20°C	Lactose	0.4735	2.838	(Cuartas- Uribe, et al. 2007)
Desal DK	Cylindrical (Dechadilok e Deen 2006) Slit-like (Dechadilok e Deen 2006)	15°C	Glycerol, xylose, glucose -average values-	0.46	2.76	(Cavaco Morao, et al. 2008)
				0.33	3.89	
Desal DK	Cylindrical	25°C	Glucose, PEG 600	0.43	1.2 from H-P eq. 0.095±0.01 from SEM + FIB images	(Déon, et al. 2013)
Desal GH				0.85	7.5 from H-P eq. 0.0325±0.025 from SEM + FIB images	
Desal GH	Cylindrical, (Bungay & Brenner, (1973))	20°C	PEG 600 $r_{\text{Stokes}}=0.61 \text{ nm}^*$	0.875±0.0015	3.96±0.74	(Escoda, Fievet, et al. 2010)
Desal DK	Cylindrical (Bowen & Sharif, (1994))	25°C	glucose	0.43 ±0.01	1.2 ± 0.1	(Escoda, Déon and Fievet 2011)
NP030 Spiral Wound	Cylindrical (Dechadilok & Deen, 2006)	25°C	Fructooligosaccharides, sucrose, glucose, fructose	0.52±0.08 (pore size distribution)	-	(Kuhn, et al. 2010)

Desal DK	Cylindrical		Glucose	0.487	3.92	
	(Bowen & Sharif, (1994))		Sucrose	0.538	4.79	(Mohammad, Basha and Leo 2010)
			Raffinose	0.673	7.49	
Desal 5 DK	Cylindrical	20°C	Glucose	0.46	3.13	(Straatsma, et al. 2002)
AFC30 (PA)	Cylindrical	25°C	Glucose	0.6 ± 0.1	2.7 ± 0.1	(Labbez, Fievet, et al. 2003)
Desal 5 DK	Cylindrical (Bowen)	25°C	Glucose	0.52-0.63	–	(Bouchoux, Roux-de Balmann and Lutin 2005)
PES 5 (Hoechst)	Cylindrical	25°C	Glucose	1.265 ^(a) ; 2.468 ^(b)	1.707 ^(a) ; 18.12 ^(b)	(Bowen, Mohammad and Hilal 1997)
			Sucrose	1.14 ^(a) ; 1.58 ^(b)	1.52 ^(a) ; 7.28 ^(b)	
			Raffinose	1.20 ^(a) ; 1.64 ^(b)	1.24 ^(a) ; 7.84 ^(b)	

*this value was calculated using the correlation proposed by (Afonso, Hagemeyer and Gimbel 2001) between the Stokes radii of PEG and their respective molar mass; (a) independent fit of the data to obtain both parameters (r_p and δ); and (b) only r_p was fitted while δ was obtained from the permeability data

As shown in table, most of data has been obtained with neutral solutes and by assuming cylindrical pore geometry, at room temperature. A common approach is in fact to calculate pore radius from asymptotic rejection, by using Stokes radius (at 25°C), and then from water permeability data and Hagen Poiseuille equation, effective membrane thickness δ is calculated as a consequence.

The state of the art about membrane characterization can be summarized as follows:

- i) r_p fitted on asymptotic rejection, by using Stokes radius;
- ii) Effective membrane thickness calculated from water permeability through Hagen-Poiseuille equation and r_p ;
- iii) Both parameters (r_p , δ) calculated at high fluxes (convective transport region, $Pe \rightarrow \infty$)
- iv) For the same membrane (r_p , δ) calculated with different solutes give different values as a function of the solute MW (i.e. pore size and thickness distribution)

4.3.2 Molecular shape of mono- and disaccharides

The primary property of a semi-permeable membrane is its sieving molecular function, and pore radius is an important parameter to characterize it. When dealing with uncharged solutes in aqueous solutions, the well known hydrodynamic model is commonly used to describe solute rejection by a NF membrane. This model assumes the membrane structure as a bundle of cylindrical or slit-like pores with uniform radius, r_p .

Pore radius can be evaluated by hydrodynamic model (*indirect method*) or by direct measurements. Atomic force microscopy studies have indeed confirmed the porous structure of NF membranes, moreover the pore radius measured with this technique is in accordance with the results obtained from hydrodynamic model calculations [(Bowen, Mohammad and Hilal 1997) (Bowen and Doneva 2000)].

Membranes can be classified according to their structural morphology, as morphology determines separation mechanism and performance. Membrane thickness affect: (i) resistance for mass transfer; (ii) permeability of solvents. Due to these reasons it is important to examine membrane morphology using SEM, this because observation of the membrane surface and section provide interesting information about membrane morphology. Fig. 4.4 put in evidence the asymmetric structure of a DK membrane.

As suggested by (Manttari, Pihlajamaki and Nystrom 2006) NF membranes do not have real pores but just free volume inside the polymer chain network, and this find confirmation in SEM images (Fig. 4.4).

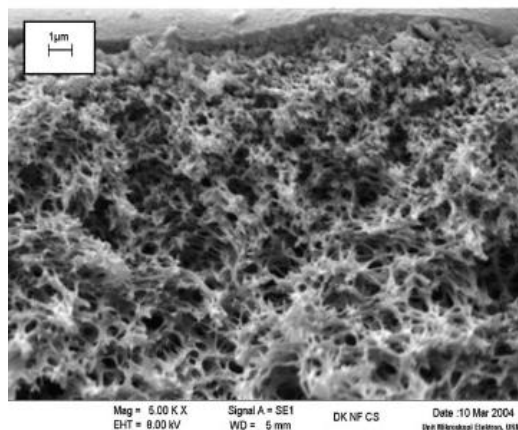


Fig.4.4: SEM pictures showing cross sectional view of GE-DK membrane (Mohammad, Basha and Leo 2010)

Evaluation of pore radius based through pore model is based on rejection data of hydrophilic organic compounds such as saccharides, because neutral solutes show weak

interaction with membrane polymer. From this point of view membrane pore radius, solute radius, water viscosity and diffusivity are critical parameters for this model.

(Afonso, Hagemeyer and Gimbel 2001) defined a correlation between the Stokes radii of the PEGs (determined by the Stokes-Einstein equation) and the respective molecular weight, although it is well known that the PEGs are not spherical molecules and that membranes bear a pore size distribution.

Nevertheless, due to the spherical geometry assumption, the Stokes-Einstein equation is not able to describe the diffusion of non-spherical solutes as well as to account for preferential solute orientation during permeation. When Stokes radius is defined, the solute is assumed to be rigid and spherical; this assumption could be true if mono-saccharides are studied (i.e. Xylose, Dextrose, as well as Fructose), but this hypothesis becomes restrictive in the case of disaccharides (Kiso, Muroshige, et al. 2010). Moreover the Stokes model is not able to take into account for solute orientation and hydration effects which occur with temperature, concentration and salt in solution (Seuvre and Mathlouthi 2010). This last assumption is valid when a generic sugar is dissolved in a solution. Sugar chemistry in aqueous solutions is quite complex and this aspect was discussed previously in *Chapter 2*. According pore model, the molecule transport is described by two main steps:

- i)* partitioning between the bulk phase and the pore area;
- ii)* transport (convective and diffusive) through the pore.

As mentioned by (Van der Bruggen, Schaep, et al. 1999) molecule orientation with respect to the pore surface may alter the partition process. The steric partition factor is defined as the ratio of the solute accessible area to the pore area. When the solute is spherical, the steric partitioning coefficient ϕ is expressed in terms of λ_i , the ratio of solute to pore radius. However when non spherical solutes are studied, the steric partitioning factor may be affected by molecular shape (Van der Bruggen, Schaep, et al. 1999).

Molecular shape influence solute transport, including convective and diffusive transport and partitioning between solution and membrane. These aspect have been discussed by some author (Van der Bruggen, Schaep, et al. 1999), (Santos, et al. 2006). When a non-spherical solute diffuses in a viscous solution, the orientation of the molecules may influence the diffusion (Kiso, Muroshige, et al. 2010).

In literature the shape of non-spherical molecules has been approximated by several simple geometric shape: typically rectangular parallelepiped (Kiso, Kon and Nishimura 2001),

cylinder (Van der Bruggen, Schaep, et al. 1999) as well as ellipsoid (Santos, et al. 2006) are used (see Tab. 4.4), while the pore was assumed to be cylindrical.

Characteristic parameters calculated non-empirically are the diameter derived from the hydrodynamic volume (Meireles, et al. 1995), the molecular length and width (L and MWd respectively) (Kiso, Muroshige, et al. 2010), the diameter derived from the molar volume and the effective diameter calculated from the molecular structure. However from the definition of these parameters, steric partition factor, diffusion coefficient and as a result rejection were calculated accordingly.

(Van der Bruggen, Schaep, et al. 1999) proposed a correlation between molecular weight and the diameter of the molecule. In literature several methods have been proposed to estimate the diffusivity on the basis of molar volumes (Lyman, Reehl and Rosenblatt 1982). According to other approaches, the Stokes radius (calculated with diffusivity in aqueous solution) was correlated with molecular width, and then the “proper” diffusivity was calculated by using the calculated Stokes radius. (Kiso, Kon and Nishimura 2001)

(Santos, et al. 2006) introduced a geometrical model that investigated how different molecular characteristics (shape, geometry, type and orientation of functional groups) can determine the rejection of neutral solutes.

Table 4.4 summarizes some of the geometries investigated in order to describe the real shape and orientation of the molecules.

Table 4.4: Definition of a molecule geometry from Literature

<i>Ref.</i>	<i>Solutes</i>	<i>Molecular shape</i>	<i>Molecular Parameter</i>	<i>Diffusivity</i>
(Kiso, Muroshige, et al. 2010)	Alcohols and polyhydric alcohols (60.10-134.17 g/mol)	Rectangular parallelepiped	Molecular length (L), Molecular width (MWd) L=0.6-1.2 nm; MWd=0.25-0.4nm	$D = \frac{k_B T}{6\pi\eta r_s}$ With $r_s = f(MWd)$ $r_s \times 10^{-9} = 1.42(MWd \times 10^{-9}) - 0.142$
(Santos, et al. 2006)	Glucose, glycerol, butanol, hexanol, octanol, hexanone, butanediol, esandiol	Ellipsoid, 3D	Geometric radius, $r_{geom}=f(\text{length, width, depth})$ L=0.571-1.172 nm; W=0.283-0.758 nm	<i>D from Wilke-Chang correlation</i>
(Van der Bruggen, Schaep,	Dextran solutions and PEG solutions (32.04-696.68 gmol ⁻¹)	sphere	Stokes diameter, d_s , equivalent molar diameter, d_m $d_s=0.51-2.65$ nm; $d_m=0.51-1.03$ nm	–

et al. 1999)	<i>cylinder</i>	calculated molecular diameter, $d_c, d_c=0.41-2.03$ nm
-----------------	-----------------	---

All geometric models proposed in literature and summarized in table allowed for a better description of the experimental rejection data which were dependent of the transmembrane pressure applied; the model could be used as an interpretative tool, allowing for a better understanding of the dominant factor (i.e. molecule orientation) that determine the rejection of uncharged solutes with different molecular geometry (Santos, et al. 2006). However these geometrical models are not taking into account possible hydration contributions, and others interactions that could occur in solution.

The influence of hydration number on friction coefficients was introduced by (Koter 1986), and later (Slezak, Grzegorzyn and Wasik 2004) introduced a relationship between the frictional coefficients and the hydration numbers of permeating species though membranes in the *Spiegler-Kedem-Katchalsky model*. Hydration shell formation around molecules is an intrinsic dynamic phenomenon and is not constant.

In this work uniform pore size is assumed and molecule shape and solution effects (i.e. Hydration) are taken into account inside hydrodynamic coefficient, independently from the definition of a Stokes radius.

4.3.3 Calculation of model parameters: a new approach

The revised *DSP&DE* model introduced has been applied to regress experimental rejection data, in order to obtain “model” parameters for each membrane tested in *Chapter 3*.

In this work a new approach is developed to calculate model parameters; it is different from those proposed in literature, and remarkably it is independent of the *Stokes* radius of solutes.

The adjustable parameters contained in *DSP&DE* model are:

- Hydraulic permeability, $L_{p,w}$;
- Effective membrane thickness, δ ;
- Solute/membrane interaction parameter, λ_i .

Key points of the parameter-calculation procedure are the following:

- 1) Determination of the hydraulic membrane permeability ($L_{p,w}$) from NF experiments with pure water, according to Eq. (4.24);
- 2) Selection of the pore geometry (*cylindrical* or *slit-like*);

- 3) Calculation of membrane permeability (L_p) from NF experiments with sugar solution and comparison with hydraulic permeability, $L_{p,w}$;
- 4) Calculation of λ_i , by fitting of asymptotic real rejection data (Fig. 4.5 b-c);
- 5) Calculation of effective membrane thickness, δ , based on neutral solute data, using real rejection data as a function of total volume flux (J_v) as well as of Péclet number (Pe), (Fig. 4.5 b-c).

Figure 4.5 shows in graphical form the sequence of elaboration.

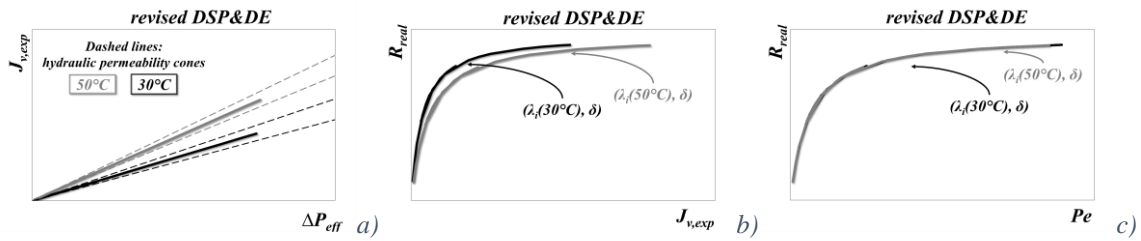


Fig. 4.5.: Graphical check for DSP&DE model parameter estimation for neutral solutes. Permeate flux (J_v) as a function of effective driving force (ΔP_{eff}) for each operating temperature (a); real rejection (R_{real}) as a function of permeate flux (J_v) for each temperature (b) and real rejection (R_{real}) as a function of Péclet number (c)

Graph (a): Elaboration of $J_{v,exp}$ vs. ΔP_{eff} data. It allows to state if membrane parameters (r_p and δ) are constant with temperature and concentration. If experimental data are located inside the water permeability cone (dashed lines), it can be concluded that sugars do not affect membrane properties, that is no swelling occurs.

Graph (b): Elaboration of R_{real} as a function of $J_{v,exp}$. It allows to fit $\lambda_i(T)$ and δ separately, under the hypothesis of r_p and δ constant with temperature; typically this kind of graph misleads, in fact the first approach is to fit separately both parameters (such as literature approach). **Graph (c)** is required to perform correctly parameter fitting.

Graph (c): Elaboration of R_{real} as a function of Péclet number, Pe . This representation shows that only one curve R_{real} vs. Pe exists, independently of δ , temperature and concentration. If λ_i changes with temperature or concentration, and r_p and δ are constant from **Graph (a)**, operating conditions affect solute properties (i.e. hydration shell), that is to say that solute properties are modified by operative conditions, whereas r_p and δ are not affected by them.

Fitting procedures are performed in order to minimize the standard variance, St_{dev} , between the calculated rejection ($R_{j,mod}$) and the experimental real rejection ($R_{j,exp}$), defined for j data points for each solute. The variance is defined as follows:

$$St_{dev} = \sqrt{\frac{\sum_{j=1}^n (R_{j,mod} - R_{j,exp})^2}{n-1}} \quad (4.51)$$

Where n is the total number of data.

4.4. Calculation of model parameters: Results

4.4.1 Check of Membrane permeability

The first step for model parameter calculation requires to checking if membrane permeability overlaps hydraulic permeability (dashed lines). The concept of hydraulic permeability cones was introduced in this study to take into account changes in membrane performances, flux decline, as well as drop in data reliability, due mainly to fouling.

For this purpose a lot of experimental data have been reworked in the form of $J_{v,exp}$ vs. ΔP_{eff} , as shown in Fig. 4.6-4.10 for GE-DL and GE-DK membranes.

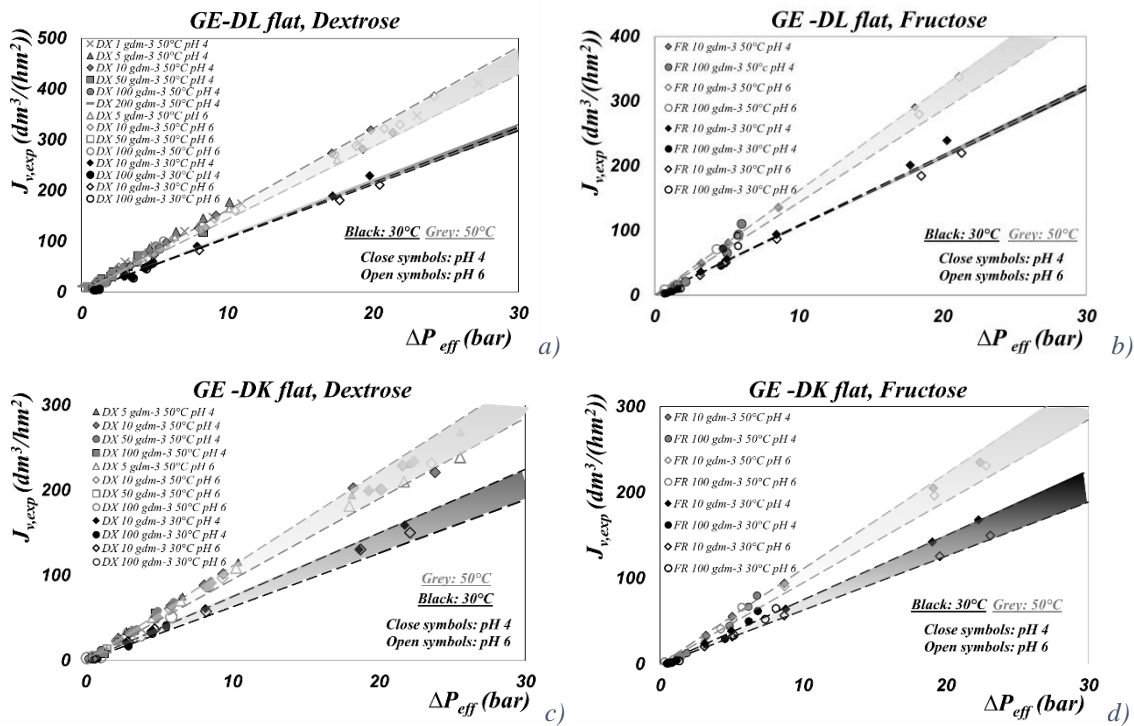


Fig 4.6. Comparison between Membrane (symbols) and Hydraulic Permeability (dashed lines). GE-DL and GE-DK flat membranes, Dextrose (a,c) and Fructose (b,d) 5-100 g/dm³, 30°C (black symbols) 50°C (grey symbols), pH 4 and 6, flow rate 400 dm³/h, ΔP_{in} ranging from 4 to 30 bar, total recirculation mode of R and P. Cones represent the confidential range of experimental hydraulic permeability

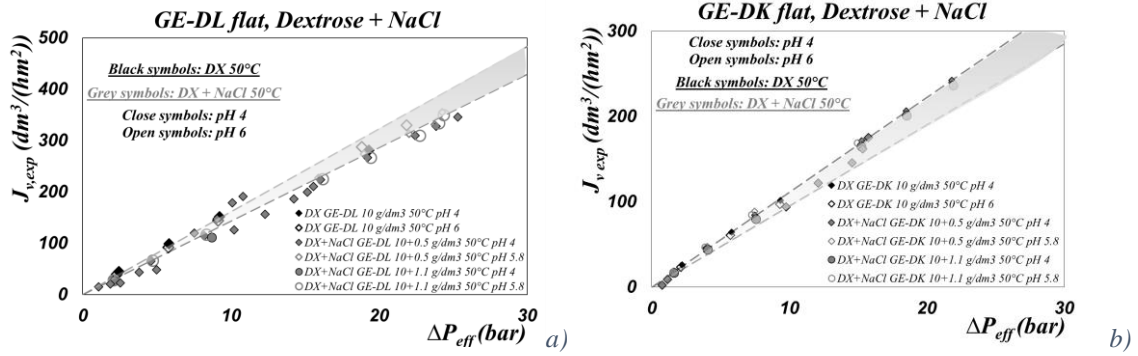


Fig 4.7. Comparison between Membrane (symbols) and Hydraulic Permeability (dashed lines). GE-DL (a) and GE-DK (b) flat membranes, Dextrose (black symbols) and Dextrose + NaCl (grey symbols) 50°C, pH 4, flow rate 400 dm³/h, ΔP_{in} ranging from 4 to 30 bar, total recirculation mode of R and P. Cones represent the confidential range of experimental hydraulic permeability

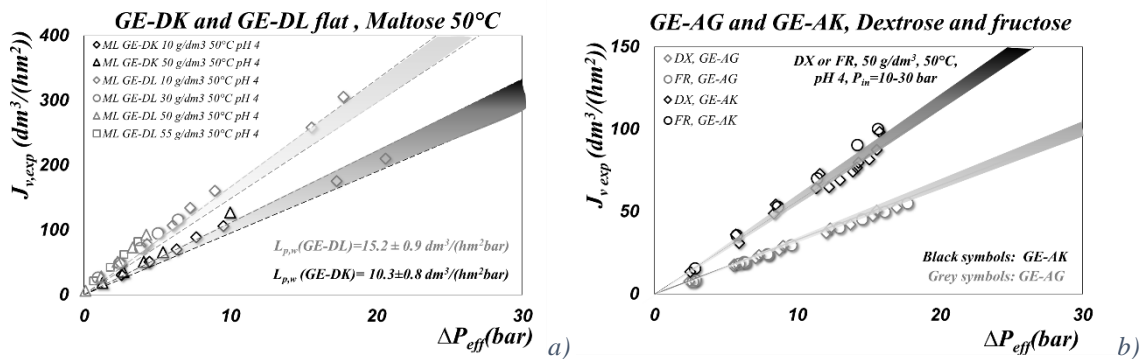


Fig 4.8. Comparison between Membrane (symbols) and Hydraulic Permeability (dashed lines). (a) GE-DL and GE-DK flat membranes, Maltose 10-55g/dm³, 50°C, Q_F=400 dm³/h pH 4; (b) GE-AG and GE-AK flat membranes, Dextrose and fructose, 50 g/dm³, 50°C, pH 4, Q_F=400 dm³/h, ΔP_{in} ranging from 4 to 30 bar, total recirculation mode of R and P. Cones represent the confidential range of experimental hydraulic permeability

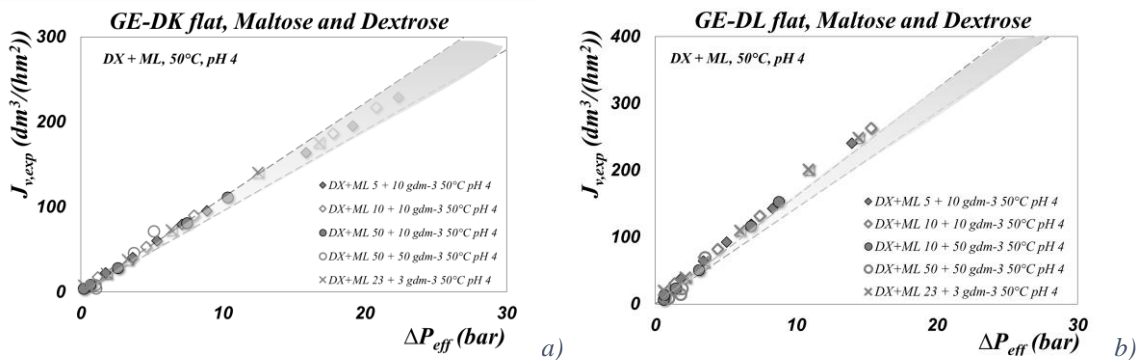


Fig 4.9. Comparison between Membrane (symbols) and Hydraulic Permeability (dashed lines). (a) GE-DK and (b) GE-DL flat membranes, Maltose and Dextrose, 50°C, Q_F=400 dm³/h pH 4, total recirculation mode of R and P. Cones represent the confidential range of experimental hydraulic permeability

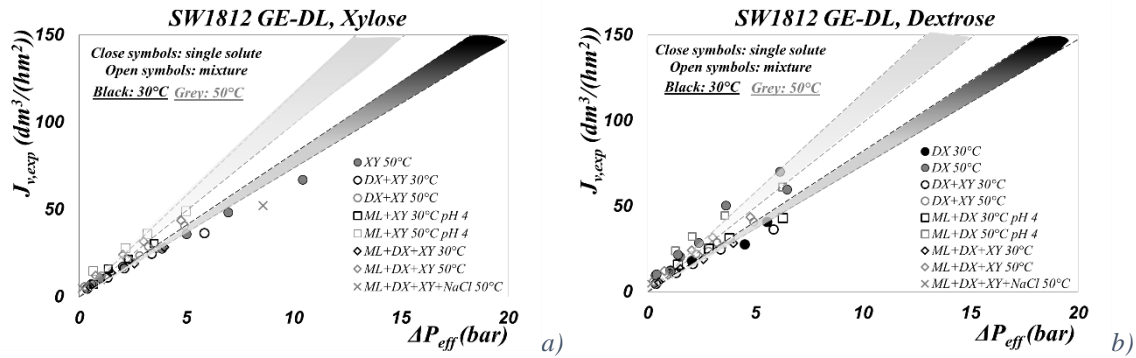


Fig 4.10. Comparison between Membrane (symbols) and Hydraulic Permeability (dashed lines). GE-DL and SW1812 membrane, (a) Xylose and (b) Dextrose, 10-50 g/dm³, 30° and 50°C, $Q_r=400$ dm³/h pH 4; ΔP_{in} ranging from 4 to 20 bar, total recirculation mode of R and P. Cones represent the confidential range of experimental hydraulic permeability

Apparently experimental results (symbols) are confined with good confidence inside hydraulic permeability cones, bordered by dashed lines, for all the case investigated. This behavior allows us to draw some conclusions:

- Porous viscous vision describes with good approximation experimental data;
- No pore swelling occurs: membrane parameters are constant with temperature and concentration.

4.4.2 Calculation of model parameters (λ_i , δ) and sensitivity from pore geometry

Once checked that membrane parameters (r_p , δ) are not affected by sugar concentration and temperature, model parameters (λ_i , δ) can be fitted on whole $R_{real,i}$ vs. $J_{v,exp}$ and $R_{real,i}$ vs. Pe curves, that means that the hydrodynamic coefficient, λ_i , as well as the membrane effective thickness δ , were estimated by fitting the intrinsic rejections of uncharged single solutes.

In contrast to what defined in literature, in this study it is more accurate refer to “model parameters”, instead of “membrane parameters”. As a matter of fact, although δ is really a membrane parameter, λ_i contains in its interior the dependence of solute and membrane properties, and it cannot be therefore defined intrinsically as a membrane parameter.

Results of model parameters calculation obtained for both membranes, and for both pore geometries is shown in Tab. 4.5 and 4.6. In the same table results are compared with parameters exploited in literature, according to procedure in which pore radius is calculated by assuming a Stokes radius, and an effective membrane thickness is calculated by Hagen Poiseuille equation (r_p and δ^* respectively).

Tab. 4.5 Model (λ , δ) and Membrane Parameter (r_p , δ^), comparison between pore geometry and temperature, GE-DK, flat sheet*

Solute	T (°C)	Slit-like pore				Cylindrical pore			
		λ	δ (μm)	r_p (nm)	δ^* (μm)	λ	δ (μm)	r_p (nm)	δ^* (μm)
<i>Dextrose</i>	30	0.987	5.8	0.366	2.9	0.860	0.1	0.420	1.4
	50	0.966	6.1	0.374	2.9	0.830	0.1	0.435	1.5
<i>Fructose</i>	30	0.986	6.0	0.362	2.8	0.859	0.1	0.416	1.4
	50	0.972	5.9	0.367	2.8	0.837	0.1	0.427	1.4
<i>Maltose</i>	50	0.998	6.0	0.471	4.7	0.932	0.1	0.504	2.0

Tab. 4.6 Model (λ , δ) and Membrane Parameter (r_p , δ^), comparison between pore geometry and temperature, GE-DL, flat sheet*

Solute	T (°C)	Slit-like pore				Cylindrical pore			
		λ	δ (μm)	r_p (nm)	δ^* (μm)	λ	δ (μm)	r_p (nm)	δ^* (μm)
<i>Dextrose</i>	30	0.977	3.7	0.369	1.9	0.853	0.045	0.423	0.9
	50	0.960	3.2	0.376	2.0	0.830	0.045	0.435	0.9
<i>Fructose</i>	30	0.980	3.2	0.364	1.8	0.848	0.045	0.421	0.9
	50	0.960	3.3	0.372	2.0	0.825	0.045	0.433	1.0
<i>Maltose</i>	50	0.997	3.3	0.472	3.2	0.903	0.046	0.521	1.4

Remarkably results highlight two key aspects: (i) effective membrane thickness remains constant for each solute used and for the temperature range investigated; (ii) it can be obtained a clear trend of the decrease of the hydrodynamic coefficient with temperature (Fig. 4.11)

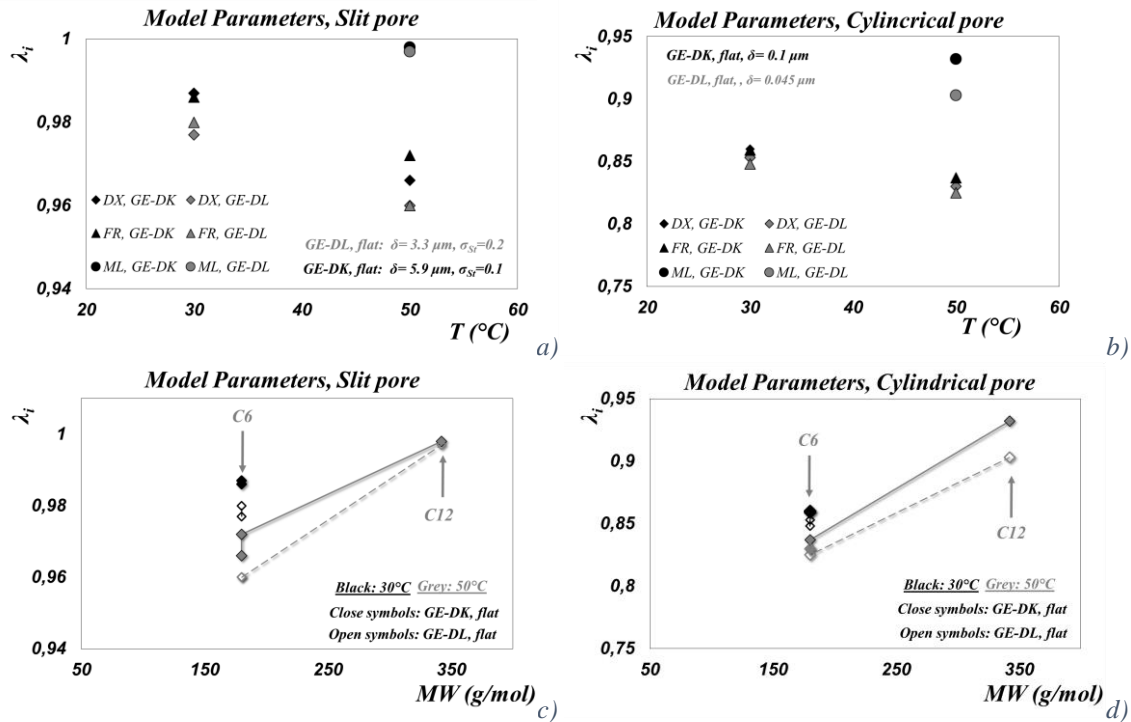


Fig.4.11: Model parameter λ_i as a function of operative temperature, 30° and 50°C. Flat sheet membranes, GE-DK and GE-DL, slit like pore geometry (a) and cylindrical pore geometry (b)

In other words these results show that temperature affects solute properties, whereas the membrane permeability is not affected by pore swelling. .

The revised *DSP&DE* model is also able to take into account the variation in viscosity and diffusion caused by temperature increase, however this effect alone is not sufficient to explain experimental data, and this is the reason why λ_i changes with temperature.

The trend obtained for flat membranes was the same observed for commercial SW1812 modules. In this study case a wide experimentation was carried on to test temperature effect on *DSP&DE* model parameters and different oligosaccharide. Results are summarized in Tab. 4.7.

Tab. 4.7: Model (λ , δ) and Membrane Parameter (r_p , δ^*), comparison between pore geometry and temperature, GE-DL, Spiral Wound DL1812C-34D

Solute	T (°C)	Slit-like pore				Cylindrical pore			
		λ	δ (μm)	r_p (nm)	δ^* (μm)	λ	δ (μm)	r_p (nm)	δ^* (μm)
Xylose	30	0.985		0.355	2.41	0.849		0.412	1.22
	40	0.975	3.4	0.359	2.55	0.835	0.072	0.419	1.31
	50	0.957		0.366	2.75	0.812		0.431	1.44
Dextrose	30	0.995		0.3628	2.52	0.884		0.408	1.20
	40	0.994	3.39	0.3633	2.62	0.877	0.069	0.412	1.26
	50	0.991		0.3643	2.74	0.860		0.420	1.36
Fructose	30	0.996		0.3585	2.46	0.892		0.400	1.15
	40	0.994	3.5	0.3592	2.56	0.875	0.072	0.408	1.24
	50	0.990		0.3605	2.68	0.861		0.415	1.33
Maltose***	30	0.999		0.4702	4.23	0.952		0.494	1.75
	50	0.9999	3.5	0.4702	4.55	0.949	0.075	0.495	1.90

Temperature effect was investigated for different sugars (from mono- to disaccharides) in a wide range of temperature (ranging from 30° to 50°C). Results confirmed flat membrane results, and added some information. From Fig. 4.12, an inversed relationship between temperature effect and sugar molecular weight exist: xylose (a C5 sugar) shows the greatest temperature effect on its λ_i coefficient, maltose hydrodynamic coefficient is constant in the whole range of temperatures, while dextrose and fructose (C6 isomers) show an intermediate behavior between xylose and maltose.

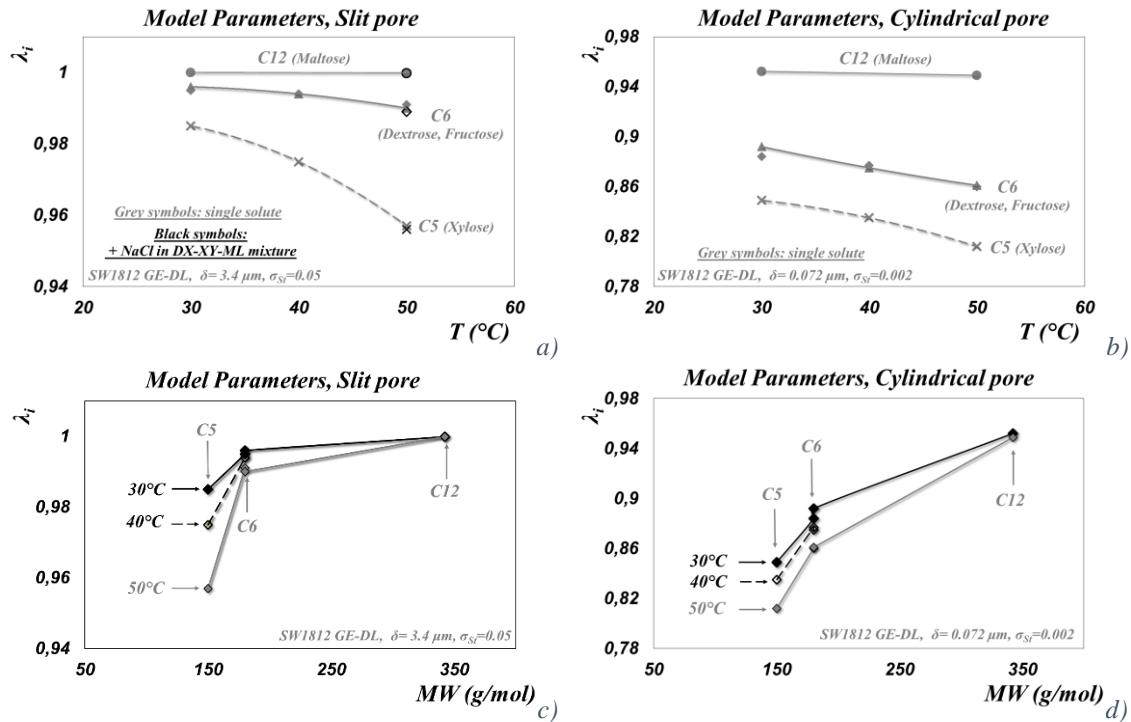


Fig.4.12: Membrane Parameters (λ , δ) fitted for both Slit-like pore and cylindrical geometry as a function of operative temperature (T) and solute molecular weight (MW), DLI812C-34D

Electrolyte effect was also investigated, but only slight decrease in rejection is observed, since apparent size of neutral solutes is influenced by ionic composition, in particular sugar is less hydrated in presence of electrolyte, a lower retention can be expected

Results obtained for both module configurations (flat sheet and spiral wound) put in evidence:

- i) model parameter sensitivity from pore geometries;
- ii) Both pore geometries fit very well experimental data, with different couple (λ_i , δ);
- iii) A proper effective membrane thickness (δ), independent from solute and temperature;
- iv) Temperature effect on hydrodynamic coefficient, λ_i , depending on sugar molecular weight

Results obtained for hydrodynamic coefficient are in accordance with sugar hydration theory [(Seuvre and Mathlouthi 2010), (Zhou, Wang and Wei 2013)]. The decrease of λ_i with increasing GE-DL can be ascribed as the sugar dehydration, when membrane parameters are constant with temperature. However the hydration layers of carbohydrates

in aqueous solutions cannot be exactly described upon present knowledge, only qualitative behavior can be derived.

Revised *DSP&DE* model was applied to predict experimental data at 50°C, starting from membrane parameters at 30°C, what has been observed is that a change in chemical-physical properties and membrane permeability with temperature is not able to describe experimental trend, that is to say that other phenomena take place as temperature increases.

Some conclusion can be drawn:

- i) The decrease in retention with temperature can't be ascribed only as reduced viscosity and increased diffusion, solute properties change with Temperature
- ii) λ_i is a parameter that contains inside it the dependence of solute size (i.e. hydration) with temperature, when r_p is constant.
- iii) The use of relationships derived from the application of the Hagen-Poiseuille equation, typically used in literature, must be careful, since it could lead to an underestimation of the membrane thickness by 5-10 times

These results are in stark contrast with literature studies. Many authors explain the reduction in sugar retention with membrane pore swelling (Sharma, Agrawal and Chellam 2003).

From this data reduction no pore swelling occurs, furthermore we are able to split membrane to solute behavior.

4.5 Revised DSP&DE model Validation

Throughout this study, it was necessary to compare the agreement between experimental data and model prediction. Once the model parameters were obtained for the solute(s)-water system of interest, the whole model (whose equations are summarized in Tab.4.1) was applied to make predictions at different pressure values (from 4 to 20 bar) in TK Solver ® environment.

The revised *DSP&DE* model was applied to the mass transfer governing fluid-dynamics in *NF* modules, whose equations are summarized in Tab. 4.8. Sherwood correlation for both radial flow test cell and SW1812 are documented in *Chapter 3*.

Table 4.8: Mass transfer equations in NF membrane modules

Mass transport model in NF modules		
<i>Film Theory</i>	$\exp\left(\frac{J_v}{k_{L,i}}\right) = \frac{c_{L,i} - c_{P,i}}{c_{bulk,i} - c_{P,i}}$	(4.52)
<i>Mass transfer coefficient</i>	$k_{L,i}^0 = \frac{Sh_i \cdot D_{S,i}}{d_h}$	(4.53)
(Aimar and Field 1992)	$k_{L,i} = k_{L,i}^0 \left(\frac{\eta_{bulk}}{\eta_i}\right)^{0.27}$	(4.54)
<i>Sherwood number</i>	$Sh_i = f(Re, Sc_i, geometry)$	(4.55)
<i>Reynolds number</i>	$Re = \frac{\rho_{bulk} \cdot v_{eff} \cdot d_h}{\eta_{bulk}}$	(4.56)
<i>Schmidt number</i>	$Sc_i = \frac{\eta_{bulk,i}}{\rho_{bulk,i} \cdot D_{S,i}}$	(4.57)

The revised DSP&DE model solution requires the knowledge of:

- Hydraulic permeability, $L_{p,w}(T)$;
- Model parameters, (λ_i, δ) ;
- Inlet conditions $(T, \Delta P, c_{bulk,i}, Q_F)$.

The discrepancy between experimental values ($J_{v,exp}$, $R_{obs,exp}$ and $R_{real, exp}$) and model prediction is put in evidence in parity diagrams (Fig. 4.13- 4.15)

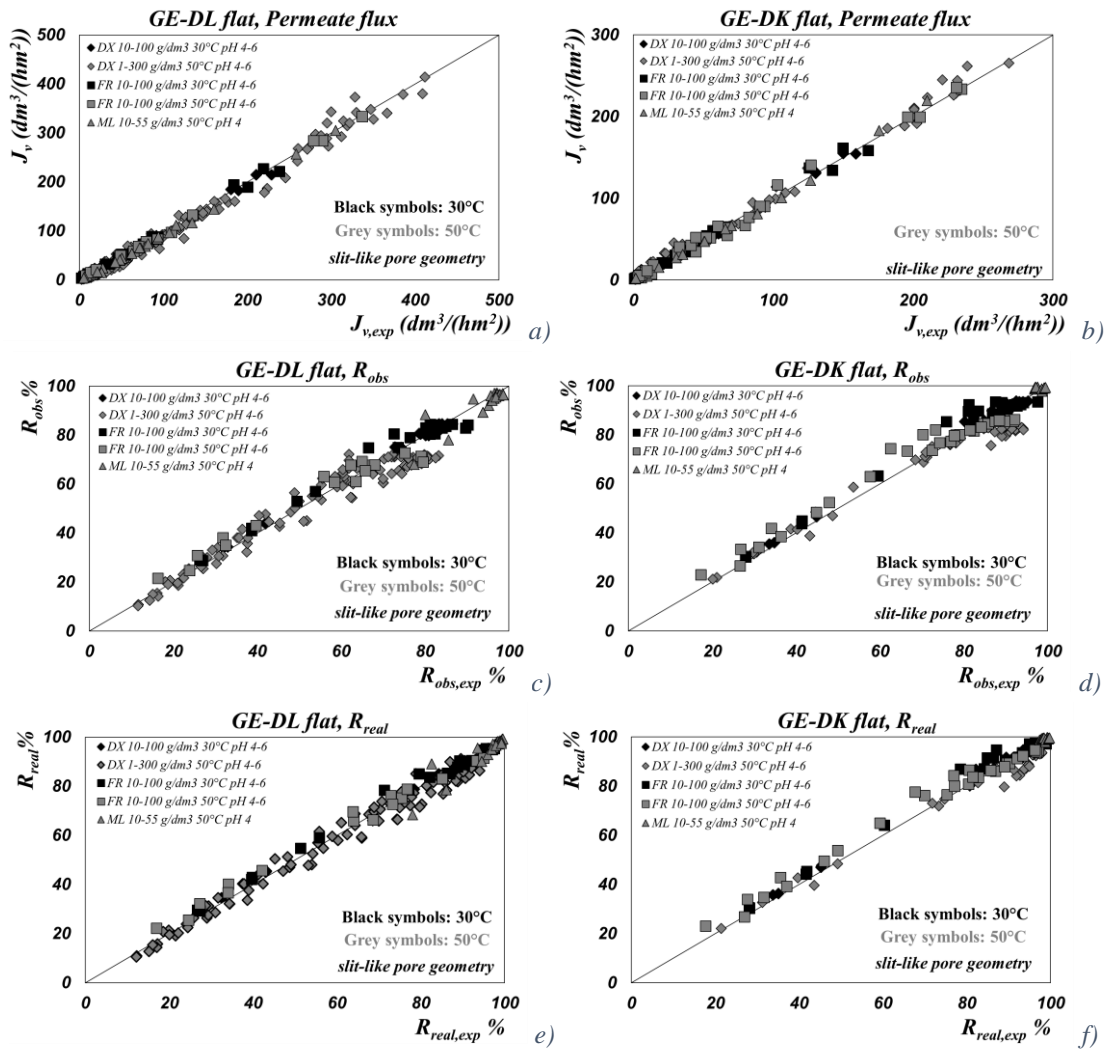


Fig. 4.13: Model validation for radial flow test cell, GE-DL and GE-DK membranes. Comparison between calculated and experimental permeate flux (a-b), observed rejection (c-d) and real rejection (e-f) respectively. Aqueous model solution of Dextrose (DX), Fructose (FR) and Maltose (ML), 1-300 g/dm³, 30-50°C, pH 4-6, $Q_F=400$ dm³/h, $P_{in}=4-30$ bar, Total recirculation mode of Retentate and Permeate

Good agreement between experimental data and model prediction was obtained in the whole range of operative conditions. DSP&DE revised model well predicts concentration and temperature effect (ranging from 1 to 300 g/dm³ and 30° to 50°C respectively) for each sugar.

The same accuracy was achieved for spiral wound module, for which experimental flux, permeate concentration, observed and real rejections are depicted as a function of model prediction. Fig.4.14.

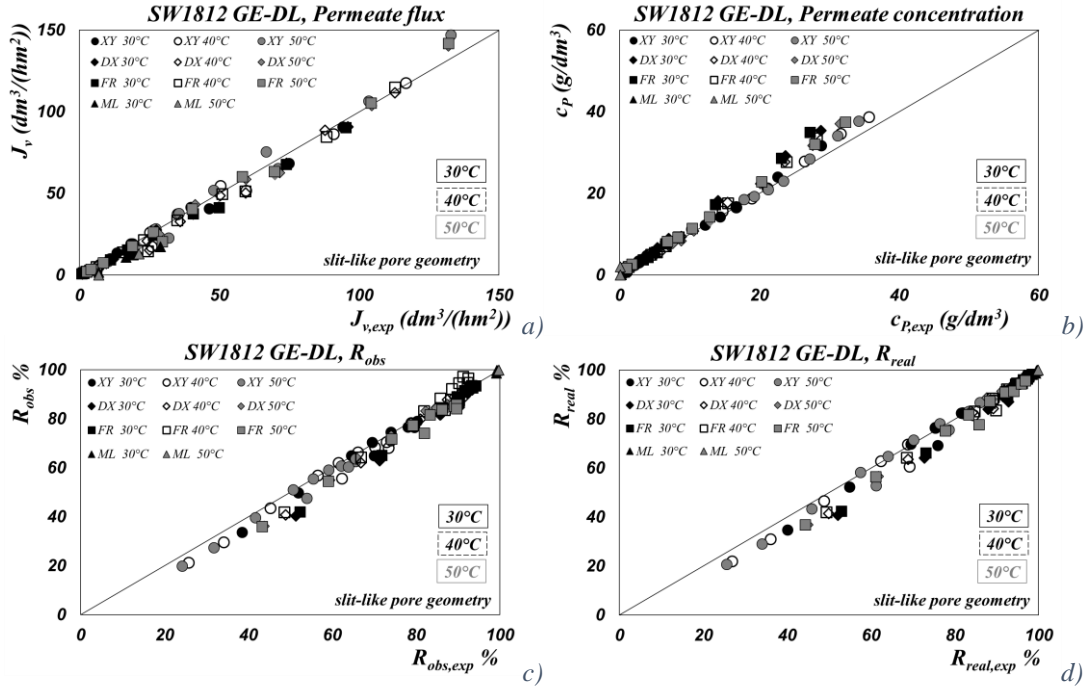


Fig 4.14: Model validation, 1812C-34D GE-DL. Comparison between calculated and experimental permeate flux (a), permeate concentration (b), observed and real rejection (c and d) respectively. Aqueous model solution of Xylose(XY), Dextrose (DX), Fructose (FR) and Maltose (ML), 10-50 g/dm³, 30-40-50°C, pH 4, $Q_F=400$ dm³/h, $P_{in}=4-20$ bar, Total recirculation mode of Retentate and Permeate

These results confirmed that the revised DSP&DE model is suitable to describe the membrane transport through these two type of membranes/modules at different operating conditions.

Once the model was validate for single solute solutions, the same validation procedure was adopted for binary and ternary mixtures. In first approximation model parameters in the mixture were assumed to be equal to membrane parameters of the single solute solution, that is to say:

$$(\lambda_i, \delta)_{mix} = (\lambda_i, \delta)_{single\ solute} , \text{ where } i=1, \dots, 3$$

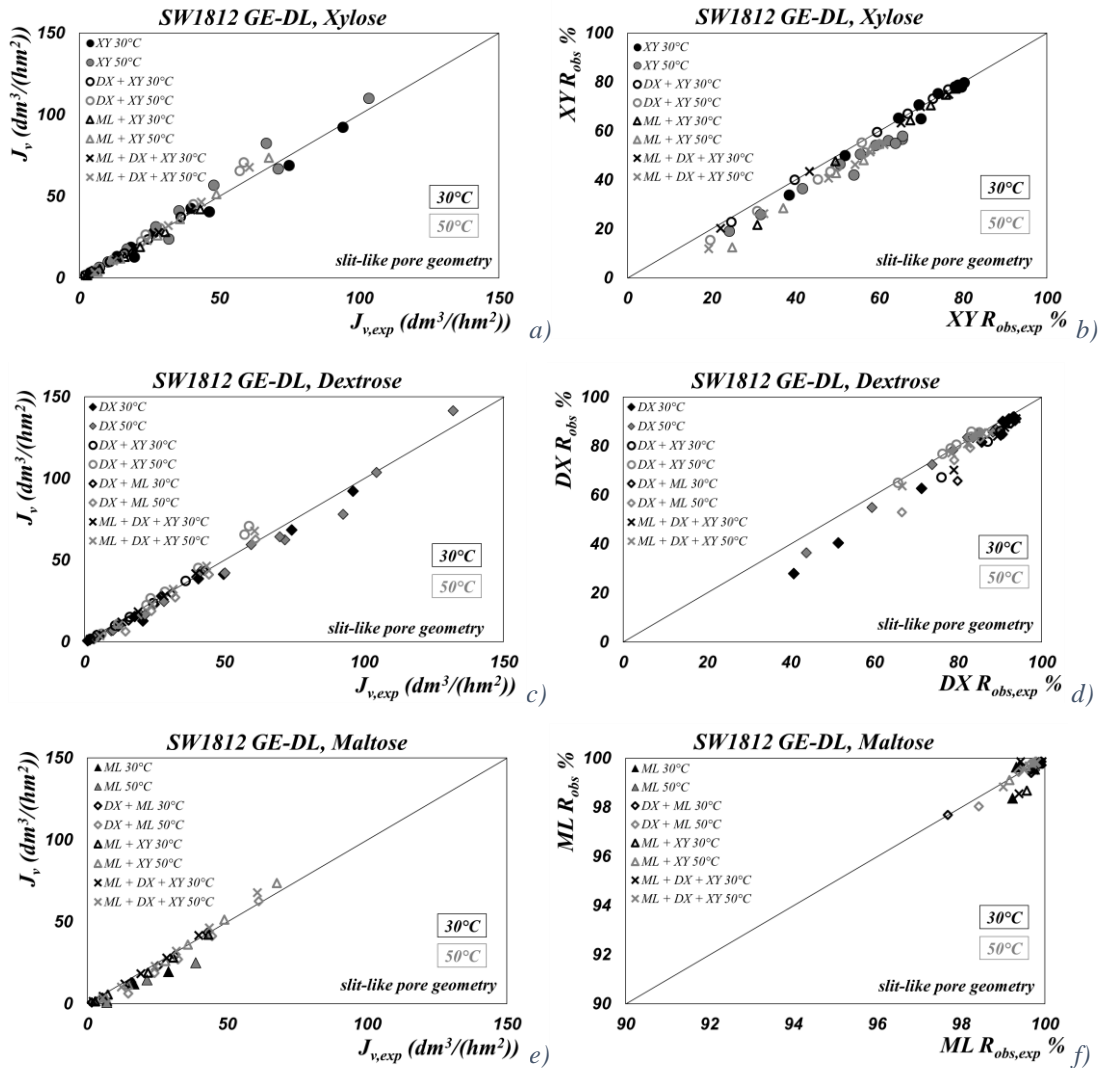


Fig 14.15: Model validation, mixtures, DL1812C-34D. Comparison between calculated and experimental permeate flux and observed rejection for Xylose (XY), Dextrose (DX) and Maltose (ML), (a, b), (c, d), (e, f) respectively. Aqueous model mixtures of Xylose(XY), Dextrose (DX), and Maltose (ML), 10-50 g/dm³, 30-50°C, pH 4, $Q_F=400$ dm³/h, $P_{in}=4-20$ bar, Total recirculation mode of Retentate and Permeate.

Good agreement between experimental and calculated membrane module performance characterizes each sugar tested, in terms of both membrane flux and rejections (observed as well as real).

The achieved results clearly shows that no interaction occurs (or in any case negligible) in mixtures between sugars, thus the approximation adopted for hydrodynamic coefficients is exact in the whole range of operating conditions.

It is also worth to mention that in order to “characterize” a membrane when oligosaccharides are processed, in term of “model parameters”, it is only necessary to perform two test at each operating temperature:

- 1) Hydraulic permeability test;

2) Filtration of model/real mixture of all n -solutes in solution.

From the first test it is possible to achieve water permeability, $L_{p,w}(T)$, afterwards filtration experiment allows to obtain $\lambda_i(T)$ and δ , with $i=1,\dots,n$.

4.6 Conclusions

A “revised” *DSP&DE* model was discussed in order to describe the transport through the membrane when sugar NF is performed.

The parameters of the revised model have been critically identified: (i) hydraulic permeability, $L_{p,w}$; (ii) hydrodynamic coefficient, λ_i , and (iii) effective membrane thickness, δ ; and a new approach was proposed for the calculation of such parameters.

Key points of this procedure are:

- Check of membrane swelling;
- (λ_i, δ) fitting on experimental data documented in *Chapter 3*.

Elaborations put in evidence that the Stokes radius is not a representative parameter of the molecule shape. The mean pore radius of the membrane should be calculated by using glucose or xylose data, whereas non spherical oligosaccharides should be represented by a parameter accounting the shape of the molecule. The model provides useful elements to understand which kind of interactions (complex formation or dehydration) can affect sugars rejections in presence of strong electrolytes, however dehydration effects caused by temperature and electrolyte are the most evident.

So doing, the model is able to predict with good confidence both the temperature effect on membrane performances and rejections in multicomponent mixtures, ranging from laboratory to process/industrial scale.

References

- Afonso, M.D., G. Hagemeyer, and R. Gimbel. "Streaming potential measurements to assess the variation of nanofiltration membrane surface charge with the concentration of salt solution." *Separation Purification Technology* 22-23 (2001): 529-541.
- Aimar, P., and R. Field. "Limiting flux in membrane separations: a model based on the viscosity dependency of the mass transfer coefficient." *Chemical Engineering Science* 47, no. 3 (1992): 579-586.
- Aydogan, N., T. Gurka, and L. Yilmaz. "Effect of operating parameters on the separation of sugars by nanofiltration." *Separation Science Technology* 33, no. 12 (1998): 1767-1785.

- Bandini, S., and D. Vezzani. "Nanofiltration modeling: The role of dielectric exclusion in membrane characterization." *Chemical Engineering Science* 58, no. 13 (2003): 3303-3326.
- Bandini, S., and L. Bruni. Transport phenomena in nanofiltration membranes. Vol. 2, in *Comprehensive membrane science and engineering*, by E. Drioli and L. Giorno, 67-89. Oxford: Elsevier, 2010.
- Bandini, S., and L. Nataloni. "Nanofiltration for dextrose recovery from crystallization mother liquors: A feasibility study." *Separation and Purification Technology* 139 (2015): 53-62.
- Bargeman, G. 2014.
- Bargeman, G., J.M. Vollenbroek, J. Straatsma, and C.G.P.H. Schroen. "Nanofiltration of multicomponent feeds. Interactions between neutral and charged components and their effect on retention." *Journal of Membrane Science* 247 (2005): 11-20.
- Bouchoux, A., H. Roux-de Balman, and F. Lutin. "Nanofiltration of glucose and sodium lactate solutions: variations of retention between single- and mixed- solute solutions." *Journal of Membrane Science* 258 (2005): 123-132.
- Bouranene, S., A. Szymczyk, P. Fievet, and A. Vidonne. "Effects of salts on the retention of polyethyleneglycol by a nanofiltration ceramic membrane." *Journal of Membrane Science* 240 (2009): 94-98.
- Bouranene, S., A. Szymczyk, P. Fievet, and A. Vidonne. "Influence of inorganic electrolytes on the retention of polyethyleneglycol by nanofiltration ceramic membranes." *Journal of Membrane Science* 290 (2007): 216-221.
- Bowen, W.R., and J.S. Welfoot. *Chemical Eng. Sci.* 57 (2002): 1121-1137.
- Bowen, W.R., A.W. Mohammad, and N. Hilal. "Characterization of nanofiltration membranes for predictive purposes - use of salt, uncharged solutes and atomic force microscopy." *Journal of Membrane Science* 126 (1997): 91-105.
- Bowen, W.R., and A. O. J. Sharif. *Colloid Interface Sci.* 168, no. 2 (1994): 414-421.
- Bowen, W.R., and H. Mukhtar. "Characterization and prediction of separation performance of nanofiltration membranes." *Journal of Membrane Science* 112 (1996): 263-274.
- Bowen, W.R., and J.S. Welfoot. "Modeling of membrane nanofiltration-pore size distribution effects." *Chem. Eng. Sci.* 57 (2002): 1393-1407.
- Bowen, W.R., and T.A. Doneva. "Atomic force microscopy studies of nanofiltration membranes: surface morphology, pore size distribution and adhesion." *Desalination* 129 (2000): 163-172.
- Bowen, W.R., J.S. Welfoot, and P.M. Williams. "Linearized transport model for nanofiltration: development and assessment." *AIChE Journal* 48, no. 4 (2002): 760-773.
- Boy, V., H. Roux-de Balman, and S. Galier. "Relationship between volumetric properties and mass transfer through NF membrane for saccharide/electrolyte systems." *Journal of Membrane Science* 390-391 (2012): 254-262.
- Bungay, P.M., and H. Brenner. *Int. J. Multiphase Flow* 1 (1973): 25-56.
- Catarino, I., M. Minhalma, L. L. Beal, M. Mateus, and M.N. de Pinho. "Assessment of saccharide fractionation by ultrafiltration and nanofiltration." *Journal of Membrane Science* 312 (2008): 34-40.
- Cavaco Morao, A.I., A. Szymczyk, P. Fievet, and A.M. Brites Alves. "Modelling the separation by nanofiltration of multi-ionic solution relevant to an industrial process." *Journal of Membrane Science* 322 (2008): 320-330.

- Cuartas-Uribe, B., M.C. Vincent-Vela, S. Alvarez-Blanco, M.I. Alcaina-Miranda, and E. Soriano-Costa. "Nanofiltration of sweet whey and prediction of lactose retention as a function of permeate flux using the Kedem-Spiegler and Donnan Steric Partitioning models." *Separation and Purification Technology* 56 (2007): 38-46.
- Dechadilok, P., and W.M. Deen. *Ind. Eng. Chem. Res.* 45 (2006): 6953-6959.
- Deen, W.M. *AIChE Journal* 33 (1987): 1409-1425.
- Déon, S., A. Escoda, P. Fievet, and R. Salut. "Prediction of single salt rejection by NF membranes: An experimental methodology to assess physical parameters from membrane and streaming potentials." *Desalination* 315 (2013): 37-45.
- Escoda, A., P. Fievet, S. Lakard, A. Szymczyk, and S. Deon. "Influence of salts on the rejection of polyethyleneglycol by a NF organic membrane: pore swelling and salting-out effects." *Journal of Membrane Science* 347 (2010): 174-182.
- Escoda, A., S. Déon, and P. Fievet. "Assessment of dielectric contribution in the modeling of multi-ionic transport through nanofiltration membranes." *Journal of Membrane Science* 378 (2011): 214-223.
- Faxen, H. *Ann. Phys.* 68, no. 10 (1922): 89-119.
- Freger, V. "Swelling and morphology of the skin layer of polyamide composite membranes: atomic force microscopy study." *Environmental Science Technology* 38 (2004): 3168.
- Godfrey, T., and West. *Industrial Enzymology*. 2nd. London: MacMillan, 1996.
- Goulas, A., A.S. Grandison, and R. A. Rastall. "Fractionation of oligosaccharides by NF." *Journal of Membrane Science* 209 (2002): 321-335.
- Kiso, Y., et al. "Effect of molecular shape of uncharged organic compounds by nanofiltration membranes and on calculated pore radii." *Journal of Membrane Science* 358 (2010): 101-113.
- Kiso, Y., T. Kon, and K. Nishimura. "Rejection properties of alkyl phthalates with nanofiltration membranes." *Journal of Membrane Science*, 2001: 205-214.
- Koter, S. "Interactions of hydrated species in transport across membranes." *Z. Phys. Chem.* 148 (1986): 247-253.
- Kuhn, R.C., F. Maugeri Filho, L. Palacio, A. Hernandez, and P. Pradanos. "Mass transfer and transport during purification of fructo oligosaccharides by nanofiltration." *Journal of Membrane Science* 365 (2010): 356-365.
- Labbez, C., et al. "Evaluation of the "DSPM model" in a titania membrane: measurement of charged and uncharged solute retention, electrokinetic charge, pore size, and water permeability." *J. Colloid Interface Sci.* 262 (2003): 200.
- Labbez, C., P. Fievet, S. Szymczyk, A. Vidonne, A. Foissy, and J. Pagetti. "Retention of mineral salts by a polyamide nanofiltration membrane." *Separation and Purification Technology* 30 (2003): 47-55.
- Lonsdale, H.K. 1965.
- Luo, J., and Y. Wan. "Effect of highly concentrated salt on retention of organic solutes by nanofiltration polymeric membranes." *Journal of Membrane Science* 372 (2011): 145-153.
- Lyman, W., W.F. Reehl, and D.H. Rosenblatt. In *Handbook of Chemical Property Estimation Methods*, 17-19. 1982.

- Manttari, M., A. Pihlajamaki, and M. Nystrom. "Effect of pH on hydrophilicity and charge and their effect on the filtration efficiency of NF membranes at different pH." *Journal of Membrane Science* 280 (2006): 311-320.
- Manttari, M., A. Pihlajamaki, E. Kaipainem, and M. Nystrom. "Effect of temperature and membrane pretreatment by pressure on the filtration properties of nanofiltration membranes." *Desalination* 145 (2002): 81.
- Marchetti, P., and A.G. Livingston. "Predictive membrane transport models for Organic Solvent Nanofiltration: How complex do we need to be?" *Journal of Membrane Science* 476 (2015): 530-553.
- Mason, E.A., and H.K. Lonsdale. "Statistical-mechanical theory of membrane transport." *Journal of Membrane Science* 51 (1990): 1-81.
- Meireles, M., A. Bessieres, I. Rogissart, P. Aimar, and V. Sanchez. "An appropriate molecular size parameter for porous membrane calibration." *Journal of Membrane Science* 103 (1995): 105-115.
- Mohammad, A.W., R.K. Basha, and C.P. Leo. "Nanofiltration of glucose solution containing salts: effects of membrane characteristics, organic component and salt on retention." *Journal of Food Engineering* 97 (2010): 510-518.
- Nabetani, H. "Prediction of the flux for reverse osmosis of a solution containing sucrose and glucose." *Journal of Chemical Engineering Jpn.* 25 (1992): 575.
- Nakao, S., and S. Kimura. "Analysis of solute rejection in ultrafiltration." *J. Chem. Eng. Jpn.* 14 (1981): 32-37.
- Nilsson, M., Gun Tragardh, and K. Ostergren. "The influence of sodium chloride on mass transfer in a polyamide nanofiltration membrane at elevated temperatures." *Journal of Membrane Science* 280 (2006): 928-936.
- Otero, J.A., et al. "Three independent ways to obtain information on pore size distribution of nanofiltration membranes." *Journal of Membrane Science* 309 (2008): 17-27.
- Otero, J.A., J. Lena, J.M. Colina, P. Prãdanos, F. Tejerina, and A. Hernandez. "Characterization of nanofiltration membranes Structural analysis by the DSP model and microscopical techniques." *Journal of Membrane Science* 279 (2006): 410-417.
- Peshev, D., and A.G. Livingston. "OSN Designer, a tool for predicting organic solvent nanofiltration technology performance using Aspen One, MATLAB and CAPE OPEN." *Chem. Eng. Sci.* 104 (2013): 975.
- Peshev, D., and A.G. Livingston. "OSN Designer, a tool for predicting organic solvent nanofiltration technology performance using Aspen One, MATLAB and CAPE OPEN." *Chemical Engineering Science* 104 (2013): 975.
- Rodrigues, C., A.I. Cavaco Morao, M.N. de Pinho, and V. Geraldes. "On the prediction of permeate flux for nanofiltration of concentrated aqueous solutions with thin-film composite polyamide membranes." *Journal of Membrane Science* 346 (2010): 1-7.
- Rosa, M.J., and M.N. de Pinho. "Separation of organic solutes by membrane pressure driven processes." *Journal of Membrane Science* 89 (1994): 235-243.

- Santos, Josè L.C., P. de Beukelaar, Ivo. F.J. Venkelcom, S. Velizarov, and G.J. Crespo. "Effect of solute geometry and orientation on the rejection of uncharged compound by nanofiltration." *Separation Purification Technology* 50 (2006): 122-131.
- Seuvre, A. M., and M. Mathlouthi. "Solution properties and solute-solvent interactions in ternary sugar-salt-water solutions." *Food Chemistry* 122 (2010): 455-461.
- Sharma, R.R., R. Agrawal, and S. Chellam. "Temperature effects on sieving characteristics of thin-film composite nanofiltration membranes: pore size distributions and transport parameters." *Journal of Membrane Science* 223 (2003): 69-87.
- Shock, G., and M. Miquel. "Mass transfer and pressure loss in spiral wound modules." *Desalination* 64 (1987): 339-352.
- Sjoman, E., M. Manttari, M. Nystrom, H. Koivikko, and H. Heikkila. "Separation of xylose from glucose by nanofiltration from concentrated monosaccharide solutions." *Journal of Membrane Science* 292 (2007): 106-115.
- Slezak, A., S. Grzegorzczyn, and J. Wasik. "Model Equations for interactions of hydrated species in transmembrane transport." *Desalination* 163 (2004): 177-192.
- Spiegler, K. S., and O. Kedem. "Thermodynamics of hyperfiltration (reverse osmosis): criteria for efficient membranes." *Desalination* 1 (1966): 311-326.
- Straatsma, J., G. Bargeman, H.C. Van der Host, and J.A. Wesslingh. "Can nanofiltration be fully predicted by a model?" *Journal of Membrane Science*, no. 198 (2002): 273-284.
- Szymczyk, A., and P. Fievet. "Investigating transport properties of nanofiltration membranes by means of a steric, electric and dielectric exclusion model." *Journal of Membrane Science* 252 (2005): 77-88.
- Van der Bruggen, B., and C. Vandecasteele. "Modelling of the retention of uncharged molecules with nanofiltration." *Water Research* 36 (2002): 1360-1368.
- Van der Bruggen, B., C. Vandecasteele, T. Van Gestel, W. Doyen, and R. Leysen. "A review of pressure driven membrane processes in wastewater treatment and drinking water production." *Environmental Progress* 22 (2003): 46-56.
- Van der Bruggen, B., J. Schaep, D. Wilms, and C. Vandecasteele. "Influence of molecular size, polarity and charge on the retention of organic molecules by nanofiltration." *Journal of Membrane Science* 156 (1999): 29-41.
- Van der Bruggen, B., J. Schaep, D. Wilms, and C. Vandercateele. "A comparison of models to describe the maximal retention of organic molecules in nanofiltration." *Separation Science Technology* 35 (2000): 169-182.
- Vanneste, Johan, Stijn De Ron, Steven Vandecruys, Sandra Adina Soare, Siavash Darvishmanesh, and Bart Van der Bruggen. "Techno-economic evaluation of membrane cascades relative to simulated moving bed chromatography for the purification of mono- and oligosaccharides." *Separation and purification technology* 80 (2011): 600-609.
- Vellenga, E., and G. Tragardh. "Nanofiltration of combined salt and sugar solutions: coupling between retentions." *Desalination* 120 (1998): 211.
- Weast, R.C. *CRC Handbook of Chemistry and Physics*. Cleveland, Ohio: CRC Press, 1973.

Zhou, F., C. Wang, and J. Wei. "Simultaneous acetic acid separation and monosaccharid concentration by reverse osmosis." *Bioresource Technology* 131 (2013): 349-356.

5. Conclusions

5.0 Module and Process prediction 139
 5.1 Simulation of industrial SW (comparison with literature data) 140
 5.2 How to perform Isomer separation? 144
 5.3 Discussions & Conclusions 146

5.0 Module and Process prediction

Until now the development of membrane process required several “crucial” stages, starting from feasibility tests at laboratory scale, passing through pilot plant tests and finishing with large industrial scale processes (Peshev & Livingston , 2013).

However, since model parameters have been estimated (at any level) and fluid dynamic inside industrial module membrane is well known, process simulation can be performed from each elemental step. In fact, once the model parameters for the solvent-solute(s) system are available, modeling can be applied to perform prediction for the same system at different operating conditions (pressure, cross-flow velocity, concentration, etc.), as shown in Fig. 5.1.

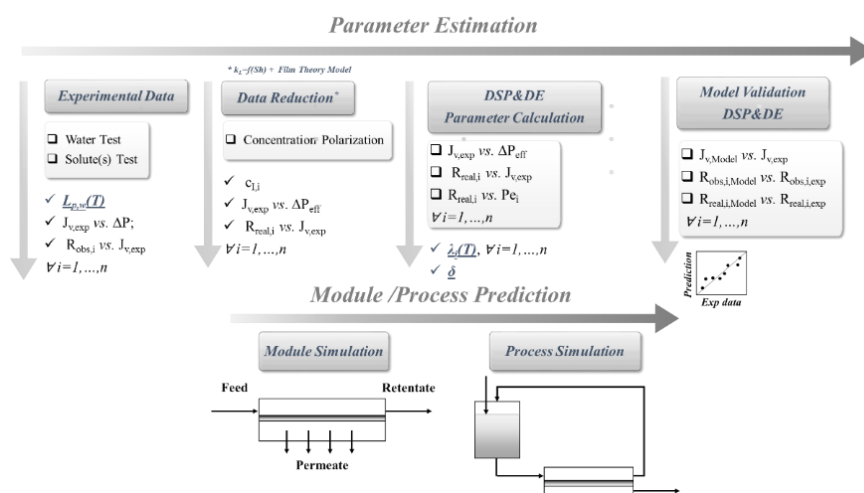


Figure 5.1: Flow sheet of the modeling steps of the thesis.

In Chapter 3 and 4 the revised DSP&DE method for Sugar NF was discussed in order to perform the Parameter estimation, in particular:

- i) Individuation of model parameters $L_{p,w}(T), \lambda_i(T), \delta$;

- ii) calculation of model parameters ;
- iii) validation on mono- and multicomponent mixtures on flat membranes and SW1812 membrane modules

According to this model, the parameters required are the hydraulic permeability, $L_{p,w}(T)$, the hydrodynamic coefficient for the specie i , $\lambda_i(T)$, and the effective membrane thickness, δ .

It means that for a n -solute solution (n =number of specie (solutes) in the solution, with $n \geq 1$), the number of model parameters required to perform a scale-up is $(n + 2)$.

Once the model parameters have been estimated, module and process can be simulated, thus scale up can be performed.

The validity of the algorithm has been tested and verified on an industrial SW module with appreciable results.

5.1 Simulation of industrial SW (comparison with literature data)

The performance of a commercial 4040C1025 GE-DL module were modeled, and compared with literature data from (Bandini & Nataloni, 2015), carried on industrial NF modules for dextrose recovery from crystallization mother liquors.

Aim of the work was primarily to compare the predictive power of the model, validated on laboratory scale modules and synthetic solutions, with experimental data performed on industrial configuration modules and real solutions.

In spite of the complexity of the mixtures investigated, solutions were modeled as ternary mixture composed of water, dextrose (DX 80-83%) and impurities modeled as maltose (ML 20-17%). Experiments on 4040C1025 GE-DL were performed in the optimal operative conditions of the module at 50°C and with a feed flow rate located in the range from 2300 to 3500 dm³/h, corresponding to an effective velocity inside the feed channel ranging from 0.18 to 0.60 m/s.

Because of the chemical nature of the solutions, chemical-physical properties necessary for data reduction were calculated assuming the solution as a binary Dextrose-water solution at the composition corresponding to the DS% content.

Concentration polarization in industrial modules at feed/membrane interface was calculated by using Sherwood correlation adopted for SW1812 module (found better than *Shock and Miquel* equation), whereas the pressure drop and mass transfer correlations are adapted from *Shock and Miquel's* work

Hydraulic permeability of the membrane is calculated from technical sheet, whereas model parameters from GE-DL flat membrane were used to predict process performances.

Simulation conditions are summarized in table 5.1

Table 5.1 Simulation of commercial 4040C1025 GE-DL spiral wound module. Test conditions, pressure drop and mass transfer correlation, and model parameters for slit-like pore geometry

Reference	Bandini & Nataloni, (2015)
Module-Membrane	4040C1025 GE-DL
Solutes	DX (1) + ML (2)
Concentration range (g/dm ³)	(1) 211.7-296.8; (2) 44.1-110.3
Temperature (°C)	50
Inlet pressure, P _{in} (bar)	20, 25, 30
Flow rate, Q _F (dm ³ /h)	2336.7-3634.8
<i>Data Reduction</i>	
Mass transfer coeff., k _L	<i>Siede & Tate</i>
ΔP _{loss}	<i>Shock & Miquel</i>
<i>DSP&DE model parameters (slit-like pore)</i>	
Water permeability, L _{p,w} (50°C)*	12.7
λ _{DX} (50°C)**	0.960
λ _{ML} (50°C)**	0.999
Membrane thickness, δ (μm)**	4.75

*Hydraulic permeability was calculated by data reported in technical sheets, according to the typical equations of the solution-diffusion model, in correspondence with the same conditions (Bandini & Nataloni, 2015); ** from GE-DL flat sheet

Since not very high fluxes across the modules were measured with sugar solutions (maximum Recovery less than 3.8%), because of the high sugar concentrations, module performances could be described by using average properties which refer to the conditions existing at the inlet section of the module itself.

Experimental set up is well described in (Bandini & Nataloni, 2015), and configuration mode is depicted in Fig. 5.2.

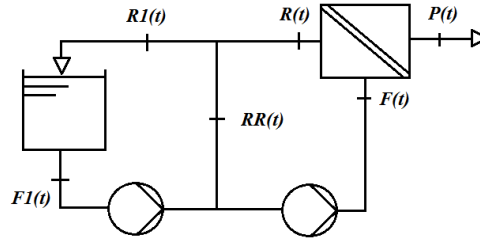


Figure 5.2: Configuration for batch operation mode, with partial recirculation of Retentate. Adapted from (Bandini & Nataloni, 2015)

The starting concentrations and purities were set to be equal to those of experimental data, the inlet pressure was set at 20, 25 and 30 bar.

In addition, as suggested by (Bandini & Nataloni, 2015) module was characterized by using few relevant quantities, such as total volume flux across the module (J_v), the average observed rejection of Dextrose ($R_{obs,DX}$) and Maltose ($R_{obs,ML}$), the *DS* composition (DS wt%), and finally the dextrose purity in Permeate and Retentate, which are independent each other. In this study each experimental quantity was compared with the same “predicted” value.

Results are shown in Fig. 5.3, where symbols represent experimental data, and lines represent model simulations from GE-DL flat membrane model parameters.

Fig. 5.4 shown the model prediction performed with parameters fitted on experimental data. The model parameters used in the simulation are reported in Table 5.2, and represent the parameters regressed from flat sheet, and 4040C1025 membranes respectively, for slit-like pore geometry.

Table 5.2 DSP&DE model paraters used in the simulation of 4040C1025 NF module. Binary mixture Dextrose-Maltose, 50°C, slit-like pore geometry.

Membrane	GE-DL	
	Flat sheet	4040C1025
$L_{p,w}(50^\circ C)$	15.2 ± 0.9	12.7
$\lambda_{DX,slit}(50^\circ C)$	0.960	0.960
$\lambda_{ML,slit}(50^\circ C)$	0.997	0.999
$\delta_{slit} (\mu m)$	3.25	4.75

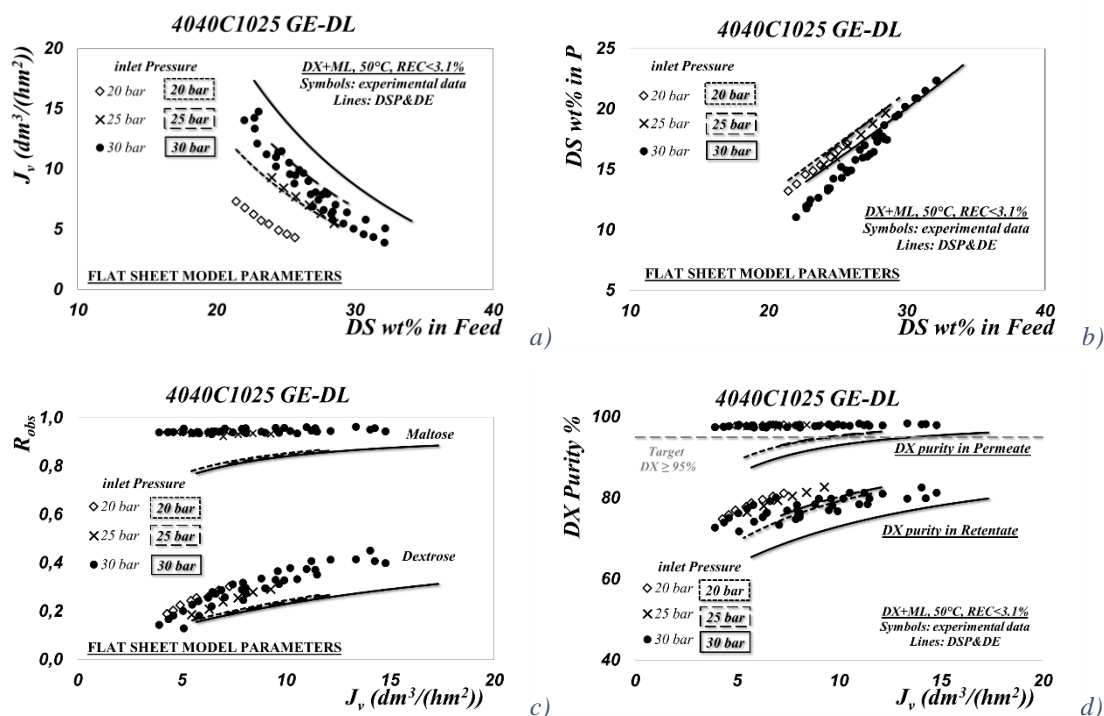


Figure 5.3: Comparison between literature experimental data ((Bandini & Nataloni, 2015)) and DSP&DE model simulation, performed with flat sheet membrane model parameters. Module GE-DL SW4040-50mil, experimental tests performed at pH 3.8-4.5, Feed flow rate=2300-3500 dm³/h, initial DX purity =81-83%. DSP&DE model simulations: (a) Total volume vs. DS wt% in the feed; (b) DS% in Permeate as a function of DS% in the feed; (c) observed rejection of DX and ML (~impurities) vs. total flux; (d) DX purity in Permeate and Retentate vs. Total flux.

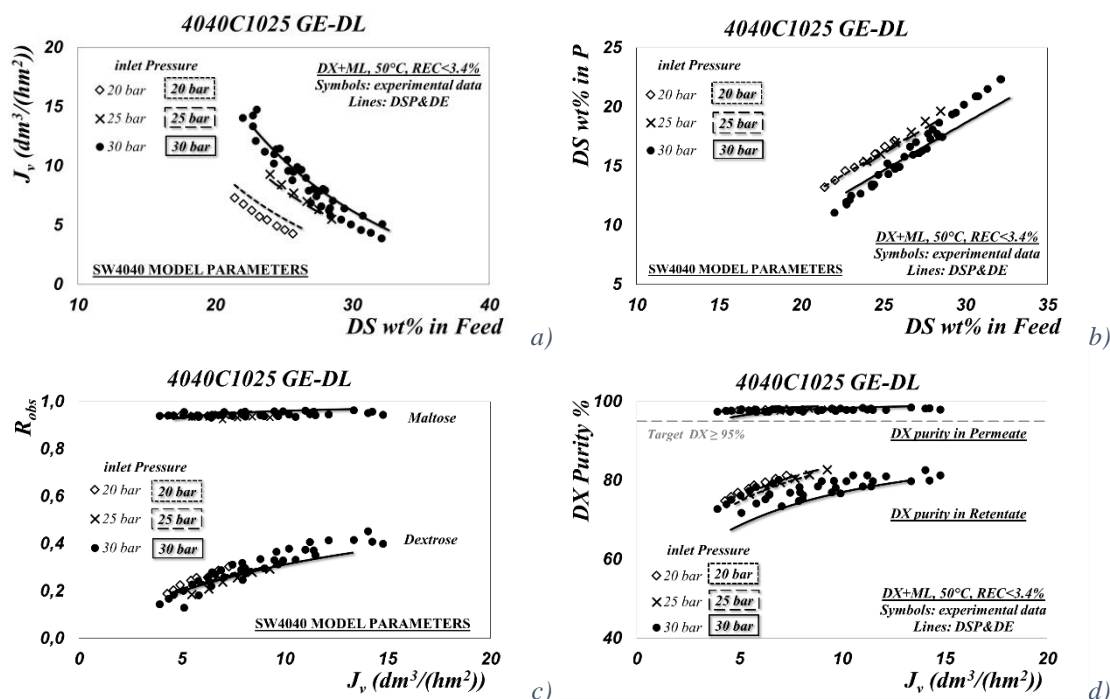


Figure 5.4: Comparison between literature experimental data ((Bandini & Nataloni, 2015)) and DSP&DE model simulation performed with 4040C1025 module model parameters. Module GE-DL SW4040-50mil, experimental tests performed at pH 3.8-4.5, Feed flow rate=2300-3500 dm³/h, initial DX purity =81-83%. DSP&DE model simulations: (a) Total volume vs. DS wt% in the feed; (b) DS% in Permeate as a function of DS% in the feed; (c) observed rejection of DX and ML (~impurities) vs. total flux; (d) DX purity in Permeate and Retentate vs. Total flux.

Results shown good agreement between modeled and experimental flux and rejection was observed as shown in Fig. 5.3 and 5.4 for each membrane sample, each solute in the whole range of temperature, pressure and concentration.

Although flat membrane show a completely different fluid dynamic and membrane area (compared to industrial spiral wound modules), is sufficient to describe module performances with good approximation.

Deviation between model prediction and experimental data may be attributed to membrane fouling. Experimentally fouling causes a flux decrease, with the respect to the values measured with the clean module at the initial condition. The flux decrease is quantified to 70% of the initial value, though rejection values as well as separation efficiency seems to be not affected by fouling.

Model is not able to take into account this flux decay, and for this reason errors may occur in predicting the permeate flux, overestimating experimental data.

This study give information useful for the process design and scale-up. The results obtained put clearly in evidence that only few well-defined experiments are sufficient to study the process feasibility with the membrane under investigation.

5.2 How to perform Isomer separation?

Isomers is a challenge in membrane separation technology.

Many studies and experiments documented the feasibility of Nanofiltration for the separation of monosaccharides from disaccharides [(Nabetani 1992), (Goulas, Grandison, & Rastall, 2002), (Aydogan, Gurka, & Yilmaz, 1998), (Bouchoux, Roux-de Balman, & Lutin, 2005), (Catarino, et al. 2008)], as well as monosaccharides fractionation (i.e. Xylose from dextrose), (Sjoman, et al. 2007), however simulated moving bed chromatography (*SMB*) is still the state of the art technology for industrial isomer purification.

One of the most challenging application is the separation of dextrose-fructose mixtures, whose production was discussed in *Chapter 2*. A schematic representation of the industrial production of *HFCS55%* id depicted in Fig. 5.5.

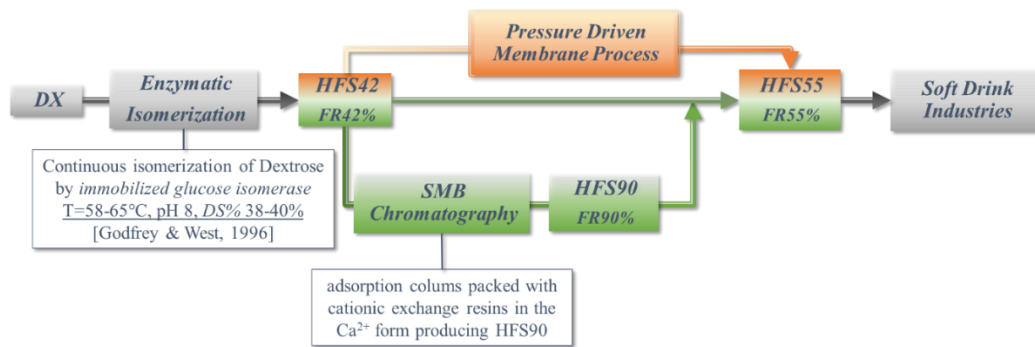


Figure 5.5: Schematic representation for the production of $HFS \geq 55\%$. Conventional pathway (SMB Chromatography step) vs. “Direct” pressure driven membrane process (Godfrey & West, 1996)

Nowadays in order to obtain a fructose syrup of 55% chromatographic technique is applied, with high efficiency.

Can we replace chromatographic step with a direct membrane process?

From experimental data and the discussion of the revised model, dextrose and fructose shown very similar hydrodynamic coefficients, that is to say that they are hard to isolate, in the whole range of operative conditions investigated.

On the basis of the revised model, module performance was simulated with total recirculation of Retentate mode on 1812C-34D GE-DL module, and results are shown in Fig. 5.6

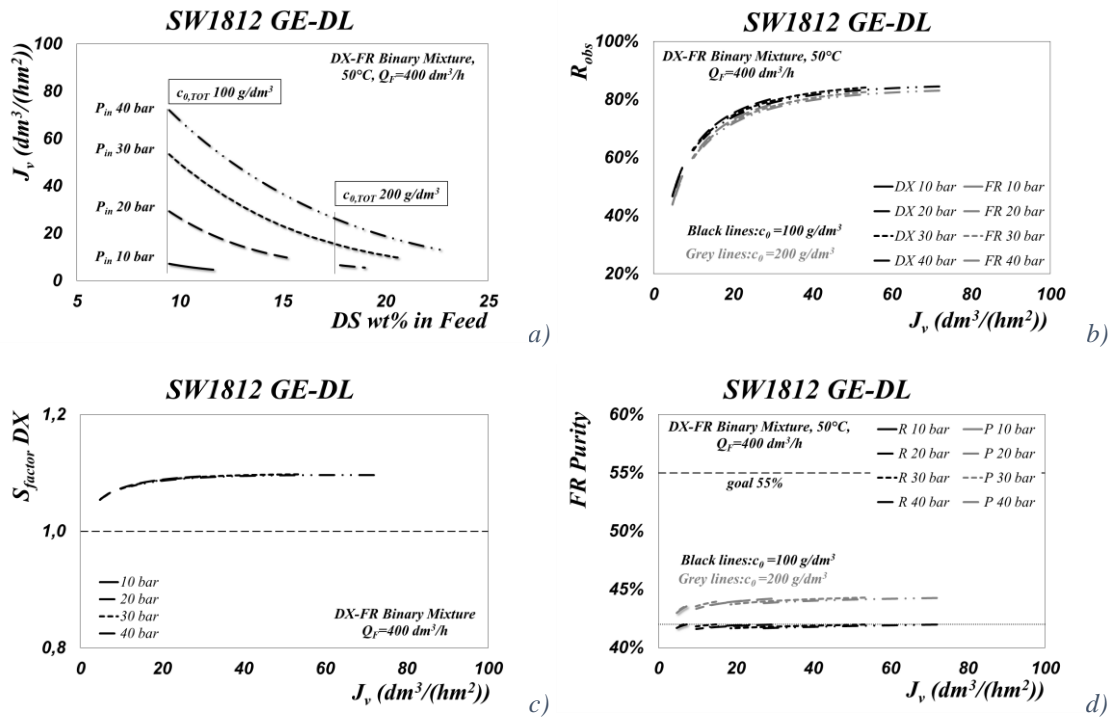


Figure 5.6: DX-FR separation. DSP&DE revised model simulation at 50°C, pressure ranging from 10 to 40 bar, total initial concentration ranging from 100 g/dm³ (black lines) to 200 g/dm³ (grey lines) and initial fructose purity 42%, $Q_F=400 \text{ dm}^3/\text{h}$. Model parameters from SW1812 GE-DL: $L_{p,w}(50^\circ\text{C})=10.7 \text{ dm}^3/(\text{h}\cdot\text{m}^2\cdot\text{bar})$, $\lambda_{FR}=0.990$, $\lambda_{DX}=0.991$, $\delta=3.45 \text{ }\mu\text{m}$, slit like pore geometry

As shown in Fig. 5.6 Dextrose-Fructose separation, with enrichment in fructose fraction from 42 to 55% is not achievable by using NF step. On the basis of model parameters achieved from experimental data, only a weak increase in fructose fraction is obtainable with small differences in hydrodynamic coefficients, especially at high total concentrations (200 g/dm³).

5.3 Discussions & Conclusions

This work reports the performance of commercial polyamide membranes assembled as flat sheet and spiral wound modules tested in aqueous solutions of oligosaccharides under various pressures, temperatures and concentrations. Spiral wound covered two module sizes (1.8”×12” and 4.0”×40”) with different feed spacer (34 mil and 50 mil respectively). A “revised” DSP&DE model was discussed to describe the transport through the membrane, starting from model parameters calculation procedure.

The unknown model parameters were determined from regression of experimental data. These parameters were then used to predict the performance of industrial spiral wound modules as well as process performances, and good agreement was observed with literature

data. This indicates that the “revised” DSP&DE model combined with the film theory is adequate to describe the transport through membranes, once Pressure drops and mass transfer coefficient correlation is known for the module geometry.

It has been shown that the correlation suited for the mass transfer coefficient determined for the 1.8”×12” module is able to describe mass transfer in industrial 4.0”×40” module too.

Model parameters regressed at each level (flat sheet, and 4040C1025 GE-DL) were used to predict process performance. Results were compared with experimental literature data (Bandini & Nataloni, 2015), and good agreement was observed, which proves that model parameters regressed at each level can be extended to describe process performance in a wide range of operating conditions.

This study proves that it is possible to identify the minimum number of experimental tests that allows to characterize oligosaccharide nanofiltration process.

The membrane transport model parameters for both flat sheet and spiral wound membrane modules were determined by regressing the performance of each module, using the DSP&DE model for single solute. According to this model, the parameters to be determined are the hydraulic permeability, $L_{p,w}(T)$, the hydrodynamic coefficient for the specie i , $\lambda_i(T)$, and the effective membrane thickness, δ .

It means that for a n -solute solution (n =number of specie (solutes) in the solution, with $n \geq 1$), the number of model parameters is $(n + 2)$.

These model parameters were then used to predict the performance on the same membrane in the whole range of test conditions. Good agreement between calculated and experimental flux and rejection was observed as shown in Fig. 5.4 and 5.5 for each membrane sample, each solute in the whole range of temperature, pressure and concentration

In conclusion

the revised DSP&DE model identifies the minimum number of experimental tests required in order to perform a process scale up for oligosaccharide NF processes at industrial level.

APPENDIX A

Materials & Methods

A.1 Solutions.....	149
A.1.1 Sugar model solutions.....	149
A.1.2 PHA and non-PHA solution.....	150
A.1.3 Model VFA Solutions.....	150
A.2 Membranes.....	150
A.3 Filtration units.....	151
A.3.1 Dead-end unit (UF/MF of PHA solution).....	151
A.3.2 Radial flow test cell (Sugar and VFA Nanofiltration).....	152
A.3.3 Lab scale spiral wound module (Sugar NF).....	153
A.3.4 Commercial SW4040 module.....	153
A.3.5 Bench-scale apparatus.....	154
A.4 Experimental Procedure.....	155
A.5 Analysis.....	157
A.5.1 Oligosaccharide Analysis.....	157
A.5.2 PHA non-PHA Analysis.....	157
A.5.3 VFA analysis.....	157

A.1 Solutions

A.1.1 Sugar model solutions

Synthetic oligosaccharide solutions were tested; analytical grade purity D(+)-glucose (molar mass equal to 180.16 g/mol) was supplied by Fagron Italia S.r.l, D(+)-fructose (180.16 g/mol), and D(-)-maltose (342.29 g/mol) were supplied from Sigma Aldrich, D(+)-Xylose (150.13 g/mol) was supplied by Carlo Erba Reagents S.r.l.. These reagents were used for the preparation of the model sugar solution and as standards for HPLC analysis. The relevant characteristics of these sugars are discussed in *Chapter 2*. All solutions were prepared in demineralized water, pH 5.6. During the experimentation solution pH was corrected, with drops of concentrated HCl and NaOH, in order to reach the value 4 and 6.

A.1.2 PHA and non-PHA solution

Ultrafiltration tests of non-PHA were performed on a real solution derived from enzymatic digestion of biomass. PHA recovery from *C. necator* cells was described in (Martino, et al. 2014). Wet PHA granules were collected by centrifugation (20,000 G for 30 min), while the supernatant represents the *non-PHA* solution.

Non-PHA consist of a mixture of cell debris and solubilized cellular materials derived from the enzymatic microbial cell ruptured. After a thermal treatment, the resultant debris are treated with enzyme cocktail and a surfactant to solubilize all non-PHA cellular materials. The solution tested is devoid of any PHA granules, presents a density closer to that of water, while viscosity and a color similar to those of an egg white.

A.1.3 Model VFA Solutions

Single VFAs (Bioreagent) were purchased from Sigma-Aldrich. Model VFA solutions were prepared at different pH (ranging from 3.5 to 4.0). The pH-shift of the feed solution was done with hydrochloric acid and sodium hydroxide, respectively. The composition of the solutions is showed in Table A.1

Table A.1: VFA model solution composition

<i>pH</i>	<i>Total VFA concentration (g/dm³)</i>	<i>Acetic Acid AA (g/dm³)</i>	<i>Propionic Acid PA (g/dm³)</i>	<i>Butyric Acid BA (g/dm³)</i>	<i>Valeric Acid VA (g/dm³)</i>	<i>Caproic Acid CA (g/dm³)</i>
3.5	10.08	2.23	2.20	2.02	2.00	1.62
4.3	11.05	2.27	2.39	2.09	2.29	1.99

A.2 Membranes

Nanofiltration

Four commercial polyamide membranes were tested in this study, GE-DK, GE-DL, GE-AG and GE-AK. Manufactured by GE Power&Water (well known as DESAL products) and supplied by Sepra S.r.l, Italy. Membranes are thin film composite, with an active layer in Polyamide, on a support of Polysulfone. This type of membrane has a good temperature and pH stability. A summary of the general properties of these membranes is reported in Table A.2

Hydraulic permeability were calculated by technical sheet data applying the typical equations of the solution-diffusion model (Mason and Lonsdale 1990) in correspondence with the same conditions.

Table A.2: General Properties for NF membranes (data from technical sheets)

Type	Classification	Cut-off (g/mol)	Rejection	pH range	IEP	P_{max} (bar)	T_{max} (°C)	$L_{p,w}$ (25°C) ($dm^3/(hm^2bar)$)
GE-DL	NF	150-300	96% MgSO ₄ ^[a]	3-9	4.1 (Manttari, Pihlajamaki and Nystrom 2006)	41.37 for T<35°C; 30.00 for T>35°C	50	5.96 ± 0.16 ^[b]
GE-DK			98% MgSO ₄ ^[a]	3-9	4.0 (Hagmeyer and Gimbel 1998)	41.37 for T<35°C; 30.00 for T>35°C	50	4.90 ± 0.20 ^[b]
GE-AK	"brackish water"	-	99 % NaCl ^[c]	4-11	-	27.56	50	5.77 ± 0.23 ^[b]
GE-AG			99.5 % NaCl ^[c]	4-11	-	31.03	50	3.19 ± 0.07 ^[b]

^[a] MgSO₄ 2000 mg l⁻¹ at 7.6 bar, 25°C, 15% Recovery; ^[b] calculated according to solution-diffusion model (Mason and Lonsdale 1990); ^[c] NaCl 2000 mg l⁻¹ at 15.5 bar, 25°C, pH 7.5 15% Recovery

Ultrafiltration and Microfiltration

Hydrophilic and hydrophobic membranes of different materials and MWCO were delivered by Septra S.r.l.. Table A.3 summarizes membrane properties.

Table A.3: UF and MF hydro -philic and -phobic membranes, delivered by Septra S.r.l.

Membrane	Material	Pore radius (μm)	MWCO	Wettability	$L_{p,w}$ ($dm^3/(hm^2bar)$)
TF-200	PTFE ¹ (PALL Corporation)	0.2	-	Hydrophobic	-
PV400R	PVDF ²	-	250 kDa	Low Hydrophobic	1470±220
PV400		0.05-0.08	100 kDa		580±87

A.3 Filtration units

A.3.1 Dead-end unit (UF/MF of PHA solution)

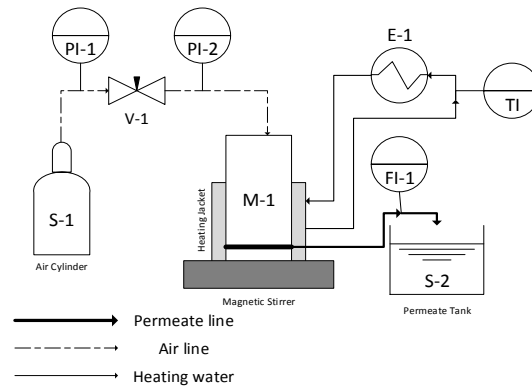
A dead-end stirred filtration (Sartorius), described in Fig. A.1, was used for the filtration of the non-PHA/PHA solution operated batchwise using compressed air ($P_{max}=7$ bar). The system consists of a stirred cell unit of 200 ml maximum process volume, a magnetic stirrer

¹ PTFE=Polytetrafluoroethylene;

² PVDF=Polyvinylidene fluoride

bar was placed just above the membrane for mixing and minimizing concentration polarization. The stirrer speed was set at 500 rpm. An external jacket surrounding the cell is connected to an external water bath for temperature control.

Discs of the flat membrane (4.3 cm in diameter, with an effective area of 14.6 cm²) were cut from flat sheets provided by the manufacturer. The pressure was provided from an air cylinder. During the experimental trial with solutions the permeate was collected in a graduated vessel (150 ml).



<i>Equipment List</i>		<i>Instruments</i>	
<i>S-1</i>	Air cylinder	<i>V-1</i>	Regulating valves
<i>S-2</i>	Permeate Tank	<i>PI-1, PI-2</i>	Manometer
<i>M-1</i>	Dead end Stirred cell	<i>TI</i>	Thermometer
<i>E1</i>	Heat exchanger	<i>FI-1</i>	Flow meter (Permeate side)

Figure A.1: Dead-end stirred cell configuration

A.3.2 Radial flow test cell (Sugar and VFA Nanofiltration)

Each NF/RO membrane were tested as circular flat sheets housed in a radial flow test cell (with an effective filtration area of $39.6 \cdot 10^{-4} \text{ m}^2$) described in a previous work C.Mazzoni and S.Bandini (2007). The radial flow unit houses in parallel two flat membrane sheets; because of the configuration of the cell each membrane is fed with half of the flow rate supplied by the pump

A.3.3 Lab scale spiral wound module (Sugar NF)

In the sugar NF study, the separation of oligosaccharides was conducted with commercial “lab-scale” 1812 spiral wound module (with an effective filtration area of 0.32 m²), purchased from Septra S.r.l

Each modules was a small size (“lab-scale”) spiral wound element with a length of 12 in. (0.35 m), a nominal diameter of 1.85 in. (0.047 m) and a feed spacer of 34 mil. The main characteristics of the module are listed in Table A.4.

Table A.4: Characteristics of NF spiral wound module used (data from technical sheets)

Parameter	Characteristics	
Model	DK1812C-34D	DL1812C-34D
Manufacturer	GE-Osmonics	
Configuration	Spiral wound- Biotech test element	
Filtration area (m ²)	0.38	
Length (m)	0.305	
Spacer (mil)	34	
Minimum MgSO ₄ rejection	98%	96%

* MgSO₄ 2000 mg l⁻¹ at 7.6 bar, 25°C, 15% Recovery

A.3.4 Commercial SW4040 module

In order to perform model validation at process scale, prediction of industrial commercial spiral wound module was performed and results compared with literature data from (Bandini and Nataloni 2015). In this study Dextrose-Maltose separation was performed on 4040C1025 GE-DL, whose characteristics are summarized in Tab. A.5

Table A.5: Characteristics of NF commercial spiral wound module (4.0” × 40”)

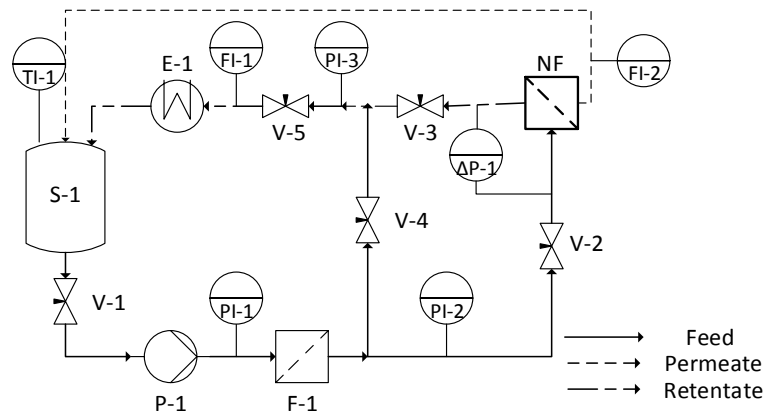
Parameter	Characteristics
Model	4040C1025 GE-DL
Manufacturer	GE-Osmonics
Configuration	Industrial Spiral wound
Filtration area (m ²)	6.1
Length (m)	1.016
Spacer (mil)	50

Minimum $MgSO_4$ rejection 96%

A.3.5 Bench-scale apparatus

Both the radial flow test cell and spiral wound modules (1.8" × 12") described previously were tested in a bench scale plant described in a simplified flow sheet in Fig. A.2.

The unit was designed to work (operate) both in total recirculation mode of retentate and permeate (constant concentration during the experimentation) and in total recirculation mode of retentate (batch operation mode) as shown in a simplified form in Fig. A.3 (a) and (b) respectively. During the total recycle operation mode a constant concentration in the feed side was obtained, and experiments were carried out by varying the inlet pressure.



Equipment List		Instruments	
S-1	Feed Tank	V-1, V-2, V-3, V-4	Regulating valves
P-1	Positive displacement pump	V-5	Needle valve
F-1	Cartridge filter	PI-1, PI-2, PI-3	Manometer
E-1	Heat exchanger	ΔP-1	Differential pressure Gauge
NF	NF module	TI-1	Thermometer
		FI-1, FI-2	Flow meter

Figure A.2: Diagram of the NF bench-scale plant used in the experiments. TK-feed tank; P1-positive displacement pump; FT-cartridge filter; E1-heat exchanger, temperature controlled water bath for temperature control of the feed; V-1-3-regulating valves; V-4-by pass valve closed during NF experiments; V-5- needle valve, for regulating the pressure; PI-1-2-3: pressure gauge; NF-nanofiltration cell (Radial flow test cell, Spiral wound element 1812); FI-1-flow meter retentate side; FI-2-flow meter permeate side; TI-1-thermometer.

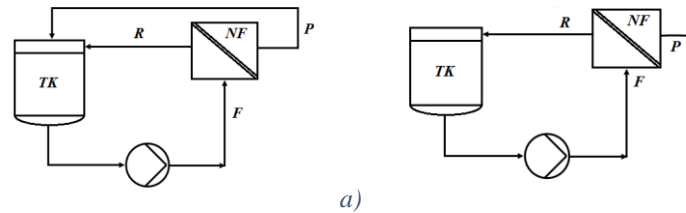


Figure A.3: Configurations for operation mode: (a) Total recirculation of Retentate and Permeate; (b) Total recirculation mode of Retentate

A.4 Experimental Procedure

Storage and Start-up

Before their use virgin membranes were stored in 1% bisulfite solution at room temperature. This conservation procedure avoids microbiological growth. Before the installation, membranes were rinsed with demineralized water (pH 5.6) in a single pass-plant configuration in order to remove any preservative solution.

The start-up procedure consists of three main steps.

Stabilization

Membranes are stabilized with ion free water in total recirculation mode operation of retentate and permeate at 20 bar, firstly at 30°C for 4 hours and then at 50°C for 4-5 hours again, with a volume flow rate of 400 dm³/h.

Stabilization is completed when permeate flux is constant in a range of 30-45 min.

Washing procedure

After the compaction membranes were subjected to a washing procedure with basic/acid solutions.

Washing is performed in total recirculation mode of permeate and retentate.

After a basic cleaning step (6.6% aqueous solution of Ultrasil-11, at maximum pH of 11, 40°C, inlet pressure 3 bar, at 400 dm³/h flow rate, for 1 h long) the acid cleaning step starts (aqueous solution of HNO₃ at pH 4, 40°C, 3 bar inlet pressure, at 400 dm³/h flow rate, for 1 h long).

Both cleaning procedures are followed by an abundant rinsing step performed with de-ionized water in single pass plant configuration, at room temperature, 3 bar inlet pressure, and 400 dm³/h volume flow rate.

Each rinsing is concluded when both permeate and retentate pH values correspond to de-ionized water pH. Flushing with de-ionized water allows to remove all traces of detergent or acid present in the plant.

A Basic/Acid washing procedure is required when a decrease higher than 20% is observed for water permeability.

Pure Water flux measurements

After the cleaning procedure measurements of total flux across membranes are performed with demineralized water, in a pressure inlet range varying from 3 to 30 bar for flat sheet membranes, and from 4 to 25 bar for spiral wound modules. Flow rate and pH are set respectively at 400 dm³/h and 4.

Water fluxes are performed at three different operating temperature is set at 30°, 40° and 50°C.

The initial water flux measurements is compared with measurements carried out under the same condition after each experiments, in order to monitor the state of the membranes (for instance fouling or damage) and control the cleanliness of the membranes.

Average permeability data measured during all the experiments are reported in *Chapter 3* for both configurations (flat-sheet and Spiral wound module).

Filtration experiments, sample analysis and model solution preparation

All the experiments were performed at controlled temperature, pressure, volume flow rate, as well as pH and concentration in the feed tank. Volume flow rates in Permeate P and Retentate R streams were measured as a function of driving force (Total recirculation mode of R and P) or as a function time (Total recirculation of R), contemporary samples were taken in the feed tank and in the Permeate P. For the entire duration of the test pH was measured and maintained constant.

Before each measurement a stabilization time of 1 hour (for the lower pressures and higher concentrations) and 40 min (for the higher pressures and lowest concentrations) was applied in order to reach the correct value.

A.5 Analysis

A.5.1 Oligosaccharide Analysis

For aqueous solutions containing single sugars a refractometer was used in order to determine the concentration (measurements were performed at constant temperature, 35°C).

When mixtures were processed total dry concentration was measured *in loco* by a refractometer, afterward sugar compositions were analysed by an HPLC followed by a refractive index detector. The HPLC system was equipped with a Transgenomic CARBOsep Coregel-87C Ca²⁺ resin based column (dimension 300 × 7.8 mm) supplied by STEP BIO S.r.l. (Bologna, Italy). Technical information about the column have been specified in Table A.6

Table A.6: Technical characteristics of HPLC column

Column Type	Coregel 87C
Part Number	CHO-99-9860
Column Size (mm)	300 × 7.8
Ionic Form	Calcium (Ca ²⁺)
Particle Size (µm)	9
Maximum pressure (psi)-(bar)	1000-(68)
Standard Flow Rate (mL/min)	0.6
pH stability	0-14
Maximum Flow Rate (mL/min)	1.0
Standard Temperature (°C)	85
Maximum Temperature (°C)	95

A.5.2 PHA non-PHA Analysis

TGA analyses were performed using a TGA 2950 (TA Instruments) thermogravimetric analyzer, from room temperature to 600°C at a heating rate of 10°C min⁻¹ under continuous airflow, as described in (Martino, et al. 2014).

Non-PHA analysis was performed by using a refractometer (measurements were performed at constant temperature, 35°C) in order to quantify the suspended solids (SS) amount.

A.5.3 VFA analysis

VFAs analysis was performed according the procedure described in VFAs were determined by CG-FID Analysis (Agilent 7890 A). For VFAs determination, a HP-INOVAX column (ID 0.25 nm, length 30 m and film thickness 0.25 µm was employed.

APPENDIX B

Fluid dynamic analysis on 1812 Spiral Wound modules

B.0 Introduction	161
B.1 Determining the mass transfer coefficient: State of art.....	162
B.2 Determination of mass transport coefficient k_L suitable for SW1812 modules: experimental results and data reduction.....	168
B.3 Data reduction	172
B.4 Results	174
B.5 Pressure Drop in a SW1812 module	179
References.....	180

List of symbols

<i>Symbol</i>	<i>Units</i>	<i>Quantity</i>	<i>Geometrical Parameters</i>		
Re	-	Reynolds number	A	[m ²]	membrane area
Sc	-	Schmidt number	R_c	[m]	semi-cell radius (=0.03551)
Sh	-	Sherwood number	b	[m]	semi-cell thickness/ flat channel width/module leaf width
ΔP_{loss}	[Pa]=[kg/(ms ²)]	pressure loss	L	[m]	module length (=0.305 m)
λ	-	friction coefficient	L^*	[m]	length of the entry region
ρ	[kg/m ³]	density	d_f	[m]	fiber diameter
η	[kg/(ms)]=[Pa·s]	dynamic viscosity	h	[m]	channel height/spacer height, feed side(=34 mil)
$\nu=\eta/\rho$	[m ² /s]	kinematic viscosity	h_p	[m]	permeate spacer height
D_S	[m ² /s]	diffusion coefficient	A_{eff}	[m ²]	effective membrane area, spiral wound module
v	[m/s]	velocity	A_{SP}	[m ²]	wetted surface of the spacer
v_{eff}	[m/s]	effective velocity	V_{SP}	[m ³]	volume of the spacer

k_L	[m/s]	mass transfer coefficient	$S_{v,SP}$	[m ⁻¹]	specific surface of the spacer
δ	[m]	boundary layer thickness	ε	-	spacer porosity (~0.9)
J_v	[m/s]	permeate flux	θ	[rad]	number of spiral turns
Q_F	[m ³ /s]	feed flow rate	r_{module}	[m]	module radius (=0.047m)
c	[g/dm ³]or [mol/dm ³]	concentration	$r_{gatherer}$	[m]	gatherer radius (=0.0159 m)
R_{obs}	-	observed rejection	s_{spiral}	[-]	spiral step
R_{real}	-	real Rejection	S	[m ²]	cross section of flow channel
L_p	[dm ³ /(hm ² bar)]	membrane permeability	P	[m]	wetted perimeter (circumference)
ΔP	[bar]	pressure difference			
$\Delta\pi$	[bar]	Osmotic pressure difference	<i>Subscript</i>		
T	[K]	temperature	i	Solute/component	
R	[J/(molK)]	Universal gas constant (=8.314)	$bulk$	bulk side	
σ_v	-	Staverman reflection coefficient	I	feed/membrane interface	
α	-	Reynolds exponent	F	feed side	
β	-	Schmidt exponent	P	permeate side	
ω	-	(d _b /L) exponent	R	retentate side	
a	-	Reynolds coefficient in friction coefficient	$inside$	inside the pore	
b	-	Reynolds exponent in friction coefficient			
φ	-	steric partitioning coefficient			

B.0 Introduction

The efficiency of membrane processes depends in general not just on the membrane properties but also on the flow conditions in front of the membrane (Schwinge, Neal, et al. 2004).

Spiral wound (SW) modules are the most common commercially available due to their high membrane area to volume ratio, however the major problems for SW units are concentration polarization and pressure loss.

In membrane research, knowledge of the concentration at the membrane surface c_I is of great interest for the description and modelling of the process.

The main purpose of this work is to measure the mass transfer coefficient, k_L , and pressure loss, ΔP_{loss} , in a “lab-scale” spiral wound module, technically SW1812.

Mass transfer coefficients are usually presented in dimensionless forms in terms of *Sherwood* number (Sh), meanwhile pressure loss is related to a proper *friction coefficient* ($\lambda=4f$).

In literature many researchers studied fluid dynamics and mass transfer through plane, spacer-filled channel, characteristics of spiral wound membrane modules, typically in aqueous solutions. To determine the mass transfer coefficient, three main methods have been used in literature (Shi, et al. 2015):

- (i) direct measurements, which made use of optical or electrochemical methods;
- (ii) indirect measurements, which are based on regression of membrane performance data using a combination of film theory and membrane transport models;
- (iii) computational fluid dynamics (CFD) simulation, based on *a priori* simulation of the module geometry.

The pressure drop characteristics of a module were usually determined either from direct measurements, using accurate pressure gauges, or via *CFD* simulation.

This study presents some experimental data processed according the second method. Transport resistances at the membrane surface will be discussed in detail, taking into account that the real retention is a function of the concentration at the membrane surface, which varies with the concentration polarization.

Furthermore the performance of the spiral wound element (i.e. permeate flux) can be calculated by numerical integration of balance equations. For this purpose a computer

program is required, which needs reliable input data regarding geometrical parameters and transport characteristics.

Literature correlations (i.e. (Shock and Miquel 1987)), experimental results and a computer program (TK-Solver ®) have been discussed and applied in order to calculate the proper correlation for mass transfer coefficient and pressure drop.

B.1 Determining the mass transfer coefficient: State of art

A number of qualitative relationships correlating the mass transfer coefficient to physical properties, flow channel dimensions, and operating parameters exists in the literature, but when no good theory exists, dimensional analysis is a powerful tool. Using the analogy with heat transfer, one can obtain general correlations.

Mass transport resistances at the membrane surface can be calculated by using mass transport coefficient. The commonly used dimensionless parameters for the description of mass transfer and pressure loss are:

$$\text{Mass-transfer number} \quad Sh = f(\text{Re}, Sc, \text{geometry})$$

$$\text{Friction coefficient} \quad \lambda = f(\text{Re})$$

Where Sh , Re and Sc are Sherwood number, Reynolds number and Schmidt number respectively. How to calculate dimensionless number is specified in Tab. B.1:

Table B.1: Dimensionless parameters for the description of mass transfer coefficient and pressure loss, specific for spiral wound element

<i>Dimensionless number for mass transfer*</i>		
<i>Sherwood number</i>	$Sh = \frac{k_L d_h}{D_s} = a \text{Re}^\alpha Sc^\beta$	<i>(B.1)</i>
<i>Reynolds number</i>	$\text{Re} = \frac{\rho v d_h}{\eta}$	<i>(B.2)</i>
<i>Schmidt number</i>	$Sc = \frac{\nu}{D_s} = \frac{\eta}{\rho D_s}$	<i>(B.3)</i>
<i>Friction coefficient</i>	$\lambda = 4f = \frac{2\Delta P}{\rho v^2} \cdot \frac{d_h}{L}$	<i>(B.4)</i>

*The dimensionless numbers are calculated using average bulk physical properties

Another geometrical parameter required is the hydraulic diameter of the spacer-filled channel in the element. As a general rule the hydraulic diameter can be expressed as:

$$d_h = 4 \cdot \frac{S}{P} \quad (B.5)$$

Where S is the cross section available for the flow, and P is the wetted perimeter of the channel.

Unlike tubes and flat channel, the hydrodynamics in a spiral wound element are critically influenced by the presence of the spacer material. The spacer materials in the feed and permeate channels reduces the void volumes of these and raises the effective velocities. The characteristic velocity in a spiral wound element can be calculated as:

$$v = v_{eff} = \frac{Q_F}{A_{eff}} \quad (B.6)$$

In the simplest approaches the SW is considered to be a flat channel, accounting for the spacer. The effective area A_{eff} can be calculated from the leaf width b , spacer thickness h , and porosity ε , according the equation:

$$A_{eff} = bh\varepsilon \quad (B.7)$$

Leaf width b can be calculated by using two different approaches. The first one as well as the easiest is the empirical rule, whereby:

$$b = \frac{1}{2} \frac{A}{L} \quad (B.8a)$$

The second one, known as “*Spiral rule*”, whereby:

$$b = \frac{1}{2} a [\mathcal{G} \sqrt{1 + \mathcal{G}^2} + \ln \mathcal{G} \sqrt{1 + \mathcal{G}^2}] \quad (B.8b)$$

$$\mathcal{G} = \frac{r_{module} - r_{gatherer}}{s_{spiral} \cdot 2\pi} \quad (B.9)$$

$$a = \frac{s_{spiral}}{2\pi} \quad (B.10)$$

$$s_{spiral} = h + h_p \quad (B.11)$$

In the “spiral” correlation h_p is an unknown value, besides, information about the spacer geometry in commercial modules is usually confidential and therefore unavailable for users without performing a module autopsy, however from literature the thickness of the

permeate spacers lies in the range from 0.2 to 0.4 mm (referred to *RO* membranes), and the porosity is significantly lower than that of feed spacer (Shock and Miquel 1987).

For this study, once fixed porosity ($\epsilon=0.9$) the value h_p has been found minimizing the difference between the area of the membrane from data sheets (0.32 m²) and the area calculated from the parameters derived from the spiral rule (Eq. B.8b). For a permeate spacer height of 0.58 mm (~23 mil) effective area for both relationships reaches the same value, which is slightly higher than typical values from literature.

Geometrical data obtained from both correlations (“empirical” (Eq. B.8a) and “spiral” (Eq. B.8b) rules) for both SW1812-34 GE-DL and GE-DK are compared in Tab. B.2.

Table B.2: Geometrical parameters for biotech spiral wound element 1812-34 Desal GE-DK and GE-DL, calculated with both Empirical rule (Eq. C.12a) and Spiral rule (Eq.C.12b)

	<i>Empirical Rule</i>	<i>Spiral Rule</i>
<i>Membrane area (m²)</i>		0.32
<i>h (mil)</i>		34
ϵ^*		0.9
<i>L (m)</i>		0.305
<i>d_h (m)</i>		$1.11 \cdot 10^{-3}$
<i>h_p (m)</i>	**	$5.85 \cdot 10^{-4}$
<i>b (m)</i>	0.525	0.525
<i>A_{eff} (m²)</i>	$4.08 \cdot 10^{-4}$	$4.08 \cdot 10^{-4}$

*hypothesis; ** not required

For simplicity in this study geometrical parameters obtained with the empirical rule will be use.

The measured Sherwood numbers for comparable Reynolds numbers are significantly higher in the spacer-filled channel than in the empty one (Shock and Miquel 1987).

In the case of forced convective flow the following relationship (Eq. B.1) is valid, at least as long as the total density and diffusivity vary only little across the boundary layer.

$$Sh = \frac{k_L d_h}{D_s} = a Re^\alpha Sc^\beta \quad (B.1)$$

The exponents α and β are constant determined by the state of development of the velocity and concentration profiles along the channel. The Schmidt number dependency (β) is

derived from dimensional considerations of the convective diffusion equation under condition in which the momentum boundary layer is much longer than the diffusion boundary layer, i.e., when $Sc \gg 1$.

For laminar flow systems, if both velocity and concentration profiles are fully developed, both α and β are zero. If velocity profile is fully developed but concentration boundary layer is developing along the entire length of the channel, the Graetz or Leveque¹ solution can be used with $\alpha = 1/3$ and $\beta = 1/3$. If both velocity and concentration profiles are developing, $\alpha = 1/2$ and $\beta = 1/3$ (Grober, Erk and Grigull 1961). When a laminar flow occurs, the entrance length, i.e. the region of flow where the profile is not fully developed, is important for mass transport, and the ratio d_h/L is taken as an additional parameter.

In situations where the concentration boundary layer is developing down the entire length of the flow channel, the Sherwood number will also be a function of the channel length, L , thus equation B.1 is usually rewritten for laminar flow models as Eq. B.12:

$$Sh = a Re^\alpha Sc^\beta \left(\frac{d_h}{L} \right)^\omega \quad (B.12)$$

Where α is 0.664 in the Grober correlation and 1.86 in the Leveque solution. The value of ω is 0.33 in the developing boundary layer and 0.5 for fully developed velocity profiles.

For turbulent flow, the Chilton-Colburn or Dittus-Boelter correlation can be used with $\alpha = 0.8$ and $\beta = 0.33$. The constant a generally is independent of the solute mobility and membrane retention, varies with geometrical parameters (channel height and distance from the inlet zone) and reflects physical property variations and other conditions of the system that one cannot explicitly account for from first principles.

Among the indirect measurements approaches, (Shock and Miquel 1987) performed regression of flat sheet membrane performance data to determine the mass transfer coefficient in a plane, feed spacer filled channel using the combination of film theory and an empirical membrane transport model. This empirical transport model assumes that the permeate flux is linearly dependent on the difference between applied pressure and osmotic pressure (see Tab. B.5). The authors used a dimensionless correlation to describe the mass transfer coefficient, in the form of Eq. B.1, where *Reynolds* and *Schmidt* numbers are expressed by using Eqs. B.2 and B.3 respectively:

¹ $L^* = 0.029 d_h Re$

$$Sh = \frac{k_L d_h}{D_s} = a Re^\alpha Sc^\beta = a \left(\frac{d_h \rho v}{\eta} \right)^\alpha \left(\frac{\eta}{\rho D_s} \right)^\beta \quad (B.1)$$

Where d_h is the hydraulic diameter of the system and D_s the diffusion coefficient. In this work (Shock and Miquel 1987), the spacer geometry was measured using a light microscope; however the authors pointed out that this might not be a very accurate technique to obtain the characteristic dimensions of permeate spacers, due to their complicated geometry, moreover they found that the geometry of the feed spacer had little effect on the friction coefficient, while the geometry of the permeate spacer showed more significant effects. Other authors [(Kuroda, Takahashi and Nomura 1983), (Da Costa, et al. 1991), (Schwinge, Wiley, et al. 2000)] also studied the effects of spacer geometry on the friction coefficient. Various type of spacers were considered in their works and a number of experimentally measured pressure drop data were reported. The significant effects of the spacer geometry on pressure drop performance were observed.

From all the literature so far, it is clear that the spacer geometry significantly affects the fluid dynamics and mass transfer characteristics in the spacer filled channels of spiral wound membrane modules. Accordingly many correlations in the form of Eqs. B.1 and B.16 were reported.

(Shock and Miquel 1987) measured the pressure drop through various feed and permeate spacer filled channels. A friction coefficient correlation was used to fit their experimental data, in the form of Eq. (B.4):

$$\lambda = \frac{2\Delta P d_h}{\rho v^2 L} = a \left(\frac{d_h \rho v}{\eta} \right)^b = a Re^b \quad (B.4)$$

λ is the friction coefficient and ΔP is the pressure drop through the channel, d_h is the hydraulic diameter of the channel, L is the length of the channel, ρ is the density of the solution, v is the velocity of the flow along the channel, η is the dynamic viscosity of the solution, and Re is the Reynolds number; a and b are the coefficient and the exponent of Reynolds number in the friction coefficient correlation, respectively.

In comparison to desalination, when sugar solutions are processed fluid dynamics and mass transfer characteristics in spiral wound membrane modules are different due to a broad range of feed concentrations, and of possible *Reynolds* and *Schmidt* numbers.

In summary, in the literature, many relationships can be found to describe the mass transfer coefficient under various conditions. Typical expression for the calculation of mass

transport coefficient in membrane literature, in the case of forced convection are summarized in Tab. B.3

Table B.3: Mass Transport and pressure loss correlations for different module geometry flow regime (Laminar and Turbulent) in Literature

Geometry	Flow Regime	Correlation	Ref.
Tube	Laminar, $L < L^*$	$Sh = 0.664 Re^{0.5} Sc^{0.33} \left(\frac{d_h}{L}\right)^{0.33}$	(Grober , Erk and Griggull 1961)
Tube or flat channel	Laminar $L > L^*$	$Sh = 1.86 \left(Re \cdot Sc \cdot \frac{d_h}{L} \right)^{1/3}$	Graetz-Leveque (Rautenbach and Albrecht 1989)
		$0.1 < Re \cdot Sc \cdot \frac{d_h}{L} < 10^4$	
Tube or Flat Channel	Turbulent, $Sc < 1, Re > 2000,$	$Sh = 0.023 Re^{0.875} Sc^{0.25}$	(Jonsson and Boesen 1977), (Schweitzer 1988) or Sieder & Tate, Dittus-Boelter
	Turbulent	$Sh = 0.04 Re^{3/4} Sc^{1/3}$	(Rautenbach and Albrecht 1989)
Flat channel + spacer (valid for SW)	Turbulent $100 < Re < 1000$	$Sh = 0.065 Re^{0.875} Sc^{0.25}$ $\lambda_{Feed} = 6.23 Re^{-0.3}; \lambda_p = 105 Re^{-0.8}$	(Shock and Miquel 1987)
SW1812**		$Sh = 0.075 Re^{0.61} Sc^{0.33}$ $\lambda_F = 6.94 Re^{-0.34}; \lambda_p = 16 Re^{-0.34}$	(Shi, et al. 2015)
SW	Laminar/Turbulent	$k = 0.753 \left(\frac{K}{2-K}\right)^{0.5} \frac{D}{h_b} Sc^{-1/6} \left(\frac{Pe h_b}{\Delta l}\right)^{0.5}$ $Pe = \frac{2h_b u_b}{D}; h_b = \frac{1}{2} h_{feed}$ Where $K=f(\text{spacer mixing efficiency}), \Delta l=\text{spacer mixing length}, u_b=\text{velocity}$	(Evangelista 1988)
Flat channel with spacer	$10 < Re < 1000$	$Sh = 0.02 Re^{0.57} Sc^{0.4}$	(Koutsou, Yiantsios and Karabelas 2009)
Tubular, RO membrane	$2600 < Re < 10000$	$Sh = 0.02 Re^{0.91} Sc^{0.25}$	(Sutzkover, Hasson and Semiat 2000)

Flat channel	Laminar	$Sh = 1.62 \left(\text{Re} Sc \frac{d_h}{L} \right)^{\frac{1}{3}}$	(Porter 1972)
	Turbulent	$Sh = 0.023 \text{Re}^{0.8} Sc^{\frac{1}{3}}$	

**Organic Solvent Nanofiltration application, SW1812 geometrical parameters were obtained by indirect regression of experimental data. $d_h=0.79$ mm, $\epsilon=0.872$ h=0.77 mm (30 mil)

Once obtained the mass transfer coefficient from the Sherwood correlation, concentration profile in front of the membrane can be estimated by the *Film model*:

$$\exp\left(\frac{J_v}{k_L}\right) = \frac{c_I - c_P}{c_{bulk} - c_P} \quad (B.13)$$

Concentration decreases exponentially from a maximum value c_I at the membrane surface to c_{bulk} in the bulk of the fluid, and obviously concentration polarization is greatly affected by both permeate flux, J_v , and the membrane-parallel flow, k_L .

B.2 Determination of mass transport coefficient k_L suitable for SW1812 modules: experimental results and data reduction

For the experimental determination of pressure drop and mass transport characteristics in SW modules, the pressure drop ΔP and mass transfer coefficient k_L must be measured.

In order to obtain reliable mass transfer coefficient relationships directly from experimental data, two methods were tested: the first method based on the variation in observed retention when cross-flow velocities are changed (“*velocity variation method*”), and the second method by using the osmotic pressure difference during NF experiments (“*osmotic pressure method*”).

B.2.1 Materials and Methods

In this work the performance of two spiral wound membrane modules tested in 0.5 wt% aqueous solutions of dextrose under various inlet pressure (from 7 to 25 bar) and flow rates (ranging from 150 to 600 dm³/h) is presented and discussed. These commercial modules were made of two different types of polyamide membranes (1812C-34D GE-DK and GE-DL). Both spiral wound modules studied have an effective membrane surface area of 0.32 m², and show the same feed and permeate spacer (the height of the feed spacer is 34 mil), as well as the parameters describing the module geometry (d_h , b and A_{eff}). Further

geometrical information are listed in *Appendix A: Materials & Methods*. All the experiments were performed in the NF-unit described in detail in *Appendix A: Materials & Methods*.

In order to investigate effect of concentration polarization on the “lab-scale” spiral wound modules, experiments were performed at a constant feed concentration of 50 g/dm³ of dextrose (a not totally rejected sugar is required for the analysis) at 50°C and pH 4, with varying volume flow rate from 150 to 600 dm³/h (corresponding to a cross flow velocity ranging from 0.10 to 0.41 m/s) and inlet pressure ranging from 7 to 25 bar.

All the spiral wound modules were initially conditioned at 10 bar for 5-7 hour at 30° and 50°C using demineralized water (pH 5.5) to remove the preservative traces from membrane. Modules were then tested with pure water (pH 4) at 30°, 40° and 50°C and various feed pressures (from 3 to 15 bar in increasing order) and a constant flow rate of 400 dm³/h in order to obtain hydraulic permeability, $L_{p,w}(T)$.

After that, modules were tested in water solution of dextrose at a constant concentration of 50 g/dm³. In each experiment, the modules were tested at each pressure (7, 10, 15, 20 and 25 bar) by increasing feed flow rate (150→ 200→ 300→ 400→ 500→ 600 dm³/h) at 50°C and pH 4.

The permeate flux, J_v , the sugar concentrations c_{bulk} and c_P of the solution and the trans-membrane pressure difference applied ΔP , were determined experimentally.

The permeate flux J_v was measured three times under each test condition after one hour; the average of the three measurements was recorded as the module flux. Feed and permeate samples were taken at different time until that concentration had remained stable for three times at least. The average of these three rejection was recorded as the module rejection.

Solute rejection, R_{obs} , and permeate flux, J_v , were calculated as reported in Eqs. B.14 and B.15, respectively.

$$R_{obs} = 1 - \frac{c_P}{c_{bulk}} \quad (B.14)$$

$$J_v = \frac{V}{t \cdot A} \quad (B.15)$$

c_I , c_{bulk} and c_P are the concentrations at feed/membrane interface, feed side and permeate side, respectively. V is the total permeate volume collected during the permeation time t , and A is the effective membrane area. Dextrose concentration was determined using a refractometer at fixed temperature (35°C)

Pressure drop was measured only with pure water on GE-DK, while for GE-DL was measured with different aqueous sugar solutions and pure water.

An average velocity over the membrane can be calculated from the feed flow rate and geometric parameters (summarized in Tab. B.2) of the element, by applying empirical rule.

B.2.2 Experimental results

Experimental results of mass transport measurements are shown in Fig. B.1 a-c.

The effect of cross flow velocity and pressure on both Permeate flux ($J_{v,exp}$) and retention ($R_{obs}\%$) is put in evidence for both modules.

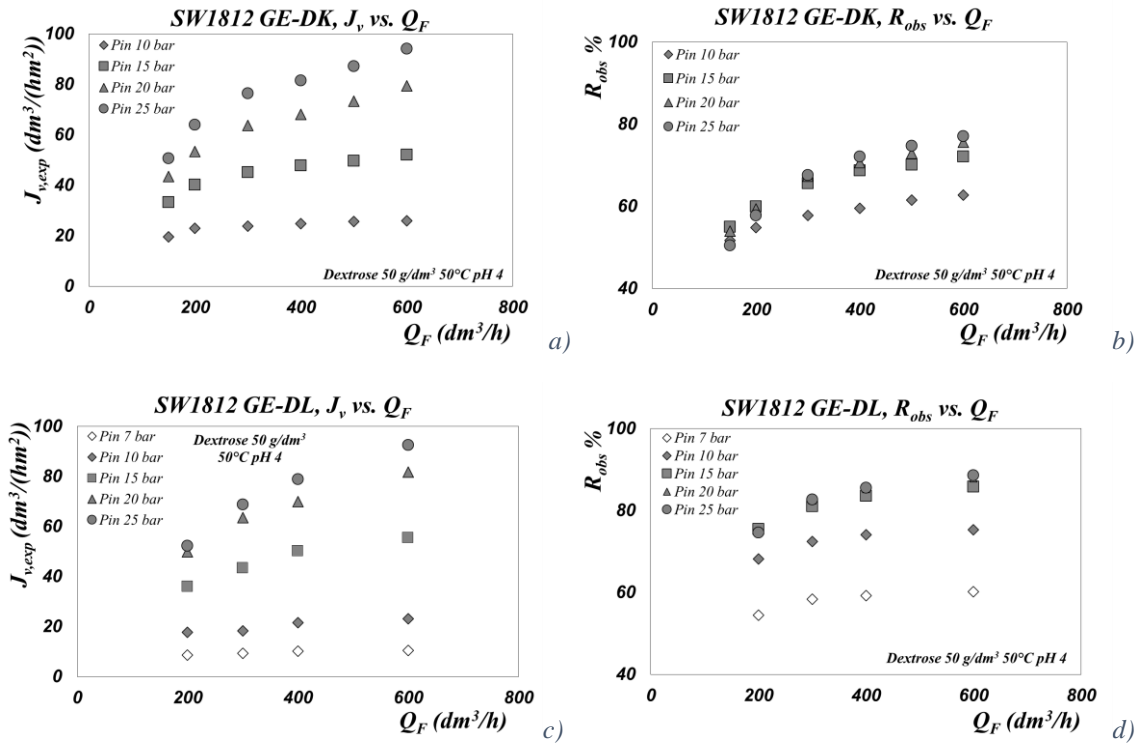


Figure B.1: Permeate flux and dextrose observed rejection for SW1812 GE-DK (a) and (b), and SW1812 GE-DL (c) and (d) respectively as a function of volume flow rate. Dextrose solution was 50 g/dm^3 , 50°C , pH 4, inlet pressure from 7 to 25 bar.

The permeate flux, J_v , through both membranes depends on applied pressure and flow rate, increases with increasing pressure and flow rate, although non linearly. Dextrose retention is positively influenced by cross-flow velocity and significantly affected by applied pressure: the higher the pressure, the higher the retention.

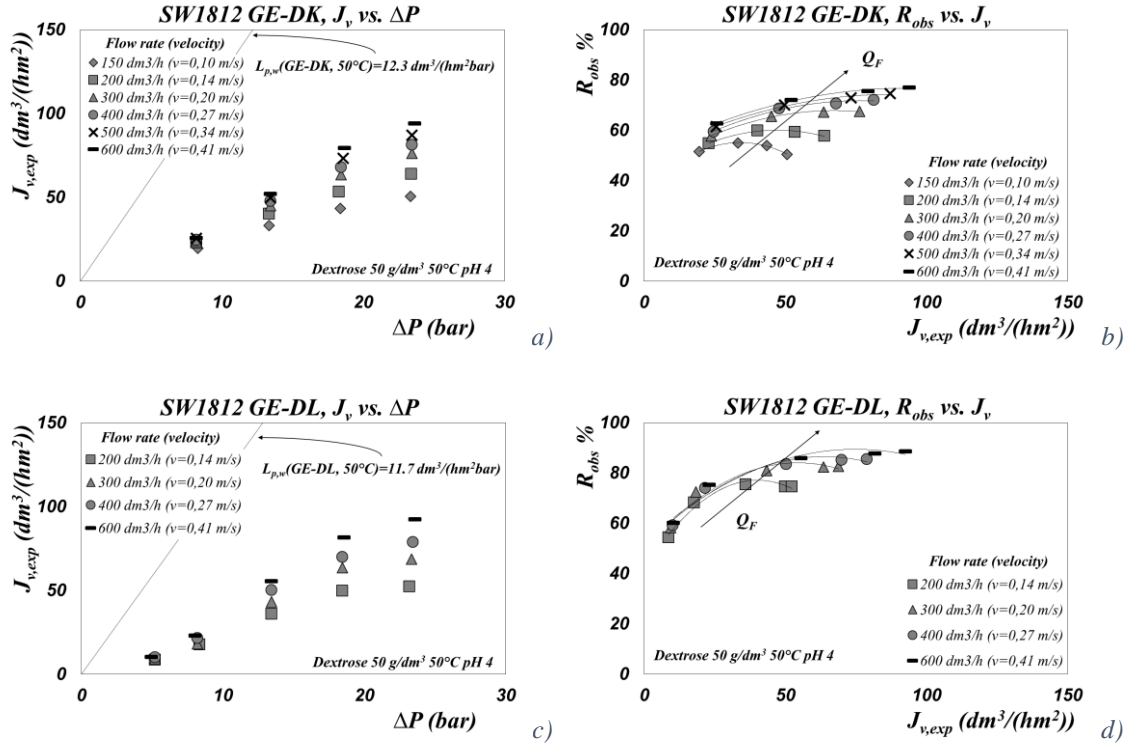


Figure B.2: Flow rate effect on experimental permeate flux ($J_{v,exp}$) and Observed Rejection (R_{obs}) in SW1812 modules of GE-DK (a-b) and GE-DL(c-d) membranes. Experimental data: Dextrose 50 g/dm³, 50°C, pH 4, Q_F ranging from 150 to 600 dm³/h, total recirculation mode of R and P

From experimental data flux is directly proportional to the applied pressure and inversely proportional to the viscosity. Viscosity is primarily controlled by two factors: solid concentration (or feed composition) and temperature. Thus increasing temperature or pressure should increase the flux; however this is true only under certain conditions such as (i) low pressure, (ii) low feed concentrations, and (iii) high feed velocity. When the process deviates from any of these conditions, flux becomes independent of pressure, sometimes even at quite low pressure. This behavior is shown in Fig. B.2 a-c for both membranes. The asymptotic pressure-flux relationship is due to the effects of concentration polarization. The general effect of pressure on flux is pronounced for both membranes. At low pressures and high feed velocities, i.e., under conditions where concentration polarization effects are minimal, flux ($J_{v,exp}$) will be affected by the transmembrane pressure (ΔP). Deviations from the linear flux-pressure relationship will be observed at higher pressures. Pressure independence occurs at lower pressure when the flow rate is lower.

B.3 Data reduction

Once gathered experimental data, sugar concentration at the membrane surface, c_I , and therefore mass transfer coefficient k_L , have been estimated through these methods:

- i) Velocity variation method (*Wilson Plot method*);
- ii) Osmotic pressure “revised” method;
- iii) Checking *G.Shock & A.Miquel (1987)* correlation suited for 2540 and 4040 modules.

For all correlation the concentration dependency of the mass transfer coefficient is taken into account according (Aimar and Field 1992) correlation (Eq. B.16):

$$k_L = k_L^0 \left(\frac{\eta(c_{bulk})}{\eta(c_I)} \right)^{0.27} \quad (B.16)$$

All methods will be discussed specifically in the following paragraphs.

B.3.1 The Velocity variation method

The first method (i) (also applied by other authors: (Bouchoux, Roux-de Balmann and Lutin 2005) (Weng, et al. 2009) (Jonsson and Boesen 1977)) is based on the description of the concentration polarization phenomenon by the film theory, which gives the following relationship:

$$\ln \left(\frac{1 - R_{obs}}{R_{obs}} \right) = \ln \left(\frac{1 - R_{real}}{R_{real}} \right) + \frac{J_v}{k_L} \quad (B.17)$$

The Sherwood relations for k_L , always show dependence on the cross-flow velocity of the type $k_L \propto v^\alpha$, where $\alpha \approx 0.33$ for laminar conditions and $\alpha = 0.75 - 0.91$ for turbulent conditions. The mass transfer coefficient k_L can be calculated from Sherwood’s relation, in the form of Eq. B.1, by assuming *Schmidt* number equal to 1/3.

By plotting the experimental values of $\ln \left[\frac{1 - R_{obs}}{R_{obs}} \right]$ as a function of $\frac{J_v}{v^\alpha}$, where the value of exponent α should be chosen in advantage, the intrinsic retention and the constant a can be determined graphically. The relationship of the mass transfer coefficient as a function of the various experimental variables can now be obtained by fitting experimental data. This semi-empirical method needs an incomplete retention of the solute.

The intrinsic retention increases with increasing permeate flux, increasing applied pressure, but is constant at increasing cross-flow velocities.

Usually, the description of the mass transfer coefficient is given for laminar and turbulent conditions separately; in this study adjustable parameters a and α were calculated for both flow regime conditions (laminar and turbulent) and independently for both modules (GE-DK and GE-DL).

B.3.2 The “revised” osmotic pressure method

The second approach used was the application of “*Osmotic Pressure Method*”, the same used in (Shock and Miquel 1987) and that in this study is presented in a “revised” form.

When the fluxes ($J_{v,exp}$) during nanofiltration of a solution are known, they can be compared to the “clean water flux” at equal applied pressure, and by using Eq. B.18 the osmotic pressure difference across the membrane can be calculated (Eq. B.19).

The unknown sugar concentration c_I at the membrane surface is commonly determined from the permeate flux, the membrane permeability and the net driving force (Shock and Miquel 1987):

$$J_v = L_p (\Delta P - \Delta \pi) \quad (B.18)$$

The osmotic pressure difference is calculated using the concentration at the membrane surface and in the permeate:

$$\Delta \pi = \pi(c_I) - \pi(c_p) \quad (B.19)$$

With the help of the relations for the osmotic pressure as a function of the concentration, the concentration at the membrane surface is obtained, then from Eq. B.18 by using experimental flux, bulk and permeate concentration, c_I and k_L can be calculated as a consequence.

The concentration dependence of osmotic pressure can be taken from literature: typically *Van't Hoff* equation is used for diluted solutions:

$$\Delta \pi = RT(c_I - c_p) \quad (B.20)$$

Together equations B.18 and B.20 yield the unknown concentration at the membrane surface, and once known membrane surface concentration, the Sherwood number is calculated.

In this study Eq. B.18 has been replaced by the following relationship:

$$J_v = L_p (\Delta P - \sigma_v \Delta \pi) \quad (B.21)$$

Where the Staverman reflection coefficient σ_v has been taken into account, and osmotic pressure difference has been calculated from literature data (Weast 1973). The equation system is summarized in Tab. B.4 and compared with (Shock and Miquel 1987) method.

Table B.4: Comparison between osmotic pressure method from (Shock & Miquel, 1987) and “revised” method adopted in this study

Osmotic Pressure Method (Shock and Miquel 1987)	Osmotic pressure “revised” method <i>this study</i>
Experimental data: NaCl 300 ppm~0.3 g/dm ³ , spacer filled channel	Experimental data: Dextrose 50 g/dm ³ 50°C, commercial SW1812
$\left\{ \begin{array}{l} J_v = L_p (\Delta P - \Delta \pi) \\ \Delta \pi = \nu RT (c_I - c_P) \\ \frac{J_v}{k_L} = \ln \frac{c_I - c_P}{c_{bulk} - c_P} \\ Sh = k_L \frac{d_h}{D_S} \end{array} \right.$	$\left\{ \begin{array}{l} J_v = L_p (\Delta P - \sigma_v \Delta \pi) \\ \Delta \pi = \pi(c_I) - \pi(c_P) \\ \frac{J_v}{k_L} = \ln \frac{c_I - c_P}{c_{bulk} - c_P} \\ L_p(T) \cdot \eta(T, c_{inside}) = L_{p,w}(T) \cdot \eta_w(T) \\ c_{inside} = \varphi \frac{c_I + c_P}{2} \\ \varphi = 1 - \sigma_v \cong 1 - R_{obs}^\infty \\ k_L = k_L^0 \left(\frac{\eta_{bulk}(T)}{\eta_l(T)} \right)^{0.27} \\ Sh = k_L^0 \frac{d_h}{D_S} \end{array} \right.$

* for the calculation of the hydraulic diameter the analogy between the flow in a spacer-filled channel and that in a packed column is used (Rautenbach and Albrecht 1989); ** Osmotic pressure was calculated by using literature data (Weast 1973); ***as fist approximation for slit-like pore geometry

B.4 Results

B.4.1 The velocity variation method application

As shown in the theoretical section, the experimental data required for a typical plot in the velocity variation method are the observed retention (R_{obs}), the permeate flux (J_v), and the cross flow velocity (v_{eff}). After choosing the exponent α of the cross flow velocity, the main variable for a certain combination of solute and membrane appears to be the applied pressure. In this study three different Reynolds exponents were chosen ($\alpha=0.33$ for laminar

flow, $\alpha = 0.8$ and $\alpha = 0.875$ for turbulent flow). The exponent 0.875 for Reynolds number in (Shock and Miquel 1987) equation (see Table B.3) was also found in the turbulent flow regime in the case of tubular and flat channel. In figure a typical example of the application of the Wilson plot method is given for turbulent conditions ($\alpha = 0.875$ and $\alpha = 0.8$)

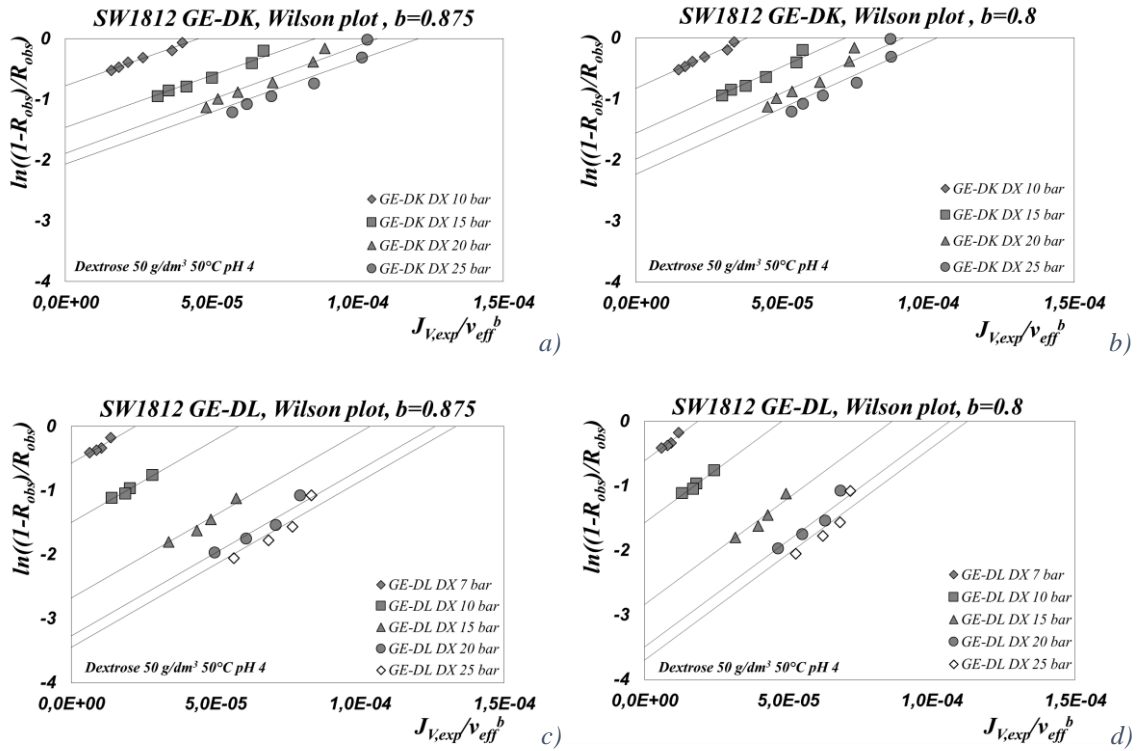


Figure B.3: the velocity variation plot for turbulent conditions ($\alpha = 0.875$ and $\alpha = 0.8$), Dextrose at bulk concentration of 50 g/dm^3 was used at 50°C using GE-DK membrane (a) and GE-DL (c) in SW1812 configuration.

The lines fitting the data show the same slope, which is $1/a$ in $k_L = av^\alpha = av^{0.875}$. This was imposed because equal slopes are expected when the applied pressure is the only variable and, more important, when a fit is made at each pressure separately the difference in slopes can be very large; the extrapolation of $J_v / v^{0.875} = 0$, to obtain the value of the intrinsic retention at the various pressures would then give nearly random values.

Both exponents ($\alpha = 0.875$ and $\alpha = 0.8$) show the same trend, although for some data a deviation can be observed (the lowest velocities at each pressure)

The range for choosing the exponent α for the cross flow velocity is fairly wide. For this study we choose “realistic” exponent like 0.875 as proposed by (Shock and Miquel 1987) and 0.8, used by Dittus-Boelter. A laminar flow regime ($\alpha = 0.33$) was rejected, because of

the scattering between lines and experimental data. It must be concluded that the exponent α should ranges from 0.8 to 0.875 instead of 0.33.

Between 0.8 and 0.875 the difference in scattering is not very large, however the problem of choosing the right exponent α still exists. The large different between the two membranes is evident, although modules have the same geometrical characteristics.

Both membranes shown different correlation for each exponent value. Results obtained for turbulent flow by using “velocity variation method” are summarized in Tab. B.5 but were rejected because inconsistent.

Table B.5: Mass transfer coefficient correlations from “velocity variation method” (Wilson Plot application)

<i>SW1812 GE-DK</i>	<i>SW1812 GE-DL</i>
$Sh = 0.018 Re^{0.875} Sc^{0.25} *$	$Sh = 0.012 Re^{0.875} Sc^{0.25} *$
$Sh = 0.015 Re^{0.8} Sc^{1/3}$	$Sh = 0.007 Re^{0.8} Sc^{1/3}$

* $Sc^{0.25}$ from Shock and A.Miquel (1987)

The application of this method provided two different correlations, in spite of the modules have same geometric characteristics (module length, feed spacer eight, effective area). The method is inconsistent to find a correct correlation for k_L .

B.4.2 “Revised” osmotic pressure method application

In this section the “revised” osmotic pressure method will be discussed in comparison with the standard osmotic pressure method applied by Shock & Miquel, (1987).

Starting from experimental results, data were reduced by applying the equation system provided in Tab B.4. This method strongly depends on the hydraulic permeability of the membrane ($L_{p,w}$), as well as the Staverman reflection coefficient (σ_V) that in first approximation is assumed equal to the asymptotic observed rejection (R_{obs}^∞).

A numerical algorithm can be used to solve the set of equations. Table B.6 summarize inputs and outputs of the system. TK-Solver® program was used to calculate mass transfer coefficient k_L .

Table B.6: Schematic representation of Input/Output data required for the resolution of the “revised” osmotic pressure method

Input	Output
$\Delta P_{,exp}, c_{bulk,exp}, T, Q_F$ $L_{p,w}(50^\circ C)=10.7 \text{ dm}^3/(hm^2bar)$ $\lambda(DX,50^\circ C)=0.991$ c_1^* (* guess value)	c_b, c_p, J_v R_{obs}, R_{real}

Results obtained for both Reynolds exponents ($\alpha=0.875$ and $\alpha=0.8$) are plotted in Fig. B.4 in terms of Sherwood as a function of Reynolds number, for both membranes.

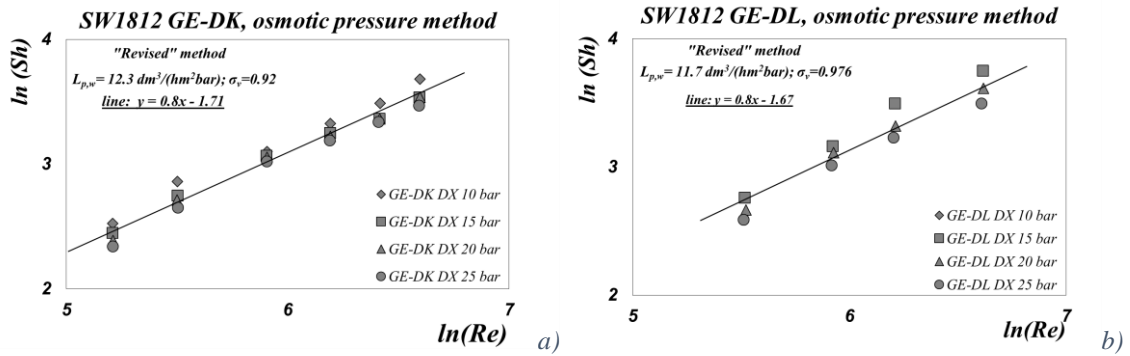


Figure B.4: Mass transport coefficient for turbulent flow from “revised” osmotic pressure methods, $\alpha=0.875$ and $\alpha=0.8$ and (lines), Spiral wound 1812 GE-DK (a) SW1812 GE-DL (b)

The best correlation identified for both membranes has the following expression (Eq. B.22):

$$Sh = 0.023 Re^{0.8} Sc^{1/3} \quad (B.22)$$

Equal to a (Sieder and Tate 1936) equation. The same equation was identified from (Jonsson and Boesen 1977) and applied later by (Weng, et al. 2009) for a similar 1812 GE-DK spiral wound module with an effective filtration area of 0.27 m^2 (equal to a feed spacer of 47 mil). (Cuartas-Uribe, et al. 2007) applied to a 2540 GE-DL Spiral Wound element the same equation derived from Schaep et al. (2001), technically defined as *Dittus & Boelter* correlation.

The “revised” osmotic pressure method provides a correlation for mass transfer already applied in literature for SW modules.

B.4.3 Comparison between Experimental data and Model

Fig. B.5 shows a comparison between model prediction and experimental data for both (Shock and Miquel 1987) and the proper Sieder & Tate equations for mass transfer (the latter found with the revised osmotic pressure method). A comparison between the two methods is proposed, for both membranes.

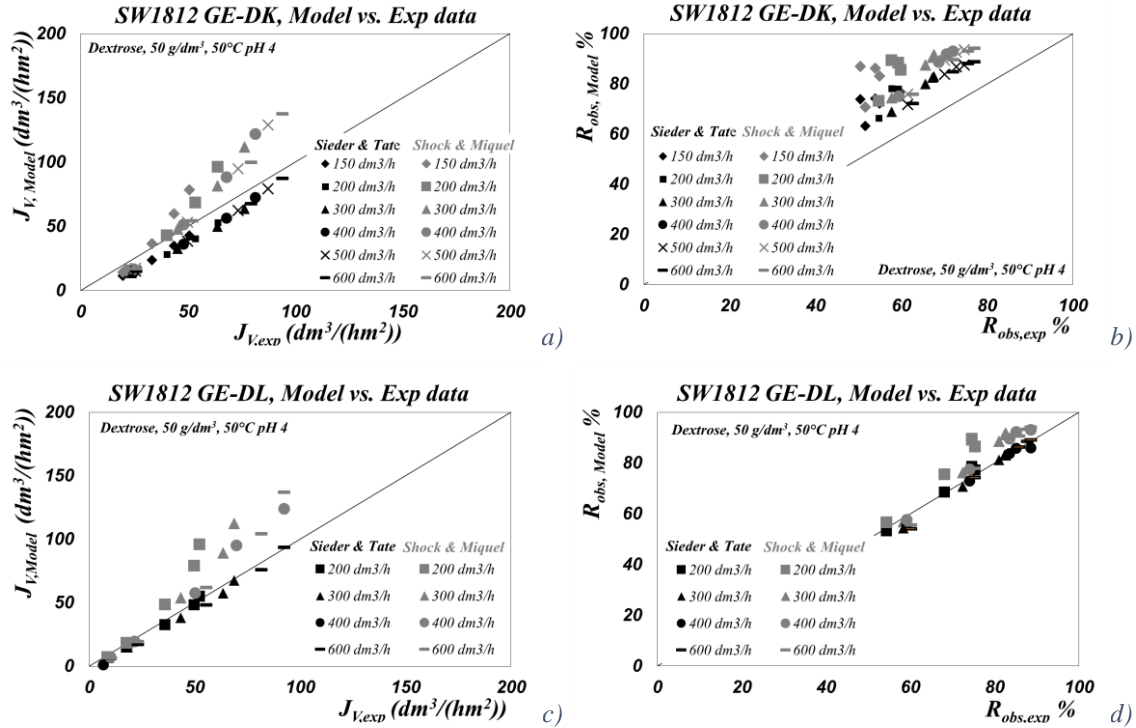


Figure B.5: Comparison between Experimental data of permeate flux ($J_{v,exp}$) and observed rejection (R_{obs}) as a function of the model prediction, by using Shock and Miquel correlation (Grey dots) and Sieder & Tate (Black dots), SW1812 GE-DL (a-b). Data: Dextrose, 50°C, 50 g/dm³, pH 4, flow rate ranging from 200 to 600 dm³/h. Total recirculation mode of R and P.

As shown graphically, a good agreement between experimental data ($J_{v,exp}$ and $R_{obs,exp}$) and the “revised” osmotic pressure correlation is obtained, however model quite overestimates rejection for GE-DK membrane, which is probably because $L_{p,w}$ and σ_V values are quite scattered compared to GE-DL membrane. For the (Shock and Miquel 1987) mass transfer correlation the experimental values are lower than predicted ones. From Figure B.5 it is further seen that Shock & Miquel equation overestimates mass transfer coefficient (that is to say that c_l is underestimated, while effective driving force, ΔP_{eff} is overestimated).

As we will see in the next session, this lack of accuracy is maybe due to the fact that 1812 module works in a transition phase, the flow should be not completely developed.

It has been proved that (Sieder and Tate 1936) correlation is able to describe (better than (Shock and Miquel 1987) equation) mass transfer in industrial spiral wound module, as

shown in *Chapter 4*, relatively to 4040C1025 GE-DL module, on the basis of literature data from (Bandini and Nataloni 2015).

B.5 Pressure Drop in a SW1812 module

For calculating the performance of a spiral wound element, knowledge about the pressure drop in the feed side is crucial, since the driving force is critically influenced by these losses. Pressure loss along the permeate channel was assumed to be negligible compared to feed channel, as well as the pressure along the permeate collector tube is usually assumed to be constant, although in practice there will be a small pressure loss.

Pressure losses in the feed side were experimentally measured in spiral wound element in order to (i) verify *G.Shock and A.Miquel (1987)* correlation (Eq. B.23) (ii) and/or identify a proper correlation able to describe pressure drop in a spiral wound element.

The (Shock and Miquel 1987) correlation for pressure drop was determined in both spiral wound elements (25''×40'') just as spacer-filled flat channel:

$$\lambda_{G.Shock \& A.Miquel} = 6.23 Re^{-0.3} \quad (B.23)$$

For the second purpose a differential pressure gauge was installed between upstream (feed side) and downstream (retentate side) of the module.

This configuration does not allow to eliminate inlet and outlet pressure losses in the element. The pressure drop of the module $\Delta P_F^{\text{module+housing}}$ includes the pressure drop of the empty housing $\Delta P^{\text{empty housing}}$, according Eq. B.24:

$$\Delta P_{loss,F}^{\text{module+housing}} = \Delta P_F^{\text{module}} + \Delta P^{\text{empty housing}} \quad (B.24)$$

To be able to transform experimental data ($\Delta P/L$ vs. Q_F) to a dimensionless form $\lambda = \lambda(Re)$ (Eq. B.4) element geometry is required. The hydraulic diameter d_h from Tab. C.2 was used. The dimensionless pressure drops for spiral wound element are compared with ones predicted from (Shock and Miquel 1987), and shown in Fig. B.6. From technical sheet the maximum pressure drop over an element is reported to be 1.03 bar.

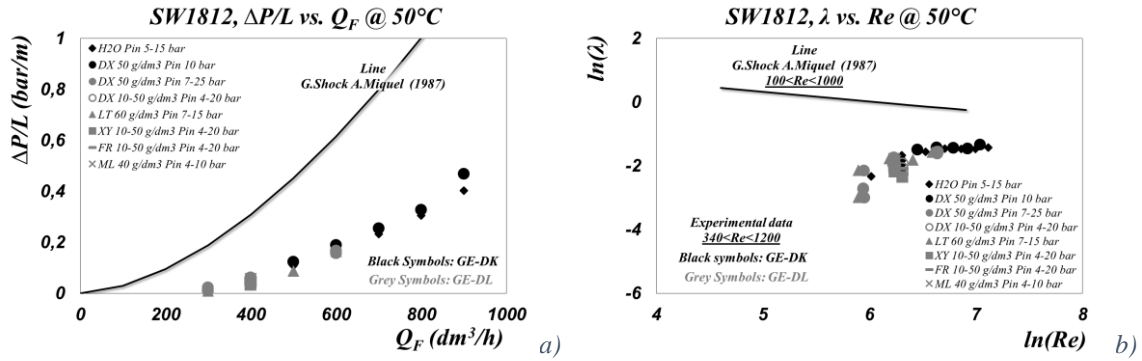


Figure B.6: Comparison between Experimental data (dots) and predicted (from (Shock and Miquel 1987)) pressure loss as a function of flow rate (a) and Reynolds number (b) for 1812C-34 D GE-DL and GE-DK. Experimental data refer to Dextrose solution, 50 g/dm³, 50°C, pH 4, Q_F ranging from 150 to 600 dm³/h, inlet pressure from 7 to 25 bar

From experimental measurements of ΔP_{loss} as a function of *Reynolds* number (Fig. B.6b) SW modules work in a transition region. No simple equation exists for accomplishing a smooth mathematical transition from laminar flow to turbulent flow. Regarding heat transfer Hausen's equation describes the transition region plotting a series of curves as a function of Reynolds number and the ration L/D as a parameter (Bird, Steward and Lightfoot 1960).

However experimental results suggest that no 1812 element will have pressure drop above 1 bar. The state of turbulence can be easily determined by the nature of the relationship between pressure drop (ΔP) and flow rate (Q_F) in the feed channel. The general relationship is:

$$\Delta P = Q^n \quad (B.25)$$

For laminar flow, $n=1$. For turbulent flow, on the other hand, $n>1$. The spiral module shows a departure from linearity, indicating that the flow is in the turbulent region.

In conclusion, in order to be conservative in prediction of pressure loss, (Shock and Miquel 1987) equation can be applied.

References

- Aimar, P., and R. Field. "Limiting flux in membrane separations: a model bases on the viscosity dependency of the mass transfer coefficient." *Chemical Engineering Science* 47, no. 3 (1992): 579-586.
- Bandini, S., and L. Nataloni. "Nanofiltration for dextrose recovery from crystallization mother liquors: A feasibility study." *Separation and Purification Technology* 139 (2015): 53-62.
- Bird, R.B., W.E. Steward, and E.N. Lightfoot. *Transport Phenomena*. New York: Wiley, 1960.

- Bouchoux, A., H Roux-de Balmann, and F. Lutin. "Nanofiltration of glucose and sodium lactate solutions variations of retention between single- and mixed- solute solutions." *Journal of Membrane Science* 258 (2005): 123-132.
- Cuartas-Uribe, B., M.C. Vincent-Vela, S. Alvarez-Blanco, M.I. Alcaina-Miranda, and E. Soriano-Costa. "Nanofiltration of sweet whey and prediction of lactose retention as a function of permeate flux using the Kedem-Spiegler and Donnan Steric Partitioning models." *Separation and Purification Technology* 56 (2007): 38-46.
- Da Costa, A.R., A.G. Fane, C.J.D. Fell, and A.C.M. Franken. "Optimal channel spacer design for ultrafiltration." *Journal of Membrane Science* 62 (1991): 275.
- Evangelista, F. "An improved analytical method for the design of spiral wound modules." *The Chemical Engineering Journal* 38 (1988): 33-40.
- Grober, H., S. Erk, and U. Grigull. *Fundamentals of heat transfer*. New York: McGrawHill, 1961.
- Jonsson, G., and C.E. Boesen. "Concentration polarization in reverse osmosis test cell." *Desalination* 21 (1977): 1-10.
- Koutsou, C.P., S.G. Yiantsios, and A.J. Karabelas. "A numerical and experimental study of mass transfer in spacer filled channels: effects of spacer geometrical characteristics and Schmidt number." *Journal of Membrane Science* 326 (2009): 234-251.
- Kuroda, O., S. Takahashi, and M. Nomura. "Characterization of flow and mass transfer rate in an electro dialyzer compartment including spacer." *Desalination* 46 (1983): 225.
- Porter, M.C. "Concentration polarization with membrane ultrafiltration." *Ind. Eng. Chem. Prod. Res. Rev.* 11, no. 3 (1972): 234-248.
- Rautenbach, R., and R. Albrecht. *Membrane Processes*. John Wiley & Sons, 1989.
- Schweitzer, P.A. *Handbook of separations Techniques for Chemical Engineers*. 2nd. McGraw-Hill, 1988.
- Schwinge, J., D.E. Wiley, A.G. Fane, and R. Guenther. "Characterization of a zigzag spacer for ultrafiltration." *Journal of Membrane Science* 172 (2000): 19.
- Schwinge, J., P.R. Neal, D.E. Wiley, D.F. Fletcher, and A.G. Fane. "Spiral wound modules and spacers Review and analysis." *Journal of Membrane Science* 242 (2004): 129-153.
- Shi, B., P. Marchetti, D. Peshev, S. Zhang, and A. Livingston. "Performance of spiral wound membrane modules in organic solvent nanofiltration-Fluid dynamics and mass transfer characteristics." *Journal of Membrane Science* 494 (2015): 8-24.
- Shock, G., and M. Miquel. "Mass transfer and pressure loss in spiral wound modules." *Desalination* 64 (1987): 339-352.
- Sieder, E.N., and G.E. Tate. "Heat transfer and pressure drop of liquids in tubes." *Ind. Eng. Chem.* 28 (1936): 1429-1435.
- Sutzkover, Iris, David Hasson, and Raphael Semiat. "Simple technique for measuring the concentration polarization level in a reverse osmosis system." *Desalination* 131 (2000): 117-127.
- van den Berg, G.B., I.G. Racz, and C.A. Smolders. "Mass transfer coefficients in cross-flow ultrafiltration." *Journal of Membrane Science* 47 (1989): 25-51.
- Weast, R.C. *CRC Handbook of Chemistry and Physics*. Cleveland, Ohio: CRC Press, 1973.

Weng, Yu-Hsiang, et al. "Separataion of acetic acid from xylose by nanofiltration." *Separation and Purification Technology* 67 (2009): 95-102.

APPENDIX C

Membrane processes in Biotechnology Applications*

* cooperation with Gonzalo Agustin Martinez and Lorenzo Bertin, DICAM, University of Bologna

C.0 Membrane processes in biotechnology	183
C.1 Biotechnology processes for bio-plastics production.....	185
C.1.1 Bio-polymers: a general introduction.....	186
C.1.2 Bacterial Polyhydroxyalcanoates (PHAs): the biosynthesis	187
C.1.3 Bacterial Polyhydroxyalcanoates (PHAs): the recovery	190
C.1.4 Experimental set up	195
C.1.5 Integration between PHA and VFA production	198
C.2 Introduction to VFAs.....	199
C.2.1 VFA recovery: state of the art	200
C.3 Conclusions	206
References.....	207

C.0 Membrane processes in biotechnology

Microbiological processes have been used for a long time in the food and beverage industry (e.g. vinegar, bakers' yeast production), in the chemical industry (ethanol production) and in the pharmaceutical industry (i.e. production of penicillin). Nowadays the importance in biotechnology increases as more and more efficient microorganism are cultivated.

Membranes have always been an integral part of biotechnology processes, they have traditionally been used for size-based separations. In many applications tangential flow microfiltration (*MF*) competes with centrifugation, depth filtration and expanded-bed chromatography for the initial cell harvesting, similarly Ultrafiltration (*UF*) has become the method of choice for protein concentration and buffer exchange, largely replacing size-exclusion chromatography in these applications.

Besides, membranes are increasingly being used in reaction, clarification, and recovery schemes for the production of molecules, emulsions and particles.

Membrane systems take advantage of their selectivity, high surface-area-per-unit-volume, and their potential for controlling the level of contact and/or mixing between two phases. They are very well suited to the processing of biological molecules since they operate at relatively low temperatures and

pressures and involve no phase changes or chemical additives, thereby minimizing the extent of denaturation, deactivation, and/or degradation of biological products (Zeman and Zydney 1996).

Ultrafiltration and microfiltration are commonly used to recover macromolecules and retain suspended colloids and particles, and are being integrated into both upstream and downstream processes. A large range of ultrafiltration and microfiltration applications is reported to concentrate proteins, exchange buffer systems, clarify suspensions for cell harvesting, and sterilize liquids to remove viruses and bacteria. Other membrane processes include membrane bioreactors (*MBR*), where enzymes, microorganisms or antibodies are suspended in solution and compartmentalized by a membrane in a reaction vessel or immobilized within the membrane matrix itself. Finally, membrane contactors involve using a pressure to force the dispersed phase to permeate through a membrane into the continuous phase, for the preparation of emulsions and various types of particles, as w/o emulsions, o/w emulsions, and polymeric particles, not to mention membrane chromatography, used as an alternative to conventional resin-based chromatography columns, for a large range of chromatographic purification schemes, including ion-exchange, hydrophobic, reversed-phase, and affinity chromatography (Charcosset 2006).

Actually, improvements in membrane technology are focused on high-resolution applications, including improved protein–virus separation, protein purification by high-performance tangential flow filtration and enhanced membrane chromatography. These developments will allow membranes to play an important role in the evolution of the next generation of biotechnology processes (van Reis and Zydney 2001).

As mentioned before, membrane processes are increasingly considered for the separation of fermentation products, next to the traditional separation methods such as centrifugation or distillation. Some special material properties of microbiological products such as sensitivity against elevated temperatures (10-40°C), small particle size (0.3-10 µm), small density differences between particles and liquids are often the reason for difficulties in conventional separation processes. Membrane processes should be capable of improving this situation generally.

There are numerous applications for membrane processes in biotechnology applications, e.g.:

- Recovery of biomolecules;
- Methane recovery from biogas;
- Separation of volatile components;

(Cheryan 1998)

Among all the applications, this study is focused mainly on two biotechnology applications:

- (i) *PHAs (Polyhydroxyalcanoates)* recovery from fermentation broth, by *UF/MF*; and
- (ii) *VFAs (Volatile Fatty Acids)* recovery by *NF*.

Nowadays biotechnology research is focused on the synthesis of bio-compounds from renewable sources. The first product is just a bio-polymer, bio-synthesized and accumulated intracellularly, that can replace synthetic production of plastics, while *VFAs* represent important compound for its fermentation pathway. A limiting factor for the production of this biopolymer, are the costs associated to its recovery. As mentioned in literature, membrane processes represent alternative methods to centrifugation, able to provide PHAs purity that exceeded 92% [(de Koning, Kellerhals, et al. 1997), (Yasotha, Aroua, et al. 2006)].

This study represent a preliminary study for the applicability of PHAs recovery by *UF/MF*, integrated by a re-use of *VFAs* during fermentation, as carbon source during polymer bio-synthesis.

C.1 Biotechnology processes for bio-plastics production

The biotechnology industry today employs recombinant bacteria almost for the production of high-value bio-molecules and chemical products, some of these latter appear to be potential candidates to replace some conventional plastics.

As a matter of fact, biopolymers, produced from renewable resources, could replace the petrochemical-based plastomers, elastomers, latexes or even high performance polymers (G.-Q. Chen 2010).

Almost all the biotechnology processes now adopted are based on an initial biological fermentation step followed by several downstream operations. The mayor cost absorbing factors are the upstream fermentation, thus part of the work consists of optimizing the fermentation conditions. However improving the downstream processing efficiency is also of great interest; in fact, to date, in many fermentation processes, downstream processing is a significant factor in determining economic feasibility, this latter significantly affects the overall process economics. Typically, carbon source and downstream process (recovery and purification) represent both 30% (approximately) of the final product cost (Choi and Lee 1999).

Various recovery technologies have been proposed and studies in small scales in the laboratory (a large amount of works and publications), as well as in industrial scales. To that respect, a large number of studies proposed new combination of traditional and/or innovative operations to be used after fermentation (Bouchoux, Roux-de Balmann and Lutin 2006):

- (i) Liquid-liquid extraction;
- (ii) Ion-exchange;
- (iii) Adsorption
- (iv) Electrodialysis, and
- (v) Other membrane separation operations.

Membrane technology can play a role in each step: many works related to cell harvesting by microfiltration, protein fractionation by ultrafiltration, desalting by electrodialysis, as well as dewatering by reverse osmosis have been published in the last decades (Cheryan 1998).

Typically, regarding biotechnology process, the first step is the separation of the biomass from its surrounding broth.

Fermentation broths are generally a complex mixture of microorganisms, unreacted substances, metabolites, un-wanted by-products and additives such as anti-foaming agents and water. The microorganism itself may be the product, as in the production of bakers' yeast, or metabolites, as in the production of antibiotics, amino acids or alcohols; in either case, the cellular components have to be separated from the dissolved components.

Regarding a bio-polymer, it is expressed within the bacterial cell in the form of an insoluble granule. The recovery of the entire biomass including the cells is performed by either preparative centrifugation or by means of tangential flow filtration systems using microporous membranes.

Since fermentation processes are usually operated discontinuously, membrane process is operated batchwise. In this preliminary feasibility study Ultrafiltration was applied for the recovery of a bio-polymer (PHA) in a dead-end stirred cell.

C.1.1 Bio-polymers: a general introduction

Plastic materials have become an integral part of contemporary life because of many desirable properties including durability and resistance to degradation. Recently, the problems concerning the global environment and solid waste management have created much interest in the development of biodegradable plastics, which must still retain the desired physical and chemical properties of conventional synthetic plastics.

Some of the biodegradable plastic materials under development include polyhydroxyalkanoates (PHAs), polylactides, aliphatic polyesters, polysaccharides, and the copolymers and/or blends of these, however the most extensively studied thermoplastic biopolymers are the polyhydroxyalkanoates (PHA) and polylactic acid (PLA) (G.-Q. Chen 2009).

It is estimated that the global market for biodegradable polymers is expected to grow. However, one of the problems facing the development of biodegradable polymers as substitutes for conventional plastics is their high price compared with petrochemical derived plastics. To date, industrial PHA production is carried out using pure microbial culture fermentation technology with high costs associated with carbon substrate, fermentation operation and downstream processing. It has been suggested, based on Life Cycle Analysis (LCA), that PHA production using mixed cultures may be

more favorable than using pure cultures in both economic and environmental terms (Gurieff and Lant 2007).

Pure cultures (wild type or genetically modified) allow getting higher productivities and PHAs content (Agustín Martínez, et al. 2015). Conversely, the employment of mixed cultures has the economic advantage that they do not need to work under sterile conditions.

Among the candidates for biodegradable plastics, PHAs have been drawing much attention because of their similar material properties to conventional plastics and complete biodegradability. A number of review articles are available on the general features of PHAs, the physiology, genetics and molecular biology of bacteria synthesizing PHAs, the development of PHAs having novel monomer constituents, the characterization of PHA polymer and the biodegradation of PHAs.

Even though PHAs have been recognized as good candidates for biodegradable plastics, their high price compared with conventional plastics limited their use in a wide range of applications. However, recently, much effort has been devoted to develop a process for the economical production of PHAs. The recovery of PHA contributes significantly to the overall economics. Development of a process that allows the simple and efficient extraction of polymers will be well rewarded. The major cost absorbing factors are the upstream fermentation processes and the downstream PHA recovery technologies

PHAs have sparked global interest due to its many advantages such as thermoplastic properties, biodegradability, biocompatibility and its ability to be synthesized from renewable resources.

For latex-like applications such as in paints (for binder, vanish hardening and sprayable films) as well as in paper coating and impregnation, a PHA purity higher than 90% is sufficient for direct applications without further treatments (Rehm, et al. 2004). However, for biomedical applications a product purity below 99% is not acceptable, thus further purification/polishing steps are required.

In the next sections the state of art about PHA bio-synthesis and recovery will be discussed.

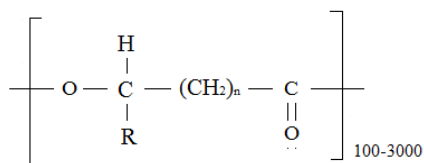
C.1.2 Bacterial Polyhydroxyalcanoates (PHAs): the biosynthesis

Polyhydroxyalcanoates (PHAs) are biodegradable polyester which are accumulated by numerous bacterial species in the form of intracellular granules and which serve as reserves of energy as shown in Fig.C.1 (Holmes and Lim 1990) :



Figure C.1: Transmission electron micrograph of recombinant *Escherichia coli* XLI-Blue (pSYL105) accumulating a large amount of poly(3-hydroxybutyrate), P(3HB). P(3HB) granules appear as electronlucent bodies. Bar represents 1 μ m (S. Lee 1996)

Polyhydroxyalkanoates (PHAs) are polyesters of hydroxyalkanoates (HAS) synthesized by numerous bacteria as intracellular carbon and energy storage compounds and accumulated as granules in the cytoplasm of cells, having the general structural formula shown in Figure C.2.



<i>n</i>	<i>R</i>	Polymer
1	hydrogen	Poly(3-hydroxypropionate)
	methyl	Poly(3-hydroxybutyrate)
	ethyl	Poly(3-hydroxyvalerate)
	propyl	Poly(3-hydroxyhexanoate)
	pentyl	Poly(3-hydroxyoctanoate)
	nonyl	Poly(3-hydroxydodecanoate)
2	hydrogen	Poly(4-hydroxybutyrate)
3	hydrogen	Poly(5-hydroxyvalerate)

Figure C.2: General structure of polyhydroxyalkanoates (S. Lee 1996)

More than 80 HAS have been detected as constituents of PHAs, which allows these thermoplastic materials to have various mechanical properties resembling hard crystalline polymer or elastic rubber depending on the incorporated monomer units. A number of bacteria including *Alcaligenes eutrophus*, *Alcaligenes latus*, *Azotobacter vinelandii*, *methylotrophs*, *pseudomonads*, and recombinant *Escherichia coli* have been employed for the production of PHAs, and the productivity of greater than 2 g PHA/L/h has been achieved. Recently (Agustín Martínez, et al. 2015) produced PHAs by feeding a pure culture of *Cupriavidus necator* with a pre-treated olive mill wastewater (OMW), accumulating up to 55% of the cells dry weight.

Recent advances in understanding metabolism, molecular biology, and genetics of the PHA synthesizing bacteria and cloning of more than 20 different PHA biosynthesis genes allowed construction of various recombinant strains that were able to synthesize polyesters having different monomer units and/or to accumulate much more polymers. Also, genetically engineered plants harboring the bacterial PHA biosynthesis genes are being developed for the economical production

of PHAs. Improvements in fermentation/separation technology and the development of bacterial strains or plants that more efficiently synthesize PHAs will bring the costs down to make PHAs competitive with the conventional plastics (S. Lee 1996).

Furthermore, improving the intracellular PHA content is important for decreasing the extraction and recovery cost of PHA downstream processing.

Numerous bacteria synthesize and accumulate PHAs as carbon and energy storage materials or as a sink for redundant reducing power under the condition of limiting nutrients (typically nitrogen, phosphorous, magnesium, or oxygen) in the presence of excess carbon source. When the supply of the limiting nutrient is restored, the PHA can be degraded by intracellular depolymerases and subsequently metabolized as carbon and energy source. The monomer HA units in these microbial polyesters are all in the D(-) configuration due to the stereospecificity of biosynthetic enzyme.

The molecular weights of polymers are in the range of 2×10^5 to 3×10^6 daltons, depending on the microorganism and growth condition.

PHA accumulates in the cells as discrete granules, the number per cell and size of which can vary among the different species; some 8 to 13 granules per cell having the diameter of 0.2 to 0.5 μm were observed in *Alcaligenes eutrophus*. These granules appear as highly refractile inclusions under electron or phase-contrast microscopic observation. The composition and quantity of PHA polymer can be determined by gas chromatography after methanolysis.

PHAs can be classified into three main groups depending on the number of carbon atoms in the monomer units:

- *short-chain-length (scl)* PHAs, which are composed of C₃ to C₅ 3-hydroxy/4-hydroxy fatty acids;
- *medium-chain-length (mcl)* PHAs, which are composed of C₆ to C₁₆ 3-hydroxy fatty acids;
- *long-chain-length (lcl)* PHAs.

Poly(3-hydroxybutyrate) P(3HB), the first of the PHAs to be studied extensively, fall into the first group of PHAs. This biopolymer shows a melting temperature close to 180°C (Kunioka and Doi 1990) and a glass transition temperature around 4°C (Mitomo, et al. 1999) and is highly crystalline (55-80%).

The composition of the general PHA produced, and thus its physical properties, depend both on the micro-organism and carbon source used (de Koning and Witholt 1997). Composition of the culture medium (particularly carbon substrate) influences the microbial polymer (e.g., range of polymers formed, molecular weight, crystallinity), which in turn determines the physical properties (e.g., mechanical and tensile strength) (Yasothea, Aroua, et al. 2007).

The discrepancy is mainly due to the substrate specificity of the PHA synthases, the key enzyme of PHA biosynthetic pathway.

The most important property of PHAs is their complete biodegradability. The family of PHAs exhibits a wide variety of mechanical properties, from hard crystalline to elastic, depending on the composition of monomer units, which broadens its application area. For example, the *mcl*-PHAs are semi crystalline elastomers with a low melting point, low tensile strength, and high elongation to break and can be used as a biodegradable rubber after crosslinking by electron-beam irradiation.

The medium-chain-length PHAs (comprising C₆ to C₁₆ monomers) produced by the Gram-negative¹ *Pseudomonas* are very much in demand due to the flexible and elastomeric applications in the global market. The *mcl* PHAs are more conducive for coating and film materials, and offer greater possibilities for chemical modifications.

PHB and its derivatives are generally produced by Gram-positive² organism such as *Bacillus megaterium* and, on an industrial scale, *Alcaligenes eutrophus*. These polymers (*PHB*) are all highly crystalline materials and therefore are suitable for polypropylene- and low-density polyethylene- type applications. Owing to their intrinsic rigidity, these materials can only cover part of the biodegradables market, unlike PHAs which can cover flexible and elastomeric applications.

C.1.3 Bacterial Polyhydroxyalkanoates (PHAs): the recovery

Following the fermentation, cells containing PHAs are separated by conventional procedures such as centrifugation, filtration, or flocculation-centrifugation: this represents the first step for the PHAs granules recovery. In order to recover the PHA granules, it is necessary to rupture the bacterial cell and remove the protein layer that coats the PHA granules; alternatively, the PHA has to be selectively dissolved in a suitable solvent. PHA recovery includes three main steps:

- (i) Biomass harvesting;
- (ii) Recovery of intracellular PHA (cell disruption and biomass solubilization) (chemical or biological/enzymatic methods) – 1st Recovery-
- (iii) Separation of PHAs from solution (centrifugation, filtration methods)-2nd Recovery-

Most importantly, by means of some of these approaches PHAs may be recovered in their native form. Within the cell, PHAs exist in an amorphous elastomeric state, surrounded by a phospholipid

¹ Gram-negative bacteria are a group of bacteria that do not retain the crystal violet stain used in the Gram staining method of bacterial differentiation making positive identification possible. The thin peptidoglycan layer of their cell wall is sandwiched between an inner cytoplasmic cell membrane and a bacterial outer membrane.

² Gram-positive bacteria are bacteria that give a positive result in the Gram stain test. Gram-positive bacteria take up the crystal violet stain used in the test, and then appear to be purple-coloured when seen through a microscope. This is because the thick peptidoglycan layer in the bacterial cell wall retains the stain after it is washed away from the rest of the sample, in the decolorization stage of the test

layer with embedded and attached proteins to form a granule. Generally, cell disruption rapidly leads to solidification of the granule and crystallization of the polymer. Where extraction is carefully carried out to obtain PHAs in their native amorphous granular form, this results in polymer latexes, which can allow unique applications such as paints, thermolyzable lacquers, and paper coatings for packaging. Recovery represents thus a critical step, because should preserve the granule integrity.

1st Recovery

After the biomass harvesting (i.e. cells are separated from the exhaust supernatant by centrifugation, 15 min at 8,000 rpm), cells are disrupted to recover polymers. A number of different methods, here discussed, have been developed in literature for the recovery of PHA.

▪ *Solvent Extraction*

The most popular PHA recovery method is carried out using the solvent extraction method, employing solvents such as chloroform and methanol (Doi 1990), which allows both high yield of recovery and degree of purity. Unfortunately this method requires large quantities of these volatile solvents which are not only cost prohibiting but also hazardous to the environment.

The first method that has most often been used involves extraction of P(3HB) from biomass with solvents. The solvents employed include chloroform, methylene chloride, propylene carbonate, and dichloroethane. Due to the high viscosity of even dilute PHA solutions, about 20 of solvent is required to extract 1 of polymer. The large amount of solvent required makes this method economically unattractive, even after the recycle of the solvent, and it is clear that the production of a “green” bioplastic should not such solvents. Biopolymers obtained through this procedure are adopted as such in biomedical applications for surgical reconstruction and tissue engineering (Chen and Wu 2005). Convenience of PHA recovery approaches alternative to solvents may be partly counterbalanced by a loss in recovery yields and/or purity of PHAs, and sometimes by production of large amounts of wastewaters. However, employment of aqueous solvents may be more easily integrated into a biorefinery scheme.

▪ *Chemical digestion*

Another popular method is the use of sodium hypochlorite which solubilizes non-PHA cellular materials and leaves PHA intact. Several methods that have been developed involve the use of sodium hypochlorite for the differential digestion of non-PHA cellular materials.

Although this method is effective in the digestion of non-PHA cellular materials, it causes severe degradation of the polymer resulting in a 50% reduction in the molecular weight; even when optimized, the hypochlorite method approximately halves the molecular weight of the PHB present in the original biomass (Berger, et al. 1998). Some author [(Berger, et al. 1998), (S. Lee 1996)]

reported a severe degradation of the polymer of up to 50% reduction in molecular weight during sodium hypochlorite digestion

This technology is simple a process, however, in view of the marked decrease in molecular weight of PHA due to sodium hypochlorite being a strong oxidant, and the appreciable amount of chlorine left behind in the recovered PHA, this technology has been modified by many researchers.

A combination of solvent extraction and hypochlorite treatment has been proposed to fight this problem, but this approach has not been developed commercially (de Koning and Witholt 1997). The use of sodium hypochlorite together with chloroform significantly reduced degradation of PHA. Such variations include using a dispersion solution made of sodium hypochlorite and chloroform as studied by (Hahn, et al. 1994). However, this also leads to a higher cost and environmental hazard.

- *Enzymatic digestion*

The aqueous enzymatic digestion method has been developed as an alternative to solvent extraction. Numerous studies in recovery process through enzymatic digestion treatments have been taken upon by many researchers [(de Koning and Witholt 1997) (de Koning, Kellerhals, et al. 1997) (Eggink and Northolt 1999) (Holmes and Lim 1990)].

In the commercial Biopol recovery process (Holmes and Lim 1990), microbial cell are ruptured by thermal treatment and the resultant debris is treated with enzyme cocktail and a surfactant to solubilize all non-PHA cellular materials.

In the enzymatic digestion process for recovery of PHAs, heat shock is employed by means of sterilizing the fermentation broth for short period of time. The heat shock enables the cells to be ruptured as well as the polynucleic acids solubilized and denatured, thereby preventing a detrimental increase in medium viscosity. Then, the solubilization of non-PHA cell material can be effected through the various enzymatic treatments (Holmes and Lim 1990).

The protease enzyme (Alcalase) was found to be effective in digesting the denatured nucleic acids and proteins (de Koning and Witholt 1997). The use of anionic detergent such as *sodium dodecyl sulfate* (SDS) can decompose any insoluble matters such as protein and lipids and solubilize the components by incorporation in micelles

(de Koning and Witholt 1997) found in their research that reaction of Alcalase and SDS simultaneously bore no synergistic effect at the optimum pH and temperature condition of Alcalase, and as such this leads to considerable time savings since the reactions can be carried out simultaneously. Further treatments with ethylene diamine tetra acetic acid (EDTA) enables chelation of divalent cations as well as degradation of the lipopolysaccharride layer enveloping membrane of the cell wall. Lysozyme is effective in degrading the peptidoglycan wall surrounding the PHA

granule, however, releasing this wall, increases viscosity, and as such, a lower concentration of lysozyme should suffice.

In the study carried out by (de Koning and Witholt 1997), the PHA was produced using sodium octanoate as the carbon source as well as different genera of the *Pseudomonas putida* strain from the one used in this study. The authors recovered the PHA by digestion with excess amounts of Alcalase, SDS and EDTA.

Other recovery technologies have been proposed in literature, including mechanical disruption, flotation techniques, use of gamma irradiation as well as aqueous two-phase system (Kunasundari and Sudesh 2011).

However, once PHA granules have been isolated from the solution, a final recovery step is required.

2nd Recovery

Final recovery of PHA granules in water suspension can be achieved through conventional methods (i.e. centrifugation) or new approaches (i.e. membrane processes).

The medium containing the solubilized cell material should be separated from the PHA granules.

Different methods have been proposed and applied for this purpose. In the PHB recovery procedures, solubilized and non-solubilized cell compounds are separated by centrifugation (Berger, et al. 1998). However, while PHB granules have a density of about 1.2 g/cm³, the submicron *mcl*-PHA granules have a density close to that of water (Marchessault, et al. 1995), therefore they form a highly stable suspension that would be difficult to centrifuge, requiring high G-forces. A clear supernatant could be obtained only by extensive centrifugation (i.e., 15,000 g for 60 min, as suggested by (de Koning and Witholt 1997).

In terms of versatility, ultra and micro filtration are perhaps the only methods able to match centrifugation processes, as shown in Fig. C.3.

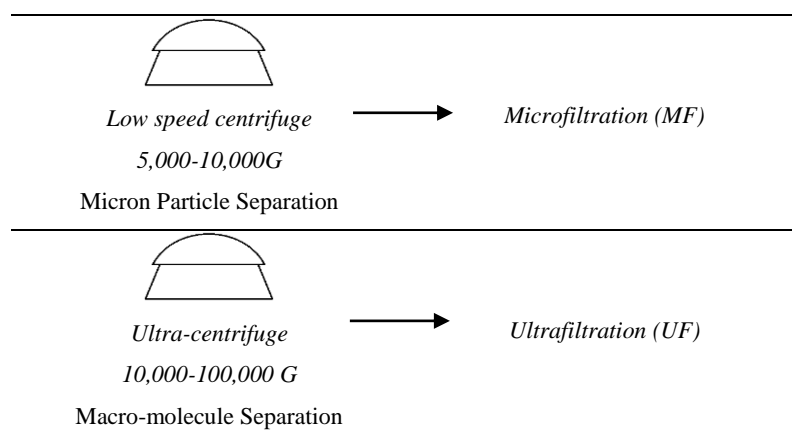


Figure C.3: Comparison of centrifugation and filtration processes (Cheryan 1998)

The filter should be selected in order to retain even the smallest PHA granules (Retentate), according to a basically scheme, depicted in Fig. C.4.

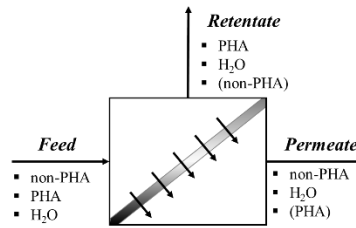


Figure C.4: Schematic representation for the recovery of PHA granules by UF/MF membranes

(Gozke, et al. 2012) recovered PHB by electrofiltration, a hybrid process combining dead-end filtration and electrophoresis, in view of the high negative zeta potential (negative charge) of PHB granules. (de Koning, Kellerhals, et al. 1997) recovered PHA granules by using ceramic tubular membrane (0.1 μm), managing to get %PHA purity that exceeded 95%. In their research tubular membrane was used in a cross flow system, however their high capital cost makes them less economics than polymeric membranes.

Table C.1 sows pressure driven membrane processes implemented for PHA recovery and documented in literature, since 1997.

Table C.1: PHA Recovery by using MF/UF membranes: state of the art

Ref.	Membranes	Apparatus	Test conditions	PHA Purity & Recovery
Yasothea et al. (2006)	PES (300 kDa) Sartocon Slice cassette (A=0.1 m ²)	Cross flow UF and DF	$\Delta P=0.5, 1.0, 1.5$ bar	Pur _{PHA} =92.6%, REC=90%
de Koning & Witholt, (1997)	KERASEP, 0.1 μm (A=0.024 m ²) ceramic tubular membrane	Cross flow	$\Delta P=3$ bar $P_{in}=1, 2, 4$ bar	–
Gozke, et al., (2012)	PES (Pall) 0.1 μm	Dead-end	Electric field=0,2,4 V/mm	–

Typically, once the optimum conditions for the enzymatic digestion treatments was decided, the solubilised non-PHA cell material was removed through crossflow ultrafiltration system with purification of PHA in water suspension through diafiltration system in a continuous mode, by replacing the non-PHA substances with water (Yasothea, Aroua, et al. 2006).

Since mcl-PHA granules are not rigid particles, but soft polymer droplets with a tendency to coalesce, plugging of the filter pores and surface posed a serious problem, cross-flow filtration is a technique typically designed to cope with this problem, in addition regular back flushing can be applied to clean plugging (ceramic) filters.

Literature studies were performed exclusively on small membrane samples or even modules, and focused on both PHA production and recovery.

The aim of this study is to evaluate the recovery feasibility by testing commercial polymeric *UF/MF* membranes.

C.1.4 Experimental set up

The simplest set up of the recovery process is one in which after fermentation, the fermentor content is heated to the sterilization temperature (121°C), and then rapidly cooled down to 55°C. The acidity is adjusted at pH=8.5, Alcalase, EDTA and SDS are added and enzymatic digestion starts. After this procedure fermentor is connected to *UF/MF* unit and filtration is started in diafiltration mode (CD), as suggested by (de Koning, Kellerhals, et al. 1997).

For this preliminary study *UF/MF* membranes (delivered by Sepra S.r.l, and described in detail in *Appendix B*) were tested housed in a dead end Stirred cell ($V=200$ ml, $A= 13.2$ cm², $P_{\max}=7$ bar), described in *Appendix A: Materials & Methods*. The following tests were performed:

- (i) Membrane screening, with water and *non-PHA* solution from *Enzymatic digestion*;
- (ii) Separation performances with *PHA* solution, derived from *Chemical digestion*.

The first step is necessary to select the membrane that enable *non-PHA* flow through the membrane. Secondly the best membrane was tested with *PHA* solution. All experiments were performed in concentration mode.

Non-PHA Recovery

UF/MF membranes selected were tested firstly with pure water (pH 5.6) and then with *non-PHA solution*. The solubilized *non-PHA* cell material was removed through a dead-end stirred cell (initial feed volume 200 ml). The closed system does not allow to perform *diafiltration* operations, by replacing the *non-PHA* substances with water, thus *non-PHA* concentration was performed batchwise only. This approach was adopted to test membrane performance, compare *non-PHA* permeate fluxes with water fluxes (hydraulic permeability), and then evaluate if *non-PHA* is permeable. In order to optimize the conditions of concentration mode, the effects of permeate flux on pressure difference across the membrane (ΔP_{in}) were tested, ranging from 0.5 to 2 bar. In this study a 100 kDa (PV400) and a 250 kDa (PV400R) PVDF membranes were tested. Results are shown in Fig. C.5 and C.6 *a-b*.

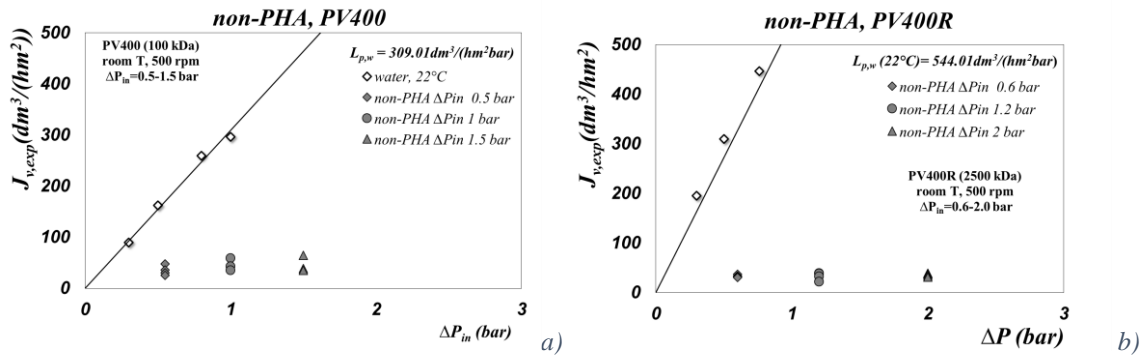


Figure C. 5: non-PHA filtration tests- Membrane screening, with PV400 (100kDa)(a) and PV400R (250 kDa) membranes, room T(22°C), 5,000 rpm, $\Delta P_{in}=0.5-2.0$ bar, dead-end stirred cell.

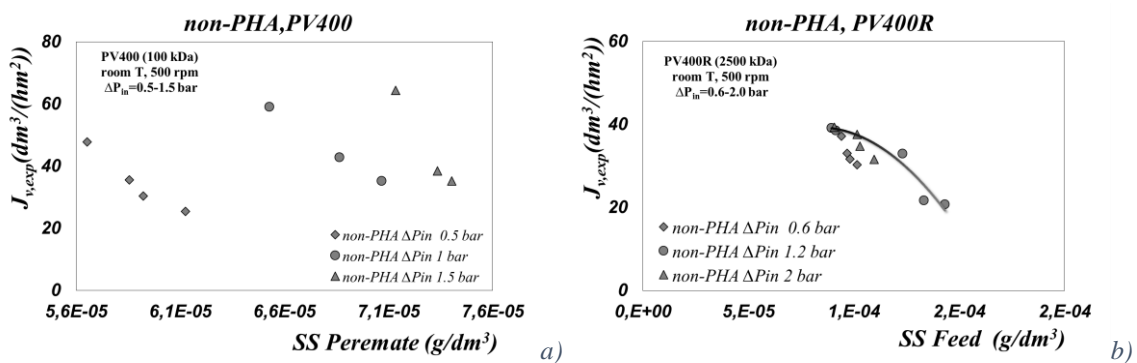


Figure C.6. non-PHA filtration test. Experimental permeate flux as a function of Suspended Solid concentration (SS) in permeate (a) and retentate (b) side. PV400 (a) and (PV400R) (b) membranes, room T, 500 rpm, ΔP_{in} ranging from 0.5 to 2 bar, dead-end stirred cell.

Concentration polarization, as we expected, is a limiting factor in UF, indeed the solute retained by the membranes tends to accumulate at the surface of the membrane and constitutes an additional barrier to the passage of the permeable specie. Furthermore, high viscosities of non-PHA solution, limits mass transfer coefficient.

The experimental results shown that for both membranes tested, concentration polarization occurred at all inlet pressures. As shown in Fig. C.5 a and C.6 a, from ΔP_{in} equal to 1 bar, permeate flux becomes quite independent from applied pressure, therefore, the optimum condition for maximal permeate flux was $\Delta P_{in}=1$ and $\Delta P_{in}=1.2$ for PV400 and PV400R respectively.

Although permeate fluxes are very low, during permeation tests the enzymatically treated suspension concentration increases in permeate side (see Fig. C.6 a, PV400 membrane), and decrease in the Feed side (Fig. C.6 b, PV400R membrane).

These behavior show that both membranes are permeable to non-PHA suspension, thus can improve PHA purity in retentate side. However, since PV400R membrane gives low reproducibility, PHA suspension has been tested on PV400 membrane.

PHA recovery

Final recovery of PHA granules was achieved through dead-end stirred cell too. Concentration experiments were performed on PV400 membrane (more stable, compared to PV400R) at 50°C (in order to increase permeate fluxes).

The effect of initial PHA concentration (ranging from 5 to 20 g/dm³) was studied on the performance separation of the membrane. Results are shown in Fig. C.7.

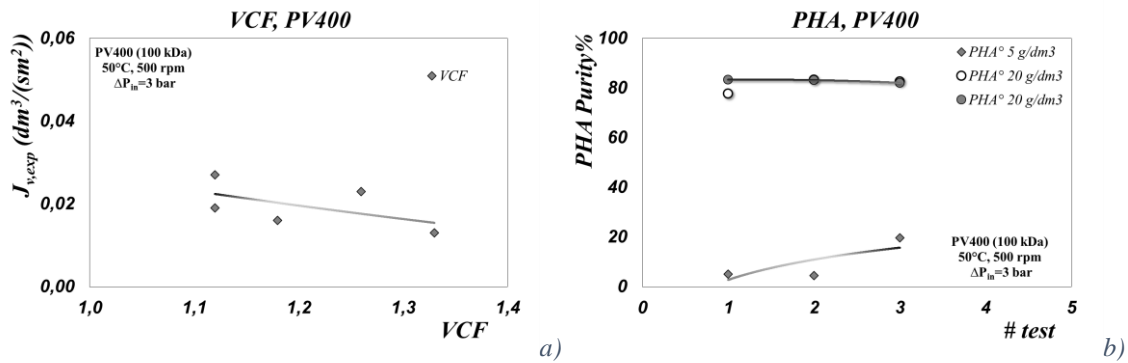


Figure C.7: PHA Recovery. Permeate flux as a function of VCF (a) and PHA purity in retentate as a function of test number. PV400 (100 kDa) membrane. Dead-end stirred cell, 50°C, 500 rpm, $c(t=0,PHA)=5$ and $20 g/dm^3$, $\Delta P_{in}=3$ bar

Experimental data put in evidence an increase in PHA concentration and purity in retentate side: the higher increment was obtained at low initial concentrations ($c_{PHA}(t=0)=5 g/dm^3$), however the highest purity (>80%) was achieved at high initial PHA concentrations, as summarized in Tab. C.2.

During tests permeate flux tend to decrease in view of the higher concentration: thus both concentration and PHA purity increase in retentate side.

Table C.2: PHA purity in retentate during experimentation, initial concentration of PHA 5 and 20 g/dm³. PV400 (100 kDa) membrane. Dead-end stirred cell, 50°C, 500 rpm, ΔP_{in}=3 bar

	PHA° 5 g/dm ³	PHA° 20 g/dm ³
#test	PHA Purity in Retentate	
1	5.09	77.77
2	4.51	83.34
3	19.69	82.59

Results obtained shown that:

- i) PHA recovery is achievable by UF/MF polymeric membranes;
- ii) In view of the concentration polarization, cross flow unit should be tested;
- iii) Higher membrane areas are necessary to confirm these behaviors;
- iv) Fouling is a key phenomenon, emphasized in a dead-end filtration unit

These results are comparable with those found in literature, however they represent only a preliminary step: a cross-flow UF should be suitable for producing a PHA latex.

C.1.5 Integration between PHA and VFA production

As a fully biodegradable and biocompatible plastic, polyhydroxyalkanoate (PHA) is an interesting alternative to petrochemical derivative plastic due to their similar characteristics.

PHA can be biosynthesized from renewable resources, allowing for a sustainable and closed-cycle process for the production and use of such polymers (Braunegg, Lefebvre and Genser 1998).

Currently, PHA synthesis at industrial scale is based on microbial isolates and well defined substrates (Patnaik 2005). However, the cost of PHA produced thus is still too high for PHA to compete with the conventional plastic commodities. Economic evaluation showed that the production expense of PHA can be reduced over half if renewable waste materials and activated sludge were used (Serafim, et al. 2004).

Above all, almost 30% of total PHA production cost is attributed to the carbon source (Salehizadeh and Van Loosdrecht 2004). Additionally, a great amount of excess sludge is generated daily worldwide. Handling, treatment and ultimate disposal of the excess sludge accounts for 40–60% of the total operational cost of an activated sludge treatment plant (Liu 2003). One strategy for excess sludge management is moving towards reutilization of sludge as useful resources, such as fermenting the excess sludge to generate carbon source for PHA production by pure culture (Lee and Yu 1997). Nowadays Volatile Fatty Acids (VFAs) is the most suitable substrate for PHA storage. PHA synthesis by activated sludge is possible to reduce PHA production cost, since its sterilization, equipment and control requirements are lower and the microbial communities in activated sludge can adapt well to the complex substrates present in the agro industrial wastes (Salehizadeh and Van Loosdrecht 2004). Basic and applied research on this field has been implemented in the past decade (Lemos, Serafim and Reis 2006).

(Mengmeng, et al. 2009) investigated the feasibility of PHA production by activated sludge by using VFAs generated from excess sludge fermentation. VFA is a suitable carbon source for PHAs production [(Serafim, et al. 2004) (Mengmeng, et al. 2009) (Albuquerque, et al. 2011)].

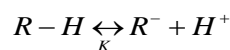
However, in some application (i.e. distillery for ethanol production) volatile solutes are known to inhibit fermentation, which makes their removal essential prior to their recycling [(Lafon-Lafourcade, Geneix and Ribereau-Gayon 1984), (Morin Couallier, Payot, et al. 2006)]. Acetic acid is one of the inhibitors in bioethanol production from the bioconversion of lignocellulosic materials.

The growth of fermentation microorganism and the production of ethanol are strongly affected by the presence of acetic acid in high concentration (Palmqvist and Hann-Hagerdal 2000).

This study aimed to evaluate the application potential of Nanofiltration (NF) membranes for the rejection of volatile fatty acids and reuse for PHA fermentation, since VFAs are used as the carbon source for PHA accumulation

C.2 Introduction to VFAs

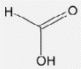
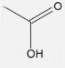
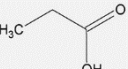
Organic acids are generally weak acids and are dissociated with regard to the pH in the solution as follows:

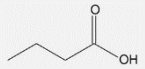
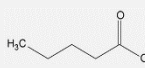


Where, R , H and K_a represent the carboxylic group, hydrogen ion and acidity constant, respectively. As rejection of weak acids and bases is highly pH-dependent, their retention in the NF process will be high in the ionized form. Thus, the organic acid rejection increases significantly at pH levels above the acidity constant (pK_a), but the rejection decreases at pH levels below pK_a (when the acids are in the neutral form). Since the pK_a values of selected organic acids are below the pH range of 3-5, an increase of the rejection observed at a pH between four and nine could be explained by an increase in the degree of dissociation. On the other hand sieving effect plays an import role in the rejection of neutralized organic acids, as shown by (Choi, Fukushi and Yamamoto 2008).

Volatile Fatty Acids (VFA) have important uses, as chemical intermediates and are central to the organic carbon cycling (Zacharof and Lovitt 2013). These acids, especially acetic, are key intracellular and extracellular metabolic intermediates. Consequently if carbon could be recovered in the form of VFA, this could represent an alternative, sustainable source of carbon based chemicals for industrial use, since these can be generated and recovered from organic degradation processes, such as fermentation and anaerobic digestion. Furthermore, these acids can be used as a substrate for a number of interesting biotransformations for sustainable production of chemical (Popken, Gotze and Gmehling 2000). In Tab. C.3 a list of the main Volatile Fatty Acids, their structures, molecular weight and pK_a constants is summarized.

Table C.3: Physical and Chemical properties and structures of Volatile Fatty Acids

VFAs	symbol	MW (g/mol)	Structure	pK_a
Formic Acid	FA	46.03		4.74
Acetic Acid	AA	60.05		4.76
Propionic Acid	PA	74.08		4.88

Butyric Acid	BA	88.10		4.82
Valeric Acid	VA	102.15		4.82
Caproic Acid (Esanoic A.)	CA	116.16	-	4.88

Although these VFAs present very similar acid dissociation constant (pK_a), their size and molecular weight are very different, ranging from 46.03 to 102.15 g/mol.

C.2.1 VFA recovery: state of the art

According to numerous work published in the last few years, the use of NF as a downstream operation in organic acids production processes is expected to be a large and new application field of this technology. Organic acids (i.e. acetic, lactic, gluconic acid...) are increasingly used in food industries, are mainly produced by fermentation [(Han and Cheryan 1995) (Timmer, Van der Horst and Robbertsen 1993) (Timmer, Kromkamp and Robbertsen 1994)]. Furthermore, the National Renewable Energy Laboratory (NREL)³ has identified some VFA (i.e. gluconic acid) as one of the top 30 building blocks for derivation of high-value chemicals.

The integration of NF process can be investigated at different stages depending on the organic acid. On one hand, for high molecular weight organic acids, NF can be considered as a concentration step, on the other hand, NF can constitute a purification step in the case of low molecular weight organic acids. It was shown for instance that NF is an appropriate method for the downstream processing of sodium acetate while retaining nutrients, like glucose, can be recycled in the fermentation tank (Han and Cheryan 1995).

The separation of organics acids from digested or fermented effluents or the discharged waste streams of these processes is not a straightforward process considering the complex physicochemical nature of these streams and the concentration of the acids in them. Often these effluents demand extensive pretreatment to make further processing workable (Masse, Masse and Pellegrini 2008).

Within this context, membrane filtration can offer a feasible option towards a cost effective fractionation and recovery of VFA.

The low molecular mass and the chemical properties of the VFA makes NF attractive choice [(Bouchoux, Roux-de Balmann and Lutin 2005), (Choi, Fukushi and Yamamoto 2008)]. However, for certain applications, fermentation-derived organic acids contain too many impurities and are usually too dilute.

³<http://www.nrel.gov/docs/fy04osti/35523.pdf>

In the literature, there are a lot of reports on the use of Nanofiltration for downstream processing of acetates, as well as many authors investigated the performance of NF membranes on enrichment and concentration of VFA as well as the influence of pH on the separation., as shown in Tab. C.4 Table D.4 focused particularly on VFA solutions (type and concentration of VFA), membrane type and configuration, operating conditions, as well as the influence of applied pressure, temperature and pH on permeate flux and rejection.

Table C.4: VFA recovery by NF applications: State of the art

VFA	VFA Concentration (g/dm ³)	Membrane	Configuration & Area	Test conditions	Ref.
Acetic A. (+ glucose)	10	DS5, DS7 (Desal); NF40, FT30 (Dow); CA, PZ, TLC (Fluid Systems), MPF20, MPF50 (Kiryat-Weizmann); NTR729, NTR759 (Nitro-Denko); MX07 (Osmonics)	Dead-end stirred cell, A=0.00145 m ²	T=30-50°C P=0-27.6 bar pH=2.7-5.8	(Han and Cheryan 1995)
Acetic A.	0.01	ES20 (Nitro-Denko)	Flat sheet, Cross flow module, A=0.006 m ²	T=25°C, P=2.9 bar, pH=3-9	(Ozaki and Li 2002)
Acetic A. (+ xylose)	2-10 (AA) + 20-100 (xylose)	Desal-5 DK	1812-47mil Spiral Wound, 0.2 m ²	T=25°C, P=4.9-24.5 bar; pH=4.9-6.9-9.1	(Weng, et al. 2009)
Acetic A. + xylose + glucose	2-10 (AA) + 10-50 (xy) + 4-20 (glu)	Desal-5 DK (GE) , Alfa Laval NF (Alfa Laval), R098pHt, RO99 (Alfa Laval)	Plate & frame DSS LABSTACK, 0.0174 m ²	T=25-40°C, P=20-50 bar	(Zhou, Wang and Wei 2013)
Acetic A. + xylose + glucose	2-10 (AA) + 10-50 (xy) + 4-20 (glu)	R098pHt (Alfa Laval)	Plate & frame DSS LABSTACK, 0.0174 m ²	T=25-40°C, P=10-40 bar; pH=3-10	(Zhou, Wang and Wei 2013)
Acetic A.	0.01-0.015	NF-90, NF-200 (Dow/Filmtec)	Flat sheet, SEPA II cross flow, A=0.0138 m ²	P=5.5 bar, pH=3-10	(Bellona and Drewers 2005)
Lactic A. + Acetic A. + Amino Acids	20.4 (LA)+ 3.31 (AA) + 19.3(amino acids)	DK, DL, HL, FT NF 270,HT, KO MPF35	Flat sheet, A=0.0127 m ²	T=25°C P=15-25 bar pH 2.5-5.5	(Eecker, Raab and Haraseka 2012)
Formic A., Acetic A., Propionic A., Succinic A., Citric A.	0.5	Flat sheet NF270 (Dow/Filmtec), ES10 (Nitro Denko)	Cross flow unit, A=0.006 m ²	T=25°C, P=2.8 bar, pH 3-9	(Choi, Fukushi and Yamamoto 2008)
Acetic A., Butyric A.	1.3 (AA) 1.4 (BA)	NF270 (Dow), HL, DL, DK (Osmonics), LF10 (Nitro-Denko)	Dead-end attired cell, Sterlitech HP4750, A=0.00146 m ²	P=0-20 bar, pH 4-9	(Zacharof and Lowitt 2014)
Acetic A., Propanoic A., Butyric A.	0.615 (AA), 0.090 (PA), 0.058 (BA)	SG, SE, CE (Osmonics); BW30, BW30LE (Filmtec); ESPA2, CPA2, LFC30 (Hydranautics)	Plate & Frame DSS LABSTACK M20-072 (Novasep), A=0.036 m ²	T=25-50°C, P=30 bar, pH 3.4-10	(Sagne, Fargues, et al. 2008)
Acetic A., Propanoic	0.8593 (AA), 0.0851 (PA),	CPA2, ESPA2 (Hydranautics); BW30 (Dow)	Spiral wound 2540, A=2.6 m ²	T=20°C, P=5-30 bar, pH 3.5-9	(Sagne, Fargues, et al. 2010)

A., Valeric	0.2399 (BA),				
A., Butyric	0.0548 (VA),				
A., Caproic	0.0329 (CA)				
A.					
Formic	<0.028 (FA),				
A., Acetic A.,	<0.016 (AA),			T=25-30°C,	(Morin Couallier,
Propionic A.,	<0.015 (PA),	Filmtec FT30 (Dow)	DSS LABSTACK M20-	P=40 bar, pH	Salgado Ruiz, et
Butyric A.,	<0.015 (BA),		0.72, A=0.18 m ²	3.0, 5.2, 7.5,	al. 2006)
Valeric A.,	<0.015 (VA),			10.0	
Hexanoic A.	<0.01 (HA)				
Formic A.,	0.46 (FA),				(Laufenberg,
Acetic A.,	0.6 (AA),		Spiral Wound module	T=18-22°C,	Hausmanns and
Propionic A.,	0.7 (PA),	TR70-2514F	(Sampas Membrantechnik	P=10 bar, pH 2-	Kunz 1996);
Butyric A.,	0.8 (BA),		GmbH), A=0.7 m ²	2.4	(Hausmanns,
Valeric A.	1.0 (VA)				Laufenberg and
					Kunz 1996)
Valeric A. (+		PCI Membrane Systems AFC99		T=20°, 40°C,	(Rodriguez, et al.
wastewater	0.5-25	(PA) tubulat	A=0.9 m ²	P=13-60 bar	2000)
stream)					

Different applications have been discussed and typically membranes performances have been investigated as a function of pressure, concentration, temperature, and the presence of other media components, however in such separations pH plays a key role in the rejection of VFAs. Many authors [(Choi, Fukushi and Yamamoto 2008), (Ozaki and Li 2002)] also reported a significant influence of pH levels on the retention of various organic acids retentions during NF. (Bellona and Drewers 2005) reported the role of membrane surface charge on the rejection of organic acids by NF membranes in a single-solute solution, and others dealt with the influence of pH on the rejection of organic acids in multicomponent systems [(Hausmanns, Laufenberg and Kunz 1996), (Laufenberg, Hausmanns and Kunz 1996)], (Sagne, Fargues, et al. 2008)].

(Timmer, Van der Horst and Robbertsen 1993) reported on the Nanofiltration of lactic acid; (Eecker, Raab and Haraseka 2012) used NF for the separation of Lactic Acid (LA) from amino acids in a “Green Biorefinery” pilot plant. (Rodriguez, et al. 2000) studied the feasibility of separate Valeric (n-pentanoic) acid (VA, 102.13 g/mol) from a wastewater stream from a nylon manufacturing process. In this study acid rejection and permeate flux as a function of temperature, acid concentration and transmembrane pressure were investigated.

A lot of study investigate Nanofiltration as a method for downstream processing of acetate fermentation broth. (Han and Cheryan 1995) were the first to study the separation of acetic acid from sugar. They firstly separated acetic acid from glucose, founding that pH is a major factor influencing the separation. In general, there is a correlation between rejection of acetate and the degree of dissociation of acetic acid, as determined from the Henderson-Hasselbach equation.

Many studies dealt with VFA-sugar separation: (Weng, et al. 2009) used a NF membrane (Desal-5 DK) to separate acetic acid from xylose, using a synthetic acetic acid-xylose solution as the model. It was found that both the solution pH and the applied pressure affected the separation performance (a high separation factor (>5) was observed at high pressure and low pH; in addition, negative retention of acetic acid was observed only in the presence of xylose. These results suggested that intermolecular interactions play an important role in the separation of xylose and AA. (Teella, Huber and Ford 2011) examined the feasibility of removing acetic acid from glucose at high feed concentration (7 wt% acetic acid and 15 wt% glucose) by Nanofiltration and reverse osmosis.

(Zhou, Wang and Wei 2013) in their work focused on the separation of acetic acid from monosaccharides, due to its toxicity for sugar fermentation. In this study the feasibility of simultaneous acetic acid separation and sugar concentration was evaluated, by using synthetic xylose-glucose-acetic acid model solution.

However the effects that several organic acids can have on each other have not been examined so far. Just (Hausmanns, Laufenberg and Kunz 1996) and (Laufenberg, Hausmanns and Kunz 1996) studied the interaction of acetic acid with 26 further acids in a RO application. It was concluded that the rejection of acetic acid was improved considerably in presence of propionic and butyric acid, as a consequence, it can be said that such interactions take place in VFA mixtures.

From the state of the art documented in Tab. C.4 we may conclude that:

- i) a wide literature exists on VFAs recovery by NF, for different applications;
- ii) ΔP , pH, T and concentration seem to be crucial parameters for VFAs recovery;
- iii) For the most part small membrane samples have been tested.

The overall objective of this preliminary research was to investigate the feasibility of using nanofiltration for the recovery and fractionation of VFA, depending on pH and organic compound..

C.2.2 VFA Nanofiltration: Results and Discussion

Experiments were carried out in NF-unit (described in *Appendix A*) in order to study the influence of different parameters, first of all pressure, feed concentration and feed pH on the membrane performances. Since previous researches have highlighted the possibility of enhancing the retention process by altering the pH of the solutions, pH was adjusted from 4 to 3.5 to investigate the influence of pH on flux and acid retention.

The rejection of the compounds under study were calculated as follows:

$$R_{obs,VFAi} = 1 - \frac{C_{P,VFAi}}{C_{bulk,VFAi}} \times 100 \quad (C.1)$$

Where $C_{P,VFAi}$ and $C_{bulk,VFAi}$ represent VFA concentration in the permeate and in the bulk solution respectively. The values obtained are shown as a function of permeate flux, $J_{v,exp}$. Volumetric flux of permeate was expressed in [$dm^3/(hm^2)$], in the form of:

$$J_{v,exp} = \frac{Q_P}{A} \quad (C.2)$$

Where Q_p is the permeate flow rate (dm^3/h) across the effective membrane area A (m^2).

To investigate the influence of applied pressure on the rejection of selected VFA, the pressure was varied from 4.4 to 24.4 bar at a total feed concentration of 10 g/dm^3 . In all the experiments temperature was set to $50^\circ C$, in order to decrease feed viscosity.

First experiments were carried out at pH 4. For both membranes, the level of applied pressure seems to have little influence on the VFAs rejection as shown in Fig. C.8 a-d.

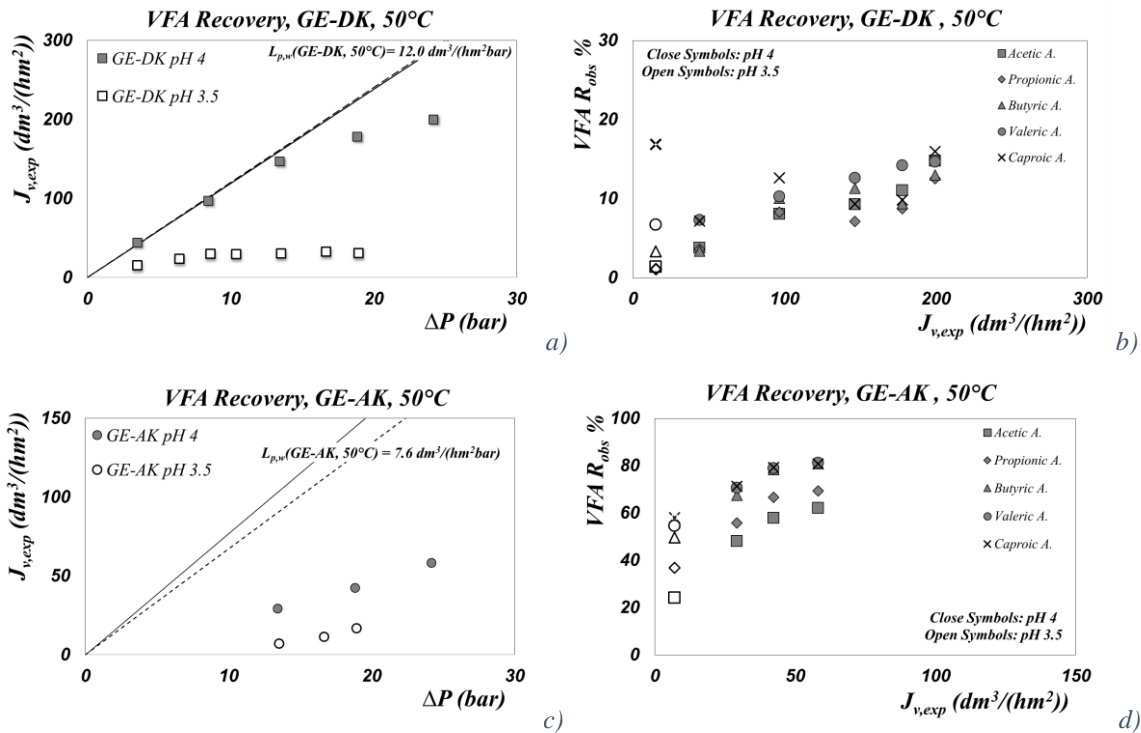


Figure C.8: Nanofiltration of model solutions of VFAs. Experimental permeate fluxes ($J_{v,exp}$) as a function of applied pressure(a,c), and observed rejections ($R_{obs,i}$) as a function of experimental permeate fluxes ($J_{v,exp}$)(b, d). Radial flow test cell, $50^\circ C$, pH 3.5 and 4, flow rate $400 \text{ dm}^3/h$, total recirculation mode of R and P.

The rejection coefficients obtained during tests at pH 4 were higher for *Caproic*, *Valeric* and *Butiric* acids. Since the pK_a values of the compounds is higher than 4, the rejection can be attributed to sieving effect, and this explains why the higher the molar mass of acids, the greater the retentions. Rejection

values are higher with GE-AK membrane (80% compared to 15% for GE-DK), as expected from permeate fluxes.

To demonstrate the role of the sieving effect on VFAs below pK_a , we have investigated observed rejections as a function of molecular weight of compound (ranging from 60.05 for *Acetic Acid* to 116.16 for *Caproic Acid*) at pH 4. The results shown that sieving effect plays an important role for GE-AK membrane. As already mentioned in literature, as the larger the acid, the higher its rejection. (Ozaki and Li 2002), (Sagne, Fargues, et al. 2008).

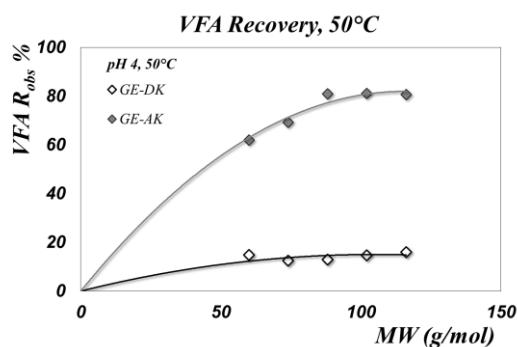


Figure C.9: Observed rejection as a function of VFAs MW for GE-DK and GE-AK membranes, at 50°C and pH 4

The effect of pH on both permeate fluxes and rejections was ambiguous. From literature the rejection of acids (particularly acetic and propionic acids) increased with the pH, because of the increased electrostatic repulsion between the ionized form of the acids and the negatively charged membranes (Ozaki and Li 2002).

Thus we would have expected at lower pH (3.5) higher fluxes and lower rejections. For both membranes, the flux becomes smaller (see Fig. C.8 a, c) when the pH of the solutions decreased from 4 to 3.5, at the same time, despite the pressure increases, permeate flux reaches an asymptotic value, corresponding to very high rejection values. The flux reducing was linked to the increase in the observed retention, thus the concentration polarization and the fouling on the membrane surface, although the osmotic pressure calculated with proper correlations was negligible (less than 1 bar).

By analyzing experimental data, it seems that membranes fouled very quickly during the tests, impairing the results obtained. High operating pressure generally results in high permeate flux; however the low pressure range is able to prevent undesired rapid membrane fouling caused by a higher permeate flux when treating VFA solutions.

Membrane fouling was observed under the experimental conditions tested. Because of the different permeability offered by the two membranes, GE-DK membrane showed a higher fouling caused by a higher permeate flux.

Separation efficiency was evaluated for both membranes, in terms of VFAs purity in feed and permeate side, as shown in Fig. C.10.

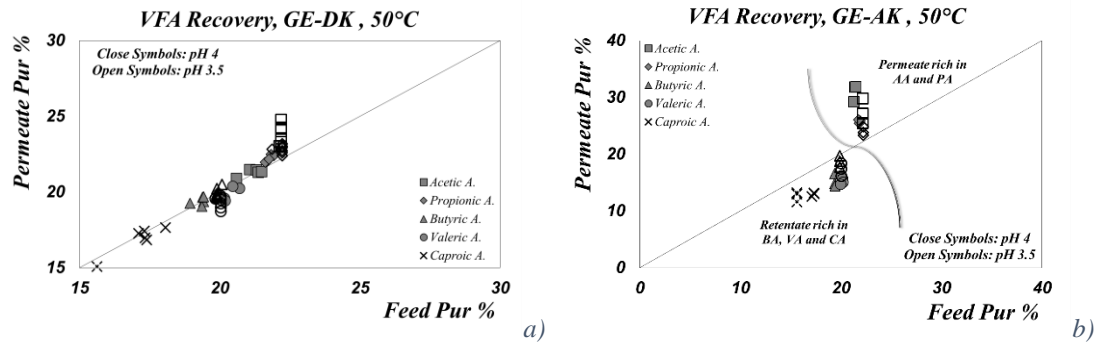


Figure C.10: Comparison between VFAs purity in the feed and permeate side. Radial flow test cell, 50°C, pH 3.5 and 4, flow rate 400 dm³/h, total recirculation mode of R and P.

GE-AK membrane were identified as the best candidate for VFAs separation and concentration. Although GE-DK membrane offered high permeate fluxes, no VFAs separation was achieved with this membrane, thus this membrane is unattractive for use as a separation step, however it can be used as a concentration step, or even testes at high pH values (with $\text{pH} > \text{p}K_a$).

C.3 Conclusions

From the results obtained, it is evident that UF and NF/RO are effective tools for the recovery of PHA and VFAs respectively.

Although studies presented are preliminary, gave interesting information. The recovery and purification of PHA in water suspension can be improved with a cross flow configuration, limiting concentration polarization, and operating in diafiltration mode, required in order to obtain a PHA latex, for which application PHA purity should be higher than 90%.

Secondly, VFA recovery by Nanofiltration seems to be attractive in order to recycle volatile fatty acids in the PHA fermentation process.

In the pH range investigated, the degree of retention of the compounds tested depended upon the membrane and the molecular weight of VFA, confirming that at pH lower than $\text{p}K_a$, separation is governed by sieving effects. Tests at higher pH are required to improve VFA concentration.

Based on the above mentioned results further investigations, especially about pH effect on retention, are required, since the pH is expected to improve the performance of the process. Furthermore it is necessary to optimize the operating parameters (pressure, recovery, fouling) on spiral wound membranes, more representative of industrial treatment conditions.

However our work suggest that membrane processes are attractive to be integrated in a biotechnology system, although some drawback exist, like membrane fouling and high concentration polarization.

References

- Agustin Martinez, G., L. Bertin, A. Scoma, S. Rebecchi, G. Braunegg, and F. Fava. "Production of polyhydroxyalcanoates from dephenolised and fermented olive mill wastewater by employing a pure culture of *Cupravidus necator*." *Biochemical Engineering Journal* 97 (2015): 92-100.
- Albuquerque, M.G.E., V. Martino, E. Pollet, L. Avérous, and M.A.M. Reis. "Mixed culture polyhydroxyalcanoate (PHA) production from volatile fatty acid (VFA)-rich streams: Effect of substrate composition and feeding regime on PHA productivity, composition and properties." *Journal of Biotechnology* 151 (2011): 66-76.
- Bellona, C., and J. Drewers. "The role of membrane surface charge and solute physico-chemical properties in the rejection of organic acids by NF membranes." *Journal of Membrane Science* 249 (2005): 227-234.
- Berger, E., B.A. Ramsay, J.A. Ramsay, and C. Chavarie. "PHB recovery by hypochlorite digestion of non-PHB biomass." *Biotechnol. Technol.* 3 (1998): 227-232.
- Bouchoux, A., H. Roux-de Balman, and F. Lutin. "Nanofiltration of glucose and sodium lactate solutions: variations of retention between single- and mixed- solute solutions." *Journal of Membrane Science* 258 (2005): 123-132.
- Bouchoux, A., H. Roux-de Balman, and F. Lutin. "Investigation of nanofiltration as a purification step for lactic acid production processes based on conventional and bipolar electro dialysis operations." *Separation and Purification Technology* 52 (2006): 266-273.
- Braunegg, G., G. Lefebvre, and K.F. Genser. "Polyhydroxyalcanoates, biopolyester from renewable resources: physiological and engineering aspects." *Journal of Biotechnology* 65, no. (2-3) (1998): 127-161.
- Charcosset, C. "Membrane processes in biotechnology: An overview." *Biotechnology Advances* 24 (2006): 482-492.
- Chen, C.Q., and Q. Wu. "The application of polyhydroxyalkanoates as tissue engineering materials." *Biomaterials* 26, no. (33) (2005): 6565-6578.
- Chen, G.-Q. "A microbial polyhydroxyalcanoates (PHA) based bio- and materials industry." *Chemical Society Reviews* 38 (2009): 2434-2446.
- Chen, G.-Q. "Plastics completely synthesized by bacteria: polyhydroxyalcanoates." In *Plastics from Bacteria*, by G.-Q. Chen, 17-37. Berlin Heidelberg: Springer, 2010.
- Cheryan, Munir. *Ultrafiltration and Microfiltration*. CRC Press, 1998.
- Choi, J., and S.Y. Lee. "Factors affecting the economics of polyhydroxyalcanoates production by bacterial fermentation." *Appl. Microbiol. Biotechnol.*, 1999: 13-21.
- Choi, J.-H., K. Fukushi, and K. Yamamoto. "A study on the removal of organic acids from wastewaters using nanofiltration membranes." *Separation and Purification Technology* 59 (2008): 17-25.
- de Koning, G.J.M., and B. Witholt. "A process for the recovery of PHAs from *Pseudomonas*, part 1. Solubilization." *Bioprocess Eng.* 17 (1997): 7-13.
- de Koning, G.J.M., M. Kellerhals, C. van Meurs, and B. Witholt. "A process for the recovery of PHAs from *Pseudomonas*, part 2. Process development and economic evaluation." *Bioprocess Eng.* 17 (1997): 15-21.
- Doi, Y. "Microbial Polyesters." In *Microbial Polyesters*, by Y. Doi, 13-27. Yokohama: VCH Publishers Inc., 1990.
- Eecker, J., T. Raab, and M. Haraseka. "Nanofiltration as a key technology for the separation of LA and AA." *Journal of Membrane Science*, 2012: 389-398.
- Eggink, G., and M.D. Northolt. Method for producing a biologically degradable polyhydroxyalcanoate coating with the aid of an aqueous dispersion of polyhydroxyalcanoates. US Patent Patent 5,958,480. 1999.
- Gozke, G., et al. «Electrofiltration as a purification strategy for microbial poly-(3-hydroxybutyrate).» *Bioresource Technology* 123 (2012): 272-278.

- Gurieff, N., and P. Lant. "Comparative life cycle assessment and financial analysis of mixed culture polyhydroxyalkanoate production." *Biores. Technol.* 98 (2007): 3393-3403.
- Hahn, S.K., Y.K. Chang, B.S. Kim, e H.N. Chang. «Optimization of microbial poly(3-hydroxybutyrate) recovery using dispersions of sodium hypochlorite solution and chloroform.» *Biotechnol.Bioeng.* 44 (1994): 256-261.
- Han, I.S., and M. Cheryan. "Nanofiltration of model acetate solutions." *Journal of Membrane Science* 107 (1995): 107-113.
- Han, I.S., and M. Cheryan. "Nanofiltration of model acetate solutions." *Journal of Membrane Science*, 1995: 107-113.
- Hausmanns, S., G. Laufenberg, and B. Kunz. "Rejection of acetic acid and its improvement by combination with organic acids in dilute solutions using reverse osmosis." *Desalination* 104 (1996): 95-98.
- Holmes, P.A., and G.B. Lim. Separation Process. US Patent Patent 4,910,145. 1990.
<http://www.nrel.gov/docs/fy04osti/35523.pdf>. s.d.
- Kunasundari, B., and K. Sudesh. "Isolation and recovery of microbial polyhydroxyalkanoates." *eXPRESS Polymer Letters* 5, no. 7 (2011): 620-634.
- Kunioka, M., and Y. Doi. "Thermal degradation of microbial copolyesters-poly(3-hydroxybutyrate-co-3-hydroxyvalerate) and poly(3-hydroxybutyrate-co-4-hydroxy butyrate)." *Macromolecules* 23 (1990): 1933-1936.
- Lafon-Lafourcade, S., C. Geneix, and Ribereau-Gayon. "Inhibition of alcoholic fermentation ofgrape must by fatty acids produced by yeasts and their elimination by yeasts ghosts." *Appl. Environ. Microbiol.* 47, no. (6) (1984): 1246-1249.
- Laufenberg, G., S. Hausmanns, and B. Kunz. "The influence og intermolecular interactions on the selectivity of several organic acids in aqueous multicomponent systems during reverse osmosis." *Journal of Membrane Science* 110 (1996): 59-68.
- Lee, S., and J. Yu. "Production of biodegradable thermoplastics from municipal sludge by a two-stage bioprocess." *Resources, Conservation and Recycling* 19, no. (3) (1997): 151-164.
- Lee, S.Y. «Bacterial Polyhydroxyalkanoates.» *Biotechnol. Bioeng.* 1996 (1996): 1-14.
- Lemos, P.C., L.S. Serafim, and M.A.M. Reis. "SYnthesis of polyhydroxyalkanoates from different short-chain fatty acids by mixed cultures submitted to aerobic dynamic feeding." *Journal of Biotechnology* 122, no. (2) (2006): 226-238.
- Liu, Y. «Chemically reduced excess sludge production in the activated sludge process.» *Chemosphere* 50 (2003): 1-7.
- Marchessault, R.H., F.G. Morin, S. Wong, and I. Saracovan. "Artificial granule suspensions of long side chain poly(3-hydroxyalkanoate)." *Can. J. Microbiol.* 41 (1995): 138-142.
- Masse, L., D.I. Masse, and Y. Pellegrini. "The effect of pH on the separation of manure nutrients with reverse osmosis membranes." *Journal of Membrane Science* 325 (2008): 914-919.
- Mengmeng, C., C. Hong, Z. Qingliang, S.N. Shirley, and R. Jie. "Optimal production of polyhydroxyalkanoates (PHA) in activated sludge fed by volatile fatty acids (VFA) generated from alkaline excess sludge fermentation." *Bioresource Technology* 100 (2009): 1399-1405.
- Mitomo, H., T. Takahashi, H. Ito, and T. Saito. "Biosynthesis and characterization of poly(3-hydroxybutyrate-co-3-hydroxyvalerate) produced by *Burkholderia cepacia* D1." *J. Biol. Macromol.* 24 (1999): 311-318.
- Morin Couallier, E., B. Salgado Ruiz, M.L. Lameloise, and M. Decloux. "Usefulness of reverse osmosis in the treatment of condensates arising from the concentration of distillery vinasses." *Desalination* 196 (2006): 306-317.

- Morin Couallier, E., T. Payot, A. Pastore Bertin, and M.L. Lameloise. "Recycling of distillery effluents in alcoholic fermentation: role in inhibition of 10 organic molecules." *Appl. Bioche. Biotechnol.* 133, no. (3) (2006): 217-238.
- Ozaki, H., and H. Li. "Rejection of organic compound by ultra-low pressure reverse osmosis membrane." *Water Research* 36 (2002): 123-130.
- Palmqvist, E., and B. Hann-Hagerdal. "Fermentation of lignocellulosic hydrolysates. II: inhibitors and mechanism of inhibition." *Bioresour. Technol.* 74 (2000): 25-33.
- Patnaik, P.R. "Perspectives in the modeling and optimization of PHB production by pure and mixed cultures." *Critical Reviews in Biotechnology* 25, no. (3) (2005): 153-171.
- Popken, T., L. Gotze, and J. Gmehling. "Reaction kinetics & chemical equilibrium of homogeneously & heterogeneously catalyzed acetic acid esterification with methanol & methyl acetate hydrolysis." *Indust. Eng. Chem. Res.* 39 (2000): 2601-2011.
- Rehm, B.H.A., N. Hoffmann, Q. Qi, S. Fiedler, and A. Steinbuchel. "Biosynthesis of latex-like polyhydroxyalkanoates." *Proceedings of the International Symposium of Bioconversion of Renewable Raw Materials*. Braunschweig, Germany, 2004. 163-175.
- Rodriguez, M., S. Luque, J.R. Alvarez, and J. Coca. "A comparative study of reverse osmosis and freeze concentration for the removal of valeric acid from wastewaters." *Desalination* 127 (2000): 1-11.
- Sagne, C., C. Fargues, R. Lewandowski, M.L. Lameloise, and M. Decloux. "Screening of reverse osmosis membranes for the treatment and reuse of distillery condensates into alcoholic fermentation." *Desalination* 219 (2008): 335-347.
- Sagne, C., C. Fargues, R. Lewandowski, M.L. Lameloise, M. Gavach, and M. Decloux. "A pilot scale study of reverse osmosis for the purification of condensate arising from distillery stillage concentration plant." *Chemical Engineering and Processing* 49 (2010): 331-339.
- Salehzadeh, H., and M.C.M. Van Loosdrecht. "Production of Polyhydroxyalkanoates by mixed culture: recent trend and biotechnological importance." *Biotechnology Advances* 22, no. (3) (2004): 261-279.
- Serafim, L.S., P.C. Lemos, R. Oliveira, and M.A.M. Reis. "Optimization of polyhydroxybutyrate production by mixed cultures submitted to aerobic dynamic feeding conditions." *Biotechnology and Bioengineering* 87, no. (2) (2004): 145-160.
- Teella, A., G.W. Huber, and D.M. Ford. "Separation of acetic acid from the aqueous fraction of fast pyrolysis bio-oils using nanofiltration and reverse osmosis membranes." *Journal of Membrane Science* 378 (2011): 495-502.
- Timmer, J.M.K., H.C. Van der Horst, and T. Robbertsen. "Mass transfer of lactic acid in reverse osmosis and nanofiltration membranes. A qualitative model." *Journal of Membrane Science* 85 (1993): 205-216.
- Timmer, J.M.K., J. Kromkamp, and T. Robbertsen. "Lactic acid separation from fermentations broths by reverse osmosis and nanofiltration." *Journal of Membrane Science* 92 (1994): 185-197.
- van Reis, R., and A. Zydney. "Membrane separations in biotechnology." *Current Opinion in Biotechnology* 12 (2001): 208-211.
- Weng, Y.-H., et al. "Separation of acetic acid from xylose by nanofiltration." *Separation and Purification Technology* 67 (2009): 95-102.
- Yasotha, K., M.K. Aroua, K.B. Ramachandran, and I.K.P. Tan. "Chemical characterization of medium-chain-length polyhydroxyalkanoates (PHAs) recovered by enzymatic treatment and ultrafiltration." *Journal of Chemical Technology and Biotechnology* 82 (2007): 847-855.

- Yasotha, K., M.K. Aroua, K.B. Ramachandran, and I.K.P. Tan. "Recovery of medium-chain-length polyhydroxyalkanoates (PHAs) through enzymatic digestion treatments and ultrafiltration." *Biochemical Engineering Journal* 30 (2006): 260-268.
- Zacharof, M.P., and R.W. Lovitt. "Complex effluent stream as potential source of volatile fatty acids." *Waste Biomass Val.*, 2013.
- Zacharof, M.-P., and R.W. Lowitt. "Recovery of volatile fatty acids (VFA) from complex waste effluents using membranes." *Water Science and Technology* 69, no. (3) (2014): 495-503.
- Zeman, L.J., and A.L. Zydney. *Microfiltration and ultrafiltration. Principles and applications*. New York: Marcel Dekker, 1996.
- Zhou, F., C. Wang, and J. Wei. "Separation of acetic acid from monosaccharides by NF and RO membranes: performance comparison." *Journal of Membrane Science* 429 (2013): 243-251.
- Zhou, F., C. Wang, and J. Wei. "Simultaneous acetic acid separation and monosaccharid concentration by reverse osmosis." *Bioresource Technology* 131 (2013): 349-356.

APPENDIX D

Experimental Data

D.1 Oligosaccharide <i>NF</i>	211
D.1.1 GE-DK, Radial flow test cell, Single Solute.....	211
D.1.2 GE-DL, SW1812-34, Single Solute	212
D.1.3 GE-DK, Radial flow test cell, Mixtures.....	213
D.1.4 SW1812 GE-DL, Mixtures	213
D.2 PHA/non-PHA Recovery by UF.....	214
D.2.1 PV400 (100 kDa) membrane	214
D.3 VFAs Recovery.....	214
D.3.1 GE-DK pH 4	214

In this Appendix some experimental data, presented and discussed in detail in *Chapter 3 (Food Applications)* and *Appendix C (Biotechnology Applications)*, is documented, in order to show the type of experimentation performed.

D.1 Oligosaccharide *NF*

D.1.1 GE-DK, Radial flow test cell, Single Solute

<i>DX GE-DK 10 g/dm3 30°C pH 4</i>								
<i>ΔP (bar)</i>	<i>J_v (dm³/(hm²))</i>	<i>C_{bulk}(g/dm³)</i>	<i>CP (g/dm³)</i>	<i>CI (g/dm³)</i>	<i>R_{obs} %</i>	<i>R_{real} %</i>	<i>ΔP-Δπ_{bulk} (bar)</i>	<i>ΔP-σνΔπ_{eff} (bar)</i>
4,2	20,26	11,11	2,19	12,31	80,26	82,19	2,87	2,83
6,3	35,08	11,36	1,49	14,11	86,84	89,41	4,84	4,59
10,3	61,03	11,36	1,10	16,86	90,35	93,50	8,78	8,16
22,25	130,34	11,26	0,85	27,06	92,48	96,87	20,71	18,66
26,2	159,25	11,01	0,65	32,81	94,12	98,03	24,67	21,77

<i>FR GE-DK 10 g/dm3 30°C pH 4</i>								
<i>ΔP (bar)</i>	<i>J_v (dm³/(hm²))</i>	<i>C_{bulk}(g/dm³)</i>	<i>CP (g/dm³)</i>	<i>CI (g/dm³)</i>	<i>R_{obs} %</i>	<i>R_{real} %</i>	<i>ΔP-Δπ_{bulk} (bar)</i>	<i>ΔP-σνΔπ_{eff} (bar)</i>
4,3	24,17	10,15	2,44	11,40	75,95	78,58	3,17	3,13
6,4	38,59	10,05	1,89	12,57	81,16	84,93	5,21	5,00
10,45	64,25	9,85	1,84	14,37	81,29	87,17	9,28	8,81
22,25	142,52	10,05	1,25	25,19	87,61	95,06	20,98	19,07
26,25	168,19	10,10	1,10	30,55	89,15	96,41	24,95	22,31

ML GE-DK 10 g/dm ³ 50°C pH 4								
ΔP (bar)	J_v (dm ³ /(hm ²))	C_{bulk} (g/dm ³)	CP (g/dm ³)	CI (g/dm ³)	R_{obs} %	R_{real} %	$\Delta P - \Delta \pi_{bulk}$ (bar)	$\Delta P - \sigma \Delta \pi_{eff}$ (bar)
3,45	30,79	9,57	0,30	11,48	96,90	97,42	2,73	2,582
5,5	50,66	9,82	0,30	13,26	96,98	97,77	4,76	4,492
7,5	70,29	9,92	0,30	15,07	97,01	98,03	6,75	6,350
9	88,68	10,17	0,30	17,27	97,08	98,28	8,23	7,677
11,05	106,09	10,32	0,30	19,49	97,13	98,48	10,27	9,552
19,7	175,67	10,57	0,25	30,80	97,66	99,20	18,90	17,294
23,7	210,17	10,72	0,30	38,79	97,23	99,24	22,89	20,649

D.1.2 GE-DL, SW1812-34, Single Solute

DX GE-DL 30°C 50 g/dm ³ pH 4								
ΔP (bar)	J_v (dm ³ /(hm ²))	C_{bulk} (g/dm ³)	CP (g/dm ³)	CI (g/dm ³)	R_{obs} %	R_{real} %	$\Delta P - \Delta \pi_{bulk}$ (bar)	$\Delta P - \sigma \Delta \pi_{eff}$ (bar)
2,13	1,11	48,64	28,82	49,00	40,75	41,19	-0,78	-0,69
3,13	1,82	48,88	23,76	49,64	51,39	52,13	-0,54	-0,47
5,18	4,33	49,16	14,09	51,74	71,35	72,78	0,10	-0,01
8,18	12,13	49,23	7,04	58,58	85,70	87,99	2,11	1,07
10,18	18,02	48,99	5,45	64,14	88,88	91,51	3,93	2,06
14,33	27,53	48,85	4,52	74,73	90,74	93,95	7,97	4,52
18,43	40,70	49,09	3,83	94,08	92,20	95,93	11,94	5,57

DX GE-DL 10 g/dm ³ 30°C pH 4								
ΔP (bar)	J_v (dm ³ /(hm ²))	C_{bulk} (g/dm ³)	CP (g/dm ³)	CI (g/dm ³)	R_{obs} %	R_{real} %	$\Delta P - \Delta \pi_{bulk}$ (bar)	$\Delta P - \sigma \Delta \pi_{eff}$ (bar)
3,18	20,85	9,92	0,96	13,31	90,37	92,82	1,94	1,56
8,18	49,80	10,09	0,69	20,96	93,14	96,70	6,88	5,50
13,33	74,10	10,06	0,66	30,38	93,45	97,83	12,03	9,37
18,43	96,04	9,96	0,76	42,19	92,39	98,20	17,16	12,84

D.1.3 GE-DK, Radial flow test cell, Mixtures

GE-DK DX+ML 5 + 10 gdm-3 50°C pH 4															
ΔP	J_v (dm ³ /(hm ²))	$C_{bulk\ DX}$ (g/dm ³)	$C_{bulk\ ML}$ (g/dm ³)	$C_{bulk,TOT}$ (g/dm ³)	$CP\ DX$ (g/dm ³)	$CP\ ML$ (g/dm ³)	CP,TOT (g/dm ³)	$CI\ DX$ (g/dm ³)	$CI\ ML$ (g/dm ³)	$Robs\ DX$ %	$Robs\ ML$ %	$Rreal\ DX$ %	$Rreal\ ML$ %	$\Delta P-\Delta\pi_{bulk}$ (bar)	$\Delta P-\sigma\Delta\pi_{eff}$ (bar)
3,45	22,40	4,81	11,50	16,32	0,44	0,08	0,52	5,29	13,09	90,96	99,27	91,78	99,35	1,92	1,76
5,45	40,62	4,81	11,50	16,32	0,85	0,04	0,89	5,63	14,56		99,62		99,70	3,98	3,65
7,50	60,30	4,81	11,50	16,32	0,16	0,04	0,20	6,31	16,33	96,61	99,69	97,42	99,78	5,93	5,37
9,50	79,58	4,81	11,50	16,32	0,15	0,02	0,18	6,89	18,29	96,82	99,80	97,78	99,87	7,93	7,13
11,50	95,43	4,81	11,50	16,32	0,00	0,00	0,00	7,50	20,09	100,00	100,00	100,00	100,00	9,90	8,88
19,70	164,00	4,81	11,50	16,32	0,00	0,00	0,00	10,36	30,22	100,00	100,00	100,00	100,00	18,10	15,87
23,75	195,41	4,81	11,50	16,32	0,00	0,02	0,02	12,05	36,52	100,00	99,83	100,00	99,95	22,16	19,17
27,95	228,73	4,81	11,50	16,32	0,00	0,00	0,00	14,19	44,92	100,00	100,00	100,00	100,00	26,35	22,38
11,50	110,24	26,10	3,03	29,13	3,41	0,00	3,41	38,38	5,32	86,94	100,00	91,12	100,00	8,14	6,02
19,70	201,72	26,10	3,03	29,13	2,80	0,00	2,80	57,79	9,08	89,28	100,00	95,16	100,00	16,25	10,87
24,75	248,91	22,85	2,58	25,43	2,74	0,00	2,74	66,30	11,02			95,87	100,00	21,56	14,42

D.1.4 SW1812 GE-DL, Mixtures

Dextrose + Xylose SW1812 GE-DL 50 gdm-3 30°-50°C pH 4															
DX+XY 30°C pH 4															
ΔP	J_v (dm ³ /(hm ²))	$C_{bulk\ DX}$ (g/dm ³)	$C_{bulk\ XY}$ (g/dm ³)	$C_{bulk,TOT}$ (g/dm ³)	$CP\ DX$ (g/dm ³)	$CP\ XY$ (g/dm ³)	CP,TOT (g/dm ³)	$CI\ DX$ (g/dm ³)	$CI\ XY$ (g/dm ³)	$Robs\ DX$ %	$Robs\ XY$ %	$Rreal\ DX$ %	$Rreal\ XY$ %	$\Delta P-\Delta\pi_{bulk}$ (bar)	$\Delta P-\sigma\Delta\pi_{eff}$ (bar)
3,18	2,21	27,16	27,64	54,80	10,30	20,79	31,09	27,79	27,89	62,07	24,78	62,93	25,46	-2,12	-0,29
5,18	4,57	26,68	27,26	53,94	6,37	16,38	22,74	28,28	28,11	76,14	39,93	77,49	41,74	-1,19	0,39
8,18	10,96	26,83	27,45	54,28	3,46	11,10	14,56	31,51	30,68	87,12	59,56	89,03	63,82	0,87	1,33
10,18	16,25	26,89	27,49	54,38	2,65	9,11	11,76	34,45	33,16	90,15	66,86	92,32	72,52	2,61	2,11
13,33	24,66	27,06	27,83	54,89	2,09	7,55	9,64	39,93	38,14	92,27	72,88	94,76	80,21	5,51	3,40
18,38	36,28	26,73	27,89	54,62	1,78	6,53	8,31	48,10	45,93	93,34	76,58	96,30	85,78	10,50	5,86

D.2 PHA/non-PHA Recovery by UF

D.2.1 PV400 (100 kDa) membrane

PV400 (100 kDa), non-PHA, room T, 500 rpm ΔP_{in} 0.5 bar				PV400 (100 kDa), non-PHA, room T, 500 rpm ΔP_{in} 1 bar				PV400 (100 kDa), non-PHA, room T, 500 rpm ΔP_{in} 1.5 bar			
	SS conc Feed (g/dm ³)	V (dm ³)		SS conc Feed (g/dm ³)	V (dm ³)			SS conc Feed (g/dm ³)	V (dm ³)		
Feed (<i>t</i> ⁰)	9,35E-05	0,20		9,15E-05	0,20			8,95E-05	0,20		
Feed (<i>t</i> _f)	1,00E-04	0,16		1,19E-04	–			1,09E-04	–		

time (min)	ΔP (bar)	<i>J_v</i> (dm ³ /hm ²)	SS Perm. Conc. (g/dm ³)	time (min)	ΔP (bar)	<i>J_v</i> (dm ³ /hm ²)	SS Perm. Conc. (g/dm ³)	time (min)	ΔP (bar)	<i>J_v</i> (dm ³ /hm ²)	SS Perm. Conc. (g/dm ³)
2	0,55	47,74	5,65E-05	5	1	59,08	–	10	1,5	64,42	0,00
14	0,55	35,54	5,86E-05	25	1	42,87	6,53E-05	30	1,5	38,42	7,34E-05
30	0,55	30,35	5,92E-05	60	1	35,23	6,86E-05	60	1,5	35,18	7,40E-05
50	0,55	25,42	6,12E-05	90	1	31,61	7,07E-05				

D.3 VFAs Recovery

D.3.1 GE-DK pH 4

GE-DK 50°C pH 4 400 dm ³ /h																					
Feed									Permeate												
<i>T</i> (°C)	<i>P_{in}</i> (bar)	ΔP_{in} (bar)	AA conc (g/dm ³)	PA conc. (g/dm ³)	BA conc. (g/dm ³)	VA conc.(g/dm ³)	CA (g/dm ³)	VFAs conc (g/dm ³)	<i>J_{v,exp}</i> (dm ³ /hm ²)	AA conc (g/dm ³)	PA conc. (g/dm ³)	BA conc. (g/dm ³)	VA conc.(g/dm ³)	CA (g/dm ³)	VFAs conc (g/dm ³)	AA <i>R_{obs}</i> %	PA <i>R_{obs}</i> %	BA <i>R_{obs}</i> %	VA <i>R_{obs}</i> %	CA <i>R_{obs}</i> %	<i>R_{obs,tot}</i> %
49,83	4,40	3,50	2,28	2,40	2,09	2,29	2,00	11,05	44,04	2,19	2,31	2,02	2,12	1,85	10,50	3,78	3,59	3,34	7,29	7,16	4,99
49,86	9,40	8,45	2,35	2,41	2,16	2,28	1,94	11,13	96,71	2,16	2,21	1,95	2,05	1,69	10,05	8,06	8,27	10,04	10,27	12,60	9,73
49,70	14,40	13,45	2,37	2,43	2,15	2,24	1,93	11,12	146,71	2,15	2,25	1,91	1,96	1,75	10,02	9,28	7,13	11,29	12,61	9,30	9,87
49,40	19,40	18,85	2,39	2,45	2,17	2,26	1,91	11,17	177,90	2,13	2,24	1,96	1,94	1,72	9,98	11,05	8,73	9,37	14,22	9,84	10,65
51,60	24,40	24,20	2,43	2,46	2,20	2,26	1,96	11,32	199,52	2,07	2,16	1,91	1,93	1,65	9,72	14,80	12,51	12,97	14,64	15,95	14,11

